NASA Tech Briefs

National
Aeronautics and
Space
Administration

A vacuum chamber previously used by a NASA contractor to test spacecraft components is now used in a unique deacidification process that extends the lifetimes of books and other valuable documents. After drying in vacuum, the documents are exposed to a penetrating vapor of diethyl zinc, which neutralizes the life-shortening acids that are normally present in the paper. Accelerated aging tests show that the process extends paper life almost fourfold, with no detrimental effects. [*See page A1.*]

Vol. 5, No. 1 SPRING 1980

About the NASA Technology Utilization Program

The National Aeronautics and Space Act of 1958, which established NASA and the United States civilian space program, requires that "The Administration shall provide for the widest practicable and appropriate dissemination of information concerning its activities and the results thereof."

To help carry out this objective, NASA's Technology Utilization (TU) Program was established in 1962. Now, as an element of NASA's Technology Transfer Division, this program offers a variety of valuable services to help transfer aerospace technology to nonaerospace applications, thus assuring American taxpayers maximum return on their investment in space research; thousands of spinoffs of NASA research have already occurred in virtually every area of our economy.

The TU program has worked for engineers, scientists, technicians, and businessmen; and it can work for you.

NASA Tech Briefs

Tech Briefs is published quarterly and is free to engineers in U.S. industry and to other domestic technology transfer agents. It is both a current-awareness medium and a problem-solving tool. Potential products . . . industrial processes . . . basic and applied research . . . shop and lab techniques . . . computer software . . . new sources of technical data . . . concepts . . . can be found here. The short section on New Product Ideas highlights a few of the potential new products contained in this issue. The remainder of the volume is organized by technical category to help you quickly review new developments in your areas of interest. Finally, a subject index makes each issue a convenient reference file.

Further Information on Innovations

Although some new technology announcements are complete in themselves, most are backed up by Technical Support Packages (TSP's). TSP's are available without charge and may be ordered by simply completing a TSP Request Card found at the back of this volume. Further information on some innovations is available for a nominal fee from other sources, as indicated. In addition, Technology Utilization Officers at NASA Field Centers will often be able to lend necessary guidance and assistance.

Patent Licenses

Patents have been issued to NASA on some of the inventions described, and patent applications have been submitted on others. Each announcement indicates patent status, if applicable.

Other Technology Utilization Services

To assist engineers, industrial researchers, business executives, city officials, and other potential users in applying space technology to their problems, NASA sponsors Industrial Applications Centers. Their services are described on page A6. In addition, an extensive library of computer programs is available through COSMIC, the Technology Utilization Program's outlet for NASA-developed software.

Applications Program

NASA conducts applications engineering projects to help solve public-sector problems in such areas as safety, health, transportation, and environmental protection. Applications teams, staffed by professionals from a variety of disciplines, assist in this effort by working with Federal agencies and health organizations to identify critical problems amenable to solution by the application of existing NASA technology.

Reader Feedback

We hope you find the information in *NASA Tech Briefs* useful. A reader-feedback card has been included because we want your comments and suggestions on how we can further help you apply NASA innovations and technology to your needs. Please use it; or if you need more space, write to the Director, Technology Transfer Division, P. O. Box 8256, Baltimore/Washington International Airport, Maryland 21240.

NASA Tech Briefs

National Aeronautics and Space Administration

SPRING 1980
Volume 5, Number 1

COVERS: Further information on the Paper Preservation Process can be found in U.S. Patent No. 3,969,549, a copy of which can be obtained for 50 cents from the Commissioner of Patents and Trademarks, Washington, D.C. 20231. To obtain more information about the Seismic Testing Facility, Circle 83 on the TSP Request Card at the back of this issue of NASA Tech Briefs.

About This NASA Publication

NASA Tech Briefs, a quarterly publication, is distributed free to qualified U.S. citizens to encourage commercial application of U.S. space technology. For information on publications and services available through the NASA Technology Utilization Program, write to the Director, Technology Transfer Division, P. O. Box 8757, Baltimore/Washington International Airport, Maryland 21240.

"The Administrator of National Aeronautics and Space Administration has determined that the publication of this periodical is necessary in the transaction of the public business required by law of this Agency. Use of funds for printing this periodical has been approved by the Director of the Office of Management and Budget."

Change of Address

If you wish to have NASA Tech Briefs forwarded to your new address, use one of the Subscriptions cards enclosed in the back of this volume of NASA Tech Briefs. Be sure to check the appropriate box indicating change of address.

Communications Concerning Editorial Matter

For editorial comments or general communications about NASA Tech Briefs, you may use the Feedback card in the back of NASA Tech Briefs, or write to: The Publications Manager, Technology Transfer Division (ETD-6), NASA Headquarters, Washington, DC 20546. Technical questions concerning specific articles should be directed to the Technology Utilization Officer of the sponsoring NASA Center (addresses listed on page A4).

Acknowledgements

NASA Tech Briefs is published quarterly by the National Aeronautics and Space Administration, Technology Utilization Branch, Washington, DC: Administrator: **Robert A. Frosch;** Director, Technology Transfer Division: **Floyd I. Roberson;** Publications Manager: **D. W. Orrick.** Prepared for the National Aeronautics and Space Administration by **Logical Technical Services Corp.:** Editor-in-Chief: **Graham L. Gross;** Art Director: **Ernest Gillespie;** Managing Editor: **Jay Kirschenbaum;** Senior Editor: **Donald Blattner;** Chief Copy Editor: **Oden Browne;** Staff Editors: **Jerry Rosen, Ted Selinsky, George Watson;** Graphics: **Concetto Auditore, Luis Martinez, Pat McDermond;** Editorial & Production: **Richard Johnson, Rose Giglietti, Beth Rogers, Vincent Susinno, John Tucker, Ernestine Walker.**

NASA TU SERVICES

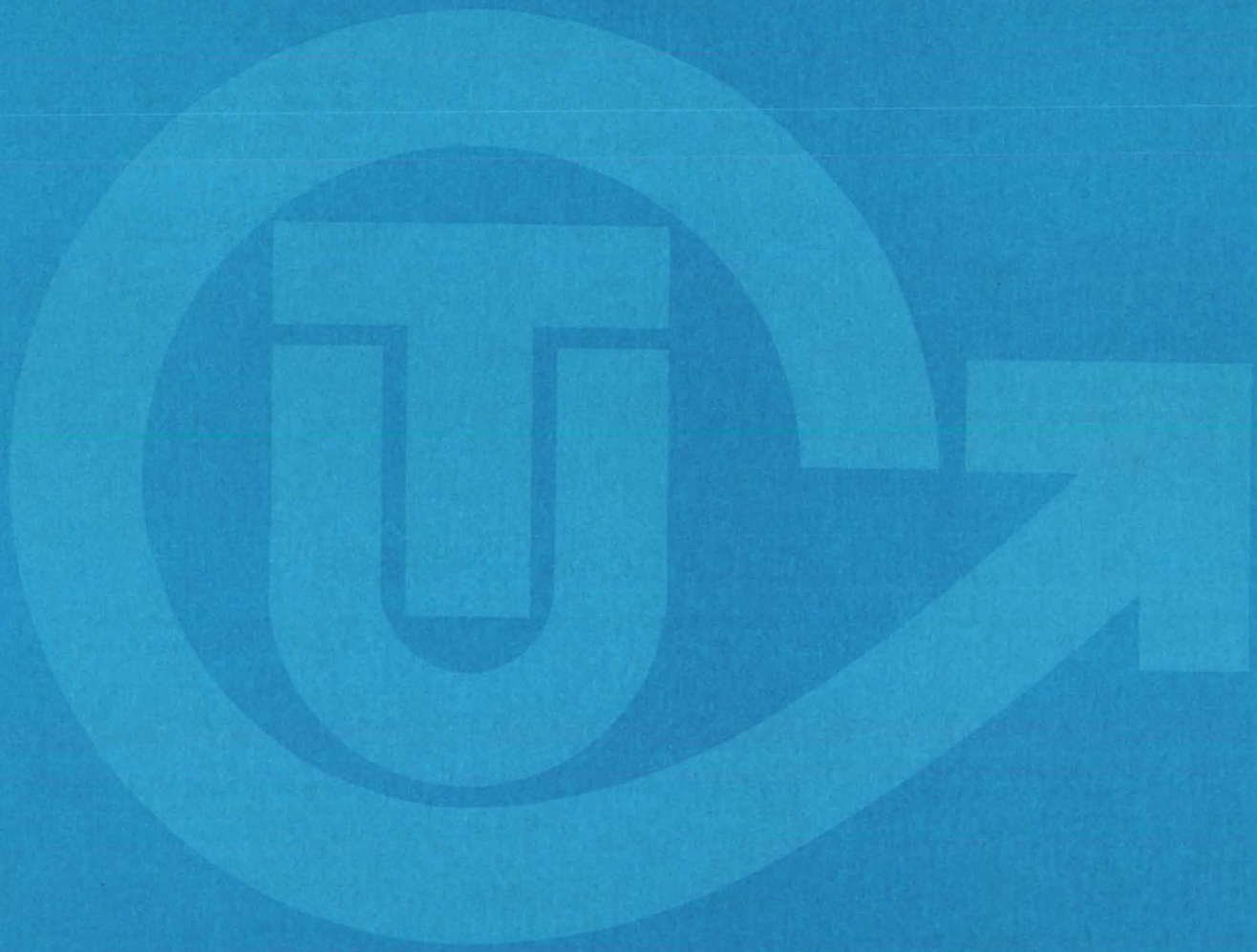

NASA TECHNOLOGY UTILIZATION NETWORK

★ TECHNOLOGY UTILIZATION OFFICERS

Charles C. Kubokawa
Ames Research Center
Code AU: 240-2
Moffett Field, CA 94035
(415) 965-5333

Gussie Anderson
Hugh L. Dryden Flight Research Center
Code OD/TU Office - Room 2015
Post Office Box 273
Edwards, CA 93523
(805) 258-3311, Ext. 787

Donald S. Friedman
Goddard Space Flight Center
Code 702.1
Greenbelt, MD 20771
(301) 344-6242

John T. Wheeler
Lyndon B. Johnson Space Center
Code AT-3
Houston, TX 77058
(713) 483-3809

Raymond J. Cerrato
John F. Kennedy Space Center
Code PT-STA-1
Kennedy Space Center, FL 32899
(305) 867-2780

John Samos
Langley Research Center
Mail Stop 139A
Hampton, VA 23665
(804) 827-3281

Harrison Allen, Jr.
Lewis Research Center
Mail Code 7-3
21000 Brookpark Road
Cleveland, OH 44135
(216) 433-4000, Ext. 6422

Aubrey D. Smith
George C. Marshall Space Flight Center
Code AT01
Marshall Space Flight Center, AL 35812
(205) 453-2224

D. W. Orrick
NASA Headquarters
Code ETD-6
Washington, DC 20546
(202) 755-2244

John H. Warden
NASA Pasadena Office
4800 Oak Grove Drive
Pasadena, CA 91103
(213) 354-6420

Gilmore H. Trafford
Wallops Flight Center
Code OD
Wallops Island, VA 23337
(804) 824-3411, Ext. 201

● INDUSTRIAL APPLICATIONS CENTERS

Aerospace Research Applications Center
1201 East 38th Street
Indianapolis, IN 46205
E. G. Buck, director
(317) 264-4644

Computer Software Management and Information Center (COSMIC)
Suite 112, Barrow Hall
University of Georgia
Athens, GA 30602
(404) 542-3265

Kerr Industrial Applications Center
Southeastern Oklahoma State University
Durant, OK 74701
Robert Oliver, director
(405) 924-0121, Ext. 413

NASA Industrial Applications Center
LIS Building
University of Pittsburgh
Pittsburgh, PA 15260
Edmond Howie, director
(412) 624-5211

New England Research Applications Center
Mansfield Professional Park
Storrs, CT 06268
Daniel Wilde, director
(203) 486-4533

North Carolina Science and Technology Research Center
Post Office Box 12235
Research Triangle Park, NC 27709
Peter J. Chenery, director
(919) 549-0671

Technology Applications Center
University of New Mexico
Albuquerque, NM 87131
Stanley Morain, director
(505) 277-3622

Western Research Applications Center
University of Southern California
University Park
Los Angeles, CA 90007
Robert Mixer, acting director
(213) 741-6132

■ STATE TECHNOLOGY APPLICATIONS CENTERS

NASA/University of Florida
State Technology Applications Center
311 Weil Hall
University of Florida
Gainesville, FL 32611
Ronald J. Thornton, director
Gainesville: (904) 392-6760
Orlando: (305) 275-2706
Tampa: (813) 974-2499

NASA/University of Kentucky
State Technology Applications Program
109 Kinkead Hall
University of Kentucky
Lexington, KY 40506
William R. Strong, manager
(606) 258-4632

◆ PATENT COUNSELS

Robert F. Kempf
Asst. Gen. Counsel for patent matters
NASA Headquarters
Code GP-4
400 Maryland Avenue, S.W.
Washington, DC 20546
(202) 755-3954

Darrell G. Brekke
Ames Research Center
Mail Code: 200-11A
Moffett Field, CA 94035
(415) 965-5104

Paul F. McCaul
Hugh L. Dryden Flight Research Center
Code OD/TU Office - Room 2015
Post Office Box 273
Edwards, CA 93523
(213) 354-2734

John O. Tresansky
Goddard Space Flight Center
Mail Code: 204
Greenbelt, MD 20771
(301) 344-7351

Marvin F. Matthews
Lyndon B. Johnson Space Center
Mail Code: AM
Houston, TX 77058
(713) 483-4871

James O. Harrell
John F. Kennedy Space Center
Mail Code: SA-PAT
Kennedy Space Center, FL 32899
(305) 867-2544

Howard J. Osborn
Langley Research Center
Mail Code: 279
Hampton, VA 23665
(804) 827-3725

Norman T. Musial
Lewis Research Center
Mail Code: 500-311
21000 Brookpark Road
Cleveland, OH 44135
(216) 433-4000, Ext. 346

Leon D. Wofford, Jr.
George C. Marshall Space Flight Center
Mail Code: CC01
Marshall Space Flight Center, AL 35812
(205) 453-0020

Monte F. Mott
NASA Pasadena Office
Mail Code: 180-601
4800 Oak Grove Drive
Pasadena, CA 91103
(213) 354-2700

▲ APPLICATION TEAMS

William N. Fetzner, director
Advisory Center for Medical Technology and Systems
University of Wisconsin
1500 Johnson Drive
Madison, WI 53706
(608) 263-2735

Edmund R. Bangs, director
IIT Research Institute
10 West 35th Street
Chicago, IL 60616
(312) 567-4191

Doris Rouse, director
Research Triangle Institute
Post Office Box 12194
Research Triangle Park, NC 27709
(919) 541-6256

Tom Anyos, director
SRI International
333 Ravenswood Avenue
Menlo Park, CA 94026
(415) 326-6200, Ext. 2864

Eugene Schmidt, program coordinator
Stanford University School of Medicine
Cardiology Division
Biomedical Technology Transfer
703 Welch Road, Suite E-4
Palo Alto, CA 94304
(415) 497-5353

David MacFadyen, project director
Technology + Economics
2225 Massachusetts Avenue
Cambridge, MA 02140
(617) 491-1500

TECHNOLOGY UTILIZATION OFFICERS

Technology transfer experts can help you apply the innovations in NASA Tech Briefs.

The Technology Utilization Officer at each NASA Field Center is an applications engineer who can help you make use of new technology developed at his center. He brings you NASA Tech Briefs and other special publications, sponsors conferences, and arranges for expert assistance in solving technical problems.

Technical assistance, in the form of further information about NASA innovations and technology, is one of the services available from the TUO. Together with NASA scientists and engineers, he can often help you find and implement NASA technology to meet your specific needs.

Technical Support Packages (TSP's) are prepared by the center TUO's. They provide further technical details for articles in NASA Tech Briefs. This additional material can help you evaluate and use NASA technology. You may receive most TSP's free of charge by using the TSP Request Card found at the back of this issue.

Technical questions about articles *in NASA Tech Briefs are answered in the TSP's. When no TSP is available, or you have further questions, contact the Technology Utilization Officer at the center that sponsored the research* [see page A4].

NASA INVENTIONS AVAILABLE FOR LICENSING

Over 3,500 NASA inventions are available for licensing in the United States — both exclusive and nonexclusive.

Nonexclusive licenses for commercial use of NASA inventions are encouraged to promote competition and to achieve the widest use of inventions. They must be used by a negotiated target date but are usually royalty-free.

Exclusive licenses may be granted to encourage early commercial development of NASA inventions, especially when considerable private investment is required. These are generally for 5 to 10 years and usually require royalties based on sales or use.

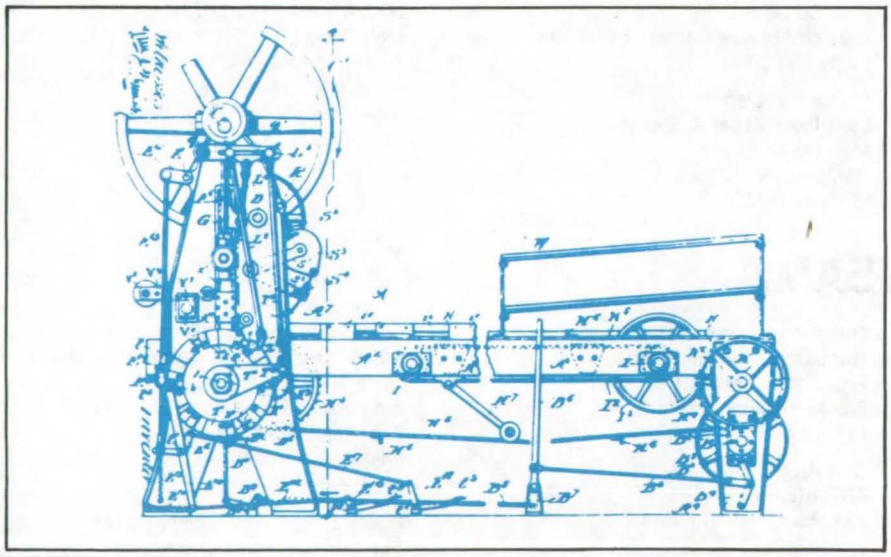

Additional licenses available include those of NASA-owned foreign patents. In addition to inventions described in NASA Tech Briefs, *"NASA Patent Abstract Bibliography"* (PAB), containing abstracts of all NASA inventions, can be purchased from National Technical Information Service, Springfield, VA 22161. The PAB is updated semiannually.

Patent licenses for Tech Briefs *are frequently available. Many of the inventions reported in NASA Tech Briefs are patented or are under consideration for a patent at the time they are published. The current patent status is described at the end of the article; otherwise, there is no statement about patents. If you want to know more about the patent program or are interested in licensing a particular invention, contact the Patent Counsel at the NASA Field Center that sponsored the research* [see page A5]. *Be sure to refer to the NASA reference number at the end of the Tech Brief.*

APPLICATION TEAMS

Technology-matching and problem-solving assistance to public-sector organizations

Application engineering projects are conducted by NASA to help solve public-sector problems in such areas as safety, health, transportation, and environmental protection. Some application teams specialize in biomedical disciplines; others, in engineering and scientific problems. Staffed by professionals from various disciplines, these teams work with other Federal agencies and health organizations to identify critical problems amenable to solution by the application of existing NASA technology.

Public-sector organization *representatives can learn more about application teams by contacting a nearby NASA Field Center Technology Utilization Office* [see page A4].

INDUSTRIAL APPLICATIONS CENTERS

Computerized access to nearly 10 million documents worldwide

Computerized information retrieval from one of the world's largest banks of technical data is available from NASA's network of Industrial Applications Centers (IAC's). The IAC's give you access to 1,800,000 technical reports in the NASA data base and to more than 10 times that many reports and articles found in 140 other computerized data bases.

The major sources include:

- *750,000 NASA Technical Reports*
- *Selected Water Resources Abstracts*
- *NASA Scientific and Technical Aerospace Reports*
- *Air Pollution Technical Information Center*
- *NASA International Aerospace Abstracts*
- *Chem Abstracts Condensates*
- *Engineering Index*
- *Energy Research Abstracts*
- *NASA Tech Briefs*
- *Government Reports Announcements*

and many other specialized files on food technology, textile technology, metallurgy, medicine, business, economics, social sciences, and physical science.

The IAC services range from tailored literature searches through expert technical assistance:

- *Retrospective Searches:* Published or unpublished literature is screened, and documents are identified according to your interest profile. IAC engineers tailor results to your specific needs and furnish abstracts considered the most pertinent. Complete reports are available upon request.
- *Current-Awareness Searches:* IAC engineers will help design a program to suit your needs. You will receive selected monthly or quarterly abstracts on new developments in your area of interest.
- *Technical Assistance:* IAC engineers will help you evaluate the results of your literature searches. They can help find answers to your technical problems and put you in touch with scientists and engineers at appropriate NASA Field Centers.

Prospective clients *can obtain more information about the services offered by NASA IAC's by contacting the nearest IAC* [see page A4] *or by checking the IAC box on a TSP Request Card in this issue.*

STATE TECHNOLOGY APPLICATIONS CENTERS

Technical information services for industry and state and local government agencies

Local government and industry in Florida and Kentucky can utilize the services of NASA's State Technology Applications Centers (STAC's). The STAC's differ from the Industrial Applications Centers described on page A7, primarily in that they are integrated into existing state technical assistance programs and serve only the host state, whereas the IAC's serve multistate regions.

Many data bases, including the NASA base and several commercial bases, are available for automatic data retrieval through the STAC's. Other services such as document retrieval and special searches are also provided. (The STAC's normally charge a fee for their services.)

To obtain information *about the services offered by NASA STAC's, write or call the STAC in your state* [see page A4].

COSMIC®

An economical source of computer programs developed by NASA and other government agencies

A vast software library is maintained by COSMIC — the Computer Software Management and Information Center. COSMIC gives you access to approximately 1,600 computer programs developed for NASA and the Department of Defense and selected programs for other government agencies. Programs and documentation are available at reasonable cost.

Available programs range from management (PERT scheduling) to information science (retrieval systems) and computer operations (hardware and software). Hundreds of engineering programs perform such tasks as structural analysis, electronic circuit design, chemical analysis, and the design of fluid systems. Others determine building energy requirements and optimize mineral exploration.

COSMIC services go beyond the collection and storage of software packages. Programs are checked for completeness; special announcements and an indexed software catalog are prepared; and programs are reproduced for distribution. Customers are helped to identify their software needs; and COSMIC follows up to determine the successes and problems and to provide updates and error corrections. In some cases, NASA engineers can offer guidance to users in installing or running a program.

Information about programs *described in NASA Tech Briefs articles can be obtained by completing the COSMIC Request Card at the back of this issue. Just circle the letters that correspond to the programs in which you are interested.*

NEW PRODUCT IDEAS

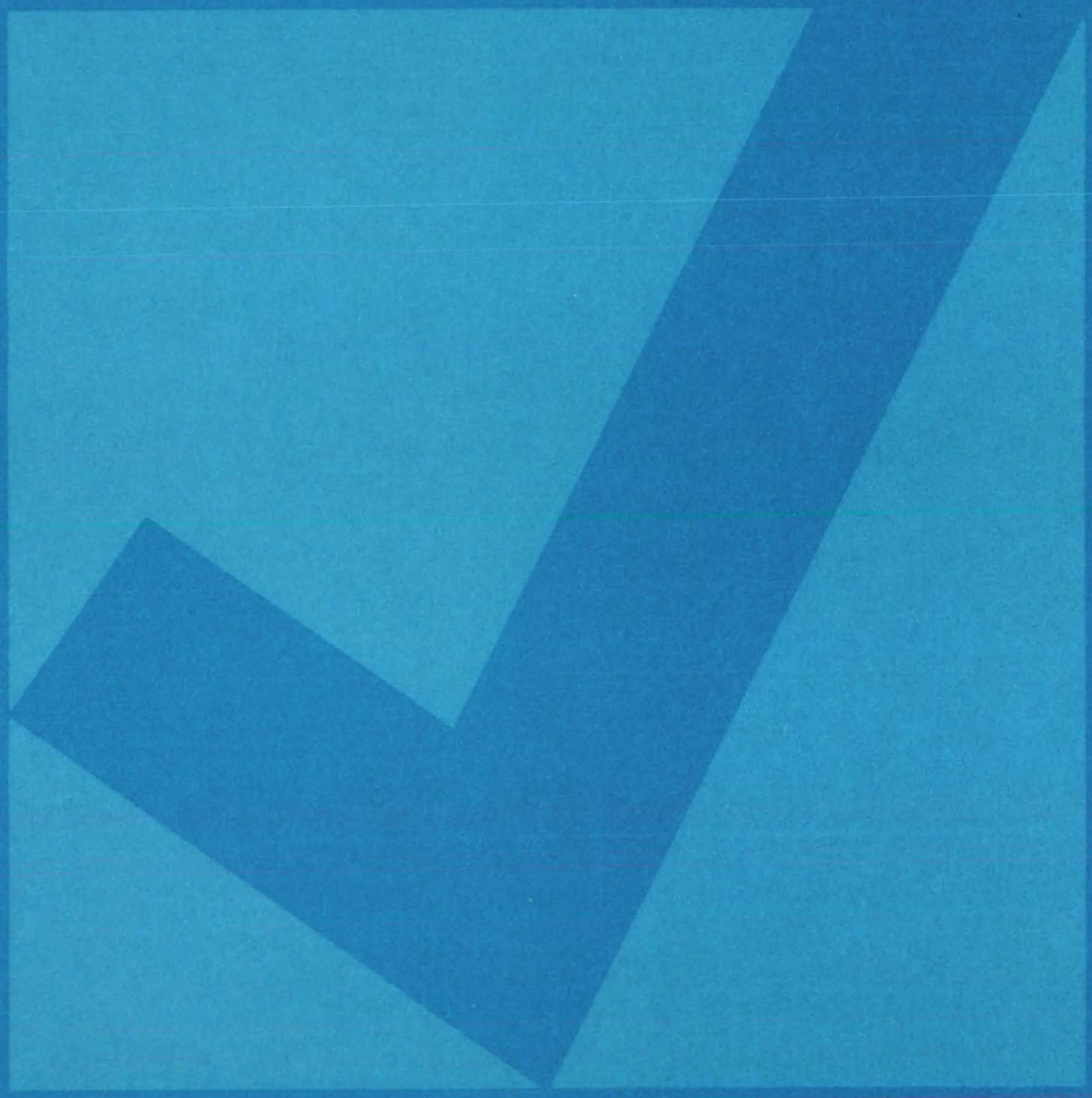

NEW PRODUCT IDEAS are just a few of the many innovations described in this issue of NASA Tech Briefs and having promising commercial applications. Each is discussed further on the referenced page in the appropriate section in this issue. If you are interested in developing a product from these or other NASA innovations, you can receive further technical information by requesting the TSP referenced at the end of the full-length article or by writing the Technology Utilization Office of the sponsoring NASA center (see page A4). NASA's patent-licensing program to encourage commercial development is described on page A6.

Multiband Microstrip Antenna

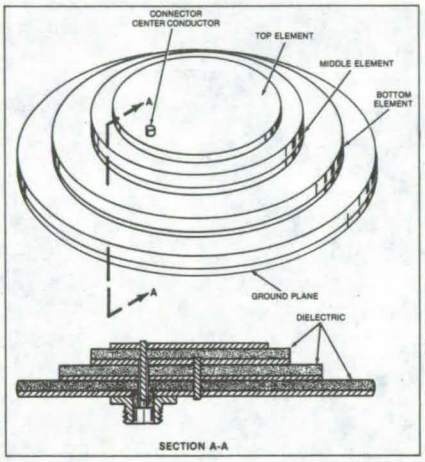

A compact, multiband microstrip antenna transmits and receives elliptically and circularly polarized radiation. The antenna consists of layers of elliptical disks separated by dielectric substrates. Each disk operates at a frequency determined by its size and the dielectric constant of the substrate. In principle, any number of elements may be included in a stack; if the sizes of the elements are close to each other in value, the individual frequency bands can be made to overlap, to yield a single broadband antenna. Standard microstrip techniques, involving sequential removal of material from a stack of conductors and insulators, can be used to build it.
(See page 3.)

Photoelectrochemical Cell With Nondissolving Anode

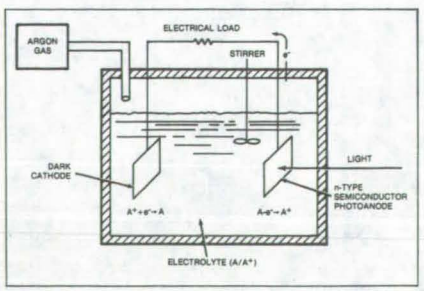

Improved electrolytic photovoltaic cells have efficiencies comparable to those of the best silicon solar cells but are potentially less expensive to manufacture. The cells consist of a light-sensitive n-type semiconductor anode and a metallic cathode immersed in an electrolytic solution. Sunlight strikes the anode and establishes a current between the two electrodes. The reversible redox cells produce no chemical change in the electrolyte and stabilize the n-type semiconducting anode against dissolving. The cell can produce more than 500 mW of power per cm^2 of anode area at an output voltage of 0.4 V.
(See page 31.)

Cable-Splice Detector

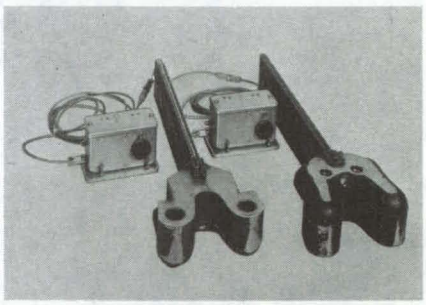

A cable-splice detector has possible uses in aerial cable-car systems, in equipment handling in mines, boreholes, and undersea operations, and in other applications where moving steel cable must be measured, monitored, or controlled. Developed for the San Francisco cable-car system, the detector consists of a Hall-effect magnetic sensor that is located close to the cable. Magnetic markings on the cable are converted to electrical signals. The signals are filtered, amplified, and counted to actuate an alarm when a splice approaches a cable car.
(See page 63.)

Tubing Cutter for Tight Spaces

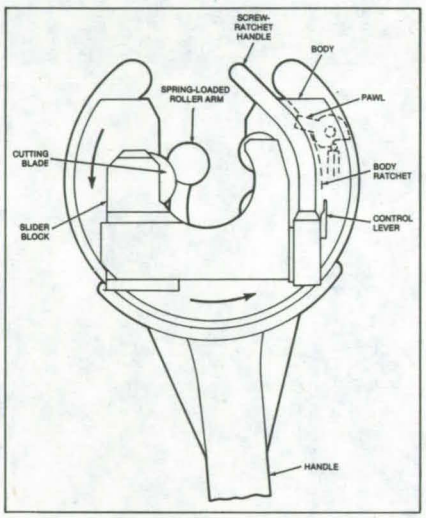

A new tubing cutter requires only a few short swings of its handle to rotate its cutting edge a full 360° around a tube. It is ideal for cutting tubing installed in a confined space that would prevent the free movement of a conventional cutter. The cutter is snapped onto the tube and held in place by a spring-loaded clamp. A screw ratchet advances the cutting wheel until it contacts the tube. After each full rotation about the tube, the screw ratchet is turned so that the cutting blade penetrates deeper into the tube for the next cut.
(See page 84.)

Mechanical End Joint for Structural Columns

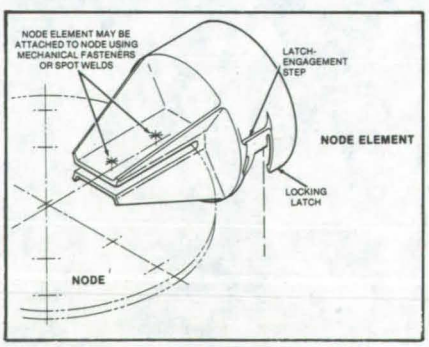

A connector for tubular struts permits the construction of lightweight frames without the use of tools or assembly equipment. The two main components are a node fitting and a strut element. To produce a structurally sound joint from the two components, they are alined approximately and pushed together. The design accommodates reasonable axial and rotational misalinement of nodes and struts. Also, individual columns can be inserted and removed between fixed nodes without affecting the integrity of the remaining structure. All joint components are interchangeable.
(See page 81.)

Fast-Response Atmospheric-Pollutant Monitor

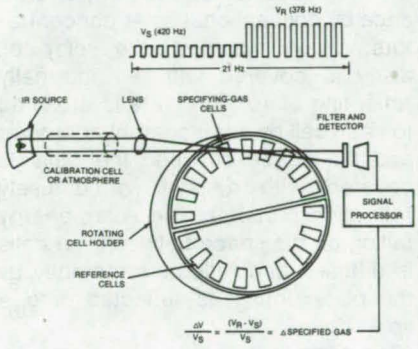

A fast-response infrared spectrometer measures atmospheric CO, CH_4, and HCl over a range of 1 to 12 ppm. With some modifications it could measure other pollutants and use natural light as a source. A cell filled with the sample to be measured filters out the spectral lines of interest. The infrared beam passes through a rotating cell holder that produces chopped signals at two frequencies. The difference in signal amplitudes depends on the amount of test gas in the sample. Signal-processing circuitry amplifies and separates the test-gas and reference signals.
(See page 48.)

Self-Energized Screw Coupling

A novel threaded coupling carries its own store of rotational energy. Originally developed to ease the task of astronauts assembling structures in space, the coupling can offer the same advantages in other hazardous

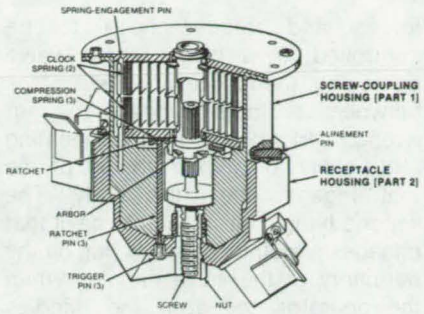

operations, such as underwater and in and around nuclear reactors. It could also be adapted to robotics. The coupling consists of two parts: a screw portion and a receptacle. When the screw portion is inserted into the receptacle and given a slight push by the operator, trigger pins release a ratchet, allowing the energy stored in springs to rotate the screw into a nut in the receptacle.
(See page 82.)

Precision Filament Cutter

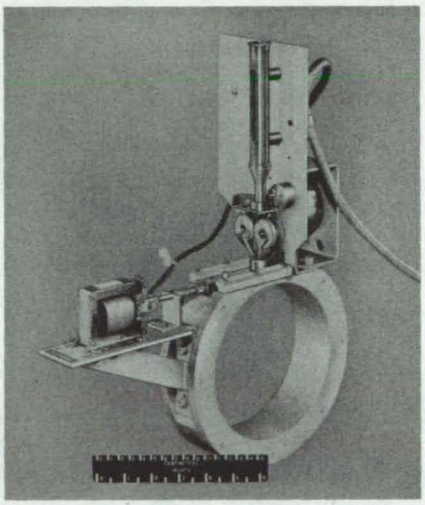

An automated filament cutter precisely chops filaments of glass, graphite, plastic, and other materials into fibers for use in composites and other applications. The cutter uses a movable blade that is pushed and pulled across a fixed blade. Because the mass of the movable blade is small and the stroke is short, operation is fast, and wear and energy consumption are low. Also, the push/pull motion of the blade speeds up operation by cutting on both forward and return movements. An operator selects the fiber length and chopping rate. After each cut, a blast of air blows the filament away so it can be collected.
(See page 79.)

Detecting a Coal/Shale Interface

A prototype coal/shale interface detector, which is intended to be used with a longwall shearer, determines when a cut has pierced through a coal layer. The detector combines the output of two optical reflectometers with that of a penetrometer. An accelerometer measures the hardness of the material struck by the penetrometer ram, while the reflectometers measure the reflectivity of the

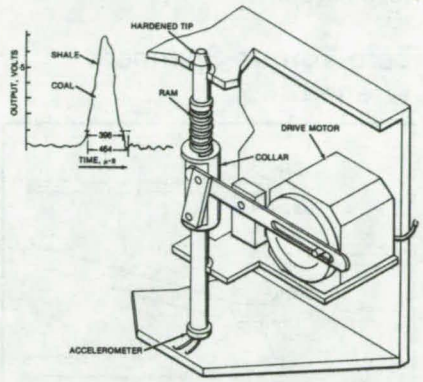

surface on both sides of the penetrometer. The signals are then combined in a voting circuit that indicates "coal" or "shale," depending on the information supplied by the three sensors. The penetrometer distinguishes between coal and shale by the differences in the accelerometer waveforms for the two materials.
(See page 47.)

Immersible Broadband Acoustic Transducer

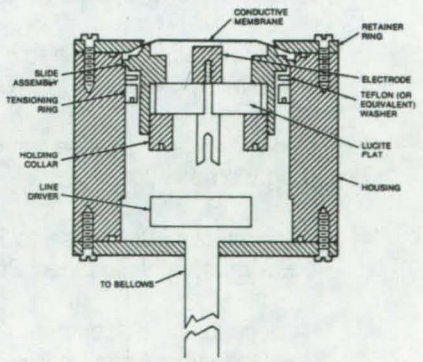

A broadband capacitive electrostatic transducer (ESAT) has been developed for use in liquids. Tests made with the transducer indicate that it may be useful as a broadband acoustic receiver with a predictable

frequency response. Since it measures the absolute displacement amplitudes of ultrasonic waves in liquids, it may be used as a calibrator for other transducers and as a probe for the nondestructive study and characterization of materials. The ESAT basically consists of a thin conductive membrane stretched over a metallic housing. Ultrasonic waves incident on the membrane cause it to vibrate and generate a signal proportional to the wave amplitude. The entire assembly is sealed for immersion in a liquid.
(See page 67.)

Zero-Torque Spanner Wrench

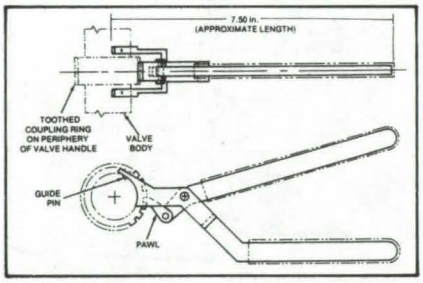

A proposed spanner wrench converts the gripping action of a hand to rotary motion. It does so without imparting reactive moments or forces on the part being turned or on the operator. The new wrench should be useful in undersea operations and other delicate work where reactive forces and torques have to be controlled. In a design for a valve tightening, the tool resembles a cross between a conventional spanner wrench and a pliers. Through locating and holding pins, one handle of the tool engages the valve body. The second handle has a ratchet pawl that engages a toothed coupling ring on the periphery of the valve handle. When the operator squeezes the handles together, the valve handle rotates with respect to the valve body.
(See page 90.)

Compact, Super Heat Exchanger

A compact, super heat exchanger uses porous media as a means of enhancing heat transfer through the walls of cooling channels, thereby lowering the wall temperature. Porous media within the cooling channel increase the internal surface area from which heat can be transferred to the coolant. Comparison data show that the wall has a lower temperature and the coolant has a higher temperature when a porous medium is used within a heat exchanger. The porous media can be sintered powdered metal, metal fibers, woven wire layers, or any porous metal having the desired permeability and porosity.
(See page 70.)

New Mounting Improves Solar-Cell Efficiency

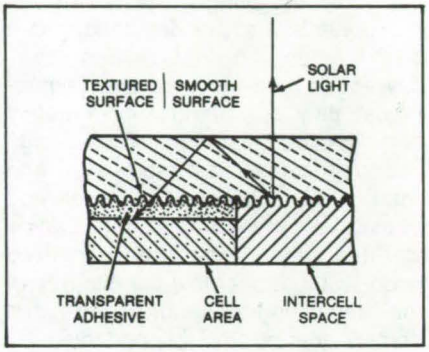

A new method of mounting and encapsulating solar cells boosts output by about 20 percent by trapping and redirecting solar radiation. This is done without the increased module depth needed for equivalent performance by conventional solar concentrators. When mounted, the solar-cell array is covered with an internally reflecting plate. The plate is attached to each cell by a transparent adhesive, and the space between the cells is covered with a layer of diffusely reflecting material. The solar energy falling on the space between the cells is diffused and reflected internally by the plate until it is reflected onto a solar cell.
(See page 32.)

Patent Licenses Recently Granted by NASA for Commercial Use of NASA-Owned Inventions

The patent licenses listed below are just a few of those recently awarded by NASA as part of its program to encourage the commercial application of its new technology. For information on how you may obtain nonexclusive or exclusive license for the commercial use of NASA inventions, see page A6 of this issue.

- A nonexclusive license to Fiber Materials, Inc., Biddeford, Maine, for U.S. Patent No. 4,072,532, covering an invention entitled "Hi-Temperature Resistant Cermet & Ceramic Compositions."
- A nonexclusive license to Foray Industries, Houston, Texas, for U.S. Patent No. 3,856,534, entitled "Anti-Fog Composition."
- A nonexclusive license to Pressure Systems, Hampton, Virginia, for U.S. Patent No. 4,111,058, entitled "Electronically Scanned Pressure Sensor Module With in Situ Calibration Capability."
- A nonexclusive license to Aerolab, Laurel, Maryland, for U.S. Patent No. 3,952,590, entitled "Apparatus for Reducing Aerodynamic Noise in a Wind Tunnel."
- A nonexclusive license to International Technology Corp., Satellite Beach, Florida, for U.S. Patent No. 4,087,975, entitled "Ocean Thermal Plant."
- A nonexclusive license to Hexcel Corp., San Francisco, California, for U.S. Patent Application Serial No. 839,963, entitled "Mixed Diamines for Lower Melting Addition Polyimide Preparation & Utilization."

Electronic Components and Circuits

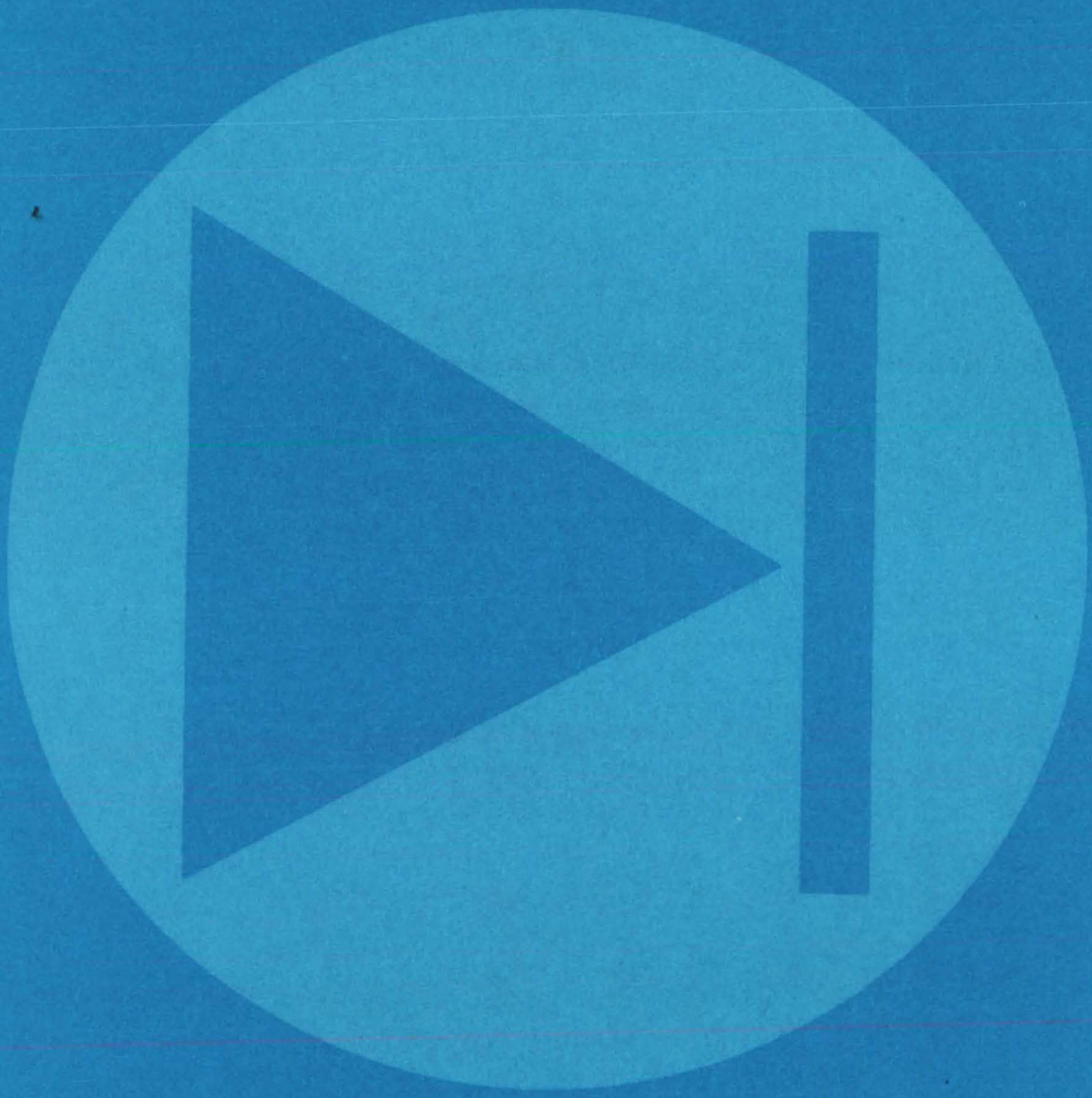

Hardware, Techniques, and Processes

Books and Reports

Multiband Microstrip Antenna

An antenna composed of stacked elliptical disks operates over broadband or multiple frequency bands.

Lyndon B. Johnson Space Center, Houston, Texas

A compact, multiband (or broadband) microstrip antenna consists of layers of elliptical disks separated by dielectric substrates (see figure). Each disk operates at the frequency determined by its size and the dielectric constant of the substrate. A single-element antenna of this type is described in "Low-Profile Communications Antenna" (MSC-16683) on page 345 of *NASA Tech Briefs*, Vol. 4, No. 3. [Also see related article, "Low-Cost Dual-Frequency Microwave Antenna" (MSC-16100), on page 513 of Vol. 1, No. 4.]

The eccentricities of the antenna elements are all within the same range, so that the sizes of the individual elements vary approximately as do their semimajor axes. To achieve an operating frequency f, the semimajor axis, a, of an antenna element is given by

$$a = kc/f\sqrt{\varepsilon}$$

where ε is the relative dielectric constant of the substrate layer, c is the speed of light, and k is an empirical constant ranging from 0.27 to 0.29. Consequently, by decreasing the semimajor axis of the ellipse, the operating frequency is made larger.

Left (right) circularly polarized radiation results if the feedpoint is located on a line at a 45° angle measured counterclockwise (clockwise) from a semimajor axis. Maintaining a 10- to 20-percent limitation on the eccentricity of an antenna element insures that the element can receive and transmit circularly polarized radiation.

For the three-element antenna shown, the disks are positioned above the ground plane in the order of length of semimajor axis, with the element with the smallest semimajor axis on top. The center conductor of the coupling connector contacts the top antenna element only. The outer conductor is attached to the bottom of the ground plane. A conducting pin passes through the center of each disk, except for the top element.

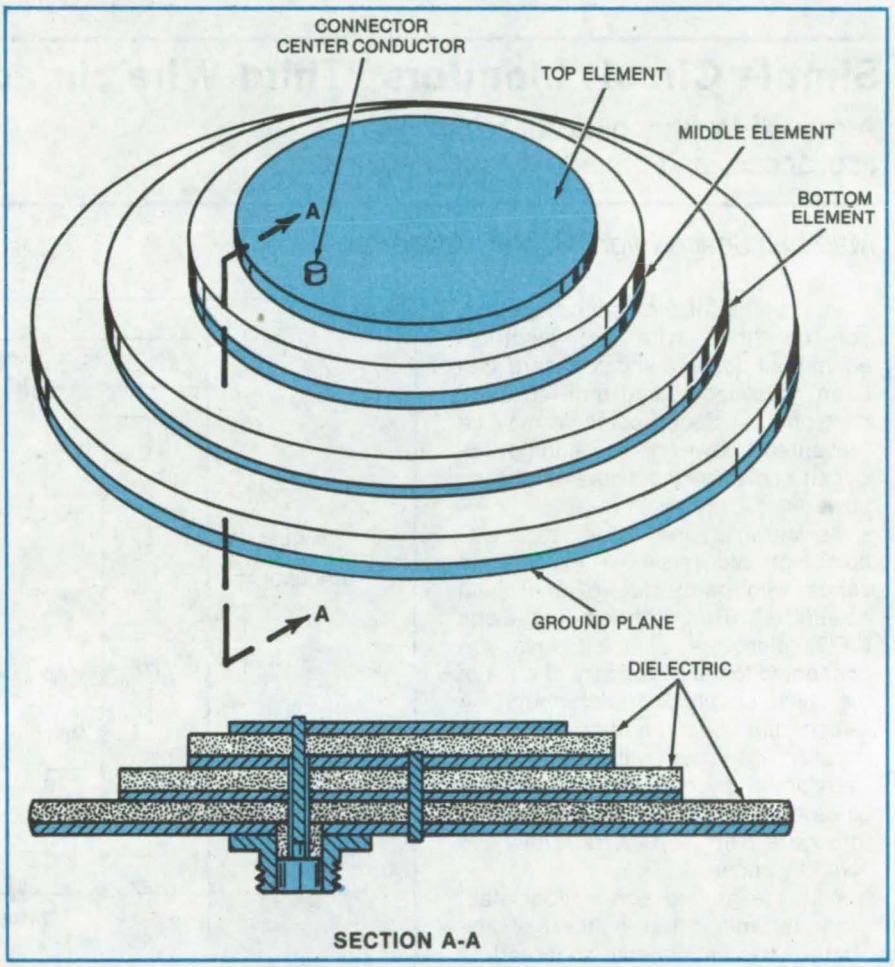

The Microstrip Construction is shown in these views of a three-element elliptical laminated antenna. Standard microstrip techniques, involving sequential removal of material from a stack of conductors and insulators, can be used to build it.

In the three-element antenna, the middle element is the ground plane for the top element, and the dielectric space is the electromagnetic cavity for the top element. At the same time, the top and middle elements are capacitively coupled. Thus, signals received by the middle element are coupled through the top element to the connector. Similarly, the bottom element is the ground plane for the middle element; and the signals it receives are capacitively coupled in turn to the middle element, to the top element, and to the connector. In the transmit mode, signals are fed through the connector to the top element and are capacitively fed to the lower elements.

The electric currents generated in the antenna elements are generally concentrated on their peripheries and are zero at their geometric centers. Consequently, no loss in signal strength or operating efficiency results from linking the lower elements at

(continued on next page)

their centers. In principle, any number of elements may be included, with all but the top element being electrically joined at their geometric centers to the ground plane. Moreover, if the sizes of the elements are close to each other in value, the individual frequency bands can be made to overlap, to yield a single broadband antenna.

This work was done by I-Ping Yu of Lockheed Electronics Co., Inc., for **Johnson Space Center.** *For further information, Circle 1 on the TSP Request Card.*

This invention is owned by NASA, and a patent application has been filed. Inquiries concerning nonexclusive or exclusive license for its commercial development should be addressed to the Patent Counsel, Johnson Space Center [see page A5]. *Refer to MSC-18334.*

Simple Circuit Monitors "Third Wire" in ac Lines

A ground-fault monitor for handtools, appliances, and other electrical equipment

Marshall Space Flight Center, Alabama

Interruption of the ground connection or "third wire" of electrical equipment poses a shock hazard that often goes undetected until an accident occurs. Such accidents may be prevented, however, by adding the circuit shown in the figure to the ac powerline.

As shown in the figure, a pair of optoelectronic relays is installed in series with each side of the main powerline. The light-emitting-diode (LED) elements of the relays are connected to the secondary circuits of the two coupling transformers. A silicon-controlled rectifier (SCR) is installed in series with each of the transformer primaries, and the SCR gates are coupled to the ground wire through a pair of 100K resistors and 1N4007 diodes.

With the ground connection intact (and assuming that neither of the "hot" wires is directly anchored to ground), each SCR gate will reach its trigger voltage once during each cycle. This will occur when the corresponding hot lead is below ground potential.

Each SCR will thus be "on" and will pass current through the corresponding transformer primary once during each cycle. The voltages thus induced in the transformer secondaries, after smoothing by the 500-μF capacitor, will keep the relays energized with a steady dc voltage.

Should the ground connection break, no current will flow through the 100K resistors, and the SCR's will not fire. This will deenergize the relays and open the main power connections.

This work was done by T. T. Kojima and D. E. Stuck of Rockwell International Corp. for **Marshall Space Flight Center.** *No further documentation is available.*
MFS-19457

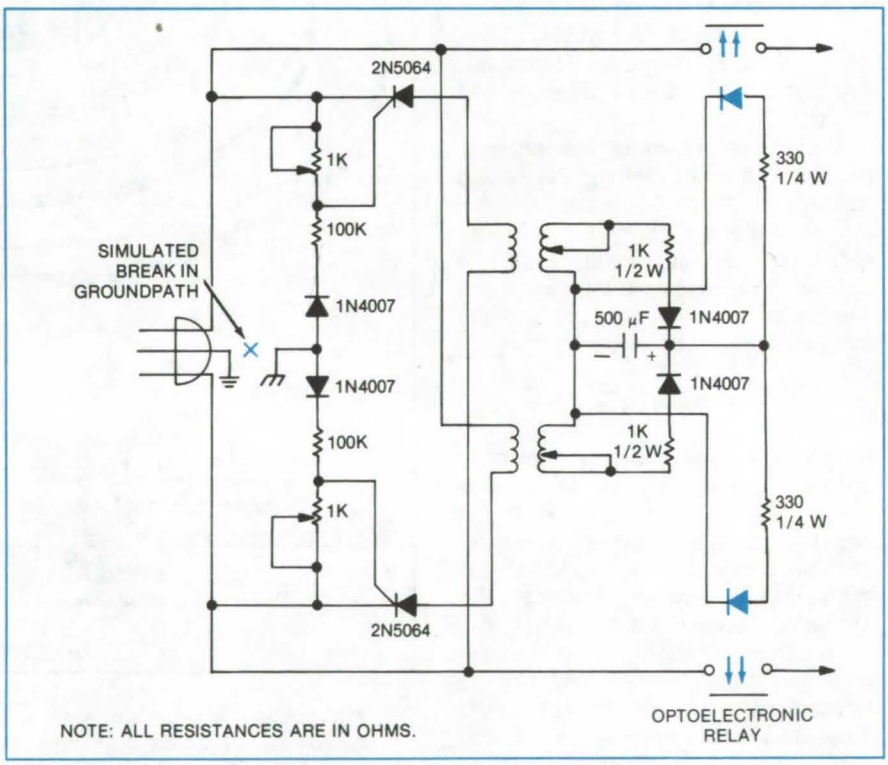

The **Ground-Fault Monitor,** originally developed to reduce shock hazard from an ultrasonic extensometer used to check bolt-tightening tension on the main engine of the Space Shuttle, includes optoelectronic relays in series with each of the main powerlines. The relays are closed unless the ground connection breaks or is disconnected. The variable resistors in the primary circuit trim the SCR trigger voltage.

Simple Buck/Boost Voltage Regulator

New circuit, with fewer components, operates more efficiently and reliably.

Goddard Space Flight Center, Greenbelt, Maryland

A new "buck/boost" voltage regulator requires fewer components than previous regulators of this type. It uses a single inductor/transformer combination to buck or boost the input voltage as it rises or falls, maintaining essentially-constant output voltage. The new regulator can handle input variations ranging from as low as one-half the output voltage to as high as the maximum rated voltage of the input transistor.

Using only one pulse-width modulator for both bucking and boosting, the regulator operates at high efficiency (90 percent in contrast to 80 percent for previous versions). In addition, the circuit subjects its switching transistors to a maximum voltage no greater than the input voltage or the output voltage, whichever is higher. These conservative operating conditions increase the lifetime of the transistors.

Potential uses for the regulator are in power sources for solar arrays, fuel cells, and thermionic generators. In a version designed for the 28-Vdc power supply aboard the Space Shuttle, the output is regulated to ±1 percent, for input voltages ranging from 21 to 35 volts.

The regulator (see figure) uses inductor L_2 and a capacitor C_2 for energy storage. C_2 keeps the output voltage constant over a complete pulse-width-modulation cycle, and L_2 maintains a net dc magnetic field. The combination of L_2 and transformer T_1, tapped as shown, provides the buck and boost voltages. The N_1 and N_2 windings of L_2 have an equal number of turns.

When switches (actually transistors) SW_1 and SW_2 are closed (conducting), power diodes D_1, D_2, and D_4 become reverse-biased, and current flows through winding N_1 of L_2 to the center tap of T_1. The current divides, half going through SW_2 to ground and half going through D_3 to the output capacitor C_2 and the load. Thus the inductor current is twice the current to C_2 and the load.

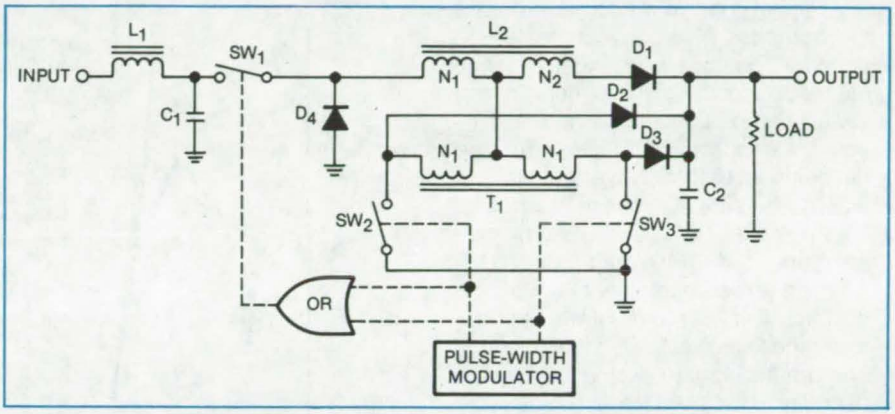

Component Count Is Reduced because the inductor/transformer combination L_2/T_1 and the pulse-width modulator do double duty, aiding both the boost and the buck functions. Switches SW_1, SW_2, and SW_3 are actually switching transistors.

However, when all switches are open (nonconducting), D_1 and D_4 become forward-biased, and D_2 and D_3 become reverse-biased. The inductor is connected to ground by D_4 and to the output by D_1. Then the inductor current is equal to one-half the original inductor current, and C_2 and the load receive the same amount of current as when SW_1 and SW_2 were closed.

The pulse-width modulator opens and closes SW_2 and SW_3 and, through an OR gate, opens and closes SW_1 in synchronism with SW_2 and SW_3. The pulse-width modulator adjusts the "on" time of the switches as necessary to regulate the output voltage.

Adding more turns to T_1 will extend the regulating range to a lower input voltage or give additional boost if a higher output voltage is needed. Adding more windings to L_2 and T_1 will provide auxiliary regulated voltages for other circuits that require isolation or voltage levels different from the output of the buck/boost voltage regulator. Overlap of the conduction period of the boost switches does not cause catastrophic failure, as it does in many conventional buck/boost regulators.

This work was done by John Paulkovich and G. Ernest Rodriguez of **Goddard Space Flight Center.** *For further information, Circle 2 on the TSP Request Card.*

This invention is owned by NASA, and a patent application has been filed. Inquiries concerning nonexclusive or exclusive license for its commercial development should be addressed to the Patent Counsel, Goddard Space Flight Center [see page A5]. *Refer to GSC-12360.*

Independent Synchronizer for Digital Decoders

Circuit maintains synchronization at low signal-to-noise ratios.

Lyndon B. Johnson Space Center, Houston, Texas

A digital logic circuit synchronizes the branches of a convolutional-code decoder, but operates independently of the decoder. The synchronizing circuit can be used with any convolutional decoder, regardless of the decoding algorithm. Nevertheless, the circuit is simple, consisting of a 15-stage shift register, three up/down counters, and a few logic gates.

In an experimental version of the synchronizer built for a Viterbi decoder using the Odenwalder 7 code, the sign bit from the input to each branch of the decoder is applied to a 15-bit shift register, and the modulo-2 sum is formed of the register 1st, 3d, 12th, 14th, and 15th stages. A second modulo-2 sum is formed of the contents of the 8th, 10th, and 11th stages, and a third modulo-2 sum is formed of the 5th and 6th stages.

The parity checks are used as an indicator of correct or incorrect node synchronization. If all three parity checks agree, an up/down counter is incremented. If the first two checks agree but the third disagrees, the same up/down counter is decremented. In any other situation, the counter is neither incremented nor decremented.

The process is repeated when the next bit is read into the shift register, but with a second up/down counter, and is repeated once more with the third input bit and a third up/down counter. The sequence starts again with the fourth input bit.

The up/down counter associated with the properly-framed code sequence is more likely than the other two counters to be augmented and less likely to be decremented when the polarity is correct. Correct node synchronization is thus determined by observing which of the counters first reaches predetermined positive and negative threshold values. Since a negative threshold crossing indicates an inverted decoder input, node synchronization and sign ambiguities are resolved simultaneously.

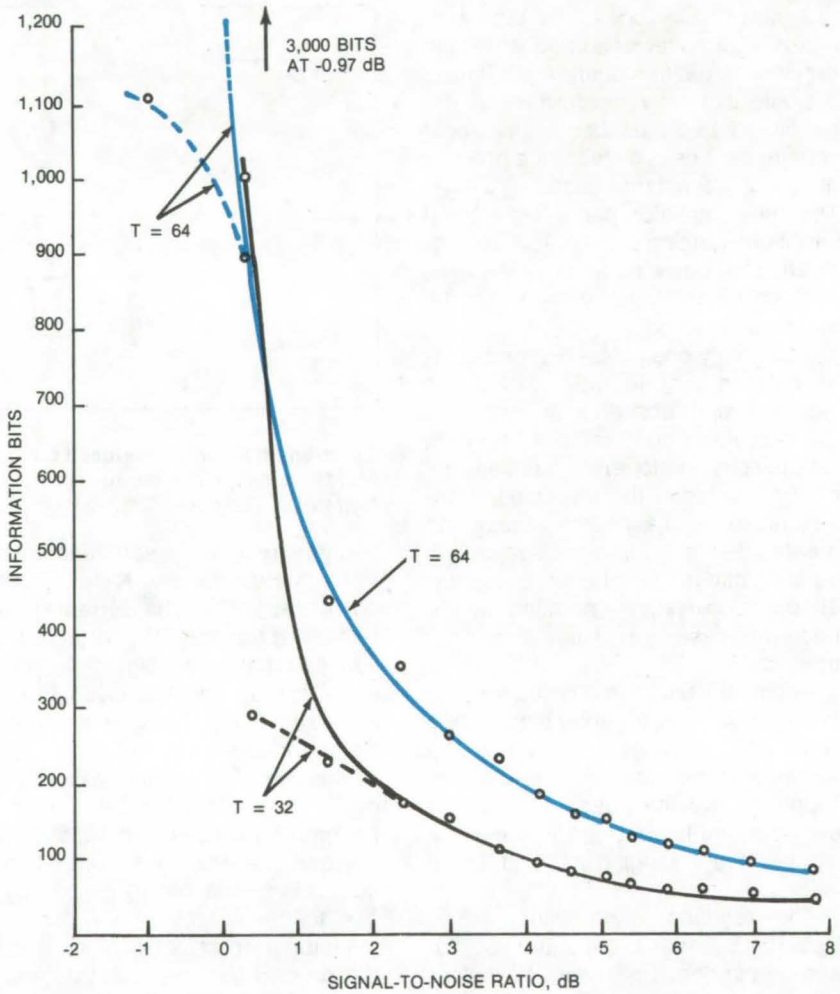

Plot of New Synchronizer Performance shows the average synchronization delay, in information bits, as a function of signal-to-noise ratio for up/down-counter thresholds of 32 (in black) and 64 (in color). The dashed lines indicate the synchronization delay to the first acceptance; the solid lines, the delay to the first correct acceptance. In both cases, the synchronizer was able to retain synchronization at all signal-to-noise ratios exceeding -3 dB.

In tests the synchronizer maintained synchronization at signal-to-noise ratios as low as -3 dB (see figure). In contrast, a conventional branch synchronizer (one based on comparisons of "unanimity" and "nonunanimity" counters) was limited to signal-to-noise ratios above 1.4 dB.

This work was done by Jack J. Stiffler of Raytheon Co. for **Johnson Space Center.** *For further information, Circle 3 on the TSP Request Card.*

MSC-16723

Multichannel Coincidence Circuit

Circuit records coincidences between pulses in two or more channels.

Langley Research Center, Hampton, Virginia

The digital circuit shown in the block diagram in Figure 1 looks for coincidences between pulses in a primary channel and those in one or more secondary channels. When two consecutive coincidence events are found, the circuit records the elapsed time (the interval time) between the leading edges of the pulses in the primary channel.

The coincidence timer has already been built for two channels of data pulses, and a three-channel version is being developed. It has been tested with both simulated and actual data sources. Originally used in a laser velocimeter to determine the time between velocity measurements, the circuit can also be used to measure time intervals in other instruments that receive data at irregular rates from two or more sources.

The timer considers a pulse of the primary channel to be coincident with one of the secondary channel pulses if both occur within a predetermined timespan or "aperture" (see Figure 2); the coincident pulses do not necessarily have to overlap as long as their leading edges are less than 1 aperture time apart.

As seen in the block diagram, the circuit is divided into three major functions:

- The *interval-time measurement subcircuit* contains binary counters, temporary data storage, and data output devices to generate a digital number related to the time between coincident pulses.
- The *measurement-control subcircuit* controls the operation of the counters, storage, and output devices.
- The *system-control and timing-sequence generator* oversees routine timing and control.

The measurement of the interval time is made from the leading edges of the pulses in the primary data channel. Since it cannot be known if the time measurement after one coincidence is valid until a second coincidence event is recorded (and this is not certain until the completion

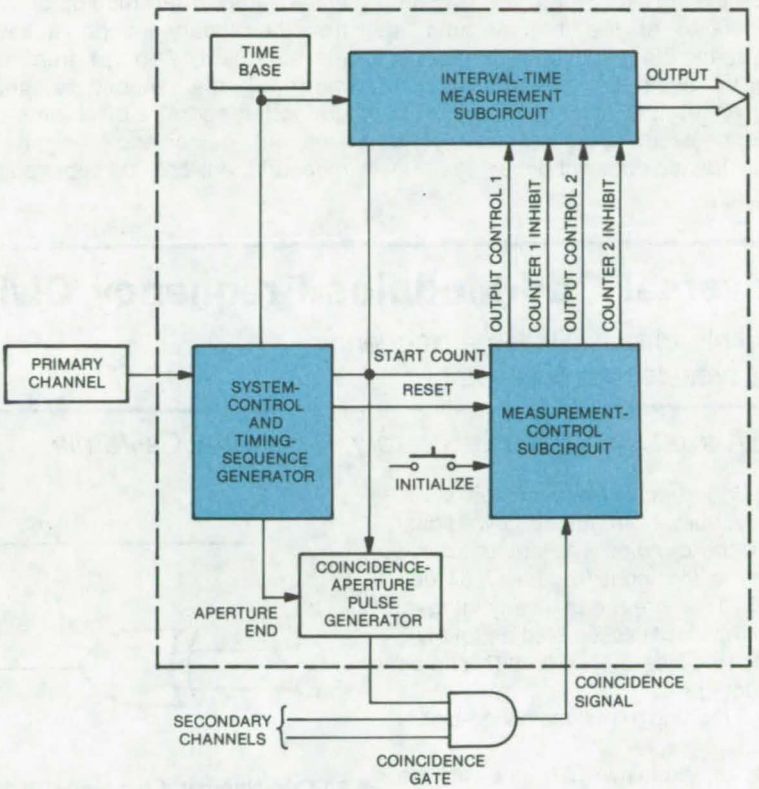

Figure 1. The **Coincidence Circuit** consists of three major blocks: Binary counters and latches are in the interval-time measurement subcircuit, the timing pulses originate in the measurement-control subcircuit, and routine timing is generated in the timing-sequence generator.

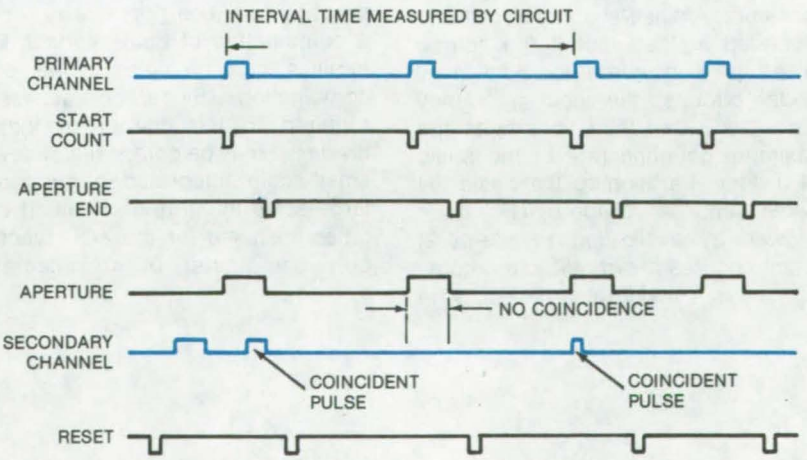

Figure 2. **Pulses From Two Channels** are "coincident" when they both fall within the same aperture period. Here, coincidence occurs in the first and third apertures. The "interval time" is thus the time between the leading edges of the first and third pulses in the primary channel.

of the aperture time for the second coincidence), two binary counters are required. While the counter making the current measurement continues its count until after the second coincidence aperture has ended, the second binary counter has already begun to measure the next interval. If a coincidence event is recorded, the leading-edge value of the interval time is stored, and the first counter is reset to zero to await a new input pulse. Meanwhile, the second counter is already measuring the next interval. If a coincidence does not occur, the first counter continues its measurement, and the second counter is reset.

A fixed series of pulses, consisting of start-count, aperture-end, and reset signals, is supplied to the coincidence-interval measurement subcircuit from the measurement-control subcircuit. The start-count pulse, generated immediately after receipt of a pulse from the primary channel, initiates the measurement. A pulse from one or more of the secondary channels during the aperture pulse time generates a coincidence signal. The measurement-control subcircuit continuously reads the count value on the active counter; when the coincidence signal is received, the count value that existed at the leading edge of the primary channel pulse is transferred to the output bus.

This work was done by James I. Clemmons, Jr., of **Langley Research Center.** *For further information, Circle 4 on the TSP Request Card.*

Inquiries concerning rights for the commercial use of this invention should be addressed to the Patent Counsel, Langley Research Center [see page A5]. Refer to LAR-12531.

Universal Odd-Modulus Frequency Divider

A simple circuit divides a frequency by a preselected odd number.

NASA's Jet Propulsion Laboratory, Pasadena, California

An odd-number frequency divider is quickly built from just a few digital integrated circuits. The output of the divider is the input frequency divided by 2N - 1, where N can be any integer.

The divider is assembled as follows:

- Select a divide-by-N circuit (N can be any integer).
- Add a flip-flop to make a divide-by-2N circuit.
- Add an exclusive-OR gate at the input.

The output frequency of the resulting circuit is $F_{out} = F_{in}/(2N - 1)$, where F_{in} is the input frequency (see figure).

The divider produces symmetrical output pulses and requires a symmetrical input. A pulse-shaping circuit can be added at the input if the source pulses are nonsymmetrical. As in all divider circuits, the input frequency must be less than one-half the maximum counting rate of the basic 2N divider. Partitioning the basic 2N divider into a divide-by-N circuit followed by a flip-flop (divide-by-2) circuit ensures a symmetrical output.

There is considerable flexibility in choosing the basic 2N divider. It can be assembled from binary, binary-coded-decimal, twisted-ring, or other counters; and it may be internally synchronous, use ripple carry, or use a combination of both. Various logic families can be used alone or in combination. Since no access is required to the interior of the 2N divider, it may be composed of several small-scale integrated circuits or a large-scale integrated circuit. If quad gates are used for the XOR function, only one-quarter of an integrated-circuit chip is needed.

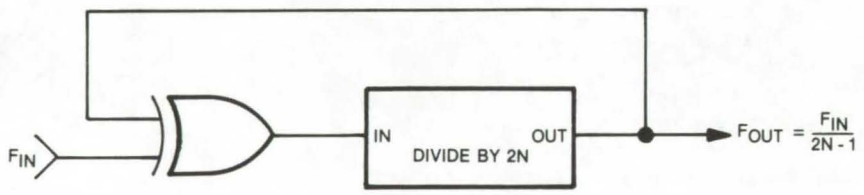

An Odd-Number Frequency Divider comprises an exclusive-OR gate and a 2N divider. The 2N divider consists of an N divider and a divide-by-2 flip-flop.

This work was done by Alexander Engel of Caltech for **NASA's Jet Propulsion Laboratory.** *For further information, Circle 5 on the TSP Request Card.*

This invention has been patented by NASA [U.S. Patent No. 3,906,374]. Inquiries concerning nonexclusive or exclusive license for its commercial development should be addressed to the Patent Counsel, NASA Resident Legal Office-JPL [see page A5]. Refer to NPO-13426.

Detecting Short Circuits During Assembly

Shorts between bus bars can be identified and eliminated as soon as they occur.

Ames Research Center, Moffett Field, California

A short-circuit detector indicates when and where a short occurs while electronic equipment is being wired. The detector is intended for use on power and ground bus bars (Figure 1) on computers and similar complex hardware. Ordinarily the bus bars are tested for shorts only after leads have been attached. Since the bus bars often have hundreds or even thousands of terminals, testing them for shorts — and a few shorts are bound to occur no matter how careful the wirer is — can be tedious and time consuming. Moreover, the equipment can be damaged if it is energized before the shorts are corrected.

The new detector sounds a buzzer to inform the wirer that a terminal is short-circuited immediately after a wire connection is made. The detector also shows the wirer, by illuminating light-emitting diodes (LED's), which bus bar conducting planes are shorted. It is then easy to make a correction by disconnecting and rewiring the affected terminals.

The short-circuit detector (Figure 2) is attached to the bus-bar assembly by a connector containing sockets for plugs on each of the bus bars to be tested. An oscillator in the detector feeds a train of positive pulses to a ring counter, and the ring counter in turn produces a corresponding positive pulse on each of its output leads (1 through n) in sequence. The output pulses bias transistors 1 through n and LED's 1 through n so that they briefly become conductive in sequence. If the oscillator frequency is 1 hertz, the LED's glow in sequence for 0.5 second.

The emitters of the transistors are connected to the pins on the bus bars. Thus, each transistor turns on when the corresponding bus bar is energized. Potentiometer R_1 is adjusted so that it produces a reference voltage that is slightly greater then the voltage across resistor R_2. R_1 and R_2 connect to separate input terminals on a comparator.

(continued on next page)

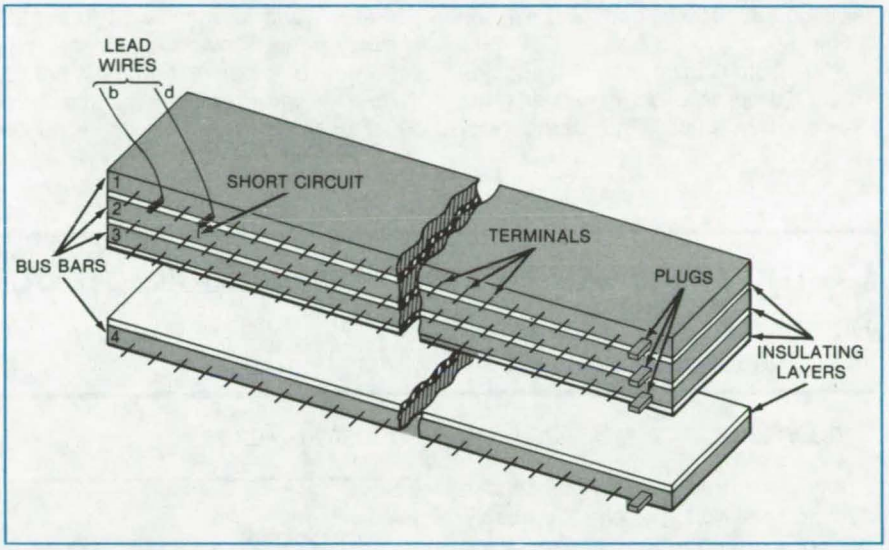

Figure 1. A **Bus-Bar Assembly** consists of conductive strips separated by sheets of insulation. Operators attach wires to terminal pins on the strips. Here, a wire wrapped around terminal d on bus bar 1 touches bus bar 2 and therefore short-circuits the two bus bars.

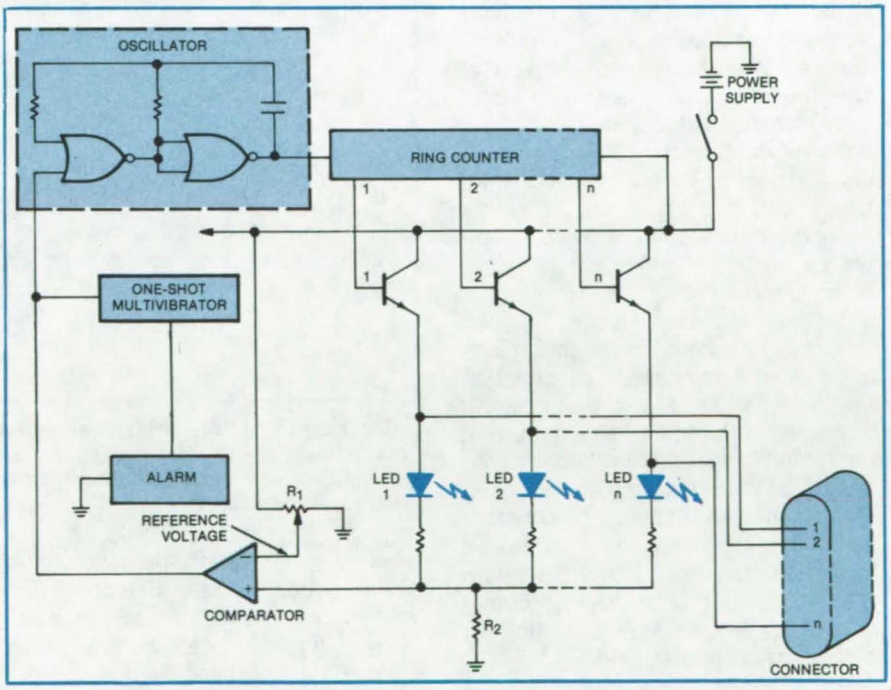

Figure 2. **Short-Circuit Detector** consists basically of a scanner (oscillator plus ring counter) that sequentially energizes a series of light-emitting diodes (LED's) and bus bars.

The detector continuously scans the bus bars until a short circuit occurs. For example, if a wire on one terminal of bus bar 1 touches bus bar 2 (as shown in Figure 1), bus bars 1 and 2 will be short-circuited. When this happens, the anode of LED 2 is connected to the anode of LED 1. Consequently, when the next pulse turns on transistor 1, both LED's 1 and 2 light up.

With both LED's conducting, the voltage drop across R_2 exceeds the reference voltage. The comparator then generates a positive output that stops the oscillator and triggers the one-shot multivibrator, which activates the alarm buzzer. With no pulses from the oscillator, the ring counter keeps transistor 1 on and LED's 1 and 2 as well.

As soon as the buzzer sounds, the wirer knows that a short has been created, and a glance at the LED display panel shows that the short is between bus bar 1 and bus bar 2. When the wirer removes the short, the buzzer stops, and the ring counter continues to scan.

This work was done by Gorden J. Deboo of **Ames Research Center.** *For further information, Circle 6 on the TSP Request Card.*

This invention is owned by NASA, and a patent application has been filed. Inquiries concerning nonexclusive or exclusive license for its commercial development should be addressed to the Patent Counsel, Ames Research Center *[see page A5].* *Refer to ARC-11116.*

Continuous Control of Phase-Locked-Loop Bandwidth

An FET circuit smooths the transition from wideband to narrow band.

Lyndon B. Johnson Space Center, Houston, Texas

When inserted between the phase detector and voltage-controlled oscillator of a second-order phase-locked loop, the filter circuit shown in the figure allows continuous electronic control of the loop bandwidth. Change from the wide bandwidth required for signal acquisition to the relatively narrow bandwidth needed for tracking occurs smoothly, without steps that can cause transients and loop instability. Already tested successfully in a delay-locked pseudonoise-code tracking loop needed for the Space Shuttle, the circuit can be used in other second-order loops. The basic principle can also be extended to higher order loops.

A field-effect transistor (FET), used as a voltage-controlled variable resistance, is the principal component of the new circuit. Since the inherent asymmetry of the FET voltage/current characteristic would introduce a voltage offset when tracking an ac signal, the circuit uses feedback to compensate for I/V nonlinearity. Detailed circuit analysis shows that the return of exactly one-half of the FET output voltage to the gate is optimum for symmetrizing the I/V curve.

An analysis of the behavior of a "perfect" second-order phase-locked loop containing the new circuit shows that the loop bandwidth is given by

$$B = \frac{K_\phi K_V (R_1 + R_2)}{4R_2} + \frac{1}{4(R_1 + R_2)C}$$

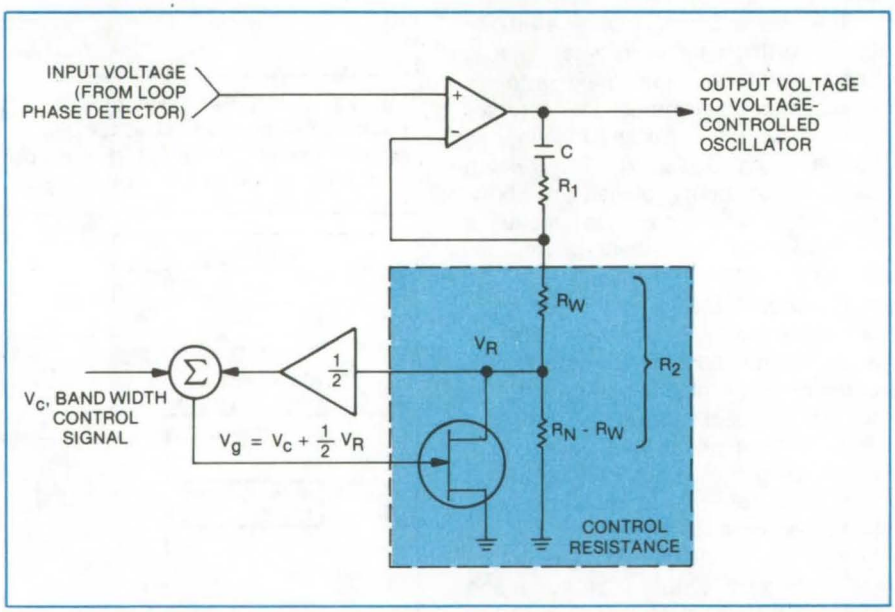

A Tracking-Loop Filter With Continuous Bandwidth Control is made by using an FET as a voltage-controlled variable resistance. Decrease of the control voltage V_C turns off the FET and increases the effective value of R_2 from R_W to R_N, narrowing the loop noise bandwidth.

where K_ϕ and K_V are the sensitivities of the loop phase detector and voltage-controlled oscillator, respectively. Thus, R_2 can be varied to change the loop bandwidth.

For the circuit shown, the control voltage is held sufficiently positive to insure that the FET is on and $R_2 = R_W$ until the loop is locked. When a signal is acquired, V_C is decreased until the FET is switched off and R_2 equals R_N. A transition period of 40 milliseconds was used for the circuit tested for the Shuttle; the bandwidth was varied between 320 Hz for acquisition and 20 Hz for tracking.

This work was done by Gary W. Motal and James C. Vanelli of Lockheed Electronics Co., Inc., for **Johnson Space Center.** *For further information, Circle 7 on the TSP Request Card.*

MSC-16684

Photocapacitive Image Converter

Solid-state converters yield high sensitivity at high information-retrieval speed.

Langley Research Center, Hampton, Virginia

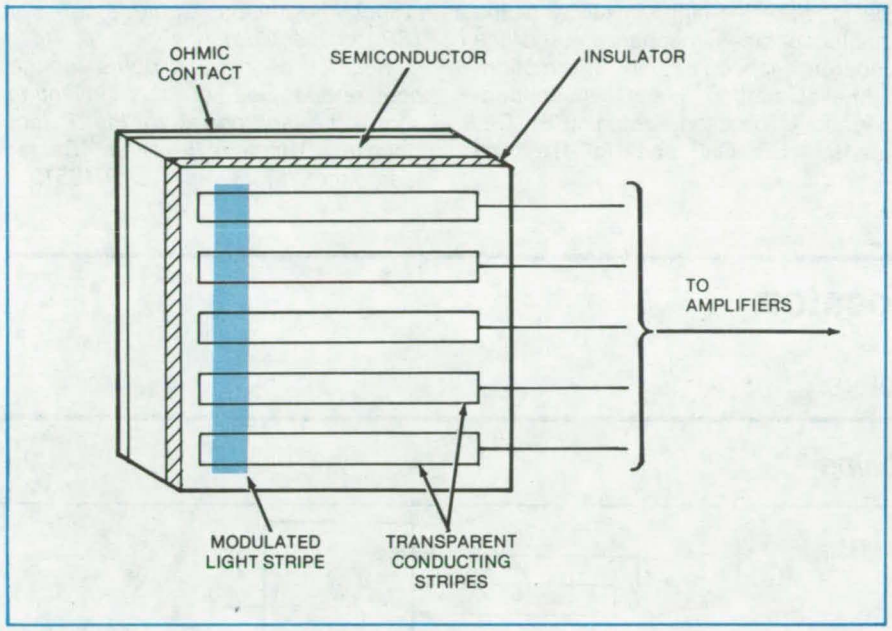

Figure 1. **CAPICON Photocapacitive Image Converter** is an insulated semiconductor structure with a depletion layer over which transparent conducting stripes are placed. An image is focused on the surface, and a modulated stripe of light is used to read out data. As the readout light stripe sweeps across the device, the photocapacitively generated voltage at each light-stripe/conducting-stripe intersection relates to the intensity of the focused image.

A sensitive, fast, solid-state imaging converter has been suggested that functions in a photocapacitive mode. Two configurations of this device have been proposed. The CAPICON version (Figure 1) reads an entire scene by sweeping a modulated light stripe across a surface of transparent conducting stripes. The PIC version (Figure 2) reads a scene by imaging it on a grid pattern of transparent conducting stripes.

The CAPICON is constructed by applying a back ohmic contact to a semiconductor wafer, applying a thin insulating layer on the front surface, and then depositing the transparent conducting stripes on the insulating layer. The ohmic contact material is chosen so that the semiconductor is in depletion when no bias is applied. An image of the scene being viewed is focused on the front surface. In regions where the light is brighter, the depletion layer is thinned more than in darker regions. A stripe of modulated light, which is perpendicular to the conducting stripes, is next focused on the surface of the device. This causes modulated voltage to be generated by the photocapacitive effect on each conducting stripe; the voltage is proportional to the intensity of the light in the scene at the intersection of the conducting stripe and the modulated light stripe. The entire scene can be read by sweeping the modulated stripe across the surface of the device. This arrangement permits the information from the set of conducting stripes to be read in parallel, thus increasing the data rate compared to a system in which a spot is swept over the surface area. The minimum width of the stripes is chosen to give the required resolution. Minimum separation between stripes is chosen so that crosstalk between them is negligible. This requires their separation to be larger than the depletion layer thickness, typically a few microns. Thus, the ultimate resolution is a few microns.

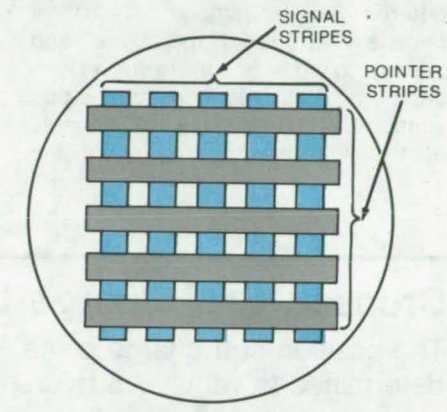

Figure 2. **PIC Photocapacitive Image Converter** is a grid of pointer and signal stripes (transparent conductors) on a semiconductor structure with a depletion layer. The focused image to be read is chopped at one frequency, and each pointer stripe is connected to a current source at a unique frequency. The voltage from each signal stripe can be analyzed to determine the intensity of the focused image (photocapacitively generated voltage) at each pointer/signal stripe intersection.

The PIC consists of a semiconductor wafer with a back ohmic contact and two layers of transparent conducting stripes separated by an insulator on the front. The two layers of stripes are fabricated in a grid pattern. A light chopper is used to modulate the focused light falling on

(continued on next page)

the image converter so that the thickness of the semiconductor depletion layer is modulated at the chopper frequency. One set of stripes, the pointer stripes, is used to sense the intensity of the voltage signal generated at a given spot on the signal stripe. Current generators of different frequencies are connected to the different pointer stripes so that a nonlinear mixing of the signal and pointer voltages occurs in the photocapacitor. This produces signal-stripe voltages with frequency components at the sum and difference of the modulating and current-generating frequencies. Each signal stripe is connected to a processing circuit that measures the amplitude of the Fourier component of the signal at the frequency equal to the sum of the two frequencies. In this way the image pattern on each stripe is determined.

The main advantages of these devices are the high sensitivity of the photocapacitive mechanism and the inherent speed of the information-retrieval method. Many semiconductors could be used, including Si, Ge, GaAs, InSb, GaP and HgCdTe. The different materials will have different spectral regions where they are most sensitive. The fabrication of both devices should be relatively simple and inexpensive.

This work was done by William E. Miller of **Langley Research Center** *and Arden Sher and Y. H. Tsuo of the College of William and Mary. For further information, Circle 8 on the TSP Request Card.*

Inquiries concerning rights for the commercial use of this invention should be addressed to the Patent Counsel, Langley Research Center [see page A5]. Refer to LAR-12513.

Crossed-Grid Charge Locator

The position of a charge pulse is determined to within 6.5 micrometers.

Marshall Space Flight Center, Alabama

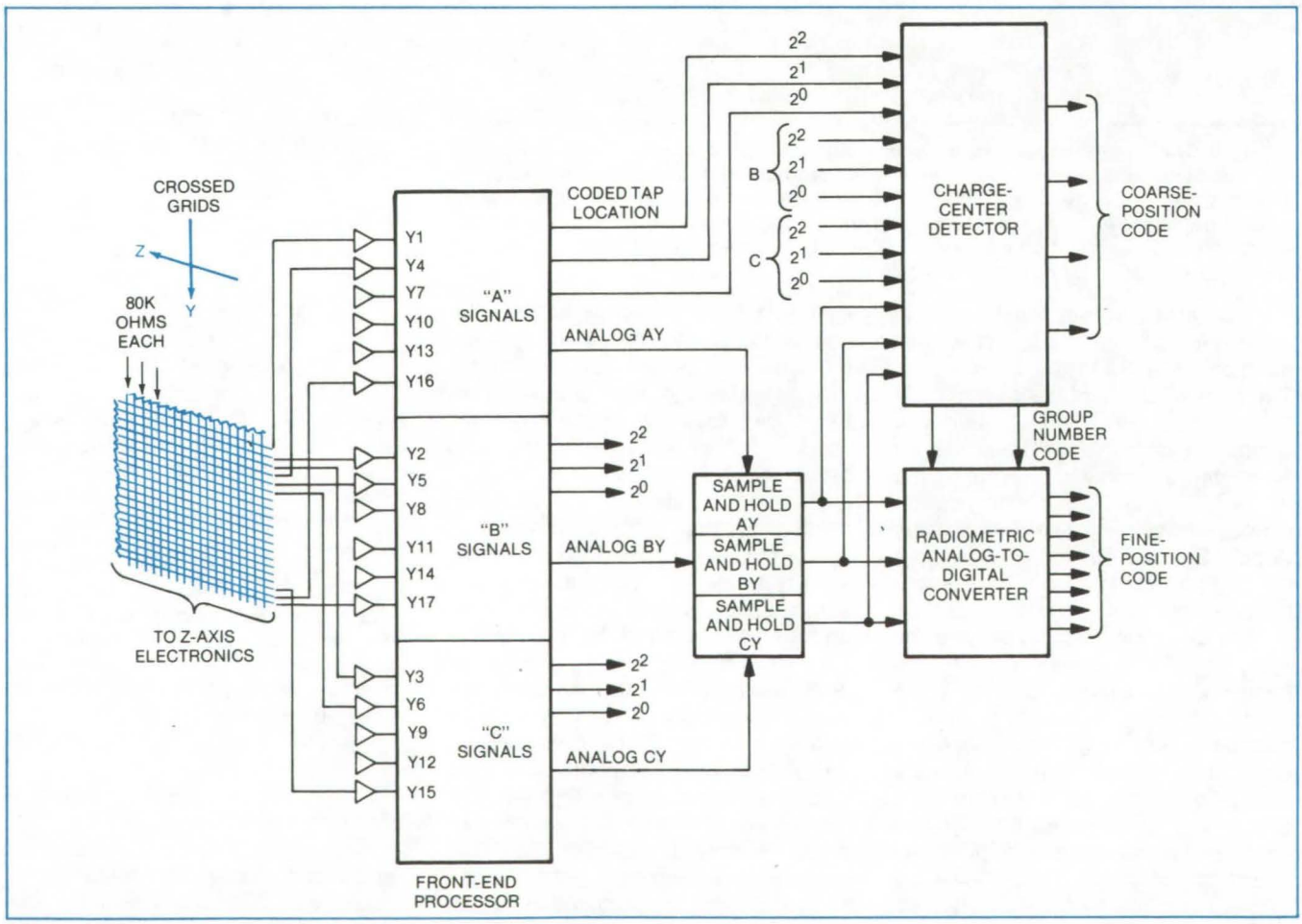

The **Crossed Grids** of the detector are tapped at 17 of the 129 wires in each grid. The wires in the vicinity of a charge cloud develop voltages that are processed, using priority encoders, to develop coarse- and fine-position codes. The coarse code is the 4-bit location of the tap nearest the center of the charge; the fine code is obtained by interpolating the signal strengths between taps.

A digital processor at the output of a crossed grid of closely spaced wires determines the position of a cloud of electrons to within 6.5 micrometers. The system is part of a high-resolution imager in the focal plane of an X-ray telescope. In this application it locates the center of the electron pulse released by a microchannel-plate ampifier in response to an incoming X-ray photon. Other possible applications of the detector are in electron microscopes and closed-circuit television.

The detector grid consists of 129 parallel wires for each axis, spaced 0.2 millimeters apart. A block diagram of the detector and the processing logic for one axis is shown in the figure. Each wire is connected to the adjacent wire by an 80-k Ω resistor. The 17 taps on each grid (at wires 1, 9, 17, 25, . . . and 129) are connected to 17 low-input-impedance preamplifiers.

A photon strikes a pair of microchannel plates in front of the grid, releasing a small group of electrons that is multiplied until it contains about 3×10^7 electrons. The grid bias is adjusted so that roughly 50 percent of the charge reaches the second grid. When this cloud of electrons arrives in the vicinity of the grid, it charges the wires in that region and is absorbed in the inputs of the nearest preamplifiers.

The processing circuit eliminates ambiguities that can arise when a large cloud, centered on a tapped wire, develops appreciable signals in the two adjacent preamplifiers. The set of 17 taps is divided into three subsets, A, B, and C, the signals of which are processed separately in the front-end processor. The five or six signals of each of these sets are summed to develop analog pulses AY, BY, and CY. The signals in each set are also sent to level detectors in the front-end processor. The outputs of each set of level detectors connect to latches, which are followed by two eight-input priority encoders.

The priority encoders are wired in reverse order so that for example encoder 1 gets signals 1, 2, 3, . . . 6 on inputs 1, 2, 3, . . . 6, while encoder 2 gets the same signals on inputs 6, 5, 4, . . . 1. Since the highest number of the input at which a signal appears in the 3-bit output of each priority encoder, the two encoders give complementary codes (e.g., 0 and 6, 1 and 5, 2 and 4, or 3 and 3) for a single signal. Noncomplementary codes are generated for multiple signals.

Single signals are recognized by their complementary codes and are classified as "valid" events, suitable for further processing, while multiple signals (noncomplementary codes) are classified as "invalid" events. The outputs from subsets A, B, and C are combined so that a valid event can be negated by an invalid event. The 3-bit-coded tap location of a valid event from each set is sent to the charge-center detector.

The three analog signals representing the sum of the charges of all elements of each set are sent through sample-and-hold circuits that maintain the signal level for the rest of the processing cycle. The outputs of these circuits are also sent to the charge-center detector, where three comparators determine the set of taps with the largest analog signal. This information, together with the 3-bit tap location, is used to develop a 4-bit "coarse-position" code that identifies the tap closest to the center of the charge cloud.

The charge-center detector also develops a 2-bit group-number code to be sent to a ratiometric analog-to-digital converter that interpolates the analog signals and determines the "fine position" of the charge center. The arithmetic for the algorithm is done by operational amplifiers.

This work was done by David C. Harrison of American Science and Engineering, Inc., for **Marshall Space Flight Center.** *No further documentation is available.*

Inquiries concerning rights for the commercial use of this invention should be addressed to the Patent Counsel, Marshall Space Flight Center [*see page A5*]. *Refer to MFS-25170.*

Books and Reports

These reports, studies, and handbooks are available from NASA as Technical Support Packages (TSP's) when a Request Card number is cited; otherwise they are available from the National Technical Information Service.

Semiconductor Step-Stress Testing

An extensive test program documents the behavior of discrete diodes and transistors under power and temperature overstress.

The behavior of discrete semiconductor components under temperature and power stress above the manufacturer's ratings is the subject of an extensive test program now underway for Marshall Space Flight Center. Twenty reports documenting some of the results of this program were described in the previous issue of *NASA Tech Briefs*. [See "Semiconductor Step-Stress Testing" (MFS-25329) on page 474 of Vol. 4, No. 4.] Described below are 19 additional reports in this series.

Details of the test program are given in the article cited above. Briefly, the effects of severe overstress on commercially available devices, including bipolar transistors, diodes, and field-effect transistors (FET's), were determined from measurements on samples obtained from various manufacturers. In broad outline, the test procedures are the same for all components. They differ in particulars, such as electrical parameters measured, for the different kinds of devices tested.

For the power-stress tests, a sample population is stressed at levels that increase in steps from half maximum rated power (MRP) to 1.75 MRP. The temperature-stress measurements are carried out in two groups. In the first group, the measurements are made in 160-hour steps starting at 75° C and increasing

(continued on next page)

in 25° C increments to 300° C. In the other group, the steps are for 16 hours duration each, commencing at 150° C and increasing in 25° C intervals to 300° C.

For all units, data are presented as graphs showing cumulative failures (in percent) for the temperature-stress group and as tables showing how the electrical parameters changed during each test phase. An analysis of the test results and the reasons for failures are given in the concluding sections of the reports. Throughout the reports, and in the following articles, the power-stress sample population is referred to as "Group I," the first temperature-stress population is "Group II," and the second temperature-stress population is "Group III."

Each of the reports described below titled "Step Stress Testing Program," presents the test procedures, results, and conclusions for one tested device. Persons wishing information about a particular unit can order the report for that device by circling the appropriate number on the TSP Request Card at the back of this issue of NASA Tech Briefs.

[*These reports were prepared to document work supported by the United States Government. They are intended solely as a vehicle for the presentation of test results and are not to be construed as an endorsement or a criticism of the companies mentioned or of their products.*]

JANTX1N2970B Zener Diode

The effects of power and temperature overstress

The testing proved strenuous for sample lots manufactured by General Semiconductor and Siemens. The Group I and Group II tests for both manufacturers were stopped due to excessive failures, although the General Semiconductor diodes underwent more hours of testings in each case.

In Group II, the predominant failure mode was detachment of the cathode lead. Failure analysis revealed that all analyzed samples failed due to the effects of excess heat. The separation of the tubulations was caused by extreme heat acting on the glass and the metal tube.

While the dice of the General Semiconductor devices were destroyed by alloying with the connecting metal, the Siemens dice were still functional and were within endpoint limits when tested by external probing of the die-lidded samples. Possibly, this difference is due to deeper junctions on the Siemens parts.

Since the General Semiconductor units had only one failure under Group III testing, only the Siemens lot underwent failure analysis. The analyzed samples were subjected to heat and power beyond their stress limits, which caused destructive damage to their internal structures. The protective junction coating charred, leading to excess leakage. The die and internal lead-attach metal melted, and the second nickel plate used on the dice peeled and separated with the connecting bonding metal. In addition, all the dice were shorted (probably due to "thermal runaway"), and two of the devices had cracks or chipouts. The die fell out of one device when it was touched.

This work was done by the Special Products Division of DCA Reliability Laboratory for **Marshall Space Flight Center**. *To obtain a copy of the report, Circle 9 on the TSP Request Card.*
MFS-25260

JANTX1N2989B Zener Diode

The effects of power and temperature overstress

Zener diodes manufactured by Siemens and General Semiconductor were tested. All three stress groups proved detrimental to both sample lots. In Group I and Group III testing, the devices were electronically intact but damaged mechanically. Electrical readings were obtained by probing the die. The bonded die connections were damaged and the cathode detached when the part was opened. This suggests that the diodes failed due to excessive temperature.

The failure mode in the Group II testing for both manufacturers was "visual catastrophic." The failed parts had cracked glass and detached cathodes caused by the excessive temperature, which also resulted in the disconnection of the internal wire lead.

This work was done by the Special Products Division of DCA Reliability Laboratory for **Marshall Space Flight Center**. *To obtain a copy of the report, Circle 10 on the TSP Request Card.*
MFS-25261

JANTX1N3016B Zener Diode

The effects of power and temperature overstress

Sample lots from Motorola and Siemens were tested. Both experienced large failure rates throughout all three stress tests. The failure mode common to all three groups was the I_R maximum-limit failure and the Zener-breakdown-voltage (B_V) maximum-limit failure. In some cases the I_R failures were shorted devices, and the B_V failures were opened devices.

In Group I testing, the diodes from both sample lots failed due to the thermal effects of excess power. In some cases the internal lead-bonding metal melted and flowed up the silver lead wire, which in turn disconnected from the die. Other devices failed due to shorting of the junction, probably caused by alloying with the melted metal at elevated temperatures.

Many devices in the Group II and Group III testing failed due to overheating. In some cases, probe testing of the dice after opening the packages showed shorts. The most probable cause of the shorts is alloying of the molten die metal into the silicon.

This work was done by the Special Products Division of DCA Reliability Laboratory for **Marshall Space Flight Center**. *To obtain a copy of the report, Circle 11 on the TSP Request Card.*
MFS-25262

JANTX1N3031B Zener Diode

The effects of power and temperature overstress

Motorola and Siemens diodes were tested. The Motorola lot experienced one failure in Group I testing and no failures in Group III. Both the Siemens and Motorola diodes failed due to exposure to excessive temperatures, which, in many cases, melted the metal on the die connections.

The electrical test results suggest that the long dwell time of the molten metal caused the metal to alloy with the silicon dice, thus shorting out their junctions. Some of the Siemens devices also had electrical leakage of the glass in the glass-to-metal seal. The glass was conductive when probed either internally or externally, with the internal conductivity being somewhat greater.

This work was done by the Special Products Division of DCA Reliability Laboratory for **Marshall Space Flight Center**. *To obtain a copy of the report, Circle 12 on the TSP Request Card.*
MFS-25263

JANTX1N5622 Diode

The effects of power and temperature overstress

All three test groups were detrimental to diodes from Semtech and Micro Semiconductor. In each case, testing was halted before the process was completed.

The failure mode of the three Semtech lots was due to excessive reverse bias leakage. Failure analysis revealed this to be due to excessive conductivity in the external paint. When the conductivity was interrupted by sanding the paint, the reverse leakage fell to acceptable levels.

The Micro Semiconductor Group I diodes also had a failure mode of excessive I_R leakage. Failure analysis showed that this was caused by damaged silicon induced by the stress test. The analyzed diodes still showed a characteristic forward breakdown curve, indicating that they were not totally destroyed, but had resistive pathways (damage sites) in parallel with the junctions.

The Micro Semiconductor diode failure modes in Group II and Group III testing were the loss of leads due to the melting of connecting metal and cracked and broken glass. The excessive glass breakage is due to residual glass strain, which was not annealed out. The strain can be seen with polarized light.

This work was done by the Special Products Division of DCA Reliability Laboratory for **Marshall Space Flight Center**. *To obtain a copy of the report, Circle 13 on the TSP Request Card.*
MFS-25280

JANTX1N5623 Switching Diode

The effects of power and temperature overstress

The three Semtech lots produced two catastrophic failures. The testing of each Micro Semiconductor lot had to be stopped because the 50-percent-failures limit was reached.

Since both Semtech failures were due to excessive reverse-leakage current, only one diode underwent failure analysis. The analysis showed that the reverse-leakage-current failure was due to surface contamination, which was driven out of the glass under the high temperature and bias of the step-stress test.

The Micro Semiconductor diodes failed because of detaching leads. During Group I testing, one diode cracked in half. Failure analysis on this group showed that the glass of the analyzed diodes cracked due to the high junction temperatures reached in the stress testing. The leads fell off where the lead-bonding material exceeded its melting temperature.

The Group II diodes that were analyzed met all the specified limits for reverse-leakage current. Those that could be tested for V_F met the limit. It was noticed that the diodes that were missing paint were quite sensitive to light, which caused a large increase in the leakage measurement.

This work was done by the Special Products Division of DCA Reliability Laboratory for **Marshall Space Flight Center**. *To obtain a copy of the report, Circle 14 on the TSP Request Card.*
MFS-25281

JANTX2N2060 Dual Transistor

The effects of power and temperature overstress

The tested units were manufactured by Raytheon and Motorola. The Motorola sample lot showed signs of weakness in Group I testing; the Raytheon lot lost the majority of its devices in Group II.

The Motorola units in Group I experienced a decline in h_{FE}, while the collector/base leakages remained within specification limits. Such a loss of h_{FE}, without any evidence of surface leakage or low breakdown voltage, suggests a change in emitter efficiency. The migration of gold or other impurities possibly continued under high-power operation with consequent loss of h_{FE}.

All of the failures in Group II testing for Raytheon experienced some marked loss of h_{FE}. There is no significant bulk or surface leakage on these parts. This implies that the h_{FE} falloff is due only to a loss of emitter efficiency. The loss of injection efficiency, in turn, is due to the migration of gold and intermetallics under the influence of heat and bias, with a consequent loss of bulk silicon lifetime.

This work was done by the Special Products Division of DCA Reliability Laboratory for **Marshall Space Flight Center**. *To obtain a copy of the report, Circle 15 on the TSP Request Card.*
MFS-25251

JANTX2N2219A Dual Transistor

The effects of power and temperature overstress

These tested units were manufactured by Texas Instruments and National Semiconductor. In Group I testing, the Texas Instruments sample lot developed two catastrophic failures in 2,500 hours of testing; the National Semiconductor lot reached the 50-percent-failures limit 450 hours before the end of the testing.

The Group II testing failure analysis discovered that many Texas Instruments parts had clumps of silicon scattered over the dice. Gold/aluminum intermetallic contamination could also be seen on many of the units. The National Semiconductor parts showed no consistent failure mode, although, like the Texas Instruments sample lot, many of the National Semiconductor parts showed signs of gold/aluminum intermetallic contamination.

This work was done by the Special Products Division of DCA Reliability Laboratory for **Marshall Space Flight Center**. *To obtain a copy of the report, Circle 16 on the TSP Request Card.*
MFS-25252

JANTX2N2369A Transistor

The effects of power and temperature overstress

National Semiconductor and Raytheon transistors suffered a loss of gain, while generally continuing to maintain good junction quality with low leakage. A loss of emitter efficiency is the probable cause of the decline in gain. The loss of emitter efficiency is in turn due to the migration of gold and possibly other impurities, resulting in a loss of minority-carrier lifetime. In some cases the migration proceeded further, so that the junctions became excessively leaky, and all of the gain was lost.

Contaminant films were seen on the dice and wires of some of the devices of both manufacturers, but the nature and source were not determined. However, the material was not easily removed by water or alcohol. The rise of emitter forward voltage (VB_{EO}) in some devices, as compared to the collector forward drop, confirmed the rise in silicon resistivity.

This work was done by the Special Products Division of DCA Reliability Laboratory for **Marshall Space Flight Center**. *To obtain a copy of the report, Circle 17 on the TSP Request Card. MFS-25254*

JANTX2N2432A Transistor

The effects of power and temperature overstress

Crystalonics and Texas Instruments were the manufacturers of these units. The Crystalonics sample lot showed no catastrophic failures in Group I. The transistors from Texas Instruments experienced six catastrophic failures toward the end of the testing. The durability of the Crystalonics lot became more apparent in the Group II (temperature-stress) testing. Although the Crystalonics lot experienced a greater total number of catastrophic failures, it was able to complete the entire Group II testing.

The Texas Instruments lot had to be stopped at the +225° C temperature step with a total of eight catastrophic failures. The majority of these were h_{FE} failures. This could indicate a change in emitter injection efficiency due to a diffusion of gold into the base under heat and bias over many hours.

In Group III, the Texas Instruments lot had 10 failures, and the Crystalonics lot had 8. Failure analysis showed that many of the failures developed weak emitter/base junctions. The high temperatures of the stress tests liberated sufficient contaminant within the devices so that both sample lots exhibited base inversions. The formation of gold/silicon intermetallics probably expedited the migration of contaminants by chemical attack on the oxide near the junctions.

This work was done by the Special Products Division of DCA Reliability Laboratory for **Marshall Space Flight Center**. *To obtain a copy of the report, Circle 18 on the TSP Request Card. MFS-25255*

JANTX2N2484 Transistor

The effects of power and temperature overstress

Transistors manufactured by Raytheon had no failures in Group I; a Teledyne sample lot suffered only one failure during Group I testing.

In the Group II (temperature-stress) process, both sample lots had to be stopped at the +250° C step, 1,280 hours into testing. The Raytheon sample lot showed 9 out of 10 failures at the +250° C step of the process. The Teledyne lot showed a more even distribution of failures starting from the +200° C step, through the +250° C step, where (like the Raytheon lot) the job was stopped because the reject rate exceeded 50 percent of the sample lot.

Both lots develop aluminum/gold intermetallic formations ("purple plague") at the +250° C step. This could possibly be caused by the high temperature stress. The Raytheon samples all suffer from excess leakage, which can reasonably be ascribed to the movement of impurities, resulting from excess die temperature. On the Teledyne samples, the gold flowed away from the wires into the aluminum. This extreme attack on the gold may be due to an unusually high proportion of silicon doping in the aluminum metalization.

The Raytheon sample lot had failures in Group III. One failure came early in the testing at the +150° C step, due to a $V_{CE(SAT)}$ limit failure. Three more failures occurred at the +275° C step of the process, due to two I_{CBO} leakage failures and one h_{FE} limit failure. A Teledyne failure, which came at the last step (+300° C), was due to an excessive I_{CBO} leakage.

This work was done by the Special Products Division of DCA Reliability Laboratory for **Marshall Space Flight Center**. *To obtain a copy of the report, Circle 19 on the TSP Request Card. MFS-25253*

JANTX2N2605 Transistor

The effects of power and temperature overstress

Group II and Group III testing proved to be the most detrimental of the three groups. Samples from Raytheon and National Semiconductor exhibited several microamperes of hysteresis in the BV_{CEO} curve trace. The pattern suggests the presence of contamination. The flow of metal from the gold leads and the intermetallics is one source of such contaminants.

The hysteresis currents in the base can inject base current that is not part of the known drive. Because of this, the h_{FE} will be high. At the same time, the contaminant may reduce emitter efficiency by reducing the lifetime of holes in the base. This tends to lower the h_{FE}.

Thus, the migration of contaminants during burn-in can have two opposite effects on the h_{FE} reading, and the net result depends upon which effect predominates in the individual sample at the moment of failure. When carried to extremes, gold migration in the base region will develop surface and junction-leakage problems and collector/emitter shorts. Possibly these failures could have been delayed to higher stress levels if aluminum wires were used in place of gold, thus removing the fast-migrating gold from the surface of the die.

This work was done by the Special Products Division of DCA Reliability Laboratory for **Marshall Space Flight Center**. *To obtain a copy of the report, Circle 20 on the TSP Request Card. MFS-25150*

JANTX2N2905A Transistor

The effects of power and temperature overstress

Thirteen Motorola and Texas Instruments parts tested were destroyed by handling, and 31 others failed for a variety of other reasons. The most common of these was intermetallic formations due to temperature stress.

Visual inspection of one failed Texas Instruments unit in Group I revealed some areas of abraded metalization. One Motorola device was destroyed by electrical overstress.

In Group III testing, one Motorola unit lost most of its current gain without exhibiting any other junction anomalies sufficient to explain that loss. This suggests that the beta falloff was due to a loss of emitter injection efficiency, specifically a loss of hole lifetime and/or mobility. Such a change could be induced by the drifting of impurities under the influence of the high power and temperature. The increase in collector/emitter breakdown voltages upon opening the packages and the hysteresis seen on those measurements are evidence that contamination was indeed present within the packages.

Four Texas Instruments samples failed in Group III due to thermal overstress, which caused gold/aluminum intermetallics to form and which degraded the collector/base junctions. The excess die temperature and intermetallic attack on the oxide allowed metallic impurities to contaminate the oxide and thus degrade the transistor characteristics. The emitter/base junctions did not degrade because the higher boron concentration of the emitter diffusions "gettered" the impurities at the emitter/base junction.

This work was done by the Special Products Division of DCA Reliability Laboratory for **Marshall Space Flight Center**. *To obtain a copy of the report, Circle 21 on the TSP Request Card.*
MFS-25256

JANTX2N2920 Dual Transistor

The effects of power and temperature overstress

The only stress test that did any notable damage to the Fairchild and National Semiconductor lots was the Group II (temperature-stress) test. Many of the failures showed a marked loss of gain. There was no significant bulk or surface leakage on these parts. This would imply that the h_{FE} falloff was due only to a loss of emitter efficiency. The loss of efficiency, in turn, was due to the migration of gold and intermetallics under the influence of heat and electrical bias.

Since Group I does not reach the high junction temperatures of Group II, and since Group III does not reach the long time steps of Group II, could explain why there were not as many failures in the Group I and Group II testings.

This work was done by the Special Products Division of DCA Reliability Laboratory for **Marshall Space Flight Center**. *To obtain a copy of the report, Circle 22 on the TSP Request Card.*
MFS-25258

JANTX2N2945A Transistor

The effects of power and temperature overstress

For the Raytheon and Teledyne parts, only Group III was detrimental to both manufacturers' sample lots. The Raytheon sample lot was stopped 160 hours before the completion of the testing because half the lot failed the h_{FE} limits. Failure analysis showed that the samples for Raytheon have extensive gold/aluminum intermetallic formations. The absence of shorts, opens, and junction leakage suggests that the loss of h_{FE} was caused by a reduction in emitter efficiency.

The Teledyne samples experienced similar contaminations; and although testing of the lot was not stopped, it ended up having more catastrophic failures than the Raytheon lot. The fact that the reject rate in the Group III testing was slight compared to the Group II testing suggests that time was a factor. Group III testing reaches high temperatures, as does Group II, but the devices are held at these high temperatures 10 times longer in Group II than in Group III.

This work was done by the Special Products Division of DCA Reliability Laboratory for **Marshall Space Flight Center**. *To obtain a copy of the report, Circle 23 on the TSP Request Card.*
MFS-25259

JANTX2N3637 Transistor

The effects of power and temperature overstress

The testing of transistors manufactured by Transitron had to be stopped during Groups I and II. Motorola lots completed the entire test times in all three groups.

The Transitron devices have two different geometries, and the Motorola units have yet a third type. Transitron uses a rectangular layout and a butterfly pattern. The rectangular layout is superior to the butterfly pattern because it employs "field-plate" extension of the emitter metalization over the base/emitter junction. This is intended to reduce the tendency of p-channel transistors toward surface inversion. The Motorola chip appears to have a longer emitter periphery than either of the Transitron parts. This design is superior for minimizing h_{FE} falloff, increasing collector current, and reducing the emitter current density.

This work was done by the Special Products Division of DCA Reliability Laboratory for **Marshall Space Flight Center**. *To obtain a copy of the report, Circle 24 on the TSP Request Card.*
MFS-25264

JANTX2N3811 Dual Transistor

The effects of power and temperature overstress

Sample lots from National Semiconductor and Motorola held up well during the Group I (power-stress) testing. The Group II testing for National Semiconductor stopped at the 225° C step. Although the Motorola lot showed a higher total number of rejects, the majority of the failures occurred at the last step of the Group II testing.

Failure analysis showed that the National Semiconductor devices are constructed with gold-ball-bonded internal wires, while the Motorola devices have ultrasonically-bonded aluminum internal wires. This difference in construction may be the reason for the difference in performance between the two sample lots.

Hysteresis or leakage was a problem with a majority of the National Semiconductor parts. This pattern suggests the presence of contamination in (or on) the base diffusion. The flow of metal from the gold leads and the intermetallics, because of the stress, was one source of such contaminants. Possibly the National Semiconductor lot failures could have been postponed to higher stress levels if aluminum wires had been used instead of gold.

This work was done by the Special Products Division of DCA Reliability Laboratory for **Marshall Space Flight Center**. *To obtain a copy of the report, Circle 25 on the TSP Request Card.*
MFS-25265

JANTX2N4150 Transistor

The effects of power and temperature overstress

In Group I testing, a General Semiconductor sample lot had to be stopped 500 hours into the 125-percent maximum-rated-power step. A Transitron lot completed the entire testing with a total of seven failures. In Group II and Group III testings, Transitron experienced one catastrophic failure in each test, and General Semiconductor experienced six and seven, respectively.

The General Semiconductor samples had surface inversions and leakage due to contamination. Bare junction areas and the extremely high temperature contributed to the contamination vulnerability of these devices. There is a voltage threshold on these devices at which the inversion and drift of I_{CBO} are triggered. The leakage continues to increase over many seconds.

One Transitron failure had low-resistance contacts to emitter, collector, and base. This suggests that changes in the bulk silicon, such as an increase in base resistivity caused by the migration of gold under the heat and bias of the stress test, were the cause.

This work was done by the Special Products Division of DCA Reliability Laboratory for **Marshall Space Flight Center**. *To obtain a copy of the report, Circle 26 on the TSP Request Card.*
MFS-25267

JANTX2N4856 Field-Effect Transistor

The effects of power and temperature overstress

The Group II and Group III stress tests were the most detrimental of the three groups for transistors manufactured by Teledyne and Texas Instruments. Because of the similar failure mode observed in both groups, failure analysis was performed on samples from the Group II testing only.

The failure analysis pointed out that the majority of the devices exhibited, in various degrees, the effects of surface charges and metal migration. In one Texas Instruments sample, the aluminum had melted. This resulted in shorting the source and drain junctions. Aluminum/silicon eutectic melts at approximately 577° C, which indicates the extreme junction temperature reached by these samples.

This work was done by the Special Products Division of DCA Reliability Laboratory for **Marshall Space Flight Center**. *To obtain a copy of the report, Circle 27 on the TSP Request Card.*
MFS-25269

Electronic Systems

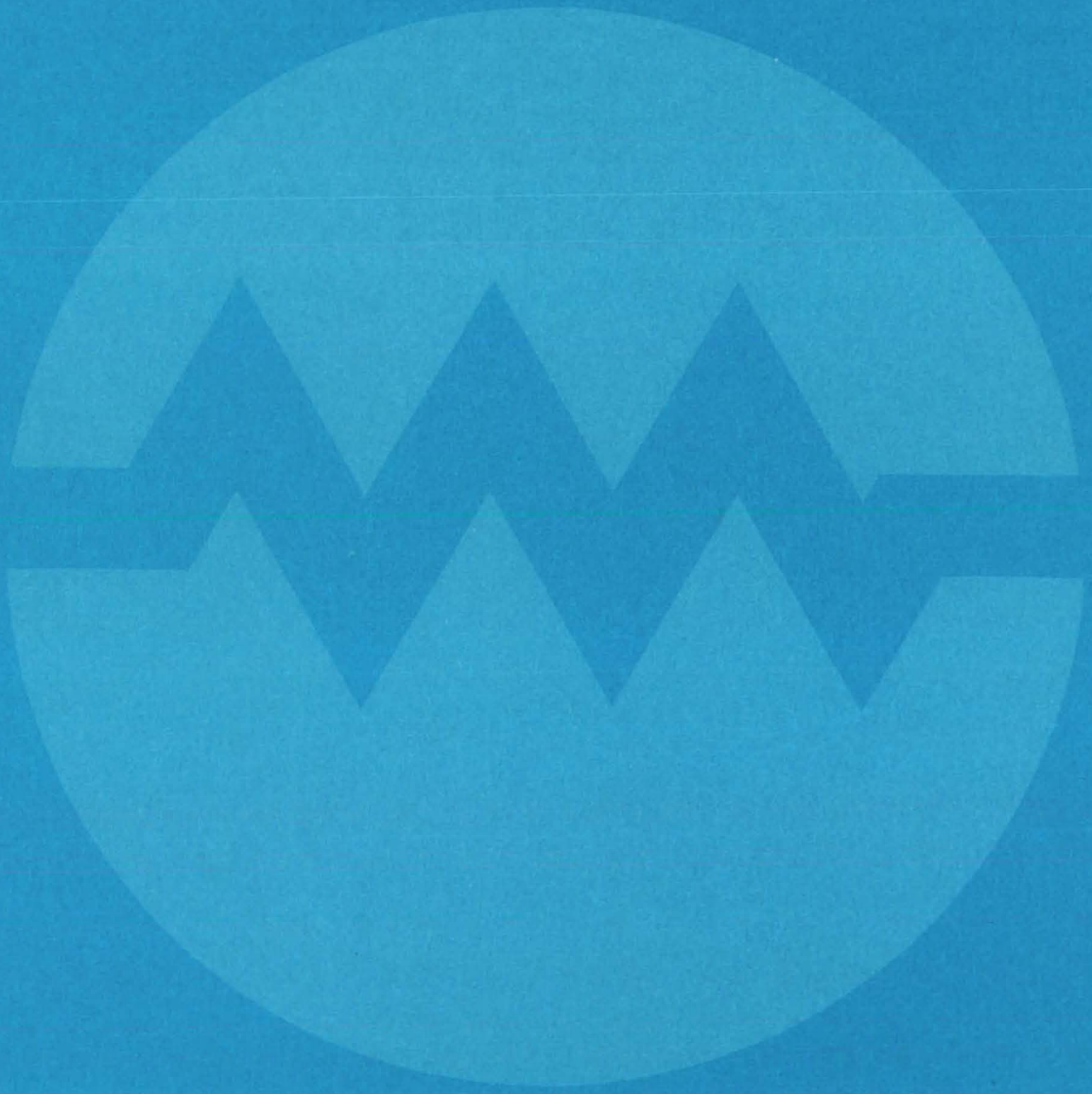

Hardware, Techniques, and Processes

Microprocessor-Controlled Data Synchronizer

A versatile receiver processes data at a variety of rates and code formats.

Lyndon B. Johnson Space Center, Houston, Texas

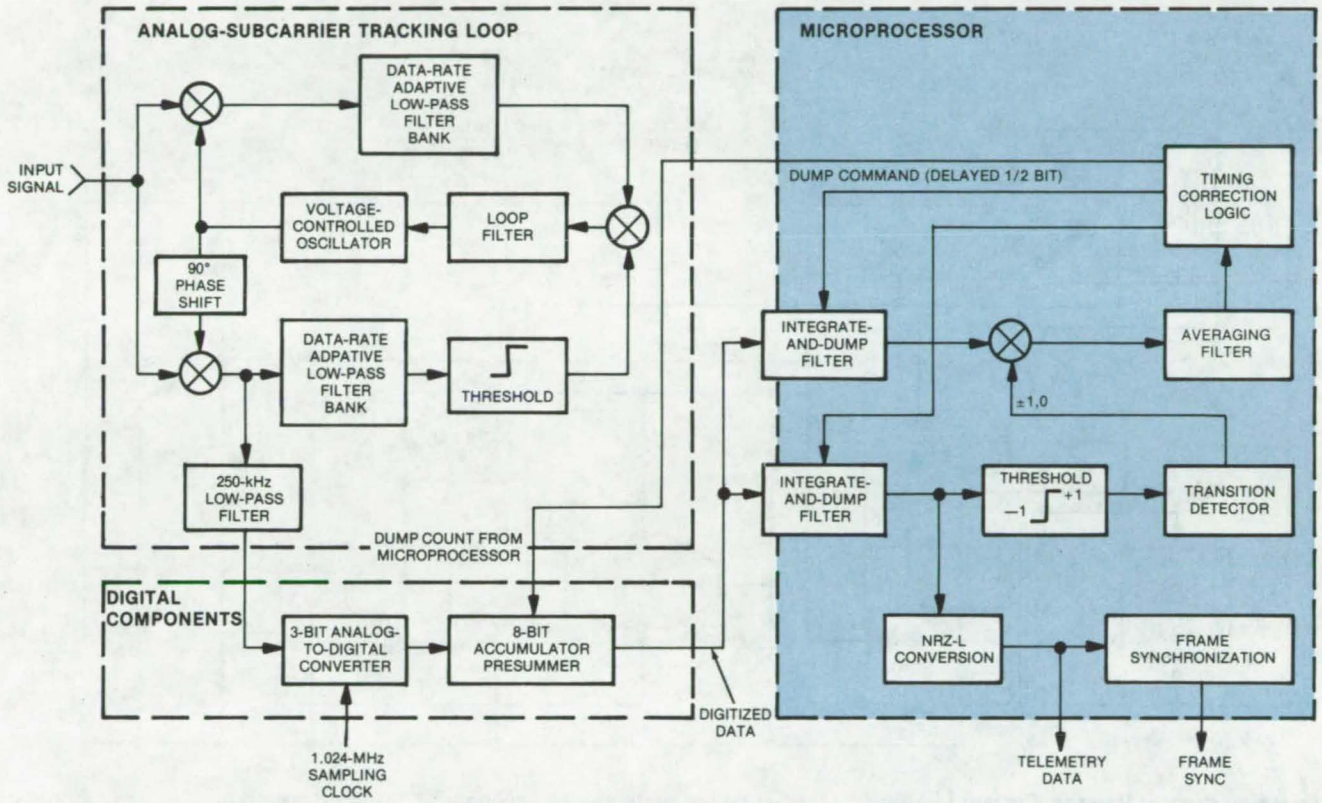

The **Microprocessor Accepts Digital Data** from the front end of the telemetry receiver. A prototype built for Shuttle communications handles phase-shift-keyed modulated signals coded in biphase-L, biphase-M, biphase-S, NRZ-L, NRZ-M, or NRZ-S data at 1, 2, 4, 8, or 16 kb/s. Signal loss is less than 1.5 dB for signal-to-noise levels ranging from 2 to 11 dB at a minimum average bit-transition density of 12-1/2 percent (64 transitions per 512 bit periods). Signal acquisition typically occurs within 2,000 bit periods with 90 percent probability.

Telemetry data in a variety of rates and formats are processed by a versatile receiver designed around a custom bit-slice microprocessor. A prototype, built for 1.024-MHz communications between the Space Shuttle orbiter and a payload deployed up to 10 miles (16 km) away, handles phase-shift-keyed signals in any of six codes at rates varying between 1 and 16 kb/s. The receiver can be reprogramed to new rates and formats by changing the programs that control the processor.

As shown in the block diagram, the received signal is filtered and demodulated by analog circuitry, and the demodulated signal is digitized. Among the functions performed by the microprocessor on the digitized signal are:

- bit detection,
- NRZ-L conversion,
- frame synchronization (with programable word length),
- bit-sync acquisition and tracking,
- error-curve normalization,
- lock detection,
- half-bit-ambiguity resolution, and
- data-rate tracking.

The receiver program, stored in read-only memory on the microprocessor chip, is not written in standard assembly language. Instead, a language that is suited to parallel data transfers among the processor registers is used. (Much of the microprocessor operation is handled in parallel, allowing high-speed processing at minimum power consumption.) The language is intermediate between a high-level language and more conventional assembly languages. The mnemonics also simplify program revisions.

This work was done by Sam W. Houston, Donald R. Martin, and Larry R. Stine of TRW, Inc., for **Johnson Space Center.** *Further information may be found in the copyrighted article "Microprocessor Bit Synchronizer for Shuttle Payload Communications" from the IEEE Transactions on Communications, Copyright IEEE. To obtain a copy of the article, along with other documentation, Circle 28 on the TSP Request Card.*

MSC-18535

Voltage Controller/Current Limiter for ac

A circuit protects ac power systems from overload failures.

NASA's Jet Propulsion Laboratory, Pasadena, California

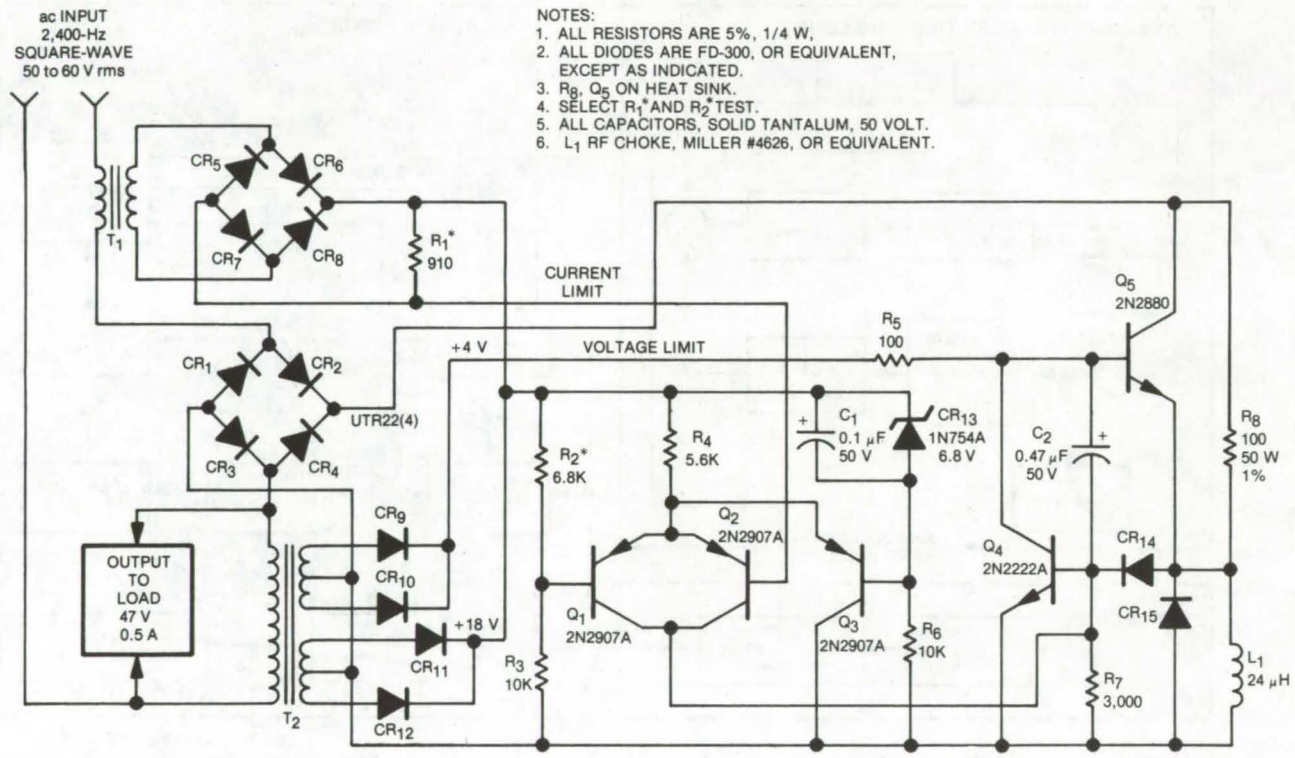

Alternating-Current Voltage/Current Limiter protects ac power systems from overload. The circuit generates a dc error signal in response to line fluctuations. When the overload level is reached, transistor Q_5 is cut off, dumping power into the power resistor R_8 and inductor L_1 branch. Excess power is dissipated in R_8, and the current rise time is limited by the L_1, limiting power to the load.

A voltage- and current-limiting circuit uses feedback to prevent excessive transients and current and voltage fluctuations in ac power systems. Positioned between the source and the load, the circuit limits power-surge and short-circuit currents to 150 percent or less of their steady-state levels. In addition, it regulates the ac output voltage to a constant level and "soft starts" the load.

Basically the circuit generates dc error signal in response to current or voltage fluctuations on the line. This signal is applied to a pass transistor that is cut off when the line current or voltage exceeds a set limit. A closed-loop feedback is formed to limit the overload.

The circuit (see figure) uses a full-wave bridge rectifier (diodes CR_1 through CR_4) that converts ac line current to dc current. Power transistor Q_5 is the pass transistor and is mounted on a heat sink. The ac line current is "sensed" by current transformer T_1 with a 100:1 current stepdown ratio. The current transformer output is converted into a dc voltage through a full-wave diode bridge (CR_5 through CR_8) and resistor R_1. This voltage, which represents ac current, is compared with a reference voltage (CR_{13}) in a modified differential-amplifier circuit (Q_2, Q_3).

The output load voltage is "sensed" by transformer T_2, which also feeds dc power for the operation of the differential amplifier and base-drive current for the pass transistor (Q_5). This signal is fed into the differential amplifier (Q_1) through the resistor divider network (R_2, R_3).

Transistor Q_4 generates additional amplifier gain and reduces the power requirement for the differential amplifier. Inductor L_1 and capacitor C_2 provide high-frequency rolloff and prevent high-frequency oscillation when the limiter circuit goes into limiting action.

The inductor L_1 also limits current rise time (di/dt) via feedback through transistor Q_4 and diode CR_{14}. Capacitor C_1 is used to reduce voltage- and current-limit set points by slow buildup of reference voltage during initial power turn-on. Capacitor C_1 thus provides a gradual buildup of reference voltage during initial power turn-on and prevents current surges that may exceed limit during this transition period. The controlled voltage and current buildup soft starts the load devices.

There is also unique short-circuit protection. If the output load is short-circuited and develops little or no voltage, transformer T_2, which is across the load, will have little or no secondary output voltage. Since the pass transistor (power transistor Q_5) obtains its base drive from transformer T_2, pass transistor Q_5 will be at cutoff. Thus, a short circuit at the load will make the pass transistor inoperative.

The load current is then carried by the power resistor R_8, connected in parallel with the pass transistor. This approach completely eliminates the danger of thermal runaway of the pass transistor and consequently failure of the control circuit, as tested in the most severe conditions of current limiting. Resistor R_8 also drastically reduces maximum power dissipation in the pass transistor Q_8 by sharing the rectified load current.

The addition of resistor R_8 can reduce maximum transistor dissipation to only one-third as much compared to that without the resistor. With the short-circuit current determined only by R_8, the maximum allowable current level in the illustrated circuit is set at 100 percent of normal load current to reduce circuit dissipation and to increase reliability.

This work was done by Ta Tzu Wu of Caltech for **NASA's Jet Propulsion Laboratory.** *For further information, Circle 29 on the TSP Request Card.*
NPO-13061

Microprocessor Control for Phase-Lock Receiver

Subsystem with complex logic, control, and memory functions is used for acquisition sequence and phase lock.

NASA's Jet Propulsion Laboratory, Pasadena, California

A new microprocessor-controlled digital subsystem optimizes phase-coherent receiver performance. The subsystem controls an involved signal-acquisition sequence and assists in precise phase-locking to the received signal. The combined software/hardware design is more compact and more reliable than a more complex all-hardware alternative. Heavy reliance on software makes the subsystem very flexible to modifications.

The subsystem is incorporated into the NASA standard-TDRSS (Tracking and Data Relay Satellite System) user transponder. Its major functions include: (a) the selection of 1 of a family of 85 sets of pseudorandom-noise (PN) codes used to spread the received and transmitted signals, (b) the selection of one of several possible command data rates, (c) automatic configuration modification to receive a nonspread signal with an alternate data rate when such signal is detected, and (d) the selection of various receiver configurations and transmitter modulation data and PN-spreading code formats in response to control-command inputs.

The subsystem incorporates a commercially available microprocessor consisting of a standard control-processing unit (CPU), one 32-by-8 static random-access memory (RAM), and seven 512-by-8 static read-only memories (ROM's). The microprocessor performs all the standard sequencing, logic, and control functions characteristic of its general performance standards.

The key to the operation lies in the software programs, which include system and code-generator initialization routines and executive routine, utility subroutines, control sequence routines for each of the receiver acquisition states, a control-command decoding routine, and lookup tables for code-generator configuration versus code-set numbers. Programmable ROM's have been used during transponder development to facilitate possible modifications of the subsystem.

Additional ROM's, RAM's, and I/O (input/output) buffers can be paralleled on the bidirectional data bus for further subsystem expansion. The multilayered printed-wiring memory board is adaptable to accept one additional RAM and three additional ROM's. Spare I/O bytes are also available for possible subsystem expansion.

The extensive use of software rather than hardware makes the subsystem much more flexible to modification. For example, receiver carrier and code-clock phase-lock-loop bandwidths and bandwidths in the suppressed carrier detector can be switched as necessary to match requirements during each step of the acquisition sequence. Steps can also be added as necessary in the acquisition sequence to extend the input-signal dynamic range by testing for false code lock on an autocorrelation side lobe.

This work was done by Lansing M. Carson and James R. Shaner of Motorola, Inc., for **NASA's Jet Propulsion Laboratory.** *For further information, Circle 30 on the TSP Request Card.*
NPO-14438

Improved Code-Tracking Loop

A new delay-locked loop is unaffected by gain imbalance.

Lyndon B. Johnson Space Center, Houston, Texas

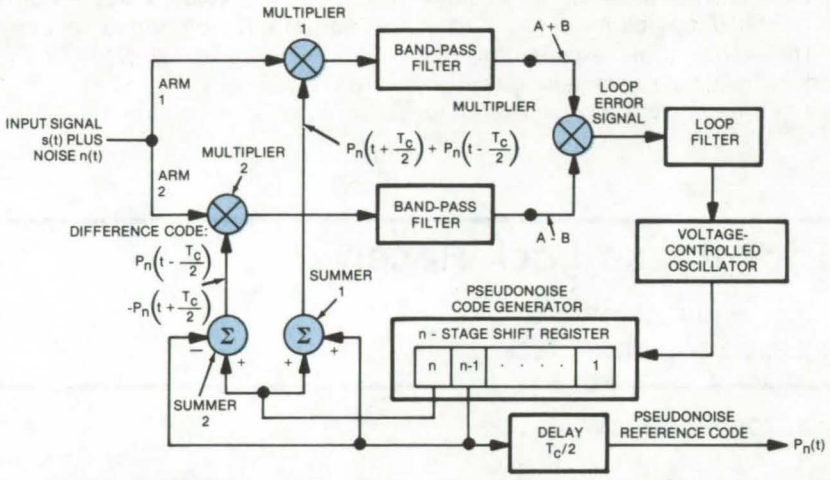

The New Delay-Locked Loop tracks pseudonoise codes without introducing dc timing errors due to gain imbalance between arms 1 and 2. Summer 1 applies the sum of the early and late codes to multiplier 1; summer 2 applies the difference between the early and late codes to multiplier 2.

An improved delay-locked loop (DLL) is insensitive to gain imbalance between its signal-processing arms and therefore eliminates dc timing errors. Loop tracking performance is equivalent to that of previous DLL circuits. The delay-locked loop is used for tracking pseudonoise codes in digital receivers.

The new circuit is arranged so that "early" and "late" reference codes pass in a combined form through both arms instead of through separate arms. Since each arm acts on both codes, differences in gain between the two arms cannot cause a timing offset at their outputs.

In the previous DLL, the received signal and its noise component are applied to the two signal-processing arms, each of which contains a multiplier and a square-law detector. One multiplier receives a late reference code from the last stage (n) of the shift register in a pseudonoise code generator; the other multiplier receives an early reference code from the next-to-last stage (n-1) of the shift register. Unless both arms have exactly equal gains, which is difficult to ensure, the loop error signal will have a dc offset or bias, and a timing error in the pseudonoise reference code will result.

In the new DLL (see figure), the received signal and noise are applied to both arms, as in the previous circuit; however, instead of receiving just the late reference code, multiplier 1 receives the late code plus the early code, and multiplier 2 receives the early code minus the late code. Multiplier 1 forms a sum product signal by multiplying the reference code sum with the incoming signal. Multiplier 2 forms a difference product signal by multiplying the reference code difference with the incoming signal. Any gain imbalance between multipliers 1 and 2 therefore has an equal effect on the data in stage n and stage n-1 of the shift register.

After going through a band-pass filter, the contents of arm 1 represent the product of the data portion S(n) of the incoming signal and the sum reference code. Similarly, after filtering, the contents of arm 2 represent the product of S(n) and the difference reference code.

The products are furnished to a multiplier, which forms an error signal. After filtering, the error signal is applied to a voltage-controlled oscillator, which provides the input to the shift register in the pseudonoise generator.

Often, a tau-dither loop is used instead of a delay-locked loop because of the gain imbalance problem. The new DLL not only is insensitive to gain imbalance but can accommodate weaker input signals; for equal tracking performance, the tau-dither loop requires a 1-dB greater signal-to-noise ratio than the new DLL.

This work was done by David T. LaFlame of Hughes Aircraft Co. for **Johnson Space Center.** *For further information, Circle 31 on the TSP Request Card.*

This invention is owned by NASA, and a patent application has been filed. Inquiries concerning nonexclusive or exclusive license for its commercial development should be addressed to the Patent Counsel, Johnson Space Center [see page A5]. *Refer to MSC-18035.*

Multipath Star Switch Controller

A function control method is proposed for multiple computer data-processing systems.

NASA's Jet Propulsion Laboratory, Pasadena, California

A proposed star switch concept is a means for a number of parallel computers to scan several common-network-connected data stations at a maximum rate. This is accomplished by using "leapfrog" sequencing to bypass any port already being serviced by another computer. A combination of functional logic techniques is used to raise the number of possible data paths in the system without installing additional connective hardware.

The output address for each path is held in individual hold registers. For internal switching of the timing control lines, their control logic is multiplexed so that only one path is in the process of being established at any one time. This avoids input-port collision between data paths. The address systems are asynchronous as to positions between systems but are otherwise synchronized to the same internal service clock.

The figure shows the concept for two sequencers X and Y. Each sequencer is implemented using a 4-bit hold register and a 4-bit adder connected end around. The second vector connected to the adder during normal operation is a constant 1. When using this sequencer implementation, a "leapfrog" operation becomes very simple. Two binary coincidence circuits are connected, one between X (the output of register X) and Y + 1 (the output from the adder in the end-around circuit) and one between Y and X + 1.

The outputs from the coincidence circuits are cross-coupled to the (2^1) terms of the second vectors in each adder. When the (2^1) term is turned on, the (2^0) term is turned off.

A sequencer leapfrogs only when the other sequencer is one step ahead and quiescent. All connections are cross-coupled so that when any one of the two sequencers is ahead one step, the second sequencer will leapfrog as they may alternate on being ahead because of their being randomly halted.

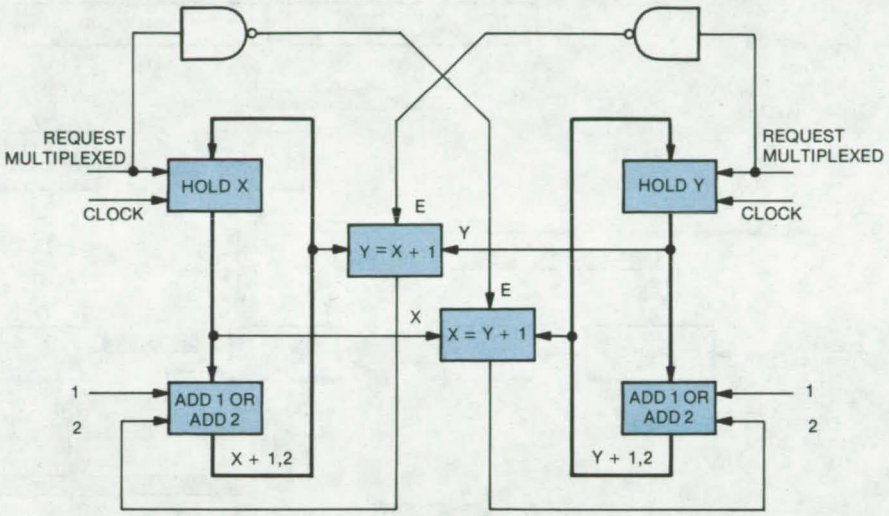

A Proposed Star Switch Controller for two sequencers X and Y would incorporate each sequencer using a 4-bit hold register and a 4-bit adder connected end around. The scheme would permit a number of parallel computers to scan a number of common-network-connected stations at a maximum rate, using "leapfrog" sequencing to bypass any part already being serviced by another computer.

For a three-sequencer system any two out of three sequencers are first cross-coupled in the same manner as for the two-sequencer system shown in the figure. In addition, any two sequencers halted at adjacent positions must be detected. When this occurs and the third is adjacent and operating, both the (2^0) and (2^1) terms of the fixed vector of the adder are energized so that it will advance three positions; i.e., leapfrog the two adjacent and quiescent sequencers.

A two-path system is only slightly more complex than a single-path system. Thus, a two-path system for a 16-port star switch controller would be cost-effective if the added bandwidth were required or the increased reliability were desired. A multiple-path system, however, becomes exponentially more complex. The triple-path system is yet manageable, but it may not be a cost-effective design for a 16-port system, although for a 32-port system it probably would.

This work was done by Tage O. Anderson of Caltech for **NASA's Jet Propulsion Laboratory.** *For further information, Circle 32 on the TSP Request Card.*

This invention has been patented by NASA [U.S. Patent No. 3,916,380]. Inquiries concerning nonexclusive or exclusive license for its commercial development should be addressed to the Patent Counsel, NASA Resident Legal Office-JPL [see page A5]. Refer to NPO-13422.

Microprocessor-Based Detector for PSK Commands

Command-detector unit operates over a wide range of data rates and signal levels in a space environment.

NASA's Jet Propulsion Laboratory, Pasadena, California

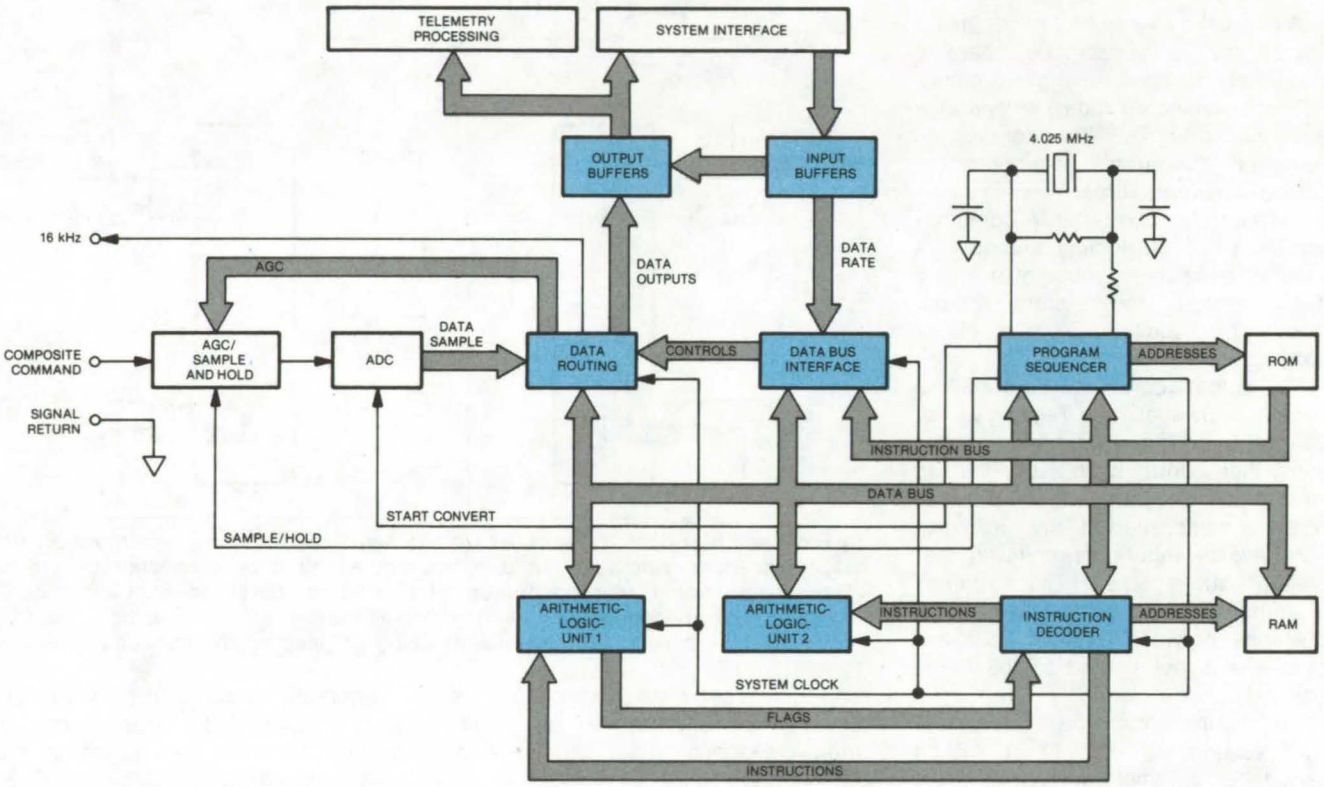

The Command Detector shown here as a block diagram consists of signal conditioning, read-only memory, random-access memory, and a digital processor. The entire command-detector unit fits on a single multilayer printed-wiring board. The components shown in color constitute the digital processor.

Command signals radioed to a spacecraft can be processed efficiently in a microprocessor-controlled command-detector unit (CDU) designed to be part of a standard transponder. The CDU is a coherent demodulator for binary phase-shift-keyed (PSK) signals on a 16-kHz subcarrier; it is readily adaptable to nine data rates ranging from 7.8 to 2,000 bits per second and can accommodate input levels over a 40-dB range. A comfortable performance margin is achieved through the power-and-weight-saving approach of digital signal processing using radiation-shielded CMOS custom large-scale integration (LSI).

Functionally, the command detector consists of a data-coherent automatic gain control (AGC), a sample-and-hold (S/H) circuit, an analog-to-digital converter (ADC), a second-order data-aided subcarrier tracking loop, a data-transition bit-synchronization loop, and a lock detector. Structurally, the detector consists (see figure) of the signal conditioning (AGC, S/H, and ADC), read-only memory (ROM), random-access memory (RAM), and a digital processor that uses a metal-gate CMOS technology.

The data-coherent AGC consists of logarithmic-linear digitally controlled attenuation with dynamic range in excess of 40 dB. Its loop performance (e.g., noise jitter and settling time) is determined by the AGC loop algorithm and coefficients stored in ROM. Upon receipt of the appropriate command from the digital processor, the sample-and-hold circuit freezes the analog input to the 8-bit successive-approximation analog-to-digital converter and holds it constant over the conversion time.

Unlike typical analog or digital data-aided loops — requiring mixers, filters, and analog-to-digital converters in both in-phase and quadrature synchronization channels — the sinusoidal subcarrier tracking loop implements the two synchronization channels with sample accumulators within

the digital processor. The sample rate is constant over all data rates, resulting in design economy without compromised performance. A second-order subcarrier loop is in the demodulator algorithm in ROM, with ROM-resident loop coefficients selected to minimize steady-state phase jitter.

The data-transition bit-synchronization loop is driven by the contents of another dedicated sample accumulator within the digital processor. The loop resolution needs only to be accurate to within a subcarrier cycle to provide effective bit-synchronization resolution of 1/64 of a subcarrier cycle. Thus, at 8 bits per second, the effective bit-synchronization resolution is about 8×10^{-6} of a data bit.

The lock detection algorithm and coefficients are also ROM-resident, allowing complete flexibility in tailoring the demodulator to meet performance requirements.

This work was done by James Durden and Stephen W. Klare of Motorola, Inc., for **NASA's Jet Propulsion Laboratory.** *No further documentation is available.*
NPO-14440

Online Assessment of a Distributed Processor

Test sequence determines the operational readiness of a multicomputer test system.

John F. Kennedy Space Center, Florida

An operational readiness test (ORT) checks out a computer complex composed of many minicomputers. Developed for the Space Shuttle prelaunch checkout, the ORT software performs morning "wakeup" testing as well as testing before and after launch to determine the readiness of the checkout complex. This approach to online assessment of a distributed processor should interest the users of similar equipment in other applications.

The prelaunch-checkout complex consists of up to 64 minicomputers connected via a common data buffer (CDBFR) — a bipolar solid-state memory — to each other, to a central data system, and to peripheral equipment (see figure). The ORT software system allows a test engineer to run a complete readiness test on the complex from one console.

The ORT first makes a "rollcall' to determine the operability of:

- the peripheral equipment directly connected to the "host" minicomputer (the host minicomputer console is the one used by the test engineer),
- the minicomputers available through the CDBFR,
- the special peripheral units available within the CDBFR, and
- the peripheral units directly connected to the minicomputers.

The system then tests all minicomputer subsystems simultaneously in their operational modes.

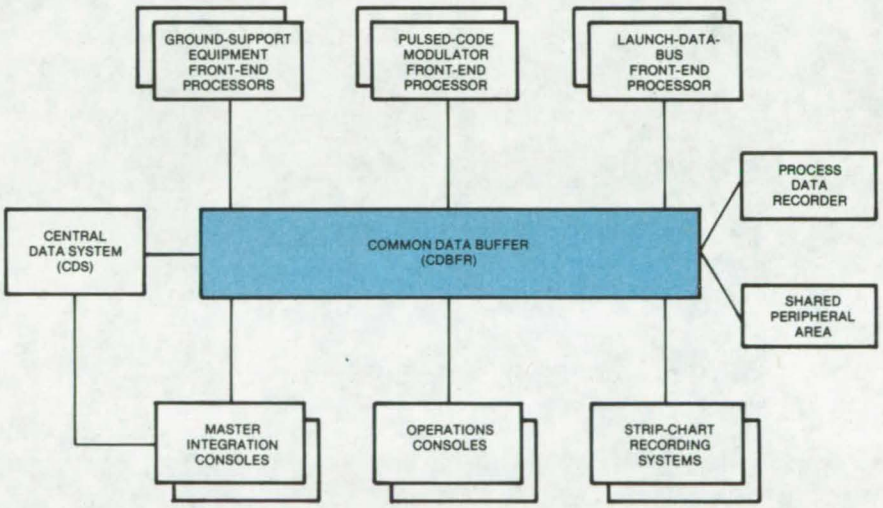

A Common Data Buffer links the many elements of a prelaunch-checkout computer complex and gives the operational-readiness-test (ORT) software system access to the various minicomputers and their peripherals.

The ORT sequences, which are integrated into the rest of the prelaunch-checkout system, are based on run tables derived from the hardware configuration used during an actual launch. The test engineer can edit the tables in real time so that the test sequence accommodates changing hardware configurations and matches the configurations available at test time. Editing also allows the engineer to test any single peripheral unit or minicomputer.

The ORT system loads the prelaunch-checkout computers with instructions and data, either from disk storage or via the CDBFR. Test results are returned to the host minicomputer and displayed. On completion of a test, the affected subsystem is restored to its original condition, ready for use. To prevent a failed subsystem from halting a test sequence, the ORT uses an automatic "watchdog" timer to terminate a given test after a preset interval; it then moves on to the next test in the sequence.

(continued on next page)

To minimize testing time, the subsystems are tested in parallel. With this scheme, a complete system rollcall can be done in about 15 minutes.

This work was done by L. F. Ehrlich of IBM Corp. for **Kennedy Space Center.** *To obtain a copy of a report describing the ORT system in more detail [program listing is not included], Circle 33 on the TSP Request Card.*

Inquiries concerning rights for the commercial use of this invention should be addressed to the Patent Counsel, Kennedy Space Center [see page A5]. Refer to KSC-11124.

Physical Sciences

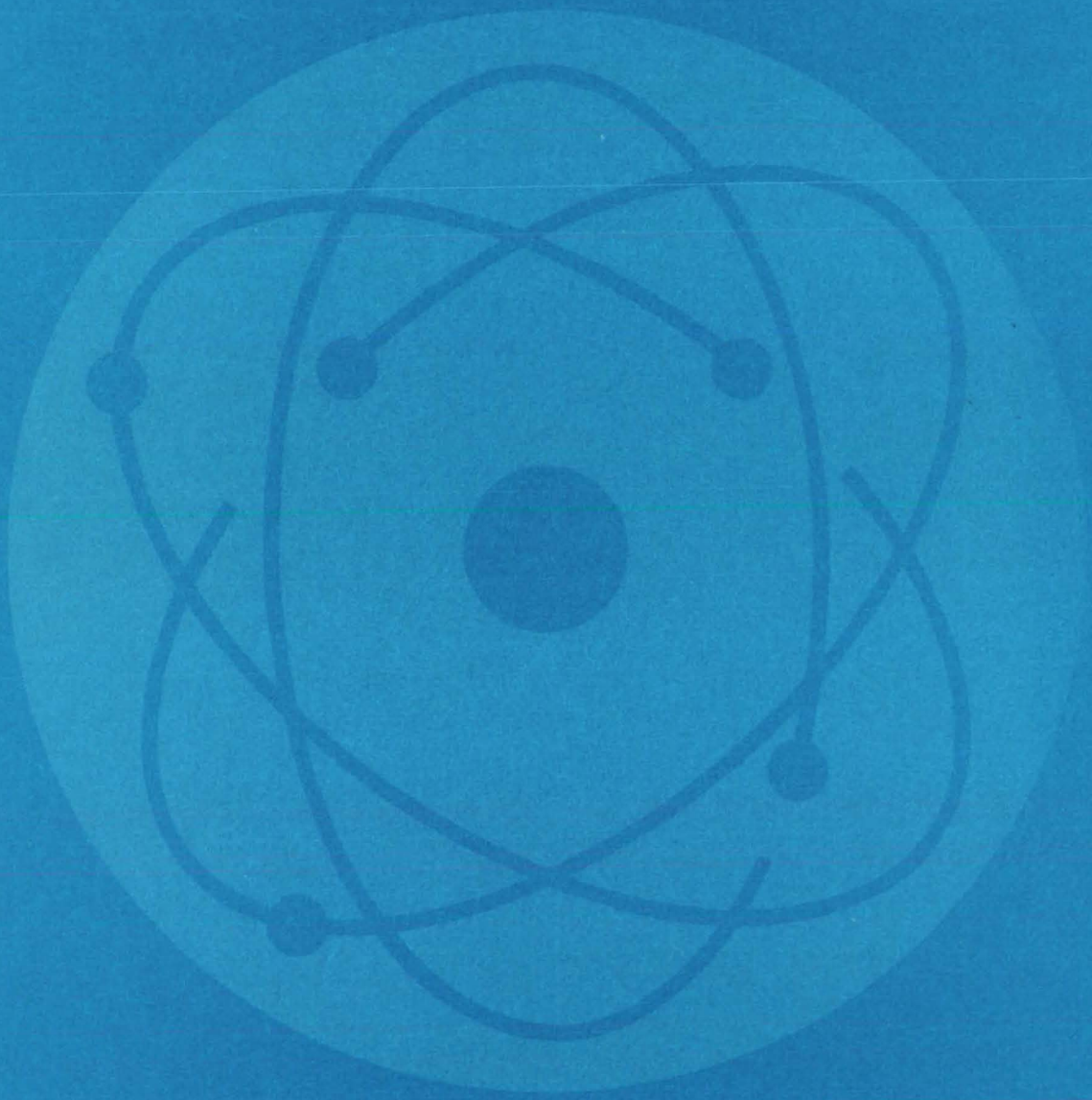

Hardware, Techniques, and Processes

Books and Reports

Computer Programs

Photoelectrochemical Cell With Nondissolving Anode

New cell may be an economical alternative to silicon solar cell.

Langley Research Center, Hampton, Virginia

An improved electrolytic photovoltaic cell converts solar energy to electricity without electrode decomposition. Cell efficiencies up to 15 percent have been measured, which are comparable to those of the best silicon solar cells. However, the costs of materials and fabrication for electrolytic cells are potentially less than for silicon cells.

Previous efforts to build practical electrolytic solar cells were hampered because the anode would dissolve in the electrolyte under the influence of the incident Sunlight. The new cell employs electrolytes that overcome this tendency.

The cell consists of a light-sensitive n-type semiconductor anode and a metallic cathode both immersed in an electrolytic solution (see figure). The cathode and the anode are electrically interconnected by an external load. Sunlight passing through the transparent container strikes the anode. The incident photons excite the anode, which establishes a current between the two electrodes.

The anode materials tested were CdS, CdSe, CdTe, GaP, GaAs, and InP; and the tested electrolytes were Na_2X/X_n, where X is S, Se, or Te. Results show that the CdS and CdSe are the most stable anode materials and that all the anode materials are stable in the Na_2Te/Te_n. Some of the other electrode/electrolyte combinations are also successful.

A key element of these cells is that the reversible redox systems employed not only result in no net chemical change in the electrolyte but also stabilize the n-type semiconductor photoelectrode to photoanodic dissolution. Presumably, the electrolyte additive is capable of undergoing photoinduced oxidation at the semiconductor electrode at a rate that completely overwhelms the general photoanodic dissolution reaction of the small-band-gap n-type semiconductors.

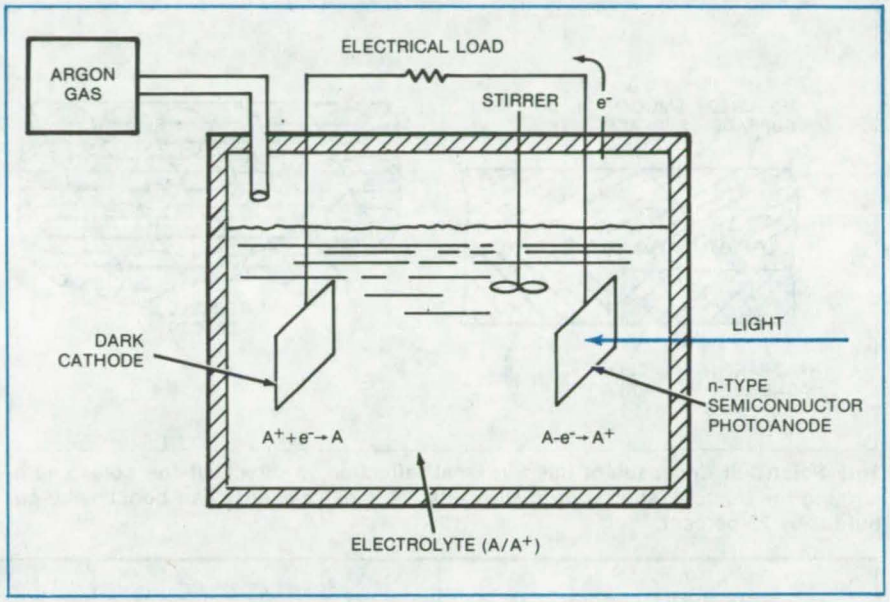

Photochemical Cell admits Sunlight through a glass window. The light strikes the semiconductor anode, which begins to conduct. A sodium compound (represented by A) oxidizes at the anode and is reduced at the cathode in a continuous cycle.

The cell can produce more than 500 mW of power per cm^2 of anode area at an output voltage of about 0.4 V. The anode has been operated at current densities as high as 16 mA/cm^2 with no deterioration.

Both single-crystal and less-costly polycrystalline semiconductors have been used as the anode. The stability of the anode is not affected by the crystal structure, although the single-crystal type is more efficient.

Argon fed over the electrolyte prevents the electrode from being oxidized by air and gently circulates the solution. Low electrolyte concentrations are circulated by using a motor-driven stirrer between the anode and cathode.

This work was done by Arthur B. Ellis, Steven W. Kaiser, and Mark S. Wrighton of the Massachusetts Institute of Technology for **Langley Research Center.** *For further information, Circle 34 on the TSP Request Card.*

Title to this invention has been waived under the provisions of the National Aeronautics and Space Act [42 U.S.C. 2457(f)], to the Massachusetts Institute of Technology, 77 Massachusetts Ave., Cambridge, MA 02139.

LAR-12591

New Mounting Improves Solar-Cell Efficiency

Solar-cell modules are modified to maximize solar-energy collection.

NASA's Jet Propulsion Laboratory, Pasadena, California

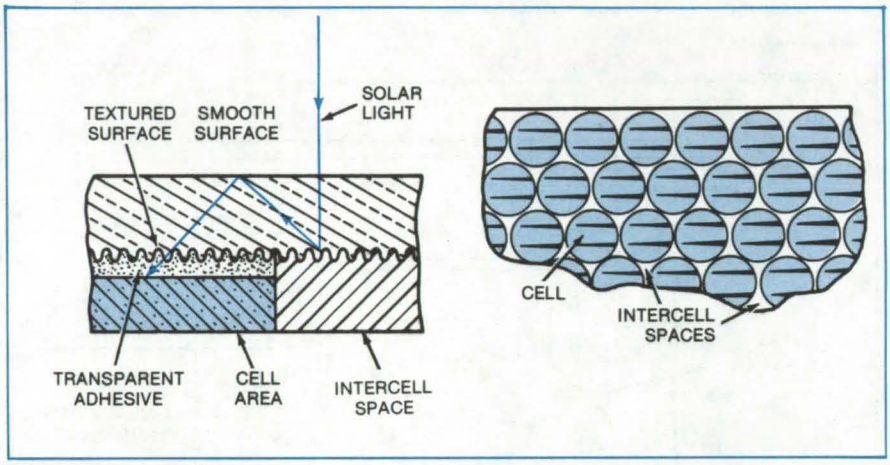

This **Solar-Cell Encapsulant** uses internal reflection to direct all the solar energy striking the intercell spaces onto the cells. This extra energy can boost solar-cell output by 20 percent.

Aperture Diameter (mm)	Short-Circuit Current at 100 mW/cm^2 and 28° C (mA)
53	672
64	752
76	792
89	812
102	823

Illumination Test Results show an increase in current for an increase in "intercell" space. Interpolation of these results indicates that for a typical interspace area equal to 55 percent of cell area, there is a 20 percent enhancement of short-circuit current.

A tested method of mounting and encapsulating solar cells traps solar radiation falling on intercell spaces and redirects it onto the cell surfaces by repeated internal reflection. This added energy can boost output by about 20 percent without increasing the module depth as is required with conventional concentrators for solar-cell arrays.

When mounted, the solar-cell array is covered with an internally reflecting plate (see figure) made from commercially-available highly transparent material. (Its outer surface is smooth, and the inner surface in contact with the module is textured.) The plate is attached to each cell by a transparent adhesive. The space between cells is covered with a layer of diffusely reflecting material.

Solar energy falling on the spaces between cells is diffused and reflected internally by the plate until it is reflected onto a solar cell. In a test of the technique, a single cell with a diameter of 53 mm was mounted as shown in the figure, with a surrounding "white space." The cell was covered with an opaque plate having a cutout the same size as the cell, and the output was measured. Plates with larger cutouts were then placed over the cell to measure the contribution of energy falling on varying amounts of intercell space. The results, as shown in the table, indicate that light falling on the "intercell" space is redirected to the cell.

This work was done by Neal F. Shepard, Jr., of General Electric Co. for **NASA's Jet Propulsion Laboratory.** *For further information, Circle 35 on the TSP Request Card.*

This invention has been patented by NASA [U.S. Patent No. 4,162,928]. Inquiries concerning nonexclusive or exclusive license for its commercial development should be addressed to the Patent Counsel, NASA Resident Legal Office-JPL [see page A5]. Refer to NPO-14467.

Energy-Saving Thermostat

Control unit and method for two-stage heating system

Langley Research Center, Hampton, Virginia

A new energy-and-cost-saving thermostat establishes a basic control concept for a two-stage heating system. It is based on a night-setback thermostat that controls a heating system according to a preprogramed schedule. The room set-point temperature schedule incorporates the desired room temperature, the time to reach the desired temperature (or target time), and the outside-air (OSA) temperature. The control turns heat off and on, according to building needs, in such a way as to reduce the amount of second-stage heating, which in two-stage systems such as heat pumps is the more-expensive resistance electrical heating.

The main purpose of the thermostat is to lower the temperature at night and to turn on the heat at the latest time necessary to have a room heated up at a chosen hour in the morning.

The second objective of the thermostat is to control second-stage heating. A typical setback thermostat initiates a large temperature set point adjustment in the morning. If after this adjustment there is still a large difference between the desired set point and actual room temperatures as could be expected the second stage is turned on even though the more-efficient first stage could raise the temperature, given enough time. In the new system, the thermostat room set-point temperature is preprogramed to rise gradually, allowing the heat pump used in the first stage to raise the room temperature. This saves considerable energy costs by reserving expensive second-stage resistance electrical heating for periods too cold for the first stage alone.

The diagram shows the desired temperature set point versus time. If the actual room temperature closely follows the adjusting set-point temperature, the second stage will not activate.

The control can be mechanical, electrical, electronic, pneumatic, or a microprocessor. A mechanical device has already been designed, and Langley Research Center is installing a microprocessor version in a building equipped with a heat pump. Sufficient data will be taken to evaluate the effectiveness of the concept.

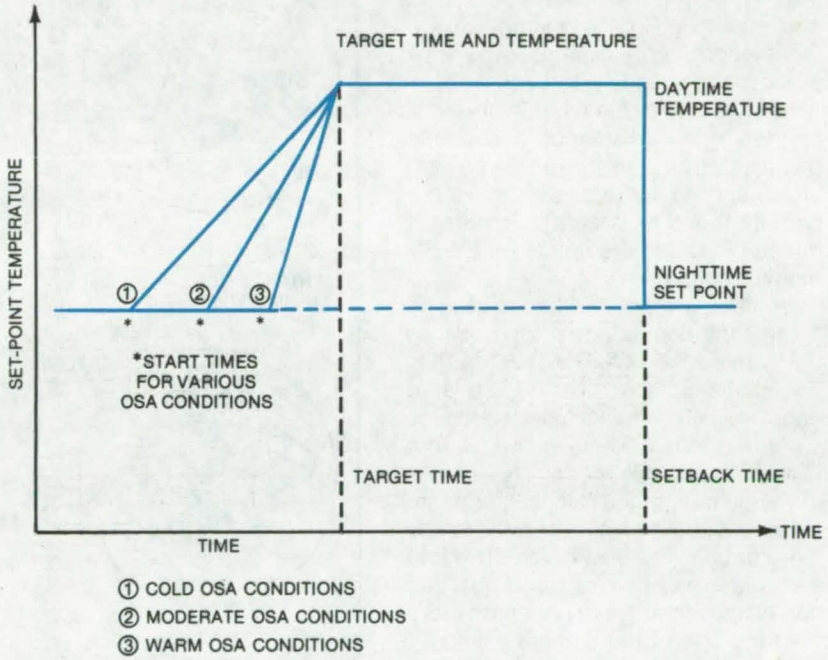

Set-Point-vs.-Time chart shows how the time required for the first (heat-pump) stage of a two-stage heating system to raise room temperature to a desired level varies with the outside-air (OSA) temperature. The new thermostat adjusts the turn-on time accordingly and reduces the amount of expensive second-stage (electrical-resistance) heating required.

The thermostat will be programed with the desired space temperature and a minimum setback temperature. A target time will be set corresponding to working hours in the building. A variable room set-point temperature will be a function of the outside-air temperature and time period before target time. If the room temperature rises above the variable set-point temperature, the heating unit shuts off; if the room temperature drops below the set-point temperature, first-stage heating is activated.

Only if the room temperature drops several degrees further below the set-point temperature is the expensive second stage activated. Correctional factors are to be included for cases where it is determined that the second-stage operation is more cost- and energy-effective than prolonged first-stage-only operation, such as when extremely-cold outside-air temperatures are encountered and the heat-pump coefficient of performance is low.

This work was done by Ronald N. Jensen of **Langley Research Center.** *No further documentation is available.*

Inquiries concerning rights for the commercial use of this invention should be addressed to the Patent Counsel, Langley Research Center [see page A5]. Refer to LAR-12450.

Rotatable Prism for Pan and Tilt

Compact, inexpensive drive changes the field-of-view of a TV camera.

Langley Research Center, Hampton, Virginia

A stationary television camera has been adapted so that it can pan and tilt with the aid of low-cost stock parts and materials. The wide-angle fixed-focal-length camera is used to view aerodynamic models through a port-hole in a wind tunnel. Commercial camera drives were not acceptable because they are expensive, too large, and, in some cases, move the camera in too wide an arc, making it difficult to orient the image on the TV monitor screen.

In the new drive, a prism rotated by a remotely controlled motor changes the camera field-of-view (see figure). For panning, the prism is rotated about an axis perpendicular to the lens surface. The viewing plane is not disoriented by this motion, regardless of the pan angle. For tilting, the prism is rotated about an axis parallel to the lens surface. The size of the drive unit and the clearance required for pan and tilt movements are not much more than the size of the camera itself.

This work was done by William B. Ball of **Langley Research Center.** *No further documentation is available.*
LAR-12388

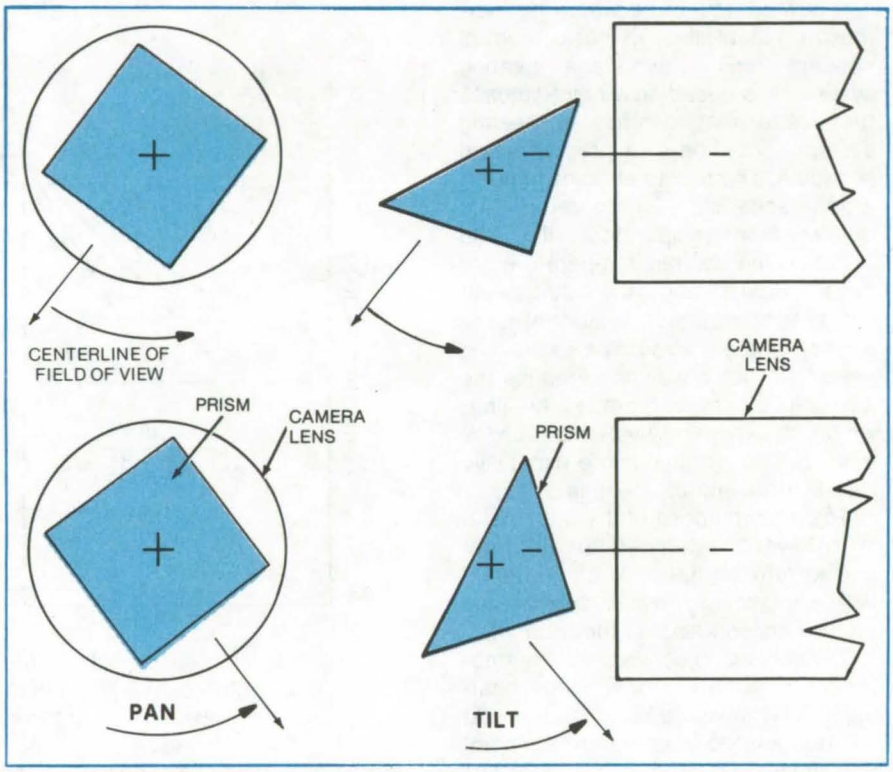

Panning Effect (left) is produced by rotating the camera and prism about the lens axis. The image is tilted by rotating the prism around an axis parallel to the lens (right).

Ultraviolet Spectrometer/Polarimeter

A combined instrument package for ultraviolet studies of solar radiation and of Earth's atmosphere

Marshall Space Flight Center, Alabama

A satellite instrument package has been developed to study solar ultraviolet radiation, particularly from flares and active regions, and to measure the constituents of Earth's atmosphere at the satellite dawn and dusk. The package consists of a telescope, a spectrometer with a polarimeter, five detectors, and the necessary electronics. The ultraviolet spectral range can be observed from 1,150 to 3,600 Å, with emphasis on the region from 1,150 to 2,000 Å. The instrument is controlled by a minicomputer that can interact with the data stream to modify the observation program.

The package is an improved version of a previously-used telescope/spectrometer system. Its major feature is the polarimeter that will allow all four Stokes parameters to be determined, giving the first such data down to about 1,200 Å. Data on possible mechanisms that produce linear and circular polarization effects will also be collected.

The telescope (see figure) is an aplanatic Gregorian with an ellipsoidal primary and a hyperboloidal secondary. This design limits the irradiation of the secondary mirror. By reducing the irradiance, ultraviolet damage to the mirror is prevented, and the instrument sensitivity is preserved. The telescope positioning range is 256 by 256 arc-seconds, and it can make rectangular rasters anywhere within this field.

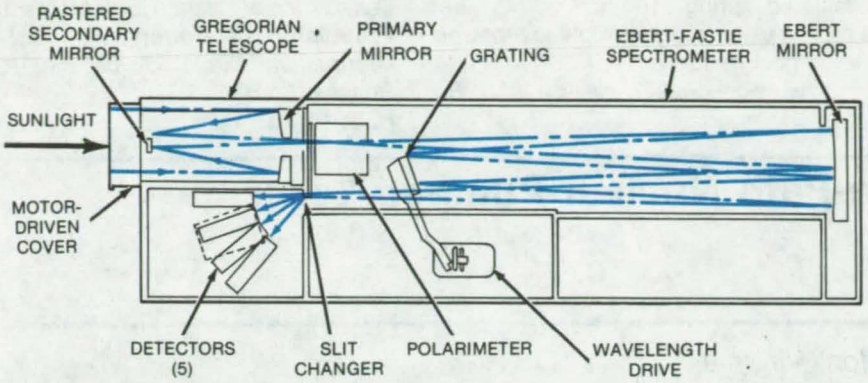

Improved Satellite Instrument Package consists of a telescope, a spectrometer with a polarimeter, five detectors, and control electronics. The instrument is designed to study solar ultraviolet radiations involving the active regions, flares, Sunspots, and corona. The polarimeter will determine four Stokes parameters and possible mechanisms for producing linear and circular polarizations. In addition, aeronomy studies will be performed using density measurements of various constituents of Earth's upper atmosphere.

The Ebert-Fastie spectrometer includes entrance slits, an Ebert mirror, a grating with its wavelength drive, and exit slits with small mirrors to deflect the light to the detectors. There are several types of slit sets: the intensity slits, the spectroscopy slits, the Lyman-α corona slits, and the aeronomy entrance slit.

The polarimeter is located behind the spectrometer entrance slit and consists of two retarders (wave plates), a linear polarizer, and drive mechanisms to insert, extract, and rotate the wave plates. In addition, the spectrometer grating, although not part of the polarimeter, participates in polarization measurement as a partial linear polarizer.

The detectors are photomultipliers operating in the pulse-counting mode. The detector pulse outputs are amplified and directed into either of two data channels. Each channel can send data to the telemetry twice every 64 ms.

The system electronics are controlled by a 4,096-word-memory minicomputer. The computer is controlled by two command channels.

This work was done by Brown Engineering of Teledyne Industries, Inc., for **Marshall Space Flight Center.** *For further information, Circle 36 on the TSP Request Card.*
MFS-25298

An Adjustable Solar Concentrator

This simple low-cost concept accommodates daily and seasonal movements of the Sun.

NASA's Jet Propulsion Laboratory, Pasadena, California

A proposed solar concentrator uses a fixed cylindrical converging lens, a movable parabolic mirror, and a conventional linear collector to accommodate daily and seasonal changes in the Sun's position. The arrangement could efficiently collect solar energy at a high temperature without costly tracking equipment. Solar rays incident on the lens are focused onto the mirror that in turn focuses them onto the collector. The collected heat is taken up by water or other working fluid.

A system would consist of several modules (see figure), each with its long axis in the east/west direction so that solar energy is focused equally well throughout the day. Seasonal changes in the Sun's position are accommodated by the movable mirror. The mirror slides on rails orthogonal to its long axis. During the winter, the mirror is moved up to

(continued on next page)

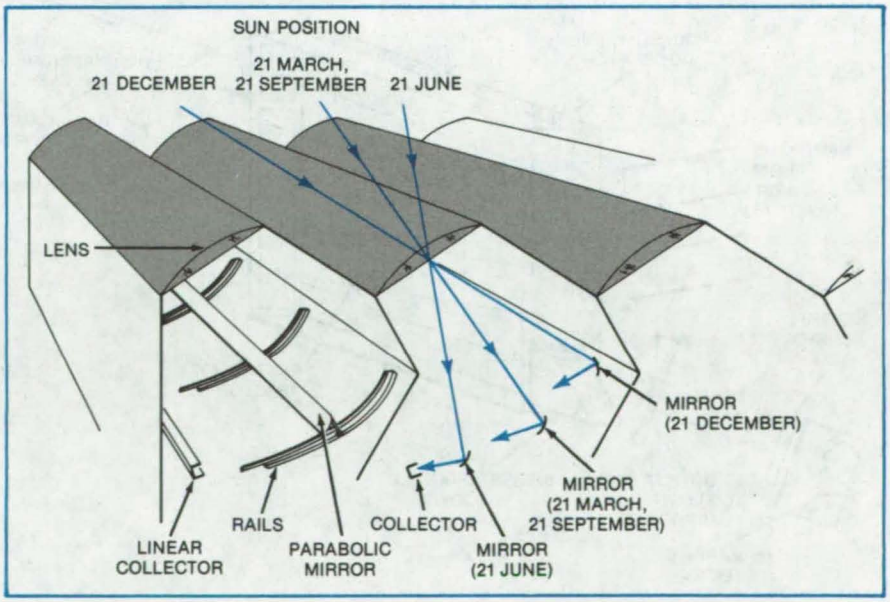

An **Adjustable Solar Concentrator** "follows" the Sun without expensive tracking devices. Each module, as shown above, contains a cylindrical converging lens with its long axis lying east/west. It collects solar energy throughout the day regardless of the Sun's angle. Seasonal adjustments are made by moving the parabolic mirror up or down, depending on the month.

accept the rays at low angles; and during the summer, it is moved down to accommodate the high angles. Intermediate positions are used in the fall and spring. The mirror may be moved using a very simple low-power electrical motor.

This work was done by Earl R. Collins, Jr., of Caltech for **NASA's Jet Propulsion Laboratory.** *For further information, Circle 37 on the TSP Request Card.*
NPO-14710

Large-Volume Multiple-Path Nuclear-Pumped Laser

Mirrors increase
laser-cavity path length.

Langley Research Center, Hampton, Virginia

The output of a nuclear-pumped laser has been increased by using multiple optical reflections to enlarge the lasing-mode volume. The new design requires a lower thermal neutron flux and uses the flux more efficiently by increasing the total area available for neutron capture. The flux needed for lasing approaches that available from a steady-state reactor. Outputs over 100 watts have been reached with $^3He/Ar$ (1.79 μm) at 600 torr and a flux of 3×10^{16} neutrons/cm^2-s.

The laser, as outlined in Figure 1, is made of aluminum cover plates on a stainless-steel frame with a polyethylene neutron moderator on the front and back. Emitted coherent light is reflected back and forth by flat aluminum or gold mirrors on the inside of the frame. Dielectric-coated mirrors outside the frame and close to the Brewster angle windows complete the optical cavity.

A He/Ne laser is used to aline the internal and external mirrors. By varying the angle of the external dielectric-coated mirrors, the number of reflections (and thus the optical path length) can be varied.

Neutrons from a fast-burst reactor are moderated by the polyethylene. These thermalized neutrons enter the optical cavity, which contains ^3He and a minority-species gas, causing $^3He(n,p)^3H$ nuclear reactions to occur. The reactions produce charged particles with a high kinetic energy that ionize and excite the gas mixture to produce an energy-state population inversion in the minority species.

The resulting photon flux is amplified in the optical cavity and escapes through the output mirror in the form of a laser beam. A typical output is shown in Figure 2.

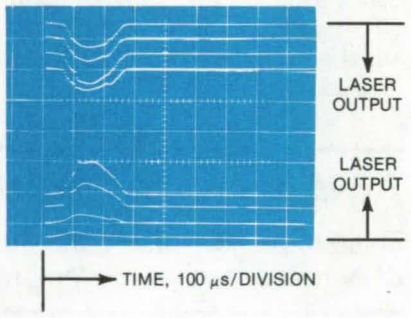

Figure 2. **Typical Output** from a multiple-path laser is shown for a ^3He-and-1-percent-Ar gas at 800 torr. Lasing (1.79 μm) was sensed by an InAr array detector. Peak thermal flux was 2.9×10^{16} neutrons/cm^2-s, and lasing-threshold thermal flux was 8.9×10^{15} neutrons/cm^2-s.

This work was done by Frank Hohl of **Langley Research Center** *and Russell J. De Young of Miami University. For further information, Circle 38 on the TSP Request Card.*

This invention is owned by NASA, and a patent application has been filed. Inquiries concerning nonexclusive or exclusive license for its commercial development should be addressed to the Patent Counsel, Langley Research Center [see page A5]. Refer to LAR-12592.

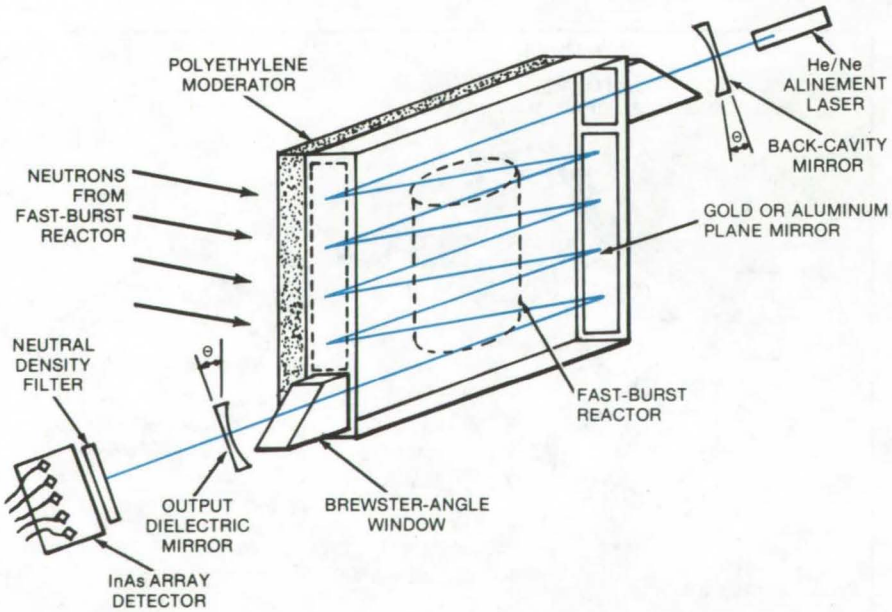

Figure 1. **Multiple-Path Laser** produces a greater output for a given size and neutron flux by replacing the conventional quartz tube with a multiple-reflection cavity. Tested versions are about 40 by 30 by 3 cm with a 5-cm-thick moderator layer front and back. By using transparent cover plates, it should be possible to make a similar laser that is homogeneously pumped by photons.

Extracting Energy From Natural Flow

Three concepts are proposed for extracting the energy from wind, waterflow, and tides.

Marshall Space Flight Center, Alabama

Three suggested flow-energy-converter geometries would utilize flow instability to generate usable energy. The configurations developed in a theoretical study are different from the traditional approach of driving the energy-generating machinery directly with natural flow sources, such as wind, waterflow, and tides. Fluid-flow instability, generally a problem in conventional engineering, is used because it is more efficient in developing a lift than the direct flow. The proposed converters would respond to one of the three instability modes: vortex excitation motion, galloping or plunging motion, and flutter.

The first converter is a spring-mounted cylinder that would oscillate at extremely high amplitudes in response to the vortex excitation. It would respond when the fluid-flow velocity past it reached a critical Strouhal reduced system frequency or reduced velocity value. This reduced velocity could be readily changed to stay tuned to the unstable conditions that generate the extreme cylinder motion. The cylinder movement can be readily converted to usable energy by conventional means, such as magnet/coil interaction.

A possibly even more effective system very much like the first except for the D-shaped cylindrical body (see figure) would respond to the galloping instability. The movement of the body would depend on the flow critical angle-of-attack α. The value of α could be maintained by turning the body when the approach flow velocity would change. This configuration is more attractive than the vortex motion because the oscillations would increase with the flow speed. Again usable energy can be extracted from the oscillation by conventional means as in the first case.

A third converter would respond to flutter — a more complex violent motion caused by the combination of two frequencies. However, this type of system would be more complex to design, and it would be difficult to maintain the unstable conditions.

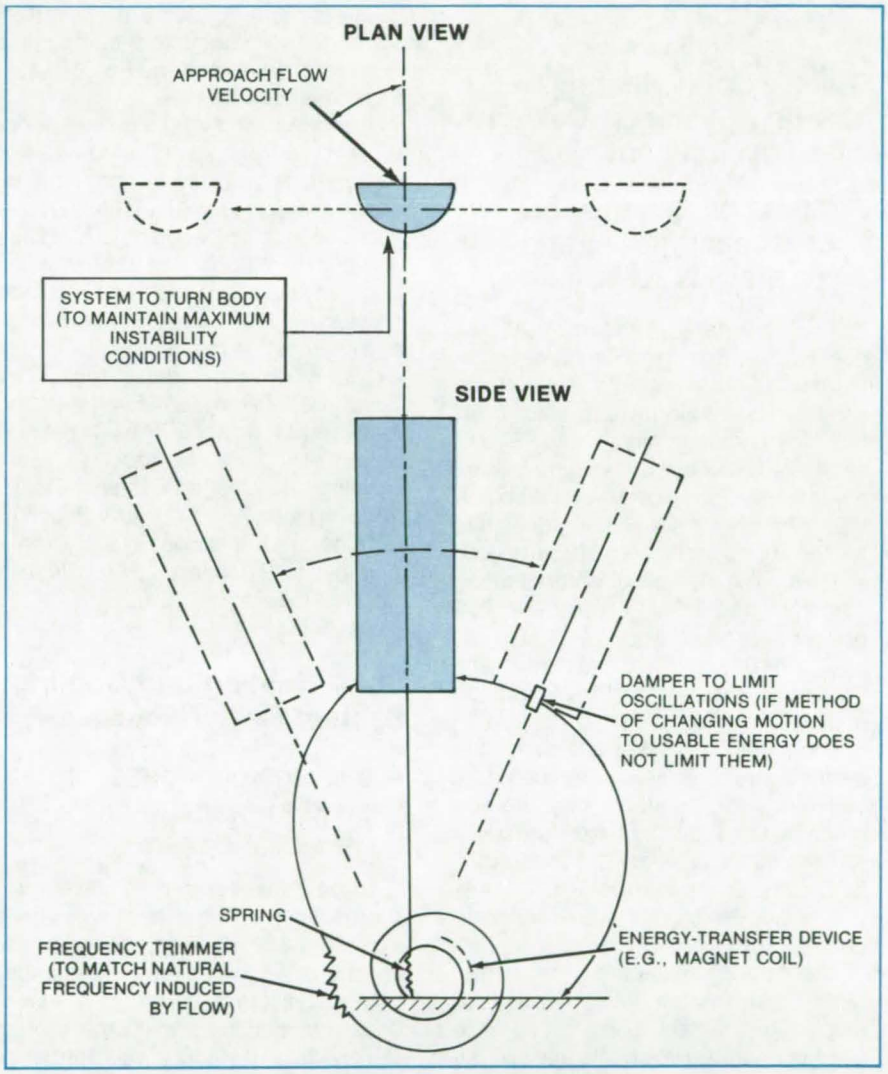

This **Spring-Mounted D-Shaped Body** would oscillate in response to galloping instability in the fluid flow, and the oscillation can be converted to usable energy. To maintain instability, the critical value of angle α could be controlled by turning the body when the flow velocity vector changes.

This work was done by Leon M. Delionback and Gilbert A. Wilhold of **Marshall Space Flight Center.** *For further information, Circle 39 on the TSP Request Card.*
MFS-23989

Books and Reports

These reports, studies, and handbooks are available from NASA as Technical Support Packages (TSP's) when a Request Card number is cited; otherwise they are available from the National Technical Information Service.

Twelve Solar-Heating/Cooling Systems: Design and Development

Progress on systems for houses, apartments, and commercial buildings

Two quarterly progress reports describe the first 6 months of development on 12 solar systems. Six systems are for heating alone, and six are for combined heating and cooling. Two of each type are for single-family, multifamily, and commercial buildings. The systems are being designed for the Minneapolis area. [See related articles "The Design of Solar-Heating Systems" (MFS-25108) on page 209 of *NASA Tech Briefs*, Vol. 4, No. 2, and "The Design of Solar-Heating and Cooling Systems" (MFS-25106) on page 210 of that issue.]

The most likely components for the systems are a liquid-cooled flat-plate collector, a water heat-storage medium, and a gas-fired forced-air furnace as the auxiliary heat source. A heat pump or an electric furnace may be considered as alternative auxiliary heat sources.

The design concept for the single-family solar system calls for two fluid loops. The primary loop, through the solar collector, gives up its energy in a heat exchanger to a secondary loop. The secondary loop incorporates a heat-storage water tank and heats domestic hot water and air for space heating.

The multiple-family system also has two fluid loops. It will heat 12 apartments through coils in the individual apartments, and it heats domestic water through a central heat exchanger.

The commercial-building system is similar but larger, being sized for a one-story, 32,500-ft^2 (3,019-m^2) structure — twice the floor area of the apartment house.

The reports discuss the basic requirements for the systems and present reasons for selecting the system configurations. The single-family, multifamily, and commercial "baseline" systems are described separately, and the major components are listed. A schematic of each system is included.

A section of the first quarterly report is devoted to tradeoff studies, with calculations of insolation in the Minneapolis area, calculations of heat loss and heating load for the buildings, and economic analyses that take into account maintenance and replacement costs, energy cost escalation, and the cost of money.

This work was done by the Energy Resources Center of Honeywell Inc. for **Marshall Space Flight Center.** *To obtain a copy of the reports, "Solar Heating and Cooling Systems Design and Development [Quarterly Report]," 9 July to 9 October 1976 and 9 October to 9 January 1977, Circle 40 on the TSP Request Card.*
MFS-25358

Solar-Heating and Cooling System Design Package

A package of information needed to evaluate one commercial system

Those considering the solar-energy alternative for home heating will be interested in the design package for a commercial system recently installed in a single-family dwelling in Akron, Ohio. Included in the package are the design data brochure, performance specifications, a hazards analysis, a spare-parts list, and detailed drawings. The documentation can help to assess the suitability of the system for a proposed installation.

The system in the Akron Metropolitan Housing Authority home combines a solar-heating unit with a heat pump for summer cooling and backup heat when solar energy is not available. The heat pump also stores offpeak electricity (supplied by utilities at reduced cost) for use during peak hours.

Using Akron solar-insolation levels, the system supplies 35 percent of the average total heating load (based on reasonable expected-load requirements). Potable water at 140° F (60° C) is delivered at a minimum of 5 gal/min (0.32 l/s). The maximum electrical power required to drive the solar portion of the system is 0.7 kW or less, and to drive the complete system, it is no more than 1.2 kW.

The system uses 546 ft^2 (50.7 m^2) of air flat-plate collectors and 27,000 lb (12,000 kg) of rock storage. It includes all the necessary control equipment, air-handling hardware, pumps, and electrical accessories.

This work was done by the Solaron Corp. for **Marshall Space Flight Center.** *To obtain a copy of the package, "System Design Package for a Solar Heating and Cooling System," Circle 41 on the TSP Request Card.*
MFS-25393

Benefit Assessment of Solar-Augmented Natural-Gas Systems

A study details how solar-energy-augmented systems can reduce natural-gas consumption.

A benefit assessment of solar-augmented natural-gas systems has been prepared as a starting point for a more extensive future project. It reveals how solar energy might be effectively utilized to reduce natural-gas consumption by 40 to 70 percent. Technology and economic factors are examined for five applications at less than 350° F (175° C).

For the first area, hot-water systems, the total solar-energy cost is presently estimated at about $14/MBtu ($0.01/MJ) for a single-family unit in a Sunny climate. In mixed climatic zones with frequent rainfall, energy costs are about $21/MBtu ($0.02/MJ). Future improvements are expected to lower energy costs to around $5.50/MBtu ($0.005/MJ) for the Sunny climatic regions.

The second area investigated is solar-assisted, gas, heat pumps for

hot water and heating and cooling space. The authors estimate that the mass-produced solar components could be marketed at about $9,000, and the projected annual household-gas savings would be about 76 MBtu (80.2×10^3 MJ) for a Sunny climate.

In the third area examined, solar energy is collected and stored (e.g., in a water tank) and is then used to heat space directly, to heat water, or to drive a chiller. Currently, direct solar heating and cooling systems do not appear generally competitive with conventional energy systems.

Efficient application of solar energy to industrial processes is limited to temperatures below 350° F (175° C). Examples include hot water or hot air for the food, paper, and chemical industries and water for carwashing, curing concrete, textile processing, laundries, and uranium mills. Such industries consume about 35 percent of industrial natural gas, which could in theory be replaced with solar energy.

Finally, energy savings may be realized on solar-assisted appliances, including furnace water heaters, stoves, dryers, heat pumps, and the like. These items are subject to further investigation before an optimum hybrid system is designed for each one.

This work was done by Edgar S. Davis, Robert L. French, and Robert L. Sohn of Caltech for **NASA's Jet Propulsion Laboratory.** *To obtain a copy of the report, Circle 42 on the TSP Request Card.*
NPO-14568.

Air-Cooled Solar-Collector Specification

Report contains information for evaluating a collector for space heating and cooling.

A short report (17 pages) summarizes performance specifications for a 72-element concentric-tube collector, versions of which have been described in several previous articles in *NASA Tech Briefs.* [See, for example, "Design Review of a Liquid Solar Collector" (MFS-25140) on page 212 of Vol. 4, No. 2.] While much of the material in this document has been covered previously, this report summarizes the essential performance data and includes assembly and installation drawings. It thus can be useful as a quick reference for information on this collector.

The collector will convert at least 1,050 Btu/ft^2 (10.3×10^6 J/m^2) per day under precisely stated conditions, including a 30° F (-1.1° C) ambient temperature and the Sun at equinox. A chart shows the minimum collector efficiency as a function of operating conditions.

This work was done by Owens-Illinois, Inc., for **Marshall Space Flight Center.** *To obtain a copy of the report, "Owens-Illinois Subsystem Design Package for the SEC-601 Air-Cooled Solar Collector," Circle 43 on the TSP Request Card.*
MFS-25336

Indoor Tests of the Concentric-Tube Solar Collector

Report describes thermal performance tests on the 12-tube, liquid-filled version.

The performance of the 12-tube, liquid-filled version of the concentric-tube solar collector (see preceding article) was recently evaluated using a solar simulator at Marshall Space Flight Center. The test procedures and results are documented in a report that is now available.

Testing was in accord with ASHRAE (American Society of Heating, Refrigerating, and Air-Conditioning Engineers) standards. Parameters measured were thermal efficiency, incident-angle modifier, and time constant.

Thermal efficiency is plotted as a function of the inlet temperature for simulated solar-flux levels of 250 and 300 Btu/h-ft^2 (788 and 945 J/s-m^2). The measurements range between about 52 percent at 85° F (29° C) inlet temperature to about 40 percent at 200° F (93° C).

The incident-angle modifier measures the change in efficiency as the Sun tracks from east to west across the sky. It is determined by tilting the collector at 10°, 20°, 30°, 40°, and 50° with respect to the direction of normal incidence and recording the efficiency. From a value of 1.0 at normal incidence, the incident-angle modifier drops to a minimum of 0.81 at a tilt angle of 40°. It rises to about 0.85 at 50°.

The time constant reflects how rapidly the temperature differential across the collector drops to 0.368 of its initial value after the solar flux is cut off. It is 20 minutes for the concentric-tube collector.

This work was done by the Solar Energy Systems Division of Wyle Laboratories for **Marshall Space Flight Center.** *To obtain a copy of the report, "Results of Thermal Performance Evaluation of the Owens-Illinois Sunpak Liquid Solar Collector at Indoor Conditions," Circle 44 on the TSP Request Card.*
MFS-25390

Evacuated-Tube Solar Collector — Performance Evaluation

Report gives curves, tables, and procedures for standard and special tests.

A report presents the procedures and results of thermal performance tests on a commercial evacuated-tube solar collector. Two models of the eight-tube collector were evaluated in a solar simulator.

Water is the working fluid in both models. One model has an outlet manifold 1 inch (2.54 centimeters) in diameter with copper orifices. The other version has a manifold 1-1/4 inches (3.18 centimeters) in diameter with heat-resistant glass orifices. Gross collector area is 17.17 ft^2 (1.6 m^2). The overall external dimensions are 48 by 51.5 by 7.8 inches (121.9 by 130.8 by 19.8 centimeters).

The collectors were subjected to standard thermal performance tests in which ambient air temperature, fluid inlet and outlet temperatures, solar flux, waterflow rate, and efficiency were measured.

The collectors also underwent other special tests. These included:

- a time-constant test to determine

(continued on next page)

how fast the water cools when insolation stops,

- an incident-angle modifier test to determine the variation in collected energy as the Sun moves from east to west, and
- a "hot-fill" test to determine whether the tubes will break if they are accidentally filled with hot water.

This work was done by Wyle Laboratories for **Marshall Space Flight Center.** *To obtain a copy of the report, "Indoor Test for Thermal Performance of the Sunmaster Evacuated Tube [Liquid] Solar Collector," Circle 45 on the TSP Request Card.*
MFS-25339

Glycol/Water Evacuated-Tube Solar Collector

A report on performance of the 8-tube and 10-tube models

The performance of two multitube commercial solar collectors is detailed in a new test report. One collector has 8 tubes with parabolic-trough reflectors; the other has 10 tubes with vee-trough reflectors. Both types use a mixture of 35 percent glycol as the working fluid. The report covers indoor tests made with a solar simulator. The collectors were tested with and without a manifold furnished by the manufacturer as optional equipment.

Each of the tubular elements is glass, with an evacuated jacket and an absorbent coating on the outside of the inner wall. The working fluid travels through a serpentine tube that is in conductive contact with the inner wall. Thus, the fluid loop is not breached if the vacuum jacket is broken. The collectors measure 57.25 by 48 by 3.25 inches (145.4 by 121.9 by 8.2 centimeters). Gross collector area is about 17.4 square feet (1.62 square meters).

The report describes conditions, equipment, and procedures for the tests. It presents data on stagnation tests (temperature rise of noncirculating working fluid), thermal efficiency as a function of inlet temperature and other conditions, time-constant tests (the cooling of working fluid after insolation ends), and incident-angle modifier tests (the variation of efficiency with position of the Sun). Flux maps show the insolation at three points in each collector tube.

The eight-tube collector performs well when the insolation angle is 90°; it is somewhat less efficient when the incidence angle departs from the normal by more than 20°. In fact, the 8-tube version is less efficient at these angles than the 10-tube collector.

For solar cooling, the efficiency of the 10-tube collector is 28 percent, and for the 8-tube collector it is 26 percent. For space heating and water heating, the efficiencies are considerably higher, as expected. Data were also gathered for the 10-tube collector on thermal efficiency with plastic covers.

This work was done by Wyle Laboratories for **Marshall Space Flight Center.** *To obtain a copy of the report, "Indoor Test for Thermal Performance of the G.E. TC-100 Liquid Solar Collector Eight- and Ten-Tube Configuration," Circle 46 on the TSP Request Card.*
MFS-25337

Thermosyphon Heat Exchanger

A report on the final development of a pumpless liquid-to-air heat exchanger

A new report summarizes the final development, testing, and certification for use of a pumpless liquid-to-air heat exchanger for solar-heating systems. The report complements documentation released previously, described in "Passive Heat Exchanger for Solar Heating" (MFS-23914) and "Passive Heat Exchanger — Installation Package" (MFS-23930) on page 214 of *NASA Tech Briefs,* Vol. 3, No. 2.

Water from the storage tank of a residential or commercial solar-heating system flows through finned tubes in the heat exchanger. From there, it returns to the tank. A blower forces air across the fins, transferring the heat from the exchanger to the room. Resistive heating elements can be added to the storage tank for backup heating.

Since the water density increases on cooling, a natural convective flow, or "thermosyphon," is set up in a vertical pipe, which eliminates the need for a pump in the water loop. The exchanger is therefore simpler and less susceptible to failure than many forced-flow units.

The heat exchanger fan is rated at 1,640 ft^3/min (774 l/s). It is operated by a 6.5-A (full-load), 115-Vac motor. The heat output is 35,000 Btu/h (10,250 W) when the water temperature is 120° F (49° C) and the entering air temperature is 70° F (21° C). When the water temperature is 160° F (71° C), up to 74,000 Btu/h (21,680 W) are delivered.

This work was done by James D. Hankins of **Marshall Space Flight Center.** *To obtain a copy of the report, "Development, Testing and Certification of the Sigma Research, Maxi-Therm S-101 Thermosyphon Heat Exchanger," Circle 47 on the TSP Request Card.*
MFS-25389

Controller for Solar-Energy Systems

Prepackaged unit includes electronic and hydronic modules.

A new report describes the operation and final development and testing of a computerized control unit for solar-heating and cooling systems. The prepackaged controller includes the electronics and "plumbing" needed to oversee the operation of a solar-energy system. The components are modular, which allows the configuration to be altered and adapted to different solar-energy systems.

The controller only requires field connection of pipes, power, and sensors. It is programed to receive input on user-defined variables, such as insolation level, room and outside temperatures, the time of day and date, and the storage-tank temperature. When the data are processed to define the appropriate operating mode, pumps, fans, valves, and switches are set to place the system in that mode. Among possible modes are heating from collectors, storing energy, and heating from storage.

Where required, the user has access to the controller through a portable printer. Access features include a 32-hour programable file of selected data, a printout of all input and output, and program editing. Field

loading of software changes is possible through an ASCII-compatible data channel.

The controller electronics are based around a microprocessor. Both ROM (read-only memory) and RAM (random-access memory) are used for program storage.

This work was done by James D. Hankins of **Marshall Space Flight Center.** *To obtain a copy of the report, "Development and Testing of the Sunkeeper Control Corporation Integrated Programmable Electronic Controller and Hydronics Package — Final Report," Circle 48 on the TSP Request Card.*
MFS-25386

Controller and Temperature Monitor for Solar Heating

A new report describes the final development and certification for public use.

The 77-171 controller is a differential thermostat with relay output for controlling a solar-heating or cooling system. It can be used with or without the 77-180, a temperature monitor that displays the indoor, outdoor, and storage temperatures. Both units, available commercially, were recently tested and certified for public use. A summary of their final development is described in a new report that is available on request.

The design package for these units is described in a previous article in *NASA Tech Briefs*. [See "Controller for Solar Heating — Design Package" (MFS-25009) on page 61 of Vol. 4, No. 1.] The new report contains a summary of their operation and performance specifications. It also references other applicable documents.

A brief summary of the background of the development program for these units is given in the report. The summary describes how this program meshes with the larger solar-energy development program managed by NASA and the Department of Energy. The larger program is part of the national effort to implement aspects of the Solar Heating and Cooling Act of 1974.

This work was done by James D. Hankins of **Marshall Space Flight Center.** *To obtain a copy of the report, "Development and Testing of the Solar Control Corporation Modular Controller and Solarstat Subsystem," Circle 49 on the TSP Request Card.*
MFS-25387

Inhibiting Corrosion in Solar-Heating and Cooling Systems

Water additives were tested in a 1-year study.

The initial phase of a program to evaluate corrosion-inhibiting additives for solar-heating and cooling systems is described in a 16-page report. A followup to this work is described in "Corrosion Inhibitors for Solar-Heating and Cooling Systems" (MFS-25023) on page 525 of *NASA Tech Briefs*, Vol. 3, No. 4.

The initial study tested 12 inhibitors, 4 of which were also evaluated in the followup. The 12 include commercial products recommended for automotive cooling systems along with several special formulations based on sodium salts.

Water, containing selected corrosive additives, was the test medium. Specimens of aluminum, steel, stainless steel, and copper were immersed at 80° C in solutions of the corrosive water mixed with the inhibiting agents. After 1 year of exposure, the specimens were removed, cleaned, and weighed.

Four of the formulations showed good promise as inhibiting agents (although the followup study revealed problems with two of these in protecting thin aluminum specimens). Others showed varying degrees of promise, depending on the temperature range and the particular metal exposed.

This work was done by G. E. DeRamus, Jr., and T. S. Humphries of **Marshall Space Flight Center**. *To obtain a copy of the report, "Corrosion Inhibitors for Solar Heating and Cooling Systems," Circle 50 on the TSP Request Card.*
MFS-23763

Computer Programs

These programs may be obtained at very reasonable cost from COSMIC, a facility sponsored by NASA to make new programs available to the public. For information on program price, size, and availability, circle the reference letter on the COSMIC Request Card in this issue.

Numerical Tracing of Electron Trajectories

For analysis and design of electron-imaging systems

The TRAJEC computer program aids the analysis and design of electron imaging systems. TRAJEC can integrate the path of a relativistic electron through a region of nonuniform, static electromagnetic fields to an accuracy of 1 micrometer in 10 centimeters. A fourth-order Runge-Kutta method with error estimation (a Kutta-Merson procedure) is used to integrate the motion equations. The force evaluation uses a third-order Legendre interpolation of the electrical potential.

The program easily interfaces with various forms of user-defined electric potentials and magnetic fields. It may be implemented interactively so that the analyst might freely experiment with combinations of trajectories and gain insight into the aberrations inherent in the imaging system under study. Several methods are provided for analyzing the imaging properties of the device under study.

The trajectory of a single electron injected from any point with arbitrary initial velocity may be studied. Lines of electrons may be studied to test linear imaging properties. TRAJEC also allows for studies of Monte Carlo point sources of electrons to simulate the characteristic emissive properties of photocathode materials and their effects on the images produced. TRAJEC has been used to evaluate

(continued on next page)

and modify designs for an imaging device used on the NASA Space Telescope.

The TRAJEC program is written in FORTRAN IV for batch or interactive execution and has been implemented on a DEC PDP-10 with a central memory requirement of 14K of 36-bit words and on a CDC 6000-series machine with a central memory requirement of 37K (octal) of 60-bit words. TRAJEC has also been utilized on PDP-11, CYBER 70, and CYBER 170-series machines. TRAJEC was developed in 1979.

This program was written by T. N. Delmer and T. C. Stephens of Science Applications, Inc., for **Goddard Space Flight Center.** *For further information, Circle A on the COSMIC Request Card.*
GSC-12535

NASA Charging Analyzer Program

Dynamic simulation of electrostatic charging of 3D objects

NASCAP (NASA Charging Analyzer Program) is able to predict how an object made of conducting sections, which may be entirely or partially covered with thin dielectric films, responds to a specified charged-particle environment with or without solar illumination. The environments of interest are those found in the Earth's magnetosphere and in a ground-based test chamber designed to simulate spacecraft charging effects. When Sunlight is present, shadowing is taken fully into account. NASCAP divides the spacecraft charging problems into two sections: (1) the tendency of materials to accumulate and emit charge when subjected to plasma environment and (2) the consequent response of the charged-particle envronment to the electrostatic field of an object. Both of these sections are treated in sufficient detail to simulate the charging of a complex satellite.

NASCAP includes formulations for electron backscatter and secondary emission, photoelectron emission, and proton-generated secondary electron emission. Dielectric constants and finite conductivity are also taken into account.

The response of the charged-particle environment to the electrostatic field of an object requires the calculation of the electric potentials on and near complex objects and the determination of how those potentials influence charged-particle trajectories. The electrostatic potential about the satellite or in the test tank is calculated by NASCAP, by using a finite-element formulation of Poisson's equation.

The computational space consists of an arbitrarily large number of nested cubic meshes. The resulting set of linear equations is solved using the Conjugate Gradient technique. The satellite or test object is defined within the innermost mesh and may have surfaces normal to any of the 26 cubic symmetry directions. It consists of one or more conductors that may be covered with thin dielectric layers. The conductors may be floating, held at fixed potentials, or biased relative to one another.

The net charge accumulation by each surface cell of the satellite is calculated in the presence of the electrostatic and magnetostatic fields about the satellite and specified environmental characteristics. In the ground test case, the incident flux is determined by forward trajectories from an electron source. In the space case, the incident flux of electrons and ions at surfaces is determined using the reverse trajectory sampling method. The ambient plasma may be isotropic and Maxwellian.

NASCAP has facilities for extensive graphical output, including several types of object display plots, potential contour plots, space charge density contour plots, current density plots, and particle trajectory plots.

NASCAP is written in FORTRAN V for batch execution and has been implemented on the 1100-series computer with a central memory requirement of approximately 62K of 36-bit words.

This program was written by J. J. Cassidy III, J. M. Harvey, I. Katz, and M. J. Mandell of Systems, Science & Software for **Lewis Research Center.** *For further information, Circle B on the COSMIC Request Card.*
LEW-12973

Materials

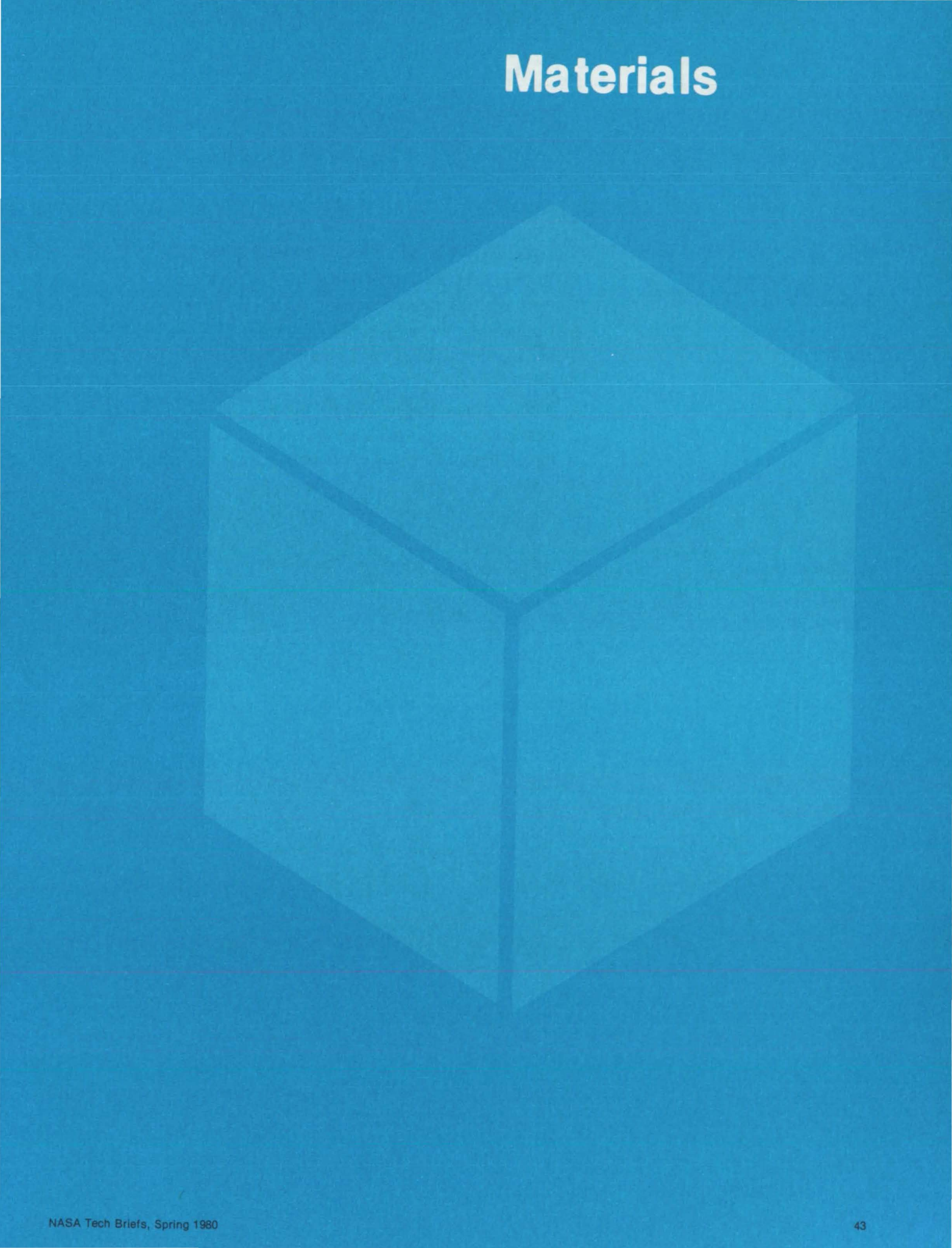

Containerless Materials Processing in the Laboratory

Drop tube makes possible the preparation of exotic materials.

Marshall Space Flight Center, Alabama

Containerless, zero-gravity materials processing, usually considered possible only in space, can now be carried out in the laboratory, using a drop tube developed at Marshall Space Flight Center. The apparatus makes possible various metastable and supercooled structures that cannot be reached easily by conventional processing. Among such structures are single crystals of high-temperature metals, bulk samples of metastable alloys and compounds, amorphous and glassy materials, and high-temperature superconductors.

The absence of a container means reduced possibility for contamination; and zero gravity implies an absence of convection currents and sedimentation, both of which disturb the uniformity of a molten sample as it solidifies. The net effect is to encourage homogeneity and supercooling, which allow the development of unusual new structures and better-quality conventional structures.

The apparatus (see figure) is similar to towers previously used to prepare spherical lead shot; however, it has substantial improvements that allow more precise control of the sample composition, shape, and environment. As shown, the primary component is a vertical stainless-steel drop tower. Samples are melted in a bell jar at the top of the tower, and the molten drops fall through the 100-foot (30.4-meter) tower to a detachable receiving chamber or "catcher" at the bottom. If the melt temperature and tower atmosphere are properly controlled, the drops are completely solidified when they reach the catcher.

The tower can be evacuated by a turbomolecular pump and a mechanical roughing pump. An inert-gas supply allows backfilling with a low-pressure inert gas. The progress of the drop as it falls can be photographed and monitored through viewing ports in the bell jar and along the tube. An optical pyrometer measures the melt temperature.

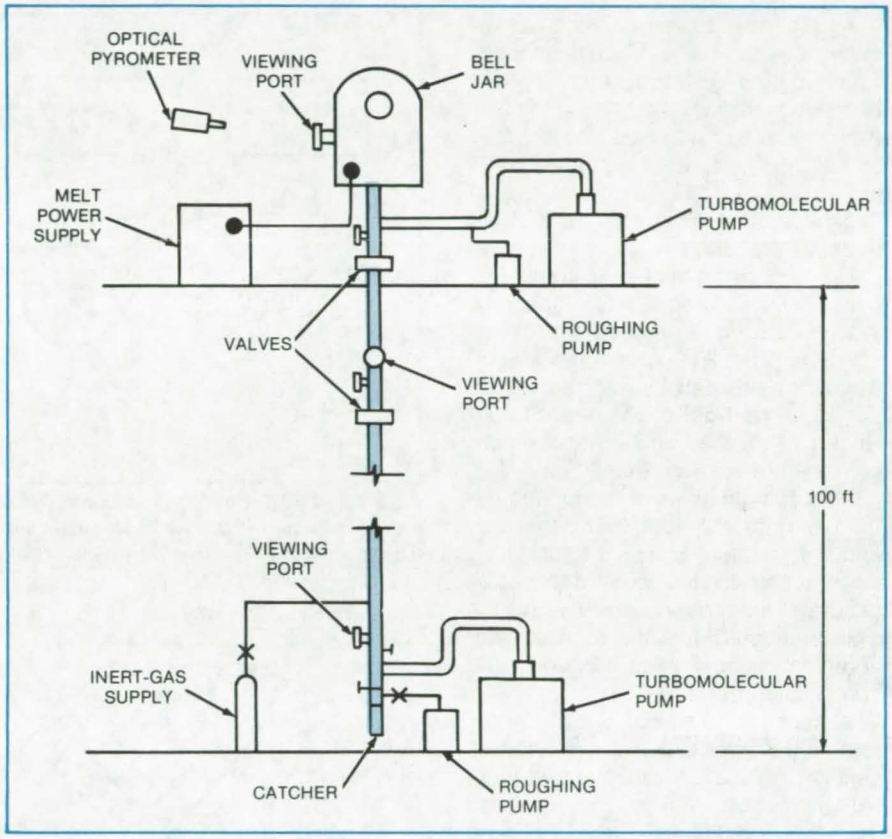

The 100-Foot Drop Tube is oriented precisely vertical to prevent a free-falling drop from hitting the tube walls. An inert-gas supply, evacuation pumps, viewing ports, and flexibility in the choice of melt technique allow precise control and monitoring of the solidification.

There is considerable flexibility in the method of melting and releasing the sample. One approach is to suspend it as a solid from a fine wire, then to melt it by electron bombardment or laser heating until it drops from the wire. Another technique is to melt the sample in a crucible fitted with a capillary tube. Drops of molten material form and are released from the end of the capillary.

This work was done by Lewis L. Lacy, Daniel B. Nisen, Thomas J. Rathz, and Michael B. Robinson of **Marshall Space Flight Center.** *For further information, Circle 51 on the TSP Request Card.*

Inquiries concerning rights for the commercial use of this invention should be addressed to the Patent Counsel, Marshall Space Flight Center *[see page A5].* *Refer to MFS-25242.*

Measuring Coal Deposits by Radar

Thickness is measured directly as a frequency difference, eliminating the need for a local oscillator.

Marshall Space Flight Center, Alabama

A recently tested system determines the thickness of coal deposits by measuring the frequency difference between microwave signals reflected from the face and back of the deposit. The system has gaged deposits 2 to 24 inches (5 to 61 centimeters) in thickness, distinguishing them from underlying shale.

Unlike conventional radio-frequency coal-thickness monitors, the new system does not compare both reflected signal frequencies with the source frequency. Instead it uses the reflection from the front of the deposit as a reference for the back-surface signal.

In the new system (see Figure 1), a 100-Hz triangular wave modulates the frequency of a 2- to 4-GHz oscillator, and the resultant signal is beamed by an antenna to the coal deposit. A separate antenna receives both the signal reflected from the front surface and the signal reflected from the coal/shale interface.

Although the front- and back-reflected signals arrive at the antenna simultaneously, the back-reflected signal traveled a longer distance and therefore originated earlier in time than the front reflection. The back reflection therefore has a lower frequency than the front-surface signal (see Figure 2), and the frequency difference is a measure of the extra travel time. The two signals are combined in a mixer diode to generate the difference frequency, and this signal is used to give a readout of the thickness of the coal layer.

The new system avoids several difficulties inherent in previous radar coal-thickness monitors. In a conventional system, the two received reflections are mixed with the local oscillator signal, and the composite signal is processed to determine the range to the front and the range to the back of the deposit. The thickness is then found by subtraction.

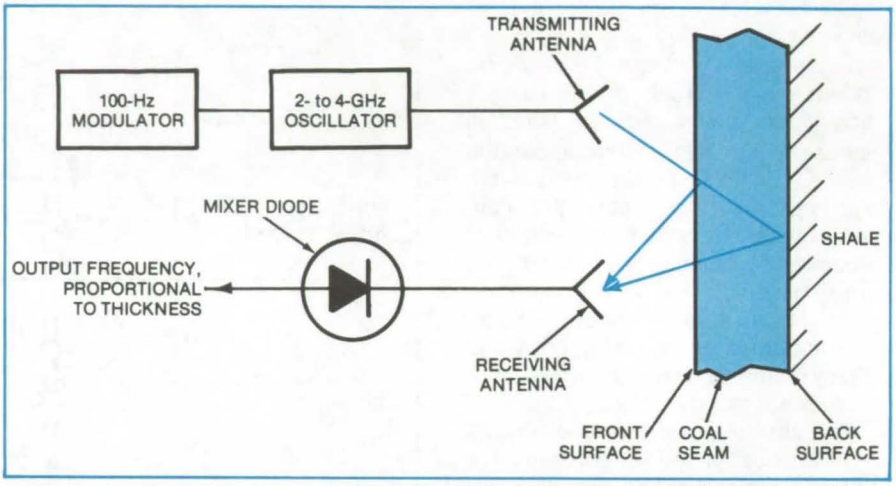

Figure 1. The **Front-Surface Local-Oscillator Radar** compares the frequency of the signal reflected from the back surface of a coal deposit with that reflected from the front surface. Previous systems compared both signals to a separate local-oscillator signal.

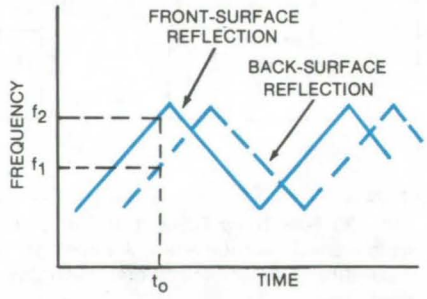

Figure 2. **Reflections From the Front and Back** of a coal deposit, received at time t_0, have different frequencies (f_1 and f_2) because they originate at different times from the frequency-modulated transmitter. The frequency difference represents the travel time through the coal and hence its thickness. The displacement between the curves is exaggerated in this figure.

In contrast, the mixer output in the new radar is a direct measure of thickness; only a frequency-to-thickness conversion is needed. Moreover, masking of the weak back reflection by the strong front reflection is greatly reduced, since the two reflections are not detected separately but in combination. Another benefit of the new system is that it is not sensitive to extraneous reflections from targets between the transmitting antenna and the coal surface, since no target information is generated until the front-surface reflection arrives at the mixer.

This work was done by Thomas A. Barr of **Marshall Space Flight Center.** *No further documentation is available.*
MFS-23922

Detecting a Coal/Shale Interface

The depth of cut is determined by combining penetrometer and reflectometer measurements.

Marshall Space Flight Center, Alabama

A prototype coal/shale interface detector combines the outputs of two optical reflectometers with that of a penetrometer. Eventually, it will be used on a longwall shearer to determine when the cut has pierced through the coal layer. Tests on the prototype in a mine show that the basic design is workable.

In the prototype, an accelerometer measures the hardness of the material struck by the penetrometer ram, while the reflectometers measure the reflectivity of the surface on both sides of the penetrometer. The signals are then combined in a voting circuit that indicates "coal" or "shale" depending on the information supplied by the three sensors.

As shown in Figure 1, one end of the penetrometer ram is hardened for striking the mine wall. The accelerometer is attached to the opposite end of the ram. The ram shaft is reciprocally driven by a spring attached to a supporting collar, and the collar is moved by linked, pivoted arms driven by a motor. As the ram strikes the mine wall, the spring compresses, preventing the impact head from damaging the surface.

The penetrometer distinguishes between coal and shale by the differences in the accelerometer waveforms for the two materials. As shown in the inset to Figure 1, the spike corresponding to shale is taller and sharper than that for coal, because shale is usually harder than coal. (There can be exceptions to this qualitative result, which is why the penetrometer output is compared to the reflectometer signals.) Discriminating circuitry can distinguish between the two signal characteristics.

The reflectometers are standard commercial units. Each includes a light source and a light-sensitive switch that trips when the reflected light exceeds a preset threshold.

The detection circuitry is shown in Figure 2. One threshold detector is biased at 6 volts, which for the prototype is the maximum accelerometer output when the ram is impacted against coal. The triggered one shot that follows the threshold detector is normally in its high state, but it goes low when the 6-volt level is exceeded (i.e., when shale is encountered).

The accelerometer output is also applied to a threshold detector that puts out a high state when the input exceeds 1 volt. At the 1-volt level (see Figure 1), the signal width is 464 microseconds for coal and 396 microseconds for shale.

A cutoff of 450 seconds is selected to distinguish a coal pulse from a shale pulse. A 450-microsecond one shot that triggers on the leading edge of the pulse is applied to the disable input of a one shot that triggers on the pulse trailing edge. Thus, the second one shot fires only if the initial pulse width exceeds 450 microseconds. Ultimately, the AND gate output of the penetrometer is enabled only if the accelerometer pulse amplitude is between 1 and 6 volts and the pulse width exceeds 450 microseconds. Of course, these values are unique to the particular penetrometer selected and would vary with impact frequency and amplitude.

The penetrometer AND gate output is supplied to the voting circuit along

(continued on next page)

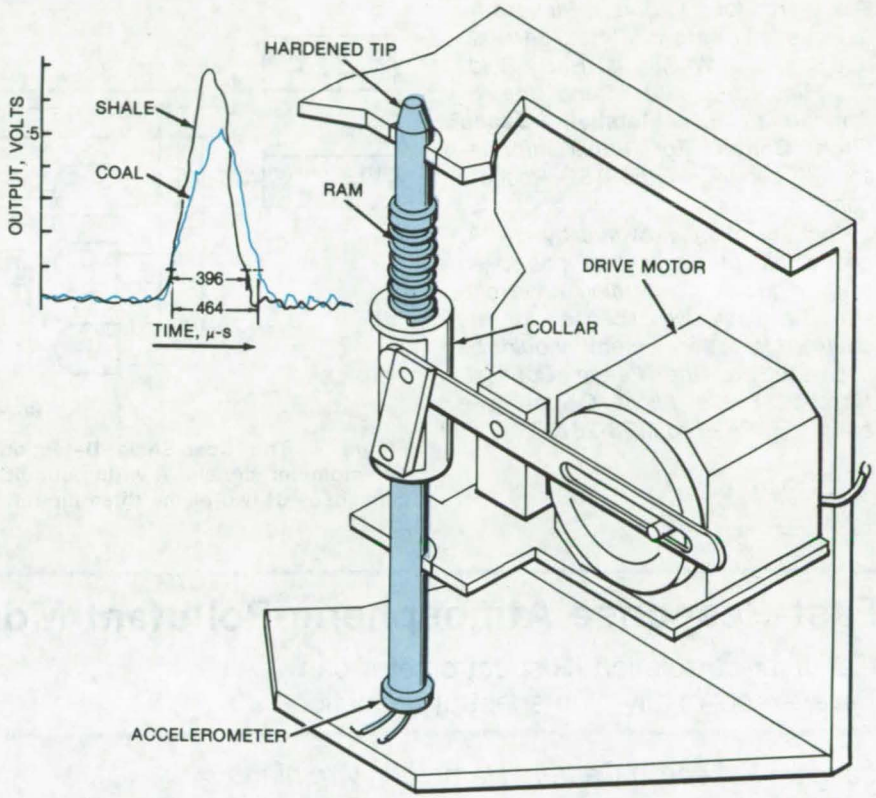

Figure 1. The **Penetrometer Portion** of the coal/shale interface detector includes a motor-driven ram with an accelerometer at the back end. Representative accelerometer outputs for coal and for shale are shown in the inset. The coal signal is identified by its broader width and lower height as compared to the shale signal.

with the reflectometer outputs, which are at logical "1" for low-light conditions (for coal). The voting circuit output is high only if two of the three inputs indicate the presence of coal. In this case, the coal indicating light is turned on. If the voting circuit output is low, the "shale" light is activated.

This work was done by Peter H. Broussard, John L. Burch, Richard A. Campbell, Edward J. Drost, Jerry L. Hudgins, Paul W. Morris, Harry Reid, Jr., Richard J. Stein, and Joe E. Zimmerman of **Marshall Space Flight Center.** *For further information, Circle 52 on the TSP Request Card.*

This invention is owned by NASA, and a patent application has been filed. Inquiries concerning nonexclusive or exclusive license for its commercial development should be addressed to the Patent Counsel, Marshall Space Flight Center [see page A5]. *Refer to MFS-23720.*

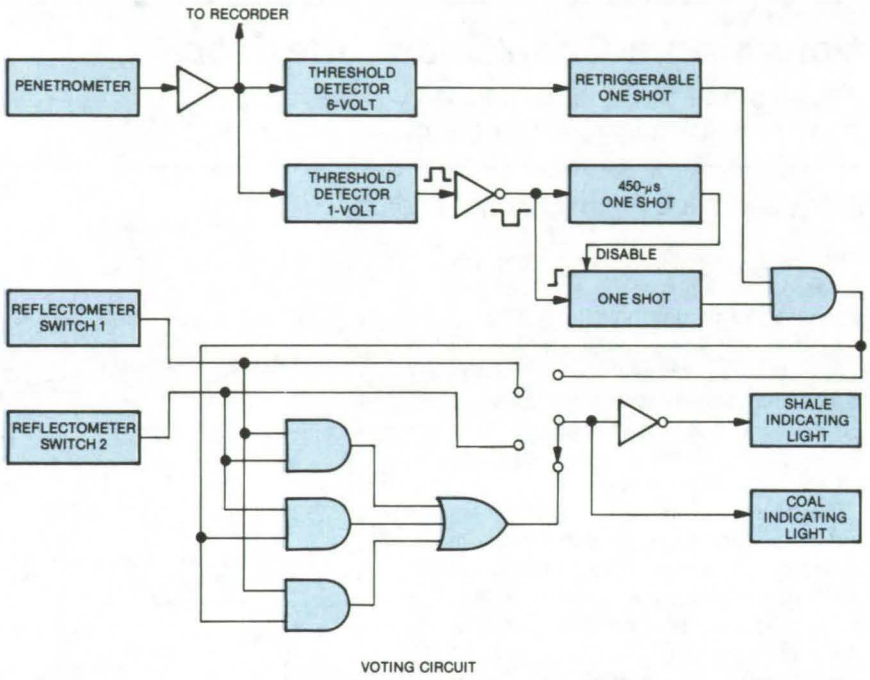

Figure 2. The **Coal/Shale Detection Circuit** processes the penetrometer and reflectometer signals. A voting circuit indicates "coal" or "shale" according to the consensus of two of the three inputs.

Fast-Response Atmospheric-Pollutant Monitor

Gas-filter-correlation IR spectrometer can have exceptionally-high spectral resolution.

Langley Research Center, Hampton, Virginia

A fast-response spectrometer has been used successfully to measure atmospheric CO, CH_4, and HCl over the range of 1 to 12 ppm. The instrument employs a modification of recent nondispersive infrared techniques, chosen for their greater resolution compared to dispersive measurements. The tested field version is relatively compact and includes its own IR source. With additional development and appropriate modifications, a similar spectrometer could measure other pollutants and use natural light as a source.

The nondispersive measurement requires no prisms or gratings. A cell filled with the gas to be measured is used to filter out selectively the spectral lines of interest. The amount of IR radiation passing through the gas-filled cell is compared to that passing through the atmosphere and an empty cell. The difference between the amounts of radiation transmitted varies with the amount of gas (of interest) in the atmosphere.

The main components of the instrument are shown in the illustration. Radiation from an IR source is focused to pass through one of several cells on a rotating disk. Ten of these cells are specifying cells; they are filled with either pure CO, CH_4, or HCl gas to attenuate the IR signal as strongly as possible at their absorption spectrum wavelengths. Nine of the cells are reference cells; they may be evacuated or may contain a nonabsorbing gas. Chopped signals are produced with an amplitude difference depending on the amount of test gas in the atmosphere (the greatest difference being when none of the gas is present).

The transmitted radiation intensity is measured by a detector that is preceded by a narrow-band-pass filter, which passes only a small part of the absorption band of interest. The filter reduces the effects of interfering gases and source variations with wavelength. The magnitude of ΔV (the change in signal for the specifying and reference cells) depends on the concentration of gas in the atmosphere. Signal ΔV is divided electronically by V_S (the detector output when the specifying cell is in the light path). Since V_S does not vary with gas concentration in the atmosphere, this procedure can be used to eliminate output-signal variations due to fluctuations in the IR source.

The signal-processing circuitry amplifies and separates the specifying and reference cell signals based upon their different frequencies. It adjusts to a null signal for a zero concentration of the test gas and divides the output signal by V_S. Varying integration times and input voltage control

are used to adjust sensitivity to span a range of gas concentrations. Output is displayed on panel meters and monitored by a strip-chart recorder.

The instrument is zeroed electronically and calibrated with a standard calibration cell containing a known amount of the gas of interest. The lowest detectable concentration for CO, CH_4, and HCl is about 5 ppm with a 1-meter light path and 1-second time constant. Placing the IR source farther away and increasing the signal-integration time constant can greatly lower the minimum detectable concentration. (Field tests were made with a 50-m light path.)

Although other atmospheric constituents can interfere with this type of measurement, tests have shown these effects on CO, CH_4, and HCl measurements to be negligible at the concentrations normally present in the atmosphere.

This work was done by Daniel I. Sebacher of **Langley Research Center.** *Further information may be found in NASA TP 1113 [N78-13408/NSP], "A Gas Filter Correlation Monitor for CO, CH_4, and HCl" [$4.50]. A copy may be purchased [prepayment required] from the National Technical Information Service, Springfield, Virginia 22161. LAR-12317*

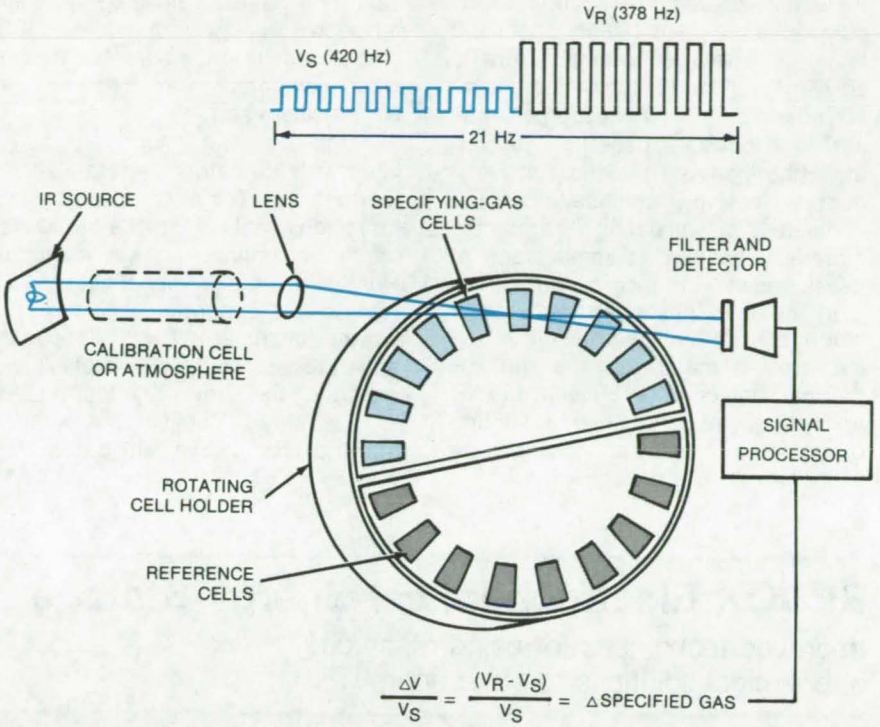

Nondispersive Trace-Gas Analyzer measures atmospheric concentrations of CO, CH_4, and HCl. A quartz lamp is used as the source for CH_4 and HCl, and a glowing SiC rod is used for CO. The IR signal after near-total absorption by gas in the specifying cell (V_S) is chopped at 420 Hz (42 rps times 10 cells), and the signal passing through the atmosphere (or calibration cell), V_R, is chopped at 378 Hz.

Fire Tests for Airplane Interior Materials

Selecting laboratory fire tests for accurate ranking of aircraft materials according to safety

Lyndon B. Johnson Space Center, Houston, Texas

A study conducted by Johnson Space Center identified reliable laboratory fire tests for evaluating the safety of airplane interior materials. Many of the existing laboratory procedures have been inaccurate in predicting how the materials would perform in actual aircraft fires, making it difficult to rank the materials according to safety. New large-scale simulated fire tests were performed in a salvaged airliner fuselage, and the results were compared with some modern laboratory tests. The conclusions are that several laboratory tests can be used to rank the materials according to heat and smoke production rates. None of the existing tests, however, is accurate in characterizing the toxic gas emissions.

The study detailed in a report, "Development of Fire Test Methods for Airplane Interior Materials," was conducted in four phases. The first involved a series of tests performed in a salvaged jetliner fuselage to determine the best methods of simulating postcrash and in-flight fires. Two "design" fire sources were selected: One simulating a crash used Jet A fuel ignited in the fuselage midsection, and the other simulating in-flight fire used a pair of polyethylene trash bags filled with paper towels, paper cups, and polystyrene glasses also ignited inside the fuselage. The characteristics of each were recorded and used as reference for a new quartz-lamp propane burner simulator that could duplicate each of the two conditions in the large-scale tests.

In the second phase, large panels of each test material were lined against the fuselage sidewall and tested one by one under each of the two conditions. The heat from the lamps and the burner was closely controlled. A total of five existing (baseline)

(continued on next page)

materials was tested, which included polyurethane foam (seat cushion), fabric-back vinyl (covering material), polyvinyl fluoride/epoxy-fiberglass/polyamide phenolic honeycomb sandwich (sidewall panel), carbonate (thermoplastic), and polyvinyl fluoride/ polyvinyl chloride/aluminum laminate (sidewall panel). Eleven new materials that are at some stage of development were also tested.

In the third phase six well-known laboratory fire tests were used to test the above materials: the Mettler thermal balance, a bunsen burner test, a radiant-panel test, a limiting oxygen-index test, an Ohio State University release-rate apparatus, and a National Bureau of Standards (NBS) smoke-density chamber. The results were compared with those of the large-scale tests.

Large-scale test results were correlated with laboratory test data in the fourth phase. The most accurate tests for ranking heat and smoke production of thermosetting organic materials were the radiant-panel test, the release-rate apparatus, and the NBS smoke chamber. The release-rate apparatus stands the best possibility of predicting the large-scale test results.

This study is published in a report that includes all the test parameters and other technical details about the tests. The test setups are illustrated in great detail.

This work was done by Everett A. Tustin of The Boeing Co. for **Johnson Space Center.** *Further information may be found in NASA CR-14568 [N79-19112/NSP], "Development of Fire Test Methods for Airplane Interior Materials" [$11.75]. A copy may be purchased [prepayment required] from the National Technical Information Service, Springfield, Virginia 22161.*

MSC-18478

REDOX Electrochemical Energy Storage

Improved techniques for using reservoirs of chemical solutions to store energy

Lewis Research Center, Cleveland, Ohio

A REDOX electrochemical storage system utilizes the oxidation and reduction reactions of two fully soluble REDOX couples to store and deliver electrical charge. Early developments in this technology were reported in *NASA Tech Briefs*, Vol. 1, No. 1, p. 78, "REDOX — Electrochemical Energy Storage" (LEW-12220). Recently, several advances have been made in this area, and prototypes have been built and tested.

The REDOX couples currently used are acidified chloride solutions of chromium (Cr^{+2}/Cr^{+3}) and iron (Fe^{+2}/Fe^{+3}). Reactant solutions are stored in tanks outside the power conversion section in which the charging and discharging reactions take place at inert electrodes. This separation of power conversion from storage is an important system design advantage. The solutions are pumped through the porous electrodes separated by a highly-selective ion-exchange membrane. The membrane prohibits the passage of iron and chromium ions and yet allows easy passage of chloride and hydrogen ions. The reactant solutions are currently 1.0 molar in iron chloride and chromium chloride and 2.0 normal in hydrochloric acid. The electrodes are highly-porous carbon felt. The chromium electrode is inexpensively catalyzed to make the chromium reactions reversible and efficient. The power conversion unit consists of a stack of cells connected together in parallel hydraulically and in series electrically. These stacks closely resemble fuel-cell batteries and water electrodialysis equipment. There are no particular temperature requirements, and operating conditions vary from -18° to +60° C. The system is 99 percent ampere-hour efficient and 75 percent watt-hour efficient. It is estimated that over a span of 25 to 30 years only a 25-percent capacity loss could occur.

Recent achievement of advancements in the ion-exchange membrane separators and electrocatalyst technologies has brought this energy-storage concept to the point where complete systems have been designed, built, and tested. Several novel features (rebalance cell, open circuit voltage cell, and trim cells) have been conceived and incorporated into complete REDOX systems that greatly enhance their ability to be kept in proper charge balance, to be capable of internal voltage regulation, and to be treated as true multicell systems rather than as many cells that are wired together.

Applications of a REDOX system will include remote power systems that are supplied either by solar-photovoltaic arrays or wind turbine generators, in traditional utility systems to reduce the need for peaking generators, and in load leveling for industry. At present, the technical requirements for solar-photovoltaic systems have been met. The development program presently underway is expected to achieve a lowered membrane resistivity that will meet electric utility requirements.

The present cost estimate for a REDOX storage system is the sum of about $325/kW of power required plus $51/kWh of storage capacity. This estimate is based on a power density of 80 watts/ft^2 (861 watts/m^2) in the power conversion section. For a 10-kW, 400-kWh application, the REDOX storage system would cost $24,000, half that of a lead-acid rechargeable battery system. A reasonable quantity market for REDOX systems will reduce the unit cost and would stimulate enough demand for

chromium chemicals to warrant the use of proved low-cost large-scale manufacturing processes. Although no detailed cases have been analyzed, it is estimated that REDOX cost could then be reduced to approximately $163/kW plus $20/kWh in sizes from stand-alone isolated installations to utility-sized storage. This would amount to about $9,360 for the 10-kW, 400-kWh application, less than one quarter the lead-acid battery system cost.

This work was done by Lawrence H. Thaller of **Lewis Research Center.** *Further information may be found in:*

NASA TM-X-71540 [N74-21688/NSP], "Electrically Rechargeable REDOX Flow Cell" [$4], and NASA TM-79186 [N79-26505/NSP], "Recent Advances in REDOX Flow Cell Storage Systems" [$4].

Copies of these reports may be purchased [prepayment required] from the National Technical Information Service, Springfield, Virginia 22161.

A copy of AIAA Terrestrial Energy Systems Conference 70-0989, "REDOX Flow Cell Energy Storage System," may be obtained from the American Institute of Aeronautics and Astronautics, Inc., 1290 Avenue of the Americas, New York, New York 10019.

Copies of U.S. Patent 4,159,366, "Electrochemical Cell for Rebalancing REDOX Flow Systems" [filed June 9, 1978], and U.S. Patent 3,996,064, "Electrically Rechargeable REDOX Flow Cell" [filed August 22, 1975], may be obtained at cost from the U.S. Patent and Trademark Office, Washington, D.C. 20231.

Inquiries concerning rights for the commercial use of this invention should be addressed to the Patent Counsel, Lewis Research Center [see page A5]. Refer to LEW-13398.

Additive Improves Engine-Oil Performance

Engine wear and the frequency of oil changes are reduced by low concentrations of tricresyl phosphate.

Goddard Space Flight Center, Greenbelt, Maryland

Tricresyl phosphate (TCP) is a well-known "extreme pressure additive" for engine oil that substantially reduces the wear rate and may extend the interval between oil changes. It does this by reacting with the fresh metal surfaces that are created as the engine parts slide past each other to form a phosphate film coating that inhibits further wear. In addition to its use as an engine additive, TCP has also been found to give substantial performance improvements in ball bearings installed in spacecraft. NASA is now considering it as an additive for all diesel and motor-vehicle engine crankcases.

The accompanying table shows the results of chemical analyses of crankcase oil changes in diesel-electric generators both with and without TCP. Eight changes, each after 250 hours with no additive, are compared with eight changes, each after 250 hours, and three changes, each after 500 hours, with 5 percent by volume TCP. Except for the tin content, the origin of which is still being investigated, the metallic and SiO_2 concentration rates were significantly lower in the samples with TCP. By these tests, the oil-change interval was extended from 250 hours to 2,000 hours without a significant increase in wear rates.

TEST CONDITIONS	CONCENTRATION OF METAL (ppm/h×10^{-2})					
	Fe	Al	Cu	Cr	Sn	SiO_2
Eight 250-h Changes (Without TCP)	7.75	1.60	1.25	0.60	0.55	5.35
Eight 250-h Changes (With TCP)	5.70	0.50	1.55	0.50	0.40	3.25
Percent Change	-26.5	-68.8	+19.4	-16.7	-27.3	-39.3
Three 500-h Changes (With TCP)	3.00	0.53	0.60	0.20	0.73	1.54
Percent Change From Values Without TCP	-61.3	-66.9	-52.0	-66.7	+32.7	-71.2

The **Wear Rate of Engine Oil** is reduced by TCP additive, as evidenced by the lowered metallic content of the used oil.

In another study, commercial 10W30 oil gave one-tenth the wear and had less degradation when mixed with 5 percent TCP, suggesting its potential for use in other lubrication applications.

This work was done by Alfred J. Babecki and Hugh C. Fletcher of **Goddard Space Flight Center.** *No further documentation is available.*
GSC-12327

Drilling Side Holes From a Borehole

Novel machine concept would take long horizontal stratum samples from a narrow vertical hole.

NASA's Jet Propulsion Laboratory, Pasadena, California

A proposed machine for drilling horizontal holes in the earth surrounding a borehole could take samples extending a few meters into the strata. Such samples will yield important data for geological studies, oil surveys, and geothermal energy surveys. The machine could also drill holes for drainage or ventilation in coal mines.

The conventional method of taking side samples is to use an explosive to drive a small sampling vessel into the borehole wall. However, since the vessel penetrates only a short distance into the wall of the borehole, the samples are likely to have been contaminated by drilling mud, distorted by the borehole drilling, and lacking in normal stratum fluids. In contrast, the new drilling machine takes samples that extend deep into the strata.

In order to take long horizontal samples from the confines of a hole 6 inches (21.2 centimeters) in diameter, a folding structure drives and advances the drilling tool. As shown in Figure 1, the rotating drill bit is advanced by a shaft composed of interlocking half-cylindrical shells, drawn from vertical storage bins. The machine is enclosed in a steel tube 30 feet (10 meters) in length, which contains pumps, motors, and a feed mechanism. The enclosure is lowered to the required depth and fixed in place by packing rings.

The feed mechanism moves upper and lower chains of half-cylindrical shells from their vertical tracks. As segments of the two chains turn horizontal, they mate to form a rigid hollow thrust tube that pushes the drill bit into the bore wall. A worm gear furnishes the motive force for the advance, driving a set of racks on the segments.

The drilling head is rotated by an extensible, flexible hollow shaft that engages an expendable drill bit stored in a magazine. (The bits are short-life tools selected to suit the stratum being

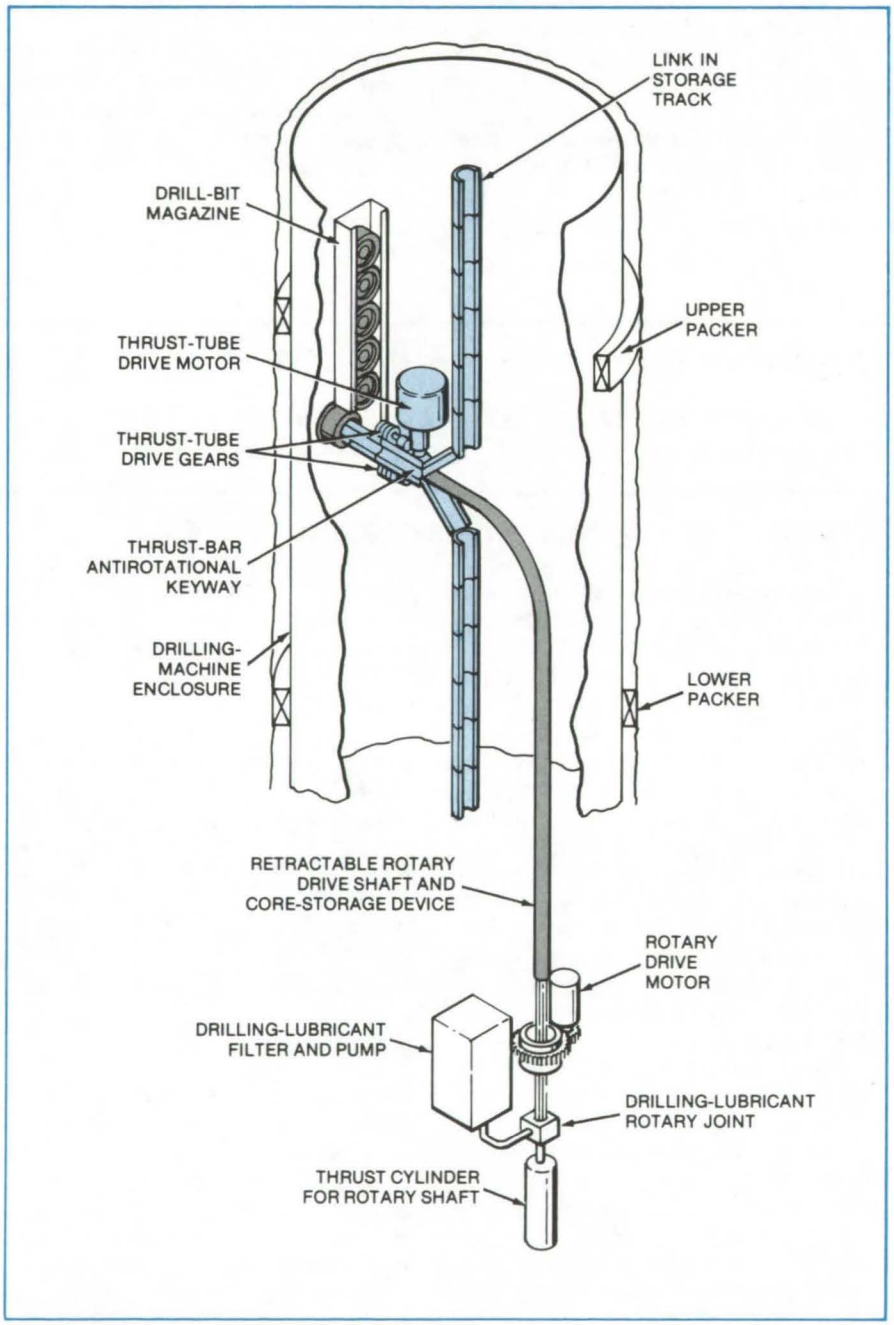

Figure 1. **At the Start of Drilling,** the thrust tube has been formed from the first links in the upper and lower chains of half-cylindrical shells. The thrust tube has engaged a drill bit and pressed it through a hole in the enclosure against the bore wall. The rotary shaft is inserted in the thrust tube and turns the drill bit.

drilled.) The flexible rotary shaft fits inside the thrust tube. Composed of segmented, slip-jointed rings in a flexible sheath, the rotary shaft holds a stratum sample in its hollow center and carries lubricating fluid for the drill bit in the space between the segments and the sheath (see Figure 2). The rotary shaft is turned by a ring gear and motor and is advanced and retracted by a hydraulic cylinder. One rotary shaft is needed for each sample to be taken.

After the sample has been taken, the rotary shaft and the thrust tube are retracted into their vertical storage positions. The expendable drill bit is left in the hole. The drilling sequence is then repeated for other strata in the borehole. Measuring instruments can be inserted in the completed hole to record dimensional data and other information.

For drilling secondary horizontal ventholes from primary vertical vents in coal mines, multiple drilling mechanisms would be installed in the machine. It is estimated that four holes 1.25 inches (3.2 centimeters) in diameter and 8 feet (2.4 meters) deep could be drilled simultaneously in 1 hour.

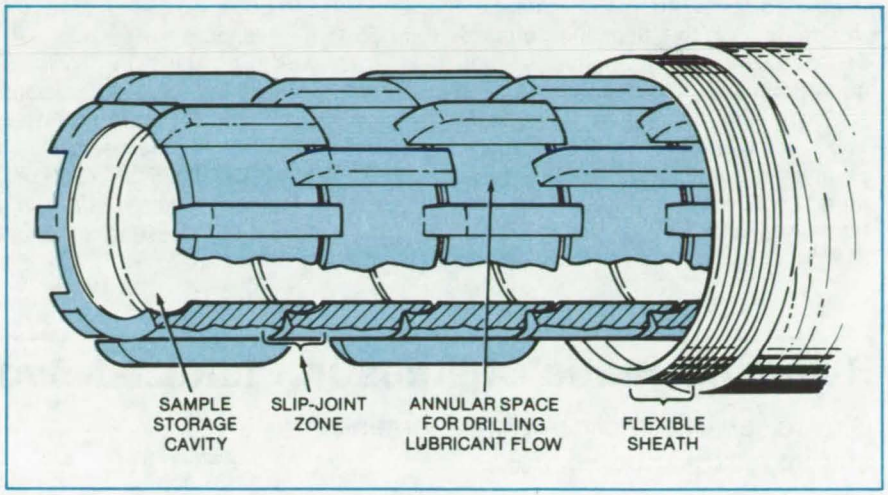

Figure 2. This **Flexible Rotary Shaft** comprising articulated segments turns the drill bit. The fins transmit rotation from one segment to the next, within a sheath. The hollow core of the shaft stores stratum samples a few meters long.

This work was done by Earl R. Collins, Jr., of Caltech for **NASA's Jet Propulsion Laboratory.** *For further information, Circle 53 on the TSP Request Card.*

Inquiries concerning rights for the commercial use of this invention should be addressed to the Patent Counsel, NASA Resident Legal Office-JPL [see page A5]. Refer to NPO-14465.

Corrosion-Resistant Ceramic Thermal-Barrier Coating

Coating for air-cooled components of gas-turbine engines better resists corrosion by fuel and air impurities.

Lewis Research Center, Cleveland, Ohio

A simple, two-layer thermal-barrier coating system that offers improved resistance to hot corrosion from fuel and air impurities has been identified for use on air-cooled components of gas-turbine engines. The coating system consists of an MCrAlY (where M is nickel, cobalt, or iron) alloy bond-coat layer and a highly-adherent, insulating, calcium silicate ceramic outer layer. The MCrAlY bond coating and the calcium silicate layer may both be deposited by plasma spraying in an air environment without the necessity of a special cover gas. The thickness of the bond coat can range from 0.008 cm (0.003 in.) to 0.018 cm (0.007 in.), and that of the calcium silicate ceramic layer may range from 0.012 cm (0.005 in.) to 0.051 cm (0.020 in.) or more. The calcium silicate coating can be polished to reduce aerodynamic frictional losses.

Ceramic coatings have low thermal conductivities and therefore impose a thermal barrier between high-temperature combustion gases and air-cooled metal parts such as the combustors, turbine blades, and vanes of power-generating turbines or the cooled components of other heat engines. As a result, the working parts can operate at reduced metal temperatures. Alternatively, increased gas temperatures or decreased coolant flows may be attained. These features provide the potential for increased engine performance, reduced fuel consumption, use of less costly materials or fabrication procedures, and increased life and durability of cooled engine components. Improved corrosion resistance is an additional attribute of the calcium silicate-based thermal-barrier coating. It offers potential to allow firing of power-generating turbines with lower-grade, corrosive fuels.

When the NASA-developed calcium silicate/MCrAlY coating was evaluated in an industrial/utility gas-turbine combustion simulation program sponsored by the Department of Energy, it was found to be more resistant to spalling in a corrosive environment than previous thermal-barrier coatings. This coating completed 675 1-hour test cycles before spalling on the leading edge compared to 80 1-hour cycles for 12 percent by weight

(continued on next page)

yttria-stabilized zirconia thermal-barrier coating. In this test, the combustion products were doped to a fuel-equivalent impurity level of 5 ppm sodium and 2 ppm vanadium. The combustion-gas temperature, ceramic-surface temperature, and metal-substrate temperature in this test were 1,370° C (2,500° F), 980° C (1,800° F), and 840° C (1,550° F), respectively.

This work was done by Philip E. Hodge, Stanley R. Levine, and Robert A. Miller of **Lewis Research Center.** *Further information may be found in NASA TM-79005 [N79-11179/NSP], "Thermal Barrier Coatings: Burner Rig Hot Corrosion Test Results"* [**$6**]. *A copy may be purchased [prepayment required] from the National Technical Information Service, Springfield, Virginia 22161.*

Inquiries concerning rights for the commercial use of this invention should be addressed to the Patent Counsel, Lewis Research Center [see page A5]. Refer to LEW-13088.

Reducing Static Charges in Fluidized-Bed Reactions

Glow discharge reduces agglomeration and increases product yield.

Ames Research Center, Moffett Field, California

Fluidized-bed reaction systems involving suspended particles often suffer unfaborable effects on their hydrodynamics due to agglomeration of the particles, caused by static charges on their surfaces. The addition of moisture or a conductive coating such as graphite on the particles can reduce the static charge, but these techniques can interfere with the chemical reactions in some processes. A new approach, ionizing the gas used to suspend the particles, introduces no foreign substances into the reaction chamber and has been shown in one case to increase the reactant-loading capacity sixfold over that in a static process, onto the same area as the diffuser plate.

The apparatus shown in the figure was used for the disproportionation of calcium peroxide diperoxyhydrate to calcium superoxide. Dry nitrogen gas is introduced at the bottom of the funnel-shaped reaction chamber to suspend the particles and create the fluidized bed. The gas is ionized by a ring-shaped high-voltage electrode (a power meter and impedance-matching circuit are not shown) to which a 5-W pulsed RF voltage is applied at 13.56 MHz.

A glow discharge makes the gas conductive enough to neutralize the static charge from the suspended particles. The particles can then react while suspended in the flowing gas stream.

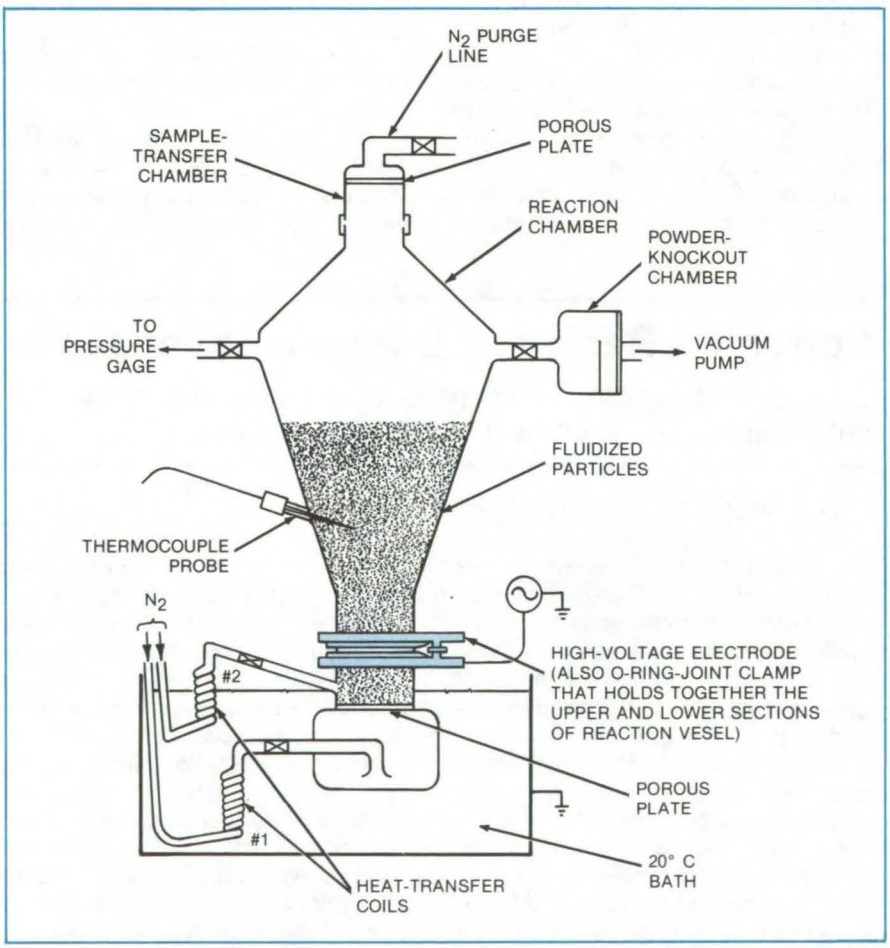

RF Glow Discharge Apparatus for a fluidized-bed reaction system ionizes the fluidizing gas to make it sufficiently conductive to neutralize static charge on the particles. In the apparatus above, the O-ring-joint pinch clamp is the high-voltage electrode.

This work was done by Theodore Wydeven of **Ames Research Center,** *E. Vernon Ballou and Peter C. Wood of San Jose State University Foundation, and LeRoy A. Spitze of San Jose State University. For further information, Circle 54 on the TSP Request Card.*

This invention is owned by NASA, and a patent application has been filed. Inquiries concerning nonexclusive or exclusive license for its commercial development should be addressed to the Patent Counsel, Ames Research Center [see page A5]. Refer to ARC-11245.

Transferring Small Samples of Viscous Liquid

Bubble-free samples are obtained for chemical analysis.

Lyndon B. Johnson Space Center, Houston, Texas

A simple technique for filling a small syringe with a viscous liquid almost completely avoids trapped air bubbles.

The sample is first drawn into an auxiliary syringe (see figure) that is large enough to avoid bubbles or allow them to be removed easily. The needle of this large syringe is used to fill the reservoir of a smaller, sample syringe from which the plunger has been removed. After the plunger is reinserted, the syringe is turned needle up, while the plunger is depressed to force out trapped air and reach the desired sample volume.

This technique makes it easy to handle and control a quantity of sample as small as 1 microliter. Such samples are often transferred by using syringes, but the vacuum created when the liquid is drawn through the hollow needle creates bubbles as the liquid reaches the barrel. It was necessary to clear the bubbles by inverting the syringe, tapping or otherwise coaxing the bubbles to rise to the needle entry, and then ejecting sufficient liquid to clear the barrel and needle of bubbles. Avoiding the bubble contamination becomes progressively more difficult for smaller syringes or for very viscous samples.

With the new technique, fewer bubbles are generated during the initial fill, and these are expelled when the plunger is reinserted. The method is thus simpler and more effective than the old approach.

This work was done by Bruce W. Miller, Shirley M. Mitchell, and John N. Olney of Rockwell International Corp. for **Johnson Space Center.** *No further documentation is available.*
MSC-18533

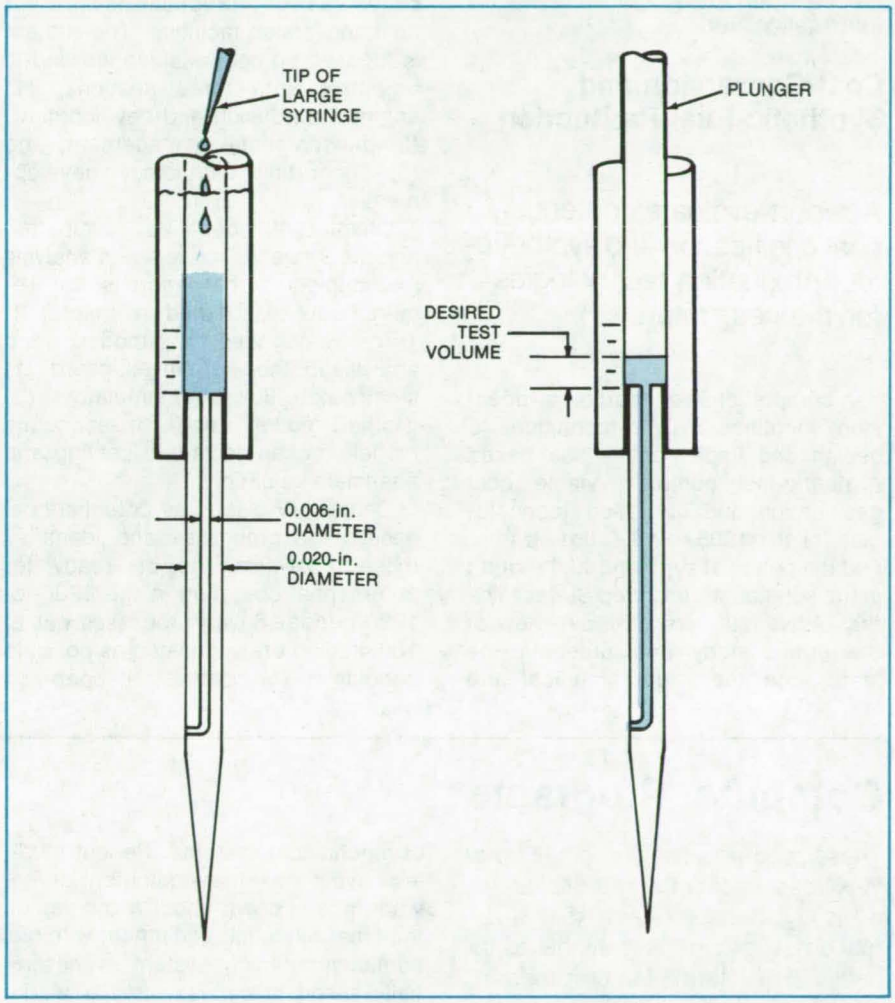

The **Viscous Fluid Is Directly Inserted** into the syringe on the left. The plunger is removed so that the fluid can be poured in or forced in from a larger auxiliary syringe. As shown on the right, the reinserted plunger forces out the air bubbles until the desired sample-volume mark is reached.

Books and Reports

These reports, studies, and handbooks are available from NASA as Technical Support Packages (TSP's) when a Request Card number is cited; otherwise they are available from the National Technical Information Service.

Coal Conversion and Synthetic-Fuel Production

A report evaluates potential coal gasification and synthetic-fuel production technologies for the near future.

A comprehensive report on a recent study identifies analytic techniques to design and implement a coal-based synthetic-fuel complex, viable coal gasification and utilization technologies for the 1985-to-1990 time frame, and the potential synthetic-fuel market in the southeastern United States. The first of five chapters is an overview of the entire study and presents the status quo and future technical and economic potentials of the coal technology.

Chapter II describes analysis methodologies, modeling capabilities, and supporting technology development required to conduct and monitor conceptual and practical designs for coal conversion facilities. The subject is focused on coal gasification and is organized into three sections: (1) engineering design and development, (2) environmental management, and (3) supporting technology development.

Chapter III identifies, evaluates, and recommends models and analysis methodologies that address the requirements established in chapter II. Three categories of models and analysis methods are investigated: (1) steady-state flowsheet simulators, (2) gasifier models, and (3) economic models broken down into costing and financial evaluations.

Chapter IV discusses potential coal gasification processes and identifies those most likely to be ready for commercial operation in the 1986-to-1990 period. Seven processes out of 100 studied are suggested as possible candidates for commercial operation (1,000 to 2,000 tons of coal/day/gasifier). Each of these is characterized by the product gas composition, byproducts, gasifier efficiency, the type of coal used, and several other factors.

Chapter V characterizes potential industrial users of coal conversion products. Major national, regional, and also specific industries in Northern Alabama are identified as potential customers for medium-Btu gas (MBG).

Two appendix sections conclude the report. The first is a catalog of 105 coal gasification systems listed alphabetically according to the manufacturers. The last is a catalog of models and analytical methodologies for coal conversion facilities.

This work was done by Rodney Bradford of **Marshall Space Flight Center** *and W. T. Atkins, Ronald M. Bass, Richard Dascher, Joseph Dunkin, Nina Luce, William Seward, and Dennis Warren of BDM Corp. To obtain a copy of the report, "Coal Conversion Processes and Analysis Methodologies for Synthetic Fuels Production," Circle 55 on the TSP Request Card.*
MFS-25330

Computer Programs

These programs may be obtained at very reasonable cost from COSMIC, a facility sponsored by NASA to make new programs available to the public. For information on program price, size, and availability, circle the reference letter on the COSMIC Request Card in this issue.

Underground Coal Mining

Closed-network queue model

Over the last 8 years, underground coal-mining productivity has declined by almost half, while the cost of coal has risen. With coal recognized as an important future energy source, it is essential that a better understanding of all aspects of coal productivity be developed. Almost all coal mining in the United States is mined with the aid of mechanical systems. Recent studies have shown that equipment at the work face is down about a quarter of the time. Since the equipment within a continuous-mining system is essentially linked in series with the workface machinery, downtime for the continuous system can be considerably more than a quarter of the time.

A new computer program that models coal-mining production, equipment failure, and equipment repair represents an underground mine as a collection of work stations that alternately require servicing by a production crew and a repair crew. Each crew is drawn from a respective pool of homogeneous crews. This interaction is modeled as a closed network of two queues in series and is solved as a classic Markov finite-state birth-and-death process. As such, the model is applicable to any cluster of processes that operate and fail independently but share pools of production and repair resources.

The model projects equipment availability and productivity based on the number of work stations, production crews, and repair crews and the equipment reliability parameters of "mean time between failure" and "mean time to repair." The sensitivity of productivity to these variables is readily derivable, suggesting appropriate areas for research and development, as well as indicating the proper balance of labor and equipment in advanced mining systems.

This program is written in FORTRAN IV for batch execution and has been implemented on a UNIVAC 1108 with a central memory requirement of approximately 14K of 36-bit words. This network queue modeling program was developed in 1978.

This program was written by Gerrie M. Hill of Caltech for **NASA's Jet Propulsion Laboratory.** *For further information, Circle C on the COSMIC Request Card.*
NPO-14704

Life Sciences

Hardware, Techniques, and Processes

Temperature Controller for Hyperthermia Device

Biomedical appliance measures and controls temperature in tumor.

Langley Research Center, Hampton, Virginia

A temperature controller was developed to support a research program investigating hyperthermia as an antineoplastic treatment modality. It closely controls temperature in the local region of a tumor in a live subject. Extensive laboratory investigations involving both leg and lung tumors in mice show that the controller is capable of maintaining a given temperature to within ±0.2° C: To allow its use by biomedical workers with little training on complex electronic systems, the controller has as few front-panel control functions as is practical. Furthermore, it is expandable for the treatment of several subjects simultaneously.

Tissue is heated by pulsed radio-frequency energy applied directly to the subject through ohmic contacts. Special applicators efficiently couple the device to the leg and thoracic regions of mice, using a conductive jelly similar to EKG grease. For the critical temperature measurements in the region of the tumor, medical-grade thermocouples (enclosed in a hypodermic needle) give the best temperature measurements. These probes are inserted subcutaneously near the tumor or, in some cases, into the tumor. At the power levels used in this investigation, no problem associated with the potential rectifying characteristic of the junction of dissimilar metals was encountered. The junction of the thermocouple probe is electrically insulated from the hypodermic needle.

The configuration illustrated shows a closed-loop system in which the subject's temperature is continuously monitored and compared to a target temperature. RF energy is supplied as needed to heat the tissue. A multiple-subject version of the hyperthermia appliance was also developed and differs from the one illustrated here in that a single temperature measurement per subject is made with measurements sequentially applied to the controller through a multiplexer. The output of the power source is multiplexed accordingly, applying heat to the subject whose temperature is being measured. The impedance-match monitor was modified to operate in a sampling mode and can be switched to read any one of the several channels.

Extensive investigations thus far have been limited to radio frequencies in the region of 30 MHz. However, the system has been tested at frequencies ranging from 10 to 100 MHz with no significant degradation in performance.

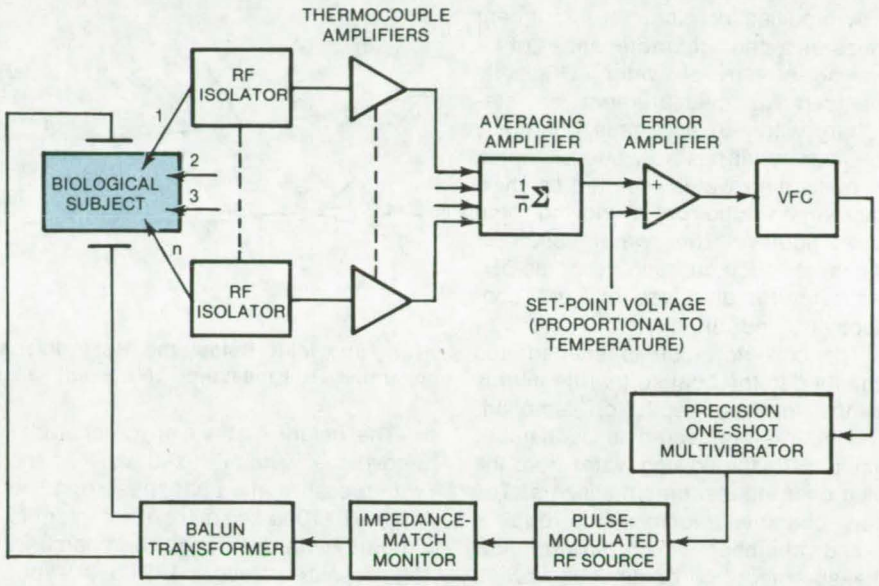

Single-Channel Hyperthermia Temperature Controller continuously monitors a subject's temperature and compares it to a target value. If the measured temperature is too high, no RF energy is applied, and the temperature drops off naturally. If the measured temperature is too low, a voltage proportional to the temperature error is generated in the error amplifier and applied to a voltage-to-frequency converter (VFC), which produces a square-wave signal with a frequency that is proportional to the input voltage. This in turn drives a precision one-shot multivibrator that produces a train of fixed-width, variable-duty-cycle pulses. This signal pulse-modulates an RF power source that provides the energy required to raise the local temperature of the subject. An impedance-match monitor allows a gross assessment of the degree to which the RF energy supplied by the generator is utilized to heat the subject. A balun transformer provides a broadband transformation from an unbalanced power source to an inherently balanced load; i.e., the subject. At the lower frequencies (≅10 MHz) the balun transformer can be eliminated.

This work was done by Richard H. Couch, Chase P. Hearn, and James B. Williams of **Langley Research Center.** *For further information, Circle 56 on the TSP Request Card.*

Inquiries concerning rights for the commercial use of this invention should be addressed to the Patent Counsel, Langley Reserach Center [see page A5]. Refer to LAR-12528.

Measuring Water Properties From a Moving Boat

Batch analyzer is modified for continuous flow.

Langley Research Center, Hampton, Virginia

A modified commercial instrument measures the characteristics of a flowing stream of water. Originally intended for measurement on stationary water in a sample chamber, the instrument has now been adapted to measuring water scooped up by a submerged tube on a moving boat (see figure). The water analyzer measures such characteristics as pH, temperature, dissolved oxygen, conductivity, and turbidity.

The collector tube is shaped and attached to the boat so that its inlet is at the required depth for sampling. The tube is connected to a chamber that passes the flowing water from the tube over the instrument sensors. The new chamber replaces the original sensor chamber, which did not allow measurements on continuous flow. If required, water samples can be taken from the tube outlet for later analysis in a laboratory.

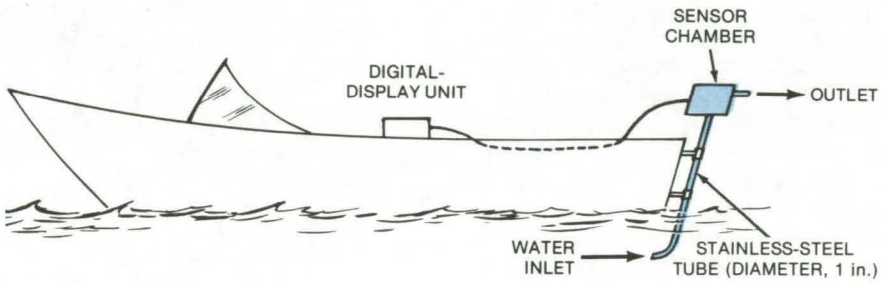

The **Tube Inlet Below the Boat** diverts a stream of water through the sensor chamber. The measured values appear on the remote digital-display unit.

The height of the sensor chamber above the water is fixed so that the ram pressure at a boat speed of 12 to 15 mi/h (19 to 24 km/h) is sufficient to force the water through the chamber. [A pressure of about 1/2 lb/in.^{2} per foot of elevation (3.4×10^6 N/m^2 per meter) is necessary.] A valve may be placed in the tube to regulate the waterflow.

This work was done by Ashby G. Lawson of **Langley Research Center.** *No further documentation is available.*
LAR-12325

Mechanics

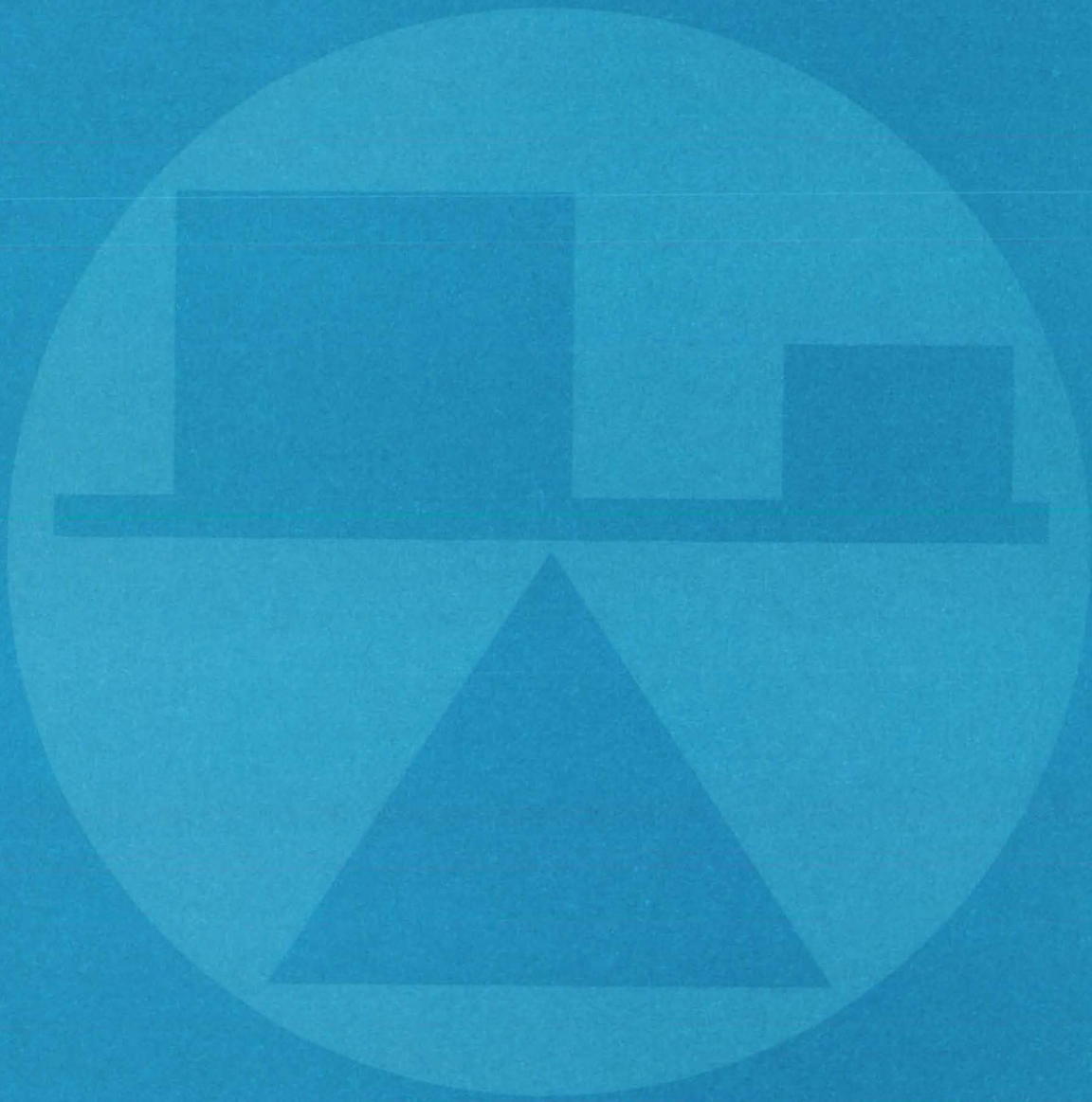

Cable-Splice Detector

An inexpensive sensor and electronic circuit reduce maintenance costs and improve the safety of San Francisco cable cars.

Ames Research Center, Moffett Field, California

A magnetic detector, originally developed to warn gripmen on San Francisco cable cars when a spliced section of cable is passing, could have other applications where moving steel cable must be measured, monitored, or controlled. Developed following a request by San Francisco city officials to a NASA Applications Team (see inside front cover), the splice detector has possible uses in aerial cable-car systems and equipment handling in mines, boreholes, and undersea operations.

In the San Francisco cable-car system, the car operator controls a lever that engages the grip mechanism with the moving underground cable; however, cable breakage at a splice has been a major problem. Such failures can occur when a spliced section [each of which is 72 feet (21.9 m) in length] is gripped, causing individual cable strands to tear. The separated cable strands can also entwine around the grip and drive the car uncontrolledly into other vehicles.

To prevent such mishaps, the splice detector sounds a buzzer when a splice approaches the car. It is activated by a Hall-effect proximity sensor that produces a linear voltage proportional to magnetic-field intensity. The sensor is attached to the bottom of the grip mechanism, 1/4 to 1 inch (0.6 to 2.5 centimeters) from the cable.

The cable contains five magnetized spots ahead of the splice. The spots are spaced 10 feet (3 meters) apart, and the last spot precedes the splice by 42 feet (12.8 meters). For a cable speed of 14 ft/s (4.3 m/s), the spot separation corresponds to 0.7 second, and the splice separation corresponds to 3 seconds.

The sensor produces voltage pulses as the magnetic spots pass it. The pulses are counted, and when at least three pulses are accumulated in rapid sequence, the circuit sounds an alarm. A 12-volt battery (such as that found in household smoke detectors) powers the circuit and alarm.

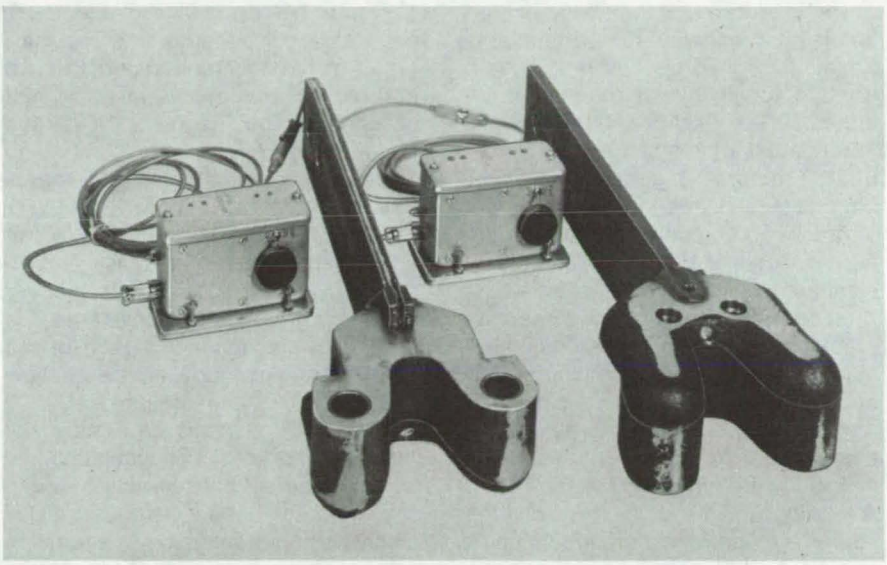

The **Cable-Splice Detector** consists of a Hall-effect magnetic sensor, which is located about 1/2 to 1 in. from the cable. Magnetic markings on the cable are converted to electrical signals by the sensor. The electrical signals are filtered, amplified, converted to pulses, and counted to actuate an audible alarm or light when a splice approaches a cable car.

In tests on cable cars, the detector worked faultlessly, provided that the cable contains no spurious magnetism and the spots are strongly magnetized. To insure these conditions, the entire length of the cable is demagnetized and the spots are remagnetized every 3 days.

Located in the main cable house, the demagnetizer is a commercial "growler" that erases magnetic noise from the cable. The magnetizer, also in the cable-car house, rotates a horseshoe magnet around the steel cable at five places separated from the splice and from each other by the requisite distances.

For reliability testing and splice monitoring, three detectors similar to those on the cable cars are also in the cable house (one detector for each of the three cable-car lines). Each detector indicates passage of a splice by lighting a 40-watt bulb and a single buzzer shared by the three detectors. An electronic timer measures the interval after the last splice indication for each of the cable-barn detectors. If the cable must be shut down, the timer readings can be read to locate the current positions of the splices.

This work was done by Robert D. Lee, Ernest J. Iufer, and Angelo Giovannetti of **Ames Research Center.** *For further information, Circle 57 on the TSP Request Card.*
ARC-11291

LVDT Gage for Fracture-Toughness Tests in Liquid Hydrogen

LVDT displacement gage can be calibrated at room temperature.

Lewis Research Center, Cleveland, Ohio

The load-carrying capability of materials at cryogenic temperatures is frequently limited by their plane-strain fracture toughness at those temperatures. The ANSI/ASTM E-399 "Standard Method of Test for Plane Strain Fracture Toughness of Metallic Materials" requires the measurement of crack-mouth-opening displacement as a function of applied load using standardized precracked specimens. It recommends a gage for measuring crack-mouth-opening displacement that incorporates conventional resistance strain gages as sensing elements. One problem encountered with this gage for fracture toughness tests in liquid hydrogen (at -423° F or 20 K) is boiling of the hydrogen on the strain-gage elements, producing noise in the output signal and obscuring the test record.

An alternative crack-mouth-opening displacement gage incorporating a linear-variable differential transformer (LVDT) has been developed for use in fracture toughness tests in liquid hydrogen.

Figure 1 is a drawing of the LVDT gage assembly. Figure 2 is a photograph of the assembly mounted on a precracked fracture toughness test specimen. The gage is held and actuated by knife edges attached to the specimen and spanning the crack mouth. Prior to testing, the LVDT movable core is positioned by an adjustment screw to establish electrical null. As the specimen is loaded, crack-mouth-opening displacement is sensed by the relative motion of the LVDT core and body as they follow separation of the knife edges.

The LVDT output is determined by the level of primary coil excitation and by the electrical phase angle between the primary and secondary coil signals. Proper selection of excitation and phase angle can produce a match in outputs at any two temperatures; e.g., room temperature and liquid hydrogen temperature. This allows gage calibration and periodic verification at room temperature rather than in liquid hydrogen. Figure 3 illustrates the technique for obtaining dual-temperature calibration. Gage output is plotted for the two selected temperatures as a function of phase angle at a given excitation level. The intersection of the two curves establishes the phase angle where the output is identical at both temperatures. Changing the excitation level shifts the curves and their intersection.

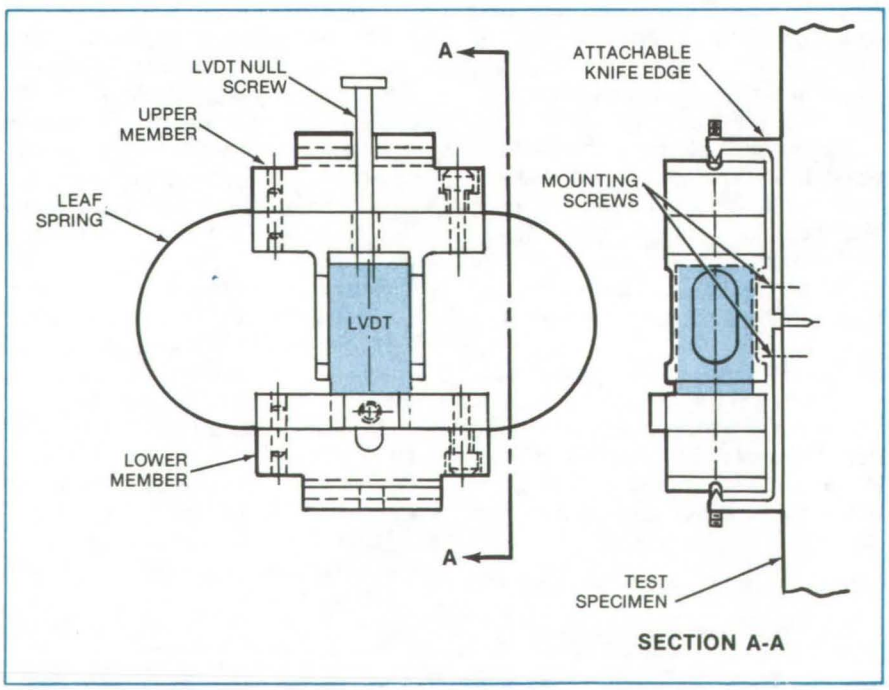

Figure 1. **LVDT Displacement Gage** is used for plane-strain fracture toughness tests in liquid cryogens.

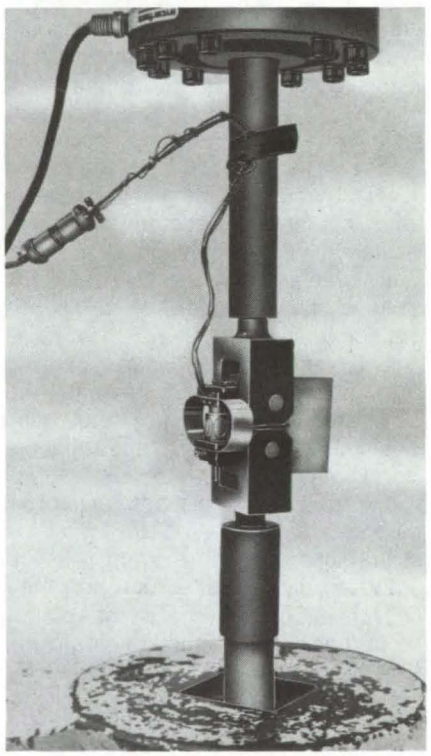

Figure 2. **Displacement Gage** is shown mounted on a test assembly.

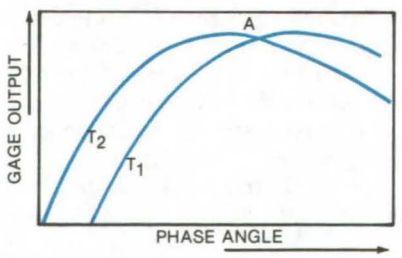

Figure 3. **Gage Output Versus Phase Angle** is plotted at temperatures T_1 and T_2 for a given displacement and excitation.

Although this gage is particularly well suited for use in cryogenic liquids, it can also be used at moderately elevated temperatures and can be encapsulated for use in corrosive or hostile environments. An encapsulated gage has been used commercially for stress corrosion cracking testing of materials in nuclear reactor environments.

This work was done by William S. Pierce and John L. Shannon, Jr., of **Lewis Research Center.** *No further documentation is available.*
LEW-13038

Tension-Mode Loading for Bend Specimens in Cryogens

Fixture allows fracture-toughness tests on standard bend specimens.

Lewis Research Center, Cleveland, Ohio

Material performance at cryogenic temperatures is frequently controlled by the plane-strain fracture toughness at those temperatures. The selection of a test specimen for determining the toughness is sometimes constrained by certain factors such as product size and configuration and crack-plane orientation. A problem arises when the necessary standard test specimen (ANSI/ASTM E-399) is incompatible with available test equipment; e.g., when only a bend specimen will do and the available equipment is suited only for tensile testing. For this particular situation, a test fixture has been developed that permits the use of tension-mode loading for fracture-toughness tests on standard bend specimens. The fixture is compatible with cryostats designed for tension testing.

Figure 1 shows the special load fixture prior to final assembly. The test specimen is centered and held in position on the support (reaction load) rollers by use of spacer blocks and wire clips. The V-block below the specimen alines the load-application roller (not shown). Figure 2 shows the load fixture assembled, with the load-application roller in place (below the specimen).

This work was done by William S. Pierce and John L. Shannon of **Lewis Research Center.** *No further documentation is available.*
LEW-13040

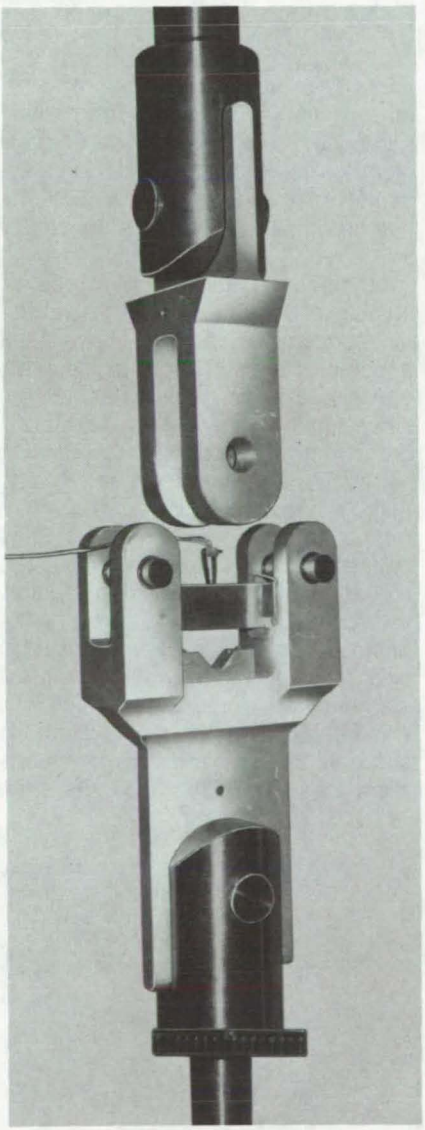

Figure 1. **Load Fixture Prior to Final Assembly**

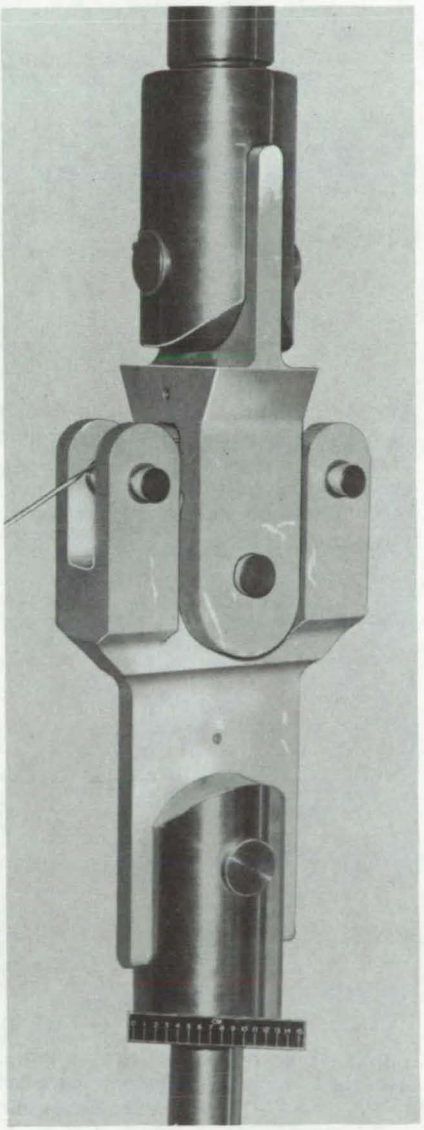

Figure 2. **Assembled Load Fixture**

Modified Displacement Gage for Cryogenic Testing

ANSI/ASTM E-399 clip-in gage for fracture toughness testing is made more stable in liquid hydrogen.

Lewis Research Center, Cleveland, Ohio

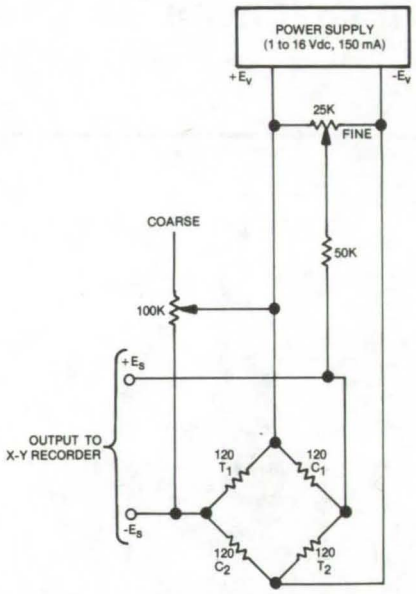

Figure 1. **Modified Strain-Gage Circuit** is more stable when immersed in liquid cryogens because the standard 10-volt excitation has been lowered to 1.5 volts to eliminate boiling on the surface of the gage.

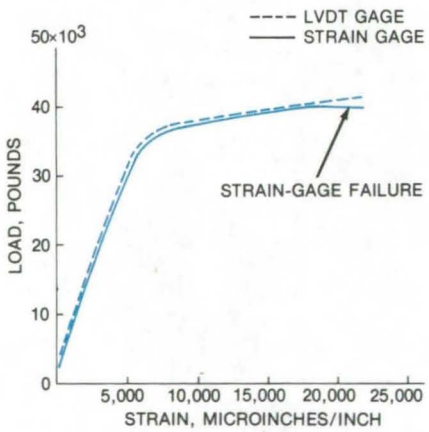

Figure 2. **Comparison Test** in liquid hydrogen shows agreement between the modified DCB gage and a calibrated LVDT gage.

Cryogenic temperatures can adversely affect the performance of electrical/mechanical measurement devices. The double-cantilever-beam (DCB) clip-in displacement gage described in ANSI/ASTM E-399 "Standard Test Method for Plane-Strain Fracture Toughness of Metallic Materials" is affected by local boiling of the cryogen on the resistance-strain-gage sensory elements mounted on its DCB arms. The boiling produces variations in strain-gage electrical resistance and turbulent motion of the gage as a whole. The output signal is, therefore, unsteady and erratic.

Modification of the gage to produce stability, accuracy, and temperature-independent calibration has been accomplished by changes in the strain gages and strain-gage circuitry. The new strain gages are a nickel/chromium alloy (similar to Karma), self-temperature compensated and fully encapsulated in a glass-reinforced epoxy-phenolic resin. Gage resistance is 120 ohms; however, higher resistance gages are preferable to reduce gage heating further. The circuitry is shown in Figure 1. Bridge excitation has been lowered from the standard 10 volts to 1.5 volts to eliminate boiling on the strain-gage surfaces. Coarse and fine potentiometers are used in the bridge circuit for output signal balancing. This circuit is capable of balancing the bridge over the entire useful range of the gage.

Sensitivity of the modified gage is 0.0333 millivolt per volt per 0.001 inch displacement. This sensitivity results in a 50X magnification at a recorder sensitivity of 1.0 millivolt per inch and 1.5 volts excitation. For higher magnification, the signal was increased by a dc amplifier with a 10X multiplier.

Calibration showed that the modified gage is linear within 0.0001 inch over the displacement range from 0.200 to 0.250 inch. Comparison tests of the modified DCB gage and a calibrated LVDT-type gage mounted on the same smooth tensile specimen gave essentially, identical results at both room temperature and liquid hydrogen temperature. The liquid hydrogen test results are shown in Figure 2.

This work was done by William S. Pierce of **Lewis Research Center.** *Further information may be found in NASA TN-D-3724 [N67-10749/NSP], "Design and Use of Displacement Gage for Crack-Extension Measurements" [$5]. A copy may be purchased [prepayment required] from the National Technical Information Service, Springfield, Virginia 22161.*

LEW-13039

Broadband Electrostatic Acoustic Transducer for Liquids

Capacitive transducer with predictable frequency response can be used to calibrate piezoelectric transducers.

Langley Research Center, Hampton, Virginia

A broadband capacitive electrostatic acoustic transducer (ESAT) has been developed for use in a liquid environment at megahertz frequencies. The ESAT is useful in the calibration of standard commercially available transducers and in pulsed or continuous-wave spectral analysis techniques for ultrasonic nondestructive-evaluation characterization of materials. The ESAT has a known electroacoustic transfer function and can be used to measure absolute ultrasonic-wave displacement amplitudes.

No previous transducer has all of these attributes. The dielectric capacitive transducer has a bandwidth and an electroacoustic transfer function comparable to the ESAT, but it cannot measure absolute displacement amplitudes. Capacitive airgap hydrophones are useful only in the kilohertz range. Piezoelectric, magnetostrictive, and electromagnetic transducers do not have the bandwidth and the desirable electroacoustic transfer characteristics of the ESAT, and they cannot measure absolute amplitude. Existing airgap capacitive transducers used in the megahertz range are not liquid-immersible.

The ESAT basically consists of a thin conductive membrane stretched over a metallic housing. The membrane functions as the ground plate of a parallel-plate capacitor; the other plate is a dc-biased electrode. An ultrasonic wave incident on the membrane causes it to vibrate and vary the membrane-electrode gap spacing; an electrical signal is generated proportional to the wave amplitude. The entire assembly (see Figure 1 and equivalent circuit in Figure 2) is sealed for immersion in a liquid. Calibration of the ESAT with incident ultrasonic waves of constant displacement amplitude from 1 to 15 MHz reveals a decrease in output signal with increasing frequency, independent of membrane tension. This is due to a coupling reaction of the membrane to the liquid in which the device is immersed.

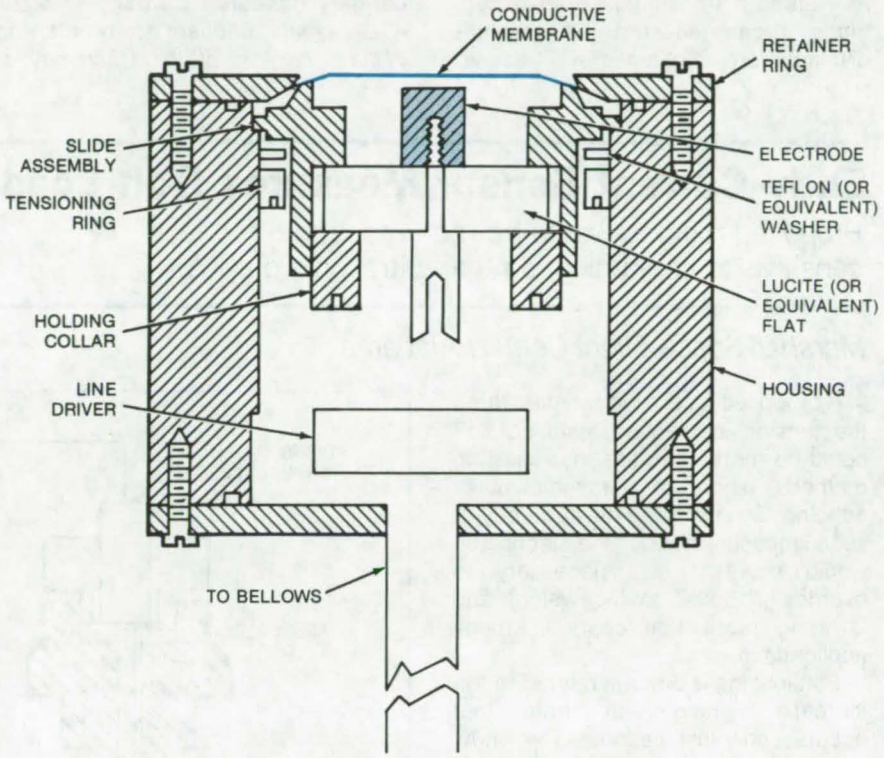

Figure 1. **Electrostatic Acoustic Transducer** is a broadband device that is sealed to allow immersion in water. The electrically grounded membrane forms a parallel-plate capacitor with the electrode, with a gap of about 10 micrometers. Ultrasonic waves incident on the membrane cause it to vibrate, producing a signal from the electrode.

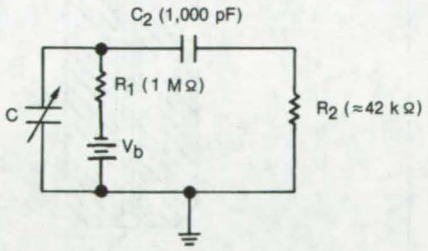

Figure 2. An **Equivalent Circuit of the ESAT** includes C, its capacitance, V_b the dc bias voltage (typically 100 volts), R_1 a large resistor used to prevent damage to the ESAT in case of arc-over, and C_2 a blocking capacitor to the load resistance R_2 (amplifier).

Tests made with the ESAT indicate that it may be useful as a broadband acoustic receiver with a predictable frequency response. Its broadband response is especially beneficial to the calibration of standard piezoelectric transducers and in spectrum analysis techniques. In addition, relative ultrasonic attenuation measurements as a function of frequency are improved

(continued on next page)

with the ESAT because of the repeatability and predictability of its frequency response as compared to conventional damped transducers. The device may be made of different materials and other sizes and shapes to accommodate specific situations. It may be used as a receiving transducer as well as a transmitting transducer. Since it can measure the absolute displacement amplitudes of ultrasonic waves in liquids, it may be used as a calibrator for other transducers and as a probe for the study and characterization of materials where absolute displacement amplitude is important.

This work was done by John H. Cantrell, Jr. [National Research Council], and Joseph S. Heyman of **Langley Research Center** *and Mack A. Breazeale, Michael A. Torbett, and William T. Yost of the University of Tennessee. For further information, Circle 58 on the TSP Request Card.*

This invention is owned by NASA, and a patent application has been filed. Inquiries concerning nonexclusive or exclusive license for its commercial development should be addressed to the Patent Counsel, Langley Research Center [see page A5]. Refer to LAR-12465.

Eddy-Current Sensor Measures Bolt Loading

Proposed method would be more accurate and less sensitive to contamination than ultrasonic probes.

Marshall Space Flight Center, Alabama

A proposed technique for measuring the tension load in an installed bolt could be more accurate than existing methods, such as ultrasonic pulse echoing. By improving the accuracy of such measurements, the technique would make it less necessary to overdesign bolts, saving weight and lowering production costs in many applications.

Bolt loading is directly related to the increase in length, or strain, that occurs on installation. The new proposal is to measure this strain by recording the displacement of a metal wire welded to the bottom of a hole along the axis of the bolt (see figure). A conventional eddy-current transducer could measure this displacement with an accuracy of about 0.0002 in. (0.05 mm). Strain (or load) values would be read directly on a digital display.

Although the required drilling and welding would be difficult and would make bolt manufacturing more complex, the needed technology does exist. Any increase in the cost to make a bolt could be offset by other production and assembly cost savings, particularly in specialty applications.

An existing bolt-load measurement, used with some success on the Shuttle main engine, is to record the time for an ultrasonic pulse to travel the length of the bolt and return. However, the accuracy of this approach is affected by dirt, oil, and other contamination in the bolthole. For each bolt size and type, it also requires a "standard" bolt for which the ultrasonic response is known at different loading levels. In contrast, the new technique is not sensitive to contamination, and it does not require a calibrated set of standard bolts. [Also see "Bolt-Tension Indicator" (MFS-19324) on page 88.]

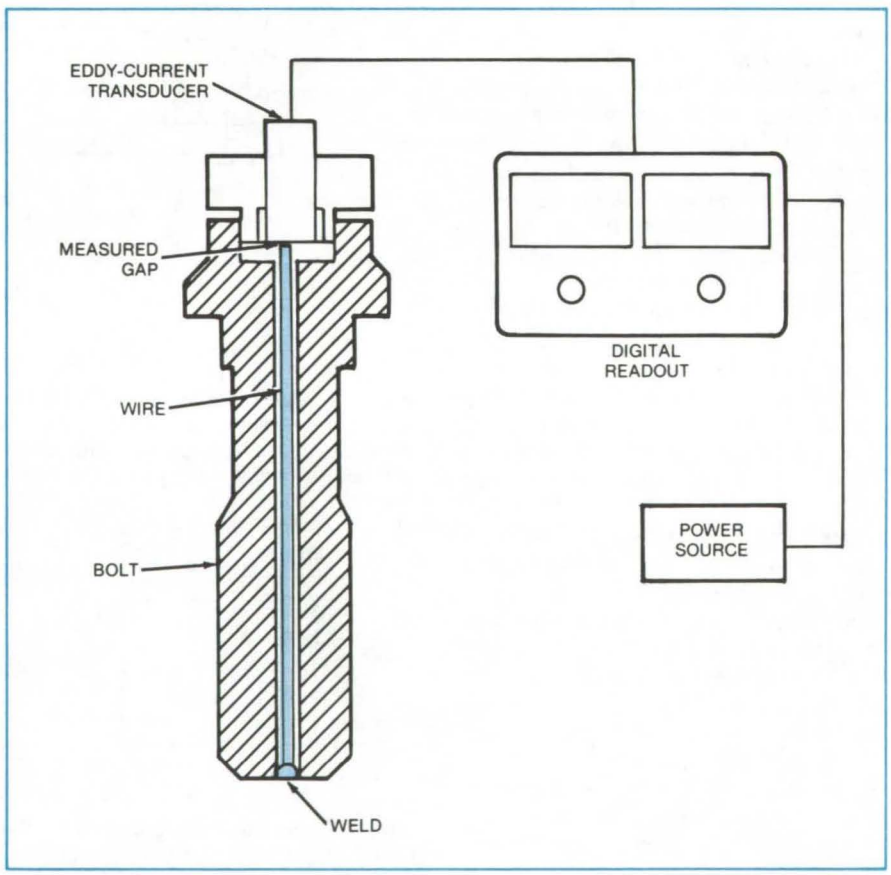

A **Thin Wire Target** welded to the bottom of a hole down the center of a bolt is the key element in a new proposal for measuring bolt loading. As the bolt stretches under load, changes in the gap between the target and the eddy-current sensing coil are measured and displayed on the digital readout.

This work was done by M. E. Burr of Rockwell International Corp. for **Marshall Space Flight Center.** *No further documentation is available.*
MFS-19486

Multiple-Creep-Test Apparatus

Simplified apparatus uses new fixtures, each supporting three samples at once.

Goddard Space Flight Center, Greenbelt, Maryland

An economical creep-testing apparatus measures flexural, compression, and shear creep of sodium iodide scintillation material. The tests are used to determine the mechanical properties of sodium iodide to design the scintillator support systems.

The apparatus (see figure) consists of a frame resting on a 4- by 6-ft (1.2- by 1.8-m) isolation table that prevents transient vibration. The heart of the apparatus is a new set of fixtures; each accommodates three samples and tests flexural, compression, or shear creep. The fixtures use a series of rods and plates that transfers a single load to all three samples at once.

The advantage of handling three samples simultaneously is that the number of loads used in any series of tests is reduced to one-third, making the apparatus more economical and compact. In addition, the samples in any given fixture are subjected to the same load. The fixtures are expandable to carry more samples by adding more rods and plates in series.

The current design accommodates 4 flexure, 3 compression, and 4 double-shear fixtures and can handle up to 24 fixtures for a maximum of 72 tests. Each vertical sample motion is independently recorded via millivolt printout from a dc-dc linear variable differential transformer responsive with a range of 0.020 in. (0.51 mm) and a sensitivity of 0.02 mil (5.1 μm). An acrylic cover protects from dust and inadvertent disturbances and retains low humidity inside.

This work was done by Carl L. Haehner of **Goddard Space Flight Center.** *For further information, Circle 59 on the TSP Request Card.*
GSC-12561

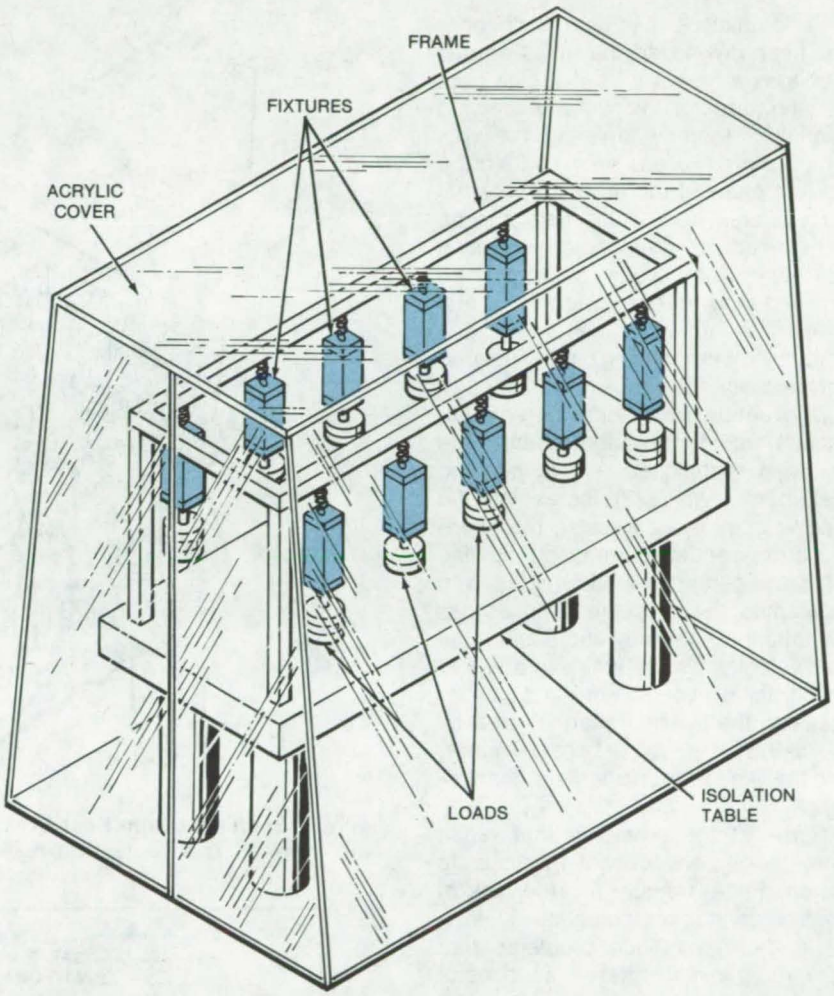

This **Creep-Test Apparatus** utilizes fixtures that can test three samples simultaneously for flexture, compression, or double-shear creep. Each fixture designed for a specific test requires a single load transferring identical forces to each sample. The arrangement reduces the amount of loads to one-third of the amount used on conventional apparatus that tests each sample separately.

Compact, Super Heat Exchanger

Porous medium enhances heat transfer.

Lewis Research Center, Cleveland, Ohio

A compact, super heat exchanger has been developed that uses porous media as a means of enhancing heat transfer through the walls of cooling channels, thereby lowering the wall temperature. Porous media within the cooling channel increase the internal surface area from which heat can be transferred to the coolant passing internally. The porous media can be sintered powdered metal, metal fibers, woven wire layers, or any porous metal having the desired permeability and porosity.

Conventional methods for enhancing heat transfer in channels utilize the following techniques: (1) roughening the internal wall; (2) increasing the fluid velocity by decreasing the channel cross-sectional area; (3) holding the cross-sectional area constant and increasing the pressure drop across the channel, thereby increasing the fluid velocity, which results in a higher heat-transfer coefficient; and (4) increasing the internal channel area by the use of fins, pins, helical inserts, and the like for heat-transfer enhancement.

Some of the problems that result from these conventional methods to increase heat transfer include lack of control of surface roughness, low-cycle thermal fatigue problems that result from joining different sections of material by welding or brazing, the difficulty of machining suitably sized channels in thin walls and confined spaces, and the difficulty of machining fins in small channels.

Figure 1 shows the physical model of a compact, super heat exchanger that is composed of a two-dimensional channel packed with porous media. The channel is exposed to the external heat flux $q_0(x)$ on one wall and $q_1(x)$ on the other wall. The heat flux is dissipated by the thermal capacity of a coolant flowing at the rate m through the porous medium in the channel.

Calculations were made to determine the cooling effectiveness of porous materials in the coolant passage of the heat-exchanger model.

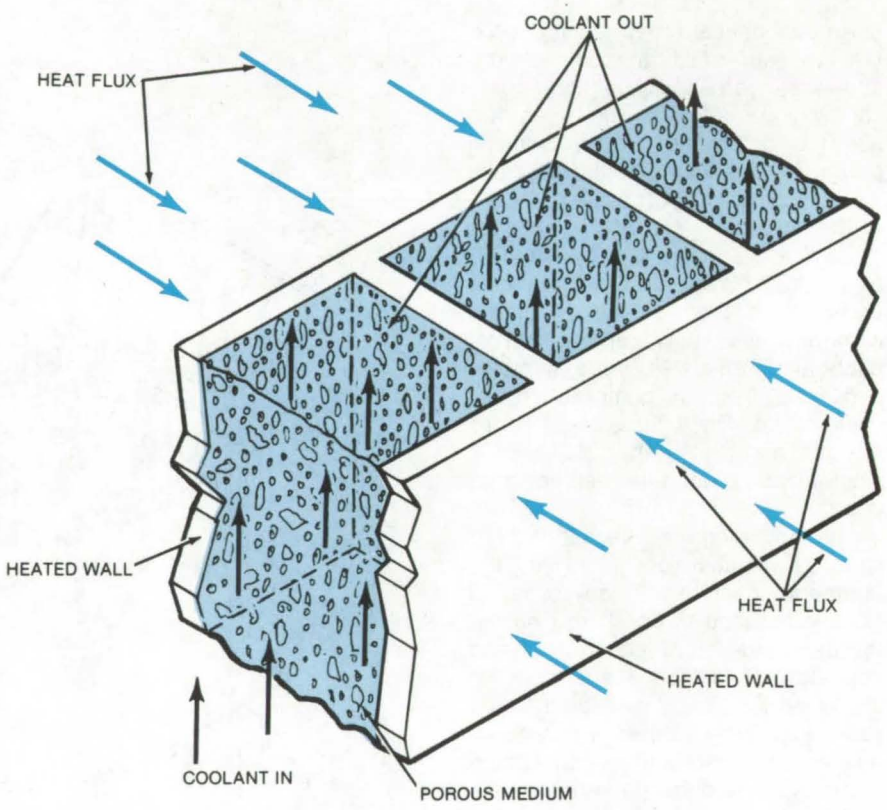

Figure 1. **Porous-Medium Heat Exchanger** has a large internal surface area for the transfer of heat to a coolant flowing through the porous material.

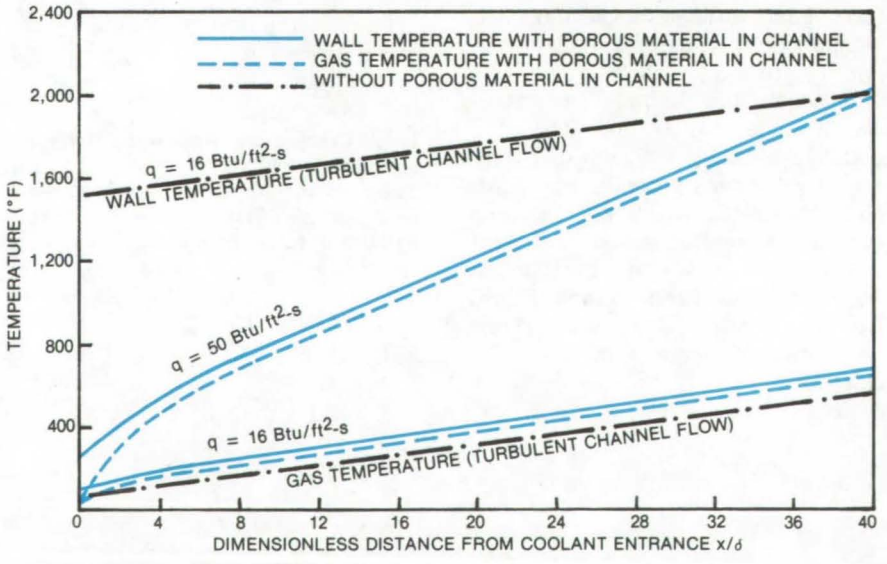

Figure 2. **Comparison Data** show that the wall has a lower temperature and the coolant gas has a higher temperature when a porous medium is used within a heat exchanger.

Figure 2 shows the result of the effects of porous media in a coolant channel. For this channel configuration and a maximum allowable wall temperature of 2,000° F (1,093° C), the wall heat flux with turbulent channel coolant flow is 16 Btu/ft^2-s (180x10^3 W/m^2). However, if the channel is packed with porous material, the wall flux can be increased to 50 Btu/ft^2-s (570x10^3 W/m^2). Thus, for a fixed wall-surface temperature, the effect of porous material is to increase the heat flux capability by over three times. On the other hand, if the heat flux is held at 16 Btu/ft^2-s, the effect of the porous material in the channel is to reduce the wall temperature from 2,000° to about 700° F (1,093° to 371° C).

The heat exchanger may be constructed by forming a body of the porous metal matrix into the desired shape. The cooling channel is then formed over the porous metal matrix by electroforming or sputtering. Both the density of the matrix and the diameter of the channel may be selected to provide the desired heat transfer and the cooling-fluid flow rate appropriate to the heat flux variations along the channel.

As an alternative, the heat exchanger may be constructed by first forming the cooling channel and then filling it with sintered metal powder, metal fibers, or the like. The unit is then heated to a temperature high enough to cause bonding or welding of the contents to form a porous metal matrix and to bond or weld the matrix to the cooling channel. The bonding or welding at all points of metal-to-metal contact provides maximum heat transfer by eliminating the normally high-thermal-resistance contact points.

Selection of the porous media depends on the amount of heat-transfer enhancement desired. Another factor to be considered in material selection relates to the structural requirements between the inner and outer walls of the cooling channel. In some applications, the porous material may serve as a structural support with the aid of ribs. The use of ribs will produce a higher enhancement factor because the ribs act as fins and are able to conduct more heat to the porous material where the heat is then transferred away by the coolant.

An important advantage in using this method of fabrication is that no distortion of the porous material occurs. As a result, prefabrication permeability and porosity characteristics are maintained. Another advantage is that no contact resistance exists at the interface of the porous material. In addition, the cooling channel structure is of one-piece construction, light weight, low cost, and high strength.

This work was done by Anthony Fortini and John M. Kazaroff of **Lewis Research Center.** *For further information, Circle 60 on the TSP Request Card.*

This invention has been patented by NASA [U.S. Patent No. 4,108,241]. Inquiries concerning nonexclusive or exclusive license for its commercial development should be addressed to the Patent Counsel, Lewis Research Center *[see page A5]*. *Refer to LEW-12441.*

Books and Reports

These reports, studies, and handbooks are available from NASA as Technical Support Packages (TSP's) when a Request Card number is cited; otherwise they are available from the National Technical Information Service.

Applications of Remote-Sensing Imagery

Aircraft and satellite imagery benefit land-development projects.

A compilation of reports discusses the usefulness of aircraft and satellite data for land-development projects. The type of imaging available and the means for analyzing it can answer some vital questions about future land development.

Remote-sensing images of the Earth are obtained using either conventional photographic cameras, scanners, or radars mounted on aircraft or satellites. The collected data are filed with different governmental agencies and are available to the general public.

The data can be analyzed using anything from sophisticated to simple equipment or with only the naked eye. For example, Landsat data may be analyzed with costly color-additive viewers and density slicers, but information sufficient for many applications can be found visually.

Landsat images are available as 70-mm and 9- by 9-in. (23- by 23-cm) positives and 9- by 9-in. and 30- by 30-in. (75- by 75-cm) prints produced in 1:500,000 or 1:250,000 scale. Three major signature categories can be determined with a naked eye: land use, biological, and geological/hydrological aspects.

The satellite images carry a lot of information about the extent of flood hazard areas, useful data for planning regional and urban developments. ERTS (Earth Resources Technology Satellites) images may be used to map the flood hazard areas. The cost of using these data for flood hazard mapping is just a few cents per kilometer of river that is being examined.

Program development and applications of remotely sensed data are also described by the Geological Survey of Alabama. This organization acquires remotely sensed data covering Alabama and has a substantial reference file about the land.

Remote-sensing imagery is also useful in estimating erosion and sedimentation rates in strip-mined areas. One lake is presented as an example of an accelerated erosion in a strip-mined area.

Lithologic mapping is also presented since it is an integral part of the proper land use. Although lithologic mapping involves regular fieldwork, it is significantly aided by aerial photographs.

The final section presents three methods how to determine the scale of a given view. The appendix includes maps of Alabama showing areas covered by various types of imagery and filed with the Geological Survey of Alabama.

This work was done by Travis H. Hughes of the University of Alabama for **Marshall Space Flight Center.** *To obtain a copy of the report, "Application of Remote Sensing for Planning Purposes," Circle 61 on the TSP Request Card.*

MFS-25107

Computer Programs

These programs may be obtained at very reasonable cost from COSMIC, a facility sponsored by NASA to make new programs available to the public. For information on program price, size, and availability, circle the reference letter on the COSMIC Request Card in this issue.

Equations of Motion for Coupled N-Body Systems

Complex systems modeled as a topological tree of idealized bodies

The dynamic characteristics of a complex system, such as a satellite or spacecraft, are best analyzed through a simulation model. The model must have the same dynamic characteristics as the complex system while lending itself to mathematical quantification. Idealized rigid bodies, point masses, and symmetric wheels are readily adapted to mathematical modeling; flexible bodies are more complex. However, if deformations are assumed to be small and if the laws of linear elasticity are applicable, their characteristics can be simulated by their natural modes and frequencies of vibration. A computer program, NBOD2, developed to help analyze spacecraft attitude dynamics, may be applied to a large class of problems involving coupled N-body systems. The program derives and solves numerically the equations of motion for any system that can be modeled as a topological tree of coupled rigid bodies, terminal flexible bodies, point masses, and symmetrical momentum wheels.

A topological-tree model of the dynamic system is used to derive vector-dyadic equations of motion for the system. To insure that the relative motion between contiguous bodies in the user-derived tree model is constrained kinematically, NBOD2 assumes that contiguous rigid and flexible bodies are connected by physically-realizable 0-, 1-, 2-, or 3-degrees-of-freedom gimbals. These gimbals prohibit relative translational motion while permitting up to 3 degrees of relative rotational freedom at hinge points.

Point masses may have 0, 1, 2, or 3 degrees of relative translational freedom, and symmetric momentum wheels have a single degree of rotational freedom relative to the body in which they are embedded. Flexible bodies must be at the end of limbs. They may possess several degrees of vibrational freedom in addition to the degrees of freedom associated with the connection gimbals. Data defining the elastic characteristics of the flexible bodies must be supplied by the user. These data can be obtained by using such programs as NASTRAN. A support program is provided for processing NASTRAN data into a format compatible with NBOD2. Program NBOD2 uses a Eulerian nested-body approach to derive the complete set of nonlinear equations of motion in a vector-dyadic format. These equations may be presented directly on a line printer for review, or they may be solved numerically; and a user-specified set of system state variables may be output.

This program is written in FORTRAN IV for batch execution and has been implemented on an IBM 360-series computer with a central memory requirement of approximately 270K of 8-bit bytes. NBOD2 was developed in 1978.

This program was written by Harold P. Frisch of **Goddard Space Flight Center.** *For further information, Circle D on the COSMIC Request Card.*
GSC-12407

Viscous Characteristics Analysis

Aid for supersonic-combustor development considers combustion and diffusion effects.

Investigations of the hydrogen-fueled supersonic combustion ramjet engine have delineated several technological problem areas. One area, the analysis of the injection, turbulent mixing, and combustion of hydrogen, requires accurate calculation of the supersonic combustion-flow fields. This calculation has proved difficult because of an interesting phenomenon: Temperature transitions in the flow field cause a change from supersonic to subsonic flow in the combustion field.

A first computer program was developed to use viscous characteristics theory to analyze supersonic combustion-flow fields with embedded subsonic regions (adjacent to boundaries). A second improved program was developed to consider both combustion and diffusive effects. It is intended to be used as a practical design tool for two-dimensional and axisymmetric supersonic-combustor development. (The first program is not presently available from COSMIC but is described in the documentation for LAR-12598, the second program.)

This second program has proved useful in the analysis of such problems as determining the flow field of a single underexpanded hydrogen jet, the internal flow of a gas-sampling probe, the effects of fuel-injector strut shape, and the effects of changes in combustor configuration. None of these problems have subsonic regions, and thus the subsonic capabilities of the program have not been tested rigorously.

Both combustion and diffusive effects can alter significantly the wave pattern in a supersonic field and can generate significant pressure gradients in the axial and radial directions. The induced pressure, in turn, substantially influences the ignition delay and reaction times as well as the velocity distribution. To analyze accurately the flow fields, the effects of finite-rate chemistry, mixing, and wave propagation must be linked to one another properly.

Viscous characteristics theory has been used in the past to describe flows that are pure supersonic; however, the interacting pressure effects in the combustor often cause the development of shock waves and embedded subsonic regions. Numerical investigation of subsonic regions (not adjacent to boundaries) awaits a new procedure that is valid within the subsonic region and can be coupled with the standard viscous characteristics procedure in the supersonic region.

Combustion and geometry shock waves, as well as expansion waves, are determined in the present program. The basic governing equations used are the viscous-inviscid equa-

tions, similar to those employed in higher-order boundary-layer analyses, with finite-rate chemistry terms included. In addition, the Rankine-Hugoniot and Prandtl-Meyer relations are used to compute shock and expansion conditions.

The program can handle up to 20 simultaneous shock waves. Chemistry terms are computed for a seven-species eight-mechanism hydrogen-and-air reaction scheme. Inputs consist of a physical description of the combustor and flow-determination parameters. Output includes detail flow-parameter values at selected points within the flow field.

This computer program is written in FORTRAN IV for batch execution and has been implemented on a CDC CYBER 175 with a central memory requirement of approximately 117K (octal) of 60-bit words. The program was developed in 1978.

This program was written by Renaldo V. Jenkins of **Langley Research Center.** *For further information, Circle E on the COSMIC Request Card.*
LAR-12598

Transonic Airfoil Design Code

Aid in design of shockless airfoils

Supercritical wing technology is expected to have a significant influence on the next generation of commercial aircraft. The use of supercritical wings could economize fuel consumption by reducing drag. An effective approach to the design of supercritical wings is through the development of shockless airfoils. In the past, the design of shockless airfoils was based on hodograph methods, which required extensive trial and error work. A recent computer program makes it possible to assign the velocity as a function of arc length and to obtain a shockless airfoil that nearly achieves the desired pressure distribution. It should enable engineers to design families of transonic airfoils for use on aircraft wings and could be useful for similar design problems, such as for turbine and compressor blades in cascade.

In gas dynamics, the partial differential equation for the velocity potential describing the isentropic flow of a compressible fluid can be derived from a variational principle. This principle asserts that the integral of the pressure over the flow field is stationary in its dependence on the velocity potential. Designing an airfoil for which the speed has been assigned as a function of arc length consists of solving a nonlinear boundary-value problem interrelating the map function and the stream function.

The solution is calculated iteratively between the map function and the stream function until a flow is determined that fits the prescribed pressure data. An exact solution cannot be expected to exist for transonic flows. However, a shockless flow is almost always obtained if there is one that closely approximates the given data.

The displacement thickness of the boundary layer is calculated from the inviscid pressure distribution by the momentum integral method of Nash and Macdonald. The displacement is subtracted from the airfoil coordinates, which are provided with a slightly-open trailing edge. The criterion of Stratford is used to impose a pressure distribution on the trailing edge of the upper surface that just avoids separation so that there is no loss of lift.

This program is written in FORTRAN IV for batch execution and has been implemented on a CDC-6000 series computer with a central memory requirement of approximately 135K (octal) of 60-bit words. This program was developed in 1977.

This program was written by Frances Bauer, Paul Garabedian, and David Korn of New York University for **Langley Research Center.** *For further information, Circle F on the COSMIC Request Card.*
LAR-12460

Improved Multielement Airfoil Analysis

Revised flow model produces results closer to experiment.

A great deal of attention has been given to the use of multielement airfoil designs, due to their high-lift capabilities. The flow around high-lift airfoils is characterized by many different inviscid and viscous flow regions. In particular, the existence of confluent boundary layers and regions of separated flow distinguishes the high-lift airfoil problem from the aerodynamic problem of standard airfoils at cruise speed.

To analyze high-lift airfoils effectively, it is necessary to compute accurately the various flow regions, including the outer potential flow, ordinary laminar and turbulent boundary layers, viscous wakes, and the confluent boundary layer. It is also necessary to predict the transition from laminar to turbulent boundary-layer flow and the onset of boundary-layer separation. The NASA/Lockheed Multielement Airfoil Analysis Program was one of the first attempts at numerically analyzing the complex viscous flow about slotted airfoils and has received worldwide usage. A recent evaluation of the Multielement Airfoil Computer Program has resulted in a major revision of the flow model. Comparisons between computed results and experimental data indicate that this version is more reliable than the older (1969) version.

The flow about a high-lift airfoil is computed assuming that the flow is attached to the airfoil surface and that the flow is two-dimensional and subcritical. The effect of the viscous flow is represented by a surface transpiration method, which uses an equivalent distribution of sources along the airfoil surface and the wake centerline to model the boundary layer and wake displacement effects. The flow model of the potential core utilizes the standard laminar and turbulent boundary-layer calculations with the addition of the lag-entrainment method of Green. The onset of separation of the confluent boundary layer is predicted by a modified version of Goradia's method with the power-law velocity profile replaced by Coles' two-parameter velocity profile. Drag prediction is based on the method of Squire and Young. The flow in the slot between adjacent airfoil components is calculated as an integral part of the overall flow computation. The airfoil to be analyzed may contain as many as 10 components with either negative or positive overlap.

(continued on next page)

This computer program is written in FORTRAN IV and Assembler for batch execution and can only be implemented on a CDC CYBER 175 with a central memory requirement of approximately 62K of 60-bit words. This version of the Multielement Airfoil Analysis Program was developed in 1978.

This program was written by G. W. Brune and J. W. Manke of The Boeing Co. for **Langley Research Center.** *For further information, Circle G on the COSMIC Request Card.*
LAR-12489

Aircraft Equilibrium Spin Characteristics

Solutions to equations of motion include spin characteristics.

Determination of the equilibrium spin characteristics of an aircraft is an essential part of the analysis step. The SPINEQ program was developed to provide analytic solutions to the nonlinear equations of motion for equilibrium spin conditions. These equations of motion require that the aircraft move along a helical trajectory with a constant angular velocity. Stability characteristics are also determined by linearization of the equations of motion about the equilibrium spin condition.

The solutions obtained by SPINEQ satisfy the requirement that a steady developed spin occurs if the equilibrium points are stable. Solutions having linear representations that are unstable either correspond to oscillatory spin conditions or are not actually developed spin conditions. The realism of the solutions is dependent on the accuracy of the aerodynamic data supplied to the program.

Inputs include aerodynamic coefficients, flight conditions, control settings, and solution control parameters. SPINEQ can be used to study the sensitivity of spin equilibrium conditions to variations in selected aerodynamic or inertial data. It can also be used in evaluating the adequacy of aerodynamic data in the spin region when accompanying experimental spin tests are available. Outputs include all values used in attaining convergence and the final state variables. With some alterations, SPINEQ could be employed to compute equilibrium conditions for steady maneuvers.

This program is written in FORTRAN IV for batch execution and has been implemented on a CDC CYBER 173 with a central memory requirement of approximately 10K (octal) of 60-bit words. SPINEQ was documented in 1978.

This program was written by William M. Adams, Jr., of **Langley Research Center.** *For further information, Circle H on the COSMIC Request Card.*
LAR-12502

Flow Field in Supersonic Mixed-Compression Inlets

Program uses 3-D method of characteristics.

The flow field in the supersonic portion of a mixed-compression aircraft inlet at nonzero angle of attack is calculated based on the method of characteristics for steady three-dimensional flow. The results of the computer program agree with those produced by the two-dimensional method of characteristics when axisymmetric flow fields are calculated. Except in regions of high viscous interaction and boundary-layer removal, the results agree well with experimental data obtained for three-dimensional flow fields.

The flow field in a variety of axisymmetric mixed-compression inlets can be calculated using the program. The bow shock wave and the internal shock-wave system are calculated using a discrete shock-wave fitting procedure. The internal flow field can be calculated either with or without the discrete fitting of the internal shock-wave system. The influence of molecular transport can be included in the calculation of the external flow about the forebody and in the calculation of the internal flow when internal shock waves are not discretely fitted.

The viscous and thermal diffusion effects are included by treating them as correction terms in the method of characteristics procedure. Dynamic viscosity is represented by Sutherland's law, and thermal conductivity is represented as a quadratic function of temperature. The thermodynamic model used is that of a thermally and calorically perfect gas.

The program assumes that the cowl lip is contained in a constant plane and that the centerbody contour and cowl contour are smooth and have continuous first partial derivatives. This program cannot calculate subsonic flow, the external flow field if the bow shock wave does not exist entirely around the forebody, or the internal flow field if the bow flow field is injected into the annulus. Input to the program consists of parameters to control execution, to define the geometry, and the vehicle orientation. Output consists of a list of parameters used, solution planes, and a description of the shock waves.

This program is written in FORTRAN IV for batch execution and has been implemented on a CDC 6000-series machine with a central memory requirement of 110K (octal) of 60-bit words when it is overlaid. This flow analysis program was developed in 1978.

This program was written by Allan R. Bishop of **Lewis Research Center** *and Joe D. Hoffman and Joseph Vadyak of Purdue University. For further information, Circle J on the COSMIC Request Card.*
LEW-13279

Shell Theory Automated for Rotational Structures

Numerical integration package for analysis of shells of revolution

Many structures, such as aircraft bodies, spacecraft, submarines, and storage tanks, can be analyzed efficiently by using shell theory. Several methods are currently available to solve the equations derived from shell theory. The program STARS (Shell Theory Automated for Rotational Structures) incorporates the method

of numerical integration into a package of programs that use Love-Reissner first-order shell theory numerically to analyze shells of revolution.

The programs in the STARS package can perform static, buckling, vibration, and plastic analyses on thin shells of revolution subjected to distributed loads, concentrated line loads, and thermal strain. A wide range of shell-wall cross sections and combinations of geometric shapes can be effectively handled by these programs.

The structure under study is divided into numerous shell regions. Each region must be a singly connected shell. The regions are further subdivided into several shell segments, each being free to have its own geometric shape. Stiffness matrices obtained for each segment are coupled to determine regional stiffnesses. The regional stiffness matrices are reduced and coupled to form the stiffness matrix of the total structure.

In the linear analysis of unsymmetrically loaded shells, the partial differential equations of shell theory are reduced to first-order differential equations and are solved using a Runge-Kutta method of numerical integration. STARS may also be used for nonlinear analysis of axisymmetric loaded shells. These plastic, large deformation cases are analyzed by a special solution iteration scheme. The user supplies STARS with segment geometric data, segment orientation and coupling data, joint freedom data, and structural material data. Output from STARS includes stresses, displacements, plastic strains, and vibration and buckling results.

The STARS package is written in FORTRAN IV for batch execution and has been implemented on a UNIVAC 1108 with a central memory requirement of 53K of 36-bit words when segmented. The STARS package was developed in 1975.

This program was written by John Key of **Marshall Space Flight Center** *and V. Sval Gonas, H. Levine, and P. Ogilvie of Grumman Aerospace Corp. For further information, Circle K on the COSMIC Request Card.*
MFS-23027

Three-Dimensional Potential Flow

Geometry package for generation of input data

It is important that the aerodynamicist be able to study the effects of configuration changes on lift, load distributions, local pressures, and flow angles. A new computer program calculates viscous effects on the lifts and pressure distributions of arbitrary three-dimensional configurations. It combines a panel method that calculates potential flow about arbitrary three-dimensional lifting configurations with a two-dimensional boundary-layer method, which is used in a strip-theory sense. The program performs all the necessary calculations without user intervention once the configuration and flow regime are given. A geometry package for input data generation reduces the user-supplied configuration data required by an order of magnitude. Calculated inviscid and viscous lift and pressure distributions agree well with experimental data for a variety of wings and wing/fuselages having both conventional and supercritical airfoil sections.

The basic procedure for combining an inviscid-flow method and a boundary-layer method is independent of dimensionality and speed regime. The program couples a three-dimensional lifting potential-flow program and a simplified finite-difference program for calculating compressible laminar and turbulent boundary layers with a program that simulates the effect of the boundary layer on the flow. Alternate subroutines allow the boundary layer to influence the potential flow by a displacement of the surface coordinates or by a simulated surface blowing. The program computes an initial potential-flow solution; then it solves the two-dimensional boundary-layer equations along strips in the stream direction and generates a distribution of displacement thickness over the body surface. This displacement is used either to generate a new set of geometry coordinates or to calculate a simulated blowing velocity over the original body surface. The final potential-flow calculation is made with the chosen boundary-layer procedure producing the simulated viscous flow.

This program is written in FORTRAN IV for batch execution and has been implemented on a CDC CYBER 175 with a central memory requirement of approximately 250K (octal) of 60-bit words using the overlay capability. The potential flow program was developed in 1977 with updates and geometry package development occurring in 1978.

This program was written by N. Douglas Halsey and John L. Hess of McDonnell Douglas Corp. for **Langley Research Center.** *Further information on this technology may be found in NASA TM-80088 [N79-31142/NSP], "Comparison of Three-Dimensional Panel Methods with Strip Boundary-Layer Simulations to Experiment" [$5.25]. A copy may be purchased [prepayment required] from the National Technical Information Service, Springfield, Virginia 22161. For further information on the computer program, Circle L on the COSMIC Request Card.*
LAR-12623

Full-Coverage Film Cooling

Coolant flows and metal temperatures for blades and vanes

A computer program, called FCFC, has been developed to calculate coolant flow and wall temperatures of a full-coverage film-cooled vane or blade. Full-coverage film cooling is an effective way of protecting turbine components from the hostile environment of high gas temperature and pressure encountered in a gas-turbine engine. Full-coverage film cooling permits higher operating temperatures and pressures than conventional cooling, resulting in greater overall cycle efficiency.

FCFC combines previous experiments and analyses of full-coverage film cooling into an overall analytical procedure. Vane or blade metal temperatures are calculated for the blade-shell inner and outer surfaces.

(continued on next page)

These temperatures are average values for a shell outer-surface area associated with each film-cooling-hole row. Heat-transfer calculations are one-dimensional through the wall and neglect conduction from adjacent areas. A thermal barrier coating may be specified on the shell outer surface. When a coating is specified, the program also calculates the outer-surface temperature of the ceramic coating.

The program inputs consist of the blade or vane internal-chamber geometry (hole sizes and hole spacing); coolant supply temperature and pressure; and main-stream-gas heat-transfer coefficients and pressure, velocity, and temperature distributions. The physical properties of the coolant and the thermal conductivities of the metal and the ceramic coating are input as functions of temperature. The coolant-flow coefficients for the impingement and film-cooling holes are input as a function of mach number. Outputs summarize the geometric data; calculated coolant flows, pressure, and temperatures; and the calculated metal-coating temperatures.

FCFC is written in FORTRAN V for batch execution and has been implemented on a UNIVAC 1100-series computer with a central memory requirement of 22K of 36-bit words. This program development was completed in 1978.

This program was written by Peter L. Meitner of the U.S. Army Research & Technology Laboratories for **Lewis Research Center.** *For further information, Circle M on the COSMIC Request Card.*
LEW-13249

Disturbance Amplification Rates

Tapered laminar-flow control wings with suction

The computer program SALLY computes the incompressible linear stability characteristics and integrates the amplification rates of boundary-layer disturbances on swept and tapered wings. For some wing designs, boundary-layer disturbances can significantly alter the wing performance. This is particularly true for swept and tapered laminar-flow control wings, which incorporate suction to prevent boundary-layer separation.

The first step in calculating the disturbance amplification rates is to solve numerically the compressible laminar-boundary-layer equation with suction for the swept and tapered wing. A two-point finite-difference method solves the governing continuity, momentum, and energy equations. A similarity transformation is used to remove the wall normal velocity as a boundary condition and to place it into the governing equations as a parameter. Thus the awkard nonlinear boundary condition is avoided.

The resulting compressible boundary-layer calculations are used to compute the incompressible linear stability characteristics. The local disturbance growth is obtained from temporal stability theory and is converted into a local growth rate for integration. The local growth rates are integrated in the direction of the local group velocity, and the logarithmic disturbance-amplitude ratio is obtained as a function of chordwise distance. This disturbance-amplitude ratio is a measure of the growth of linear disturbances within the boundary layer and can serve as a guide in transition prediction.

This program is written in FORTRAN IV and Assembler for batch execution and has been implemented on a CDC CYBER 70-series computer with a central memory requirement of approximately 67K (octal) of 60-bit words. SALLY was developed in 1979.

This program was written by Andrew J. Srokowski of **Langley Research Center,** *Steven A. Orszag of Cambridge Hydrodynamics, Inc., and Tuncer Cebeci and Kalle Kaups of McDonnell Douglas Corp. For further information, Circle N on the COSMIC Request Card.*
LAR-12556

Machinery

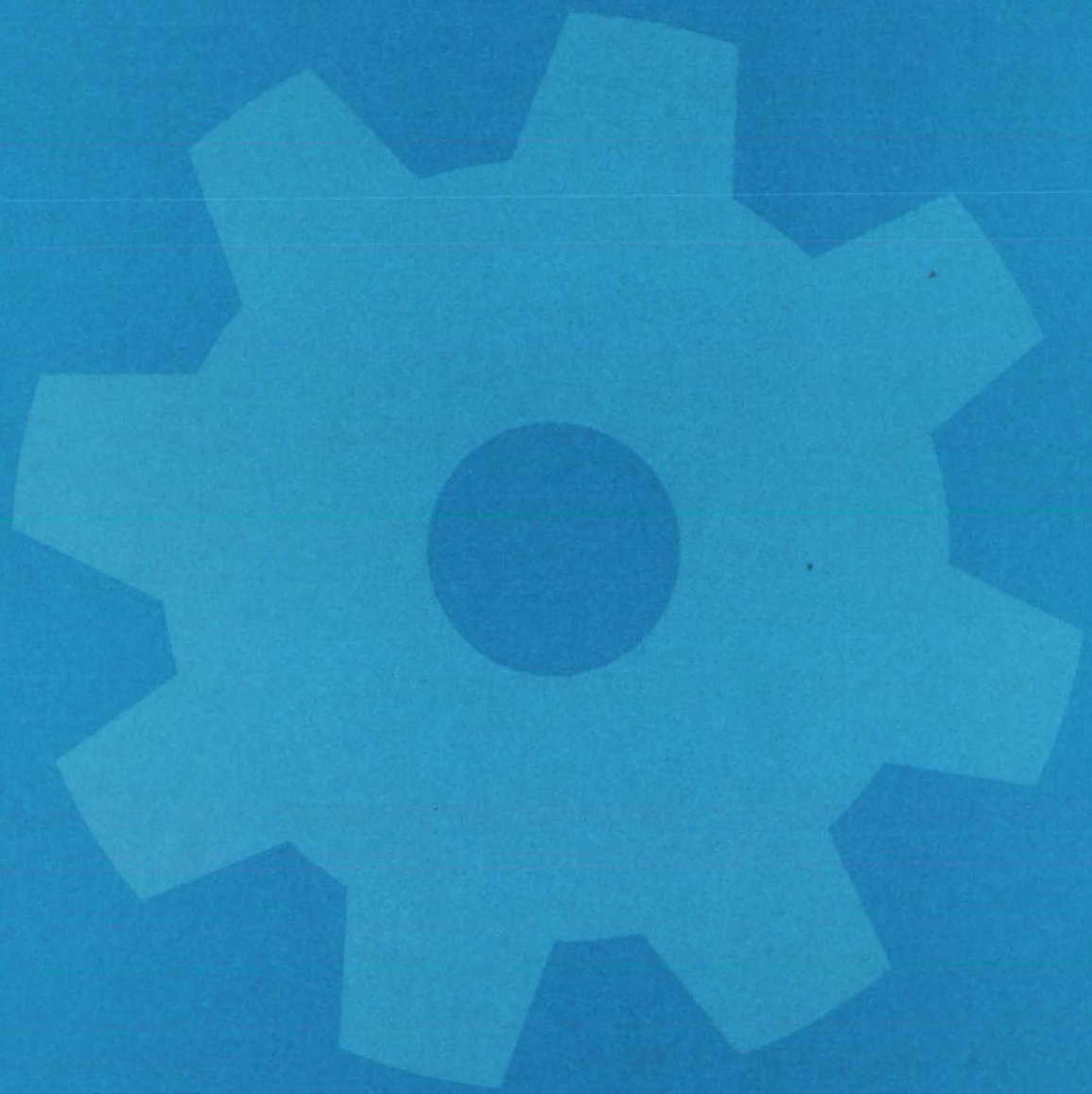

Hardware, Techniques, and Processes

Books and Reports

Precision Filament Cutter

Digital control lets an operator choose the fiber length and chopping rate.

Langley Research Center, Hampton, Virginia

The machine illustrated in the figure chops filaments of glass, graphite, plastic, or other material into fibers for use in composites and other applications. The fiber length and the chopping rate can be selected independently, and fiber length is accurate to within 0.2 millimeter of the length setting. A prototype has undergone successful operational tests and is in continuous use at Langley Research Center.

For a 10-millimeter fiber length, a single chop sequence requires 33 milliseconds. Longer fibers require an additional 0.8 millisecond per millimeter. Thus the maximum chopping rate for 10-millimeter fibers is 30 cuts per second; for 15-millimeter fibers it is 27 chops per second. The operator can select slower rates.

The machine contains a fixed blade, a double-edged moving blade actuated by opposed solenoids, a motor-driven precision indexing mechanism, and fixtures for guiding the filaments to the blades (see figure). Logic circuits control the indexing motor, the solenoids, and an air jet for dispersing the cut filaments.

An operator selects the fiber length and the chopping rate by adjusting controls on the front panel. The drive motor advances a length of multifilament tow according to the length setting. When the fiber is in position between the blades, the logic circuit actuates a solenoid, pulling the movable blade over the fixed blade and snipping off the filaments. The motor again advances a length of tow, and the circuitry actuates the opposite solenoid, pulling the other edge of the movable blade over the fixed blade. The sequence repeats automatically until the machine is turned off. After each cut, a blast of air blows the filament away so it can be collected.

Because the mass of the movable blade is small and the stroke is short, operation is fast, and wear and energy consumption are low. The push/pull motion of the blade speeds up operation by cutting on both forward and return movements.

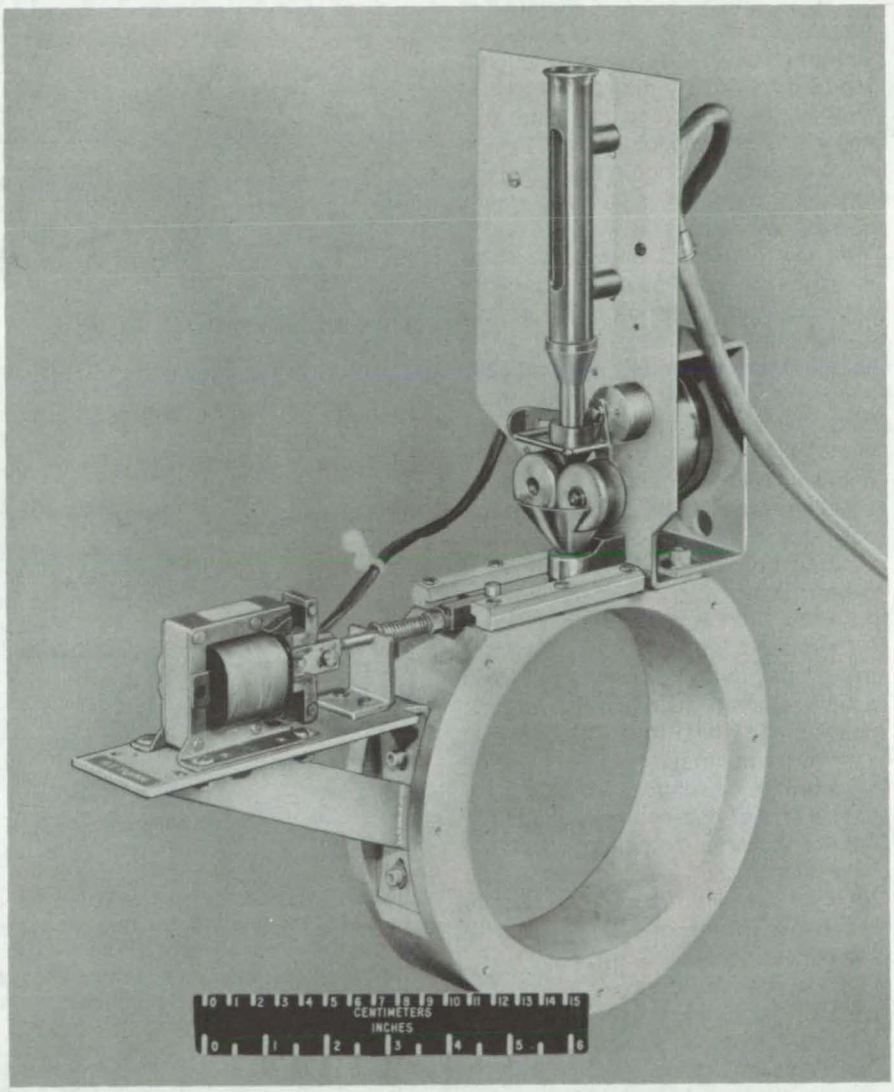

The **Push/Pull Blade** in this prototype filament cutter chops a length of multifilament tow as it is drawn back and forth over a fixed blade (not visible). The drive motor advances a precise length of tow each time the blade moves. Only one solenoid is used in this prototype; the final version will have two.

This work was done by Austin D. McHatton and Arthur L. Newcomb, Jr., of **Langley Research Center** *and Gregory Schluge of Bionetics Corp. For further information, Circle 62 on the TSP Request Card.*

This invention is owned by NASA, and a patent application has been filed. Inquiries concerning nonexclusive or exclusive license for its commercial development should be addressed to the Patent Counsel, Langley Research Center [see page A5]. *Refer to LAR-12564.*

Automatic Connector for Structural Beams

A novel beam connector allows quick alinement, connection, and disconnection.

Marshall Space Flight Center, Alabama

Typical structural-beam connectors are permanent and cannot easily be separated without destroying the joint. Moreover, much manual work is needed to aline, engage, and disengage these connectors; and, though most beam connectors withstand tension and compression loads, many do not tolerate torsion.

A new connector allows for longitudinal and transverse structural-beam assembly and needs no tools for easy connection or disconnection. The lightweight connector automatically alines the beams and absorbs torque loads, tension, and compression. Its automated trigger engagement and release make the connector faster to use than many others. Though originally designed for in-space assembly of large orbiting structures, the connector may also be suitable for assemblies on Earth as well.

The beam connector (see figure) has a four-prong shaft that is retracted against a compression spring within a housing. It is held in position by two locking arms that rest in recessed slots on the housing.

The end of one beam is fitted with the connector; a matching receptor is placed on the other beam. The receptor is cylindrical and has slots to receive the three or more prongs of the beam connector shaft.

An alinement bracket alines the axes of the connector and receptor. When a release lever is actuated, the compressed spring expands and pushes the connector shaft into the receptor. The prongs, which have engagement hooks, snap and lock into the receptor slots to complete the connection. The lever can be remotely actuated, mechanically or electrically, for fully automated connection.

To disconnect the beam, a simple release, consisting of a sliding ring with a prong depressor, is used. The retractor ring is pushed along the slots of the receptor to depress the connector prongs. The connector can then be retracted by the actuating levers and secured, and the beams can be separated.

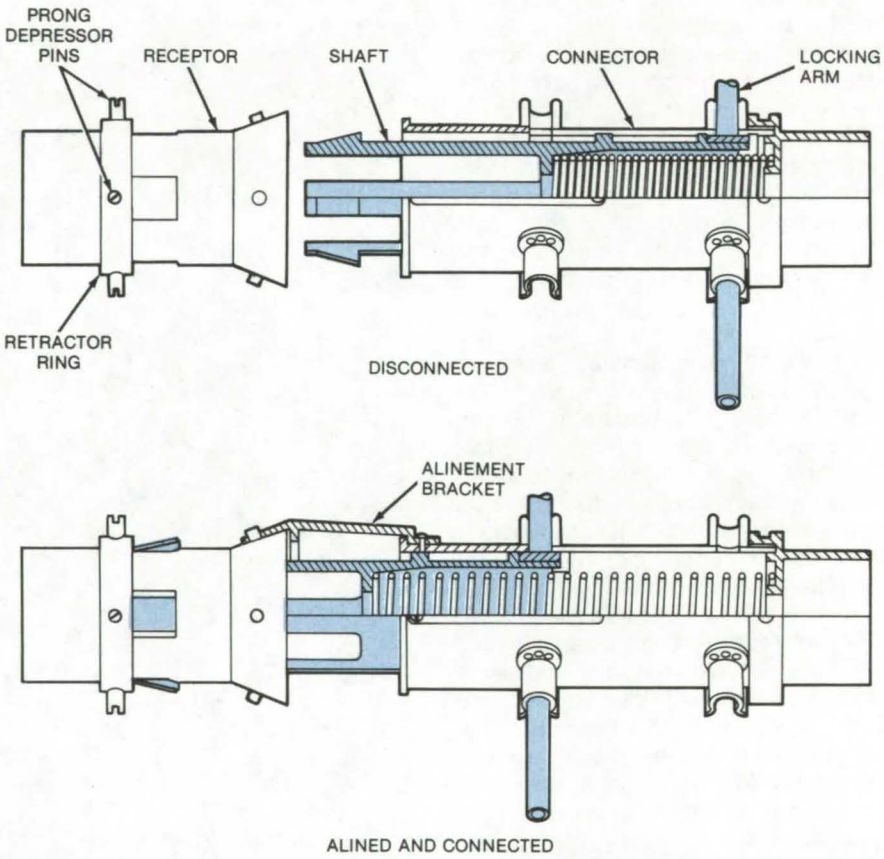

The Beam Connector is shown disconnected and connected. When the locking arms move out of their slots, the hooked prongs are pushed out of the connector housing by the compressed spring and into the receptor, where they lock into slots. To disconnect the beam, the retractor ring is pushed along the receptor slots to depress the connector prongs; the connector can then be retracted by the actuating levers.

This work was done by Georg F. von Tiesenhausen of **Marshall Space Flight Center.** *For further information, Circle 63 on the TSP Request Card.*

Inquiries concerning rights for the commercial use of this invention should be addressed to the Patent Counsel, Marshall Space Flight Center [see page A5]. Refer to MFS-25134.

Mechanical End Joint for Structural Columns

Lightweight, side-entry system assembles without tools.

Langley Research Center, Hampton, Virginia

A column-end joint system that connects tubular struts in various lightweight skeletal-framework structures consists of two main components (see figure):

1. A node fitting with attached mechanical-joint halves at locations required by individual structures; and
2. Strut elements with machined joint halves attached to ends, with length adjustments made.

To produce a structurally sound joint from the two components, the two parts are alined approximately and pushed together. As the integral semicircular tongues enter their mating grooves, their tapered form compensates for small longitudinal misalinement. The radial alinement pins engage stops on the mating joint half to compensate for small radial misalinement. During this assembly sequence, the locking latches contact and subsequently ride the crests of the semicircular tongues until the tongues mate with their corresponding grooves. At that time the pawls on the locking latches engage their corresponding latch-engagement steps.

A small transverse force is required to effect this joint due to the wedge action of the engaging faces. Normal finger pressure is adequate. The node fitting, along with its joint-node elements, could be produced as a single piece; material could be cast or molded metal or filament-reinforced or thermoformed plastic.

Previous methods of making such structural connections have utilized mechanical fasteners, threaded fittings, or welding operations. When assembly is in situ, such procedures are time consuming and costly, and the resulting joints are normally heavy. Some prior joint systems do not permit struts to be inserted or removed between fixed nodes without taking the nodal joint apart.

The new arrangement circumvents this restriction and permits the construction of skeletal frameworks without the use of tools or assembly equipment. Node fittings can be custom designed easily for various degrees of column fixity without affecting operative joint fixtures, and the design accommodates reasonable axial and rotational misalinement of nodes and struts. Individual columns can be inserted and removed between fixed nodes without affecting the integrity of the remaining structure, and all operative joint components are interchangeable. In addition, this joint system is lightweight and mass producible, and it contains no moving parts.

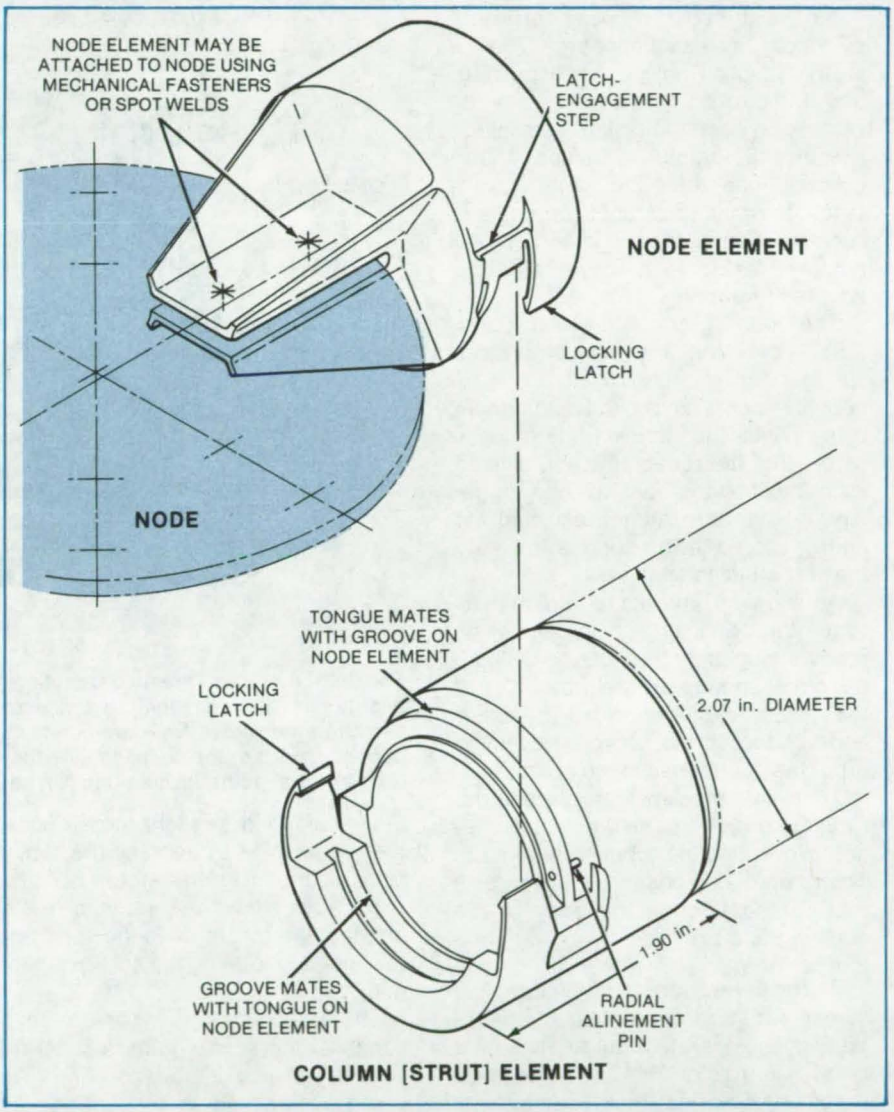

Mechanical End-Joint System for structural columns consists of a node fitting and a strut element. The node and node-element shown are typical; they may be varied to meet specific requirements.

This work was done by Harold G. Bush of **Langley Research Center** *and Richard E. Wallsom of Vought Corp. For further information, Circle 64 on the TSP Request Card.*

Inquiries concerning rights for the commercial use of this invention should be addressed to the Patent Counsel, Langley Research Center [see page A5]. Refer to LAR-12482.

Self-Energized Screw Coupling

A spring-loaded threaded fastener is actuated by just a push.

Marshall Space Flight Center, Alabama

A novel threaded coupling carries its own store of rotational energy. The operator supplies only a small push to trigger the rotary motion. Originally developed to ease the task of astronauts assembling structures in space, the coupling can offer the same advantages in other hazardous operations, such as underwater and in and around nuclear reactors. It could also be adapted for robotics.

The coupling consists of two parts: Part 1 contains a screw, two clock springs, and a ratchet. Part 2 is a receptacle containing a nut and trigger pins. When the screw portion is inserted into the receptacle and given a slight push by the operator, the trigger pins release the ratchet, allowing the energy stored in the springs to rotate the screw into the nut.

As shown in the figure, which illustrates the coupling with the screw already engaged by the nut, the cylindrical clock springs are held by a pin at their outer circumference. The other ends of the springs power a rotating arbor that it attached to the screw.

Three compression springs load the ratchet so that it bears against the arbor, preventing the arbor from turning. The ratchet also has three sliding pins that extend through the body of the coupling and protrude through its bottom surface.

As the screw portion of the coupling is inserted into the receptacle, it is rotated by the operator until an alinement pin falls into a slot. This alines the three trigger pins so that they bear against the sliding pins. A slight force causes the trigger pins to depress the sliding pins, disengaging the ratchet from the arbor. This allows the arbor to rotate, and the energy stored in the springs is expended in rotating the screw into the nut.

The rotation stops when the mid-flange of the screw bears against the seating surface in the coupling. The energy remaining in the springs assures positive locking.

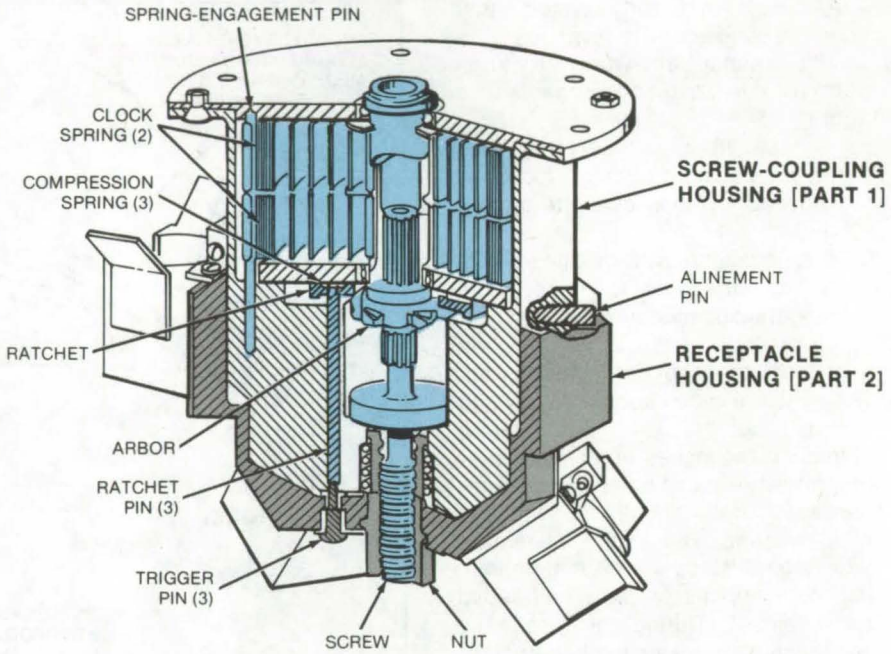

The Self-Energized Threaded Coupling has two clock springs that carry the rotational energy needed to engage the screw and nut. The adapter is disengaged by manually resetting the screw. A square-nosed speed wrench is inserted in one of two holes on opposite sides of the coupling, and the screw is turned until the ratchet reengages the arbor. At that point the coupling can be demated.

This work was done by Alan E. LeFever and Raymond S. Totah of Rockwell International Corp. for **Marshall Space Flight Center.** *No further documentation is available.*

Inquiries concerning rights for the commercial use of this invention should be addressed to the Patent Counsel, Marshall Space Flight Center [see page A5]. Refer to MFS-25340.

Automatic Shutoff Valve

A cellulose-sponge-activated valve bars water from the vent line.

Lyndon B. Johnson Space Center, Houston, Texas

A relatively-simple shutoff valve proposed for the Space Shuttle wastewater-tank vents is activated by a cellulose-sponge disk. The sponge absorbs incoming water and expands with enough force to shut the valve. This direct mechanical action is expected to be more reliable than an electrically-activated solenoid valve.

Preshaped sponge disks are prepared by first wetting and compressing them to about one-eleventh of the

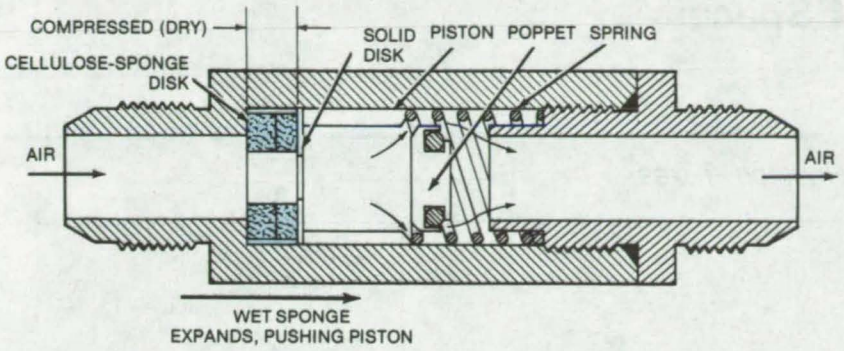

Cellulose-Sponge-Activated Valve prevents water from entering the air vent system. The sponge disk absorbs moisture and expands, driving a spring-loaded piston against a plunger and shutting off the valve. When the water recedes, the piston squeezes the sponge back to its original shape and opens the valve.

original dry thickness [e.g., 1-3/8 in. to 1/8 in. (3.5 cm to 0.3 cm)] for vacuum drying to a "permanent" thickness. Samples of wet finished disks are reported to expand from 1/8 in. (0.3 cm) to 3/4 in. (1.9 cm), developing 5 lb/in.^{2} (34.5×10^3 N/m^2) pressure — sufficient to close the valve.

The dry disk (see figure) is inserted into the valve cavity and is backed up by a solid disk that drives a spring-loaded piston. When the sponge is dry, spring force keeps the piston open, allowing air to escape through the vent. When water enters the system, the sponge expands, overcoming the spring force and driving the piston against the plunger to shut the valve. When the water recedes, the valve opens up by squeezing the sponge dry to its original shape.

This work was done by Scott F. Hawkins and Charles W. Overbey of Rockwell International Corp. for **Johnson Space Center.** *No further documentation is available.*
MSC-19385

Vise Holds Specimens for Microscope

A convenient, miniature, spring-loaded mechanism holds specimens for scanning electron microscope.

Lyndon B. Johnson Space Center, Houston, Texas

A simple vise (see figure) made from three components holds specimens for display in a scanning electron microscope. The specimen is secured with a jawlike structure without being cemented and can be easily reused after the analysis.

The vise consists of a studded aluminum angle and a threaded mating nesting angle. The specimen is simply inserted between the two, and a spring-loaded screw is tightened into the nesting angle until the spring becomes tight enough to depress the aluminum angle against the specimen. When the specimen is secured, the vise is inserted into the microscope mount. The stud at the bottom fits the standard mounts.

The vise eliminates a more involved method of using conductive adhesives to secure the samples. Samples cemented to flat studs with silver paint are more difficult to remove.

This work was done by Walter N. Greule of Rockwell International Corp. for **Johnson Space Center.** *No further documentation is available.*
MSC-18690

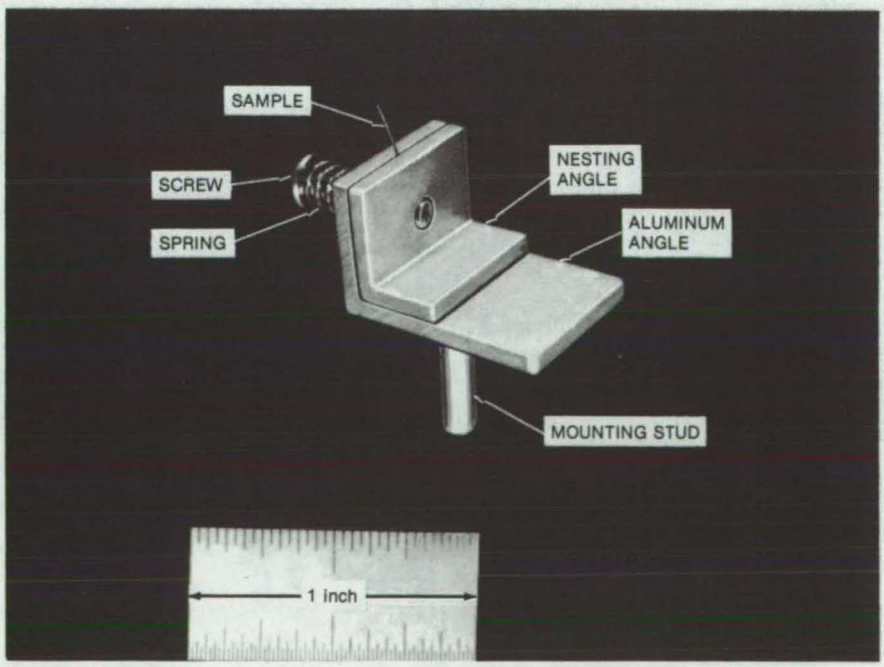

Miniature Spring-Loaded Vise holds specimens for scanning electron microscope analysis. A wire specimen shown is held in a jawlike structure formed by two mating angles. A spring-loaded screw driven into the nesting angle tightens the grip.

Tubing Cutter for Tight Spaces

Two-ratchet handtool cuts tubing in confined installations.

Lyndon B. Johnson Space Center, Houston, Texas

A new tubing cutter requires only a few short swings of its handle to rotate its cutting edge a full 360° around a tube. It is therefore useful for cutting tubing that has been installed in a confined space that would prevent the free movement of a conventional cutter.

The essential parts of the new cutter are seen in the figure. The cutting blade is mounted on a slider block that travels on a screw ratchet. A spring-loaded roller clamps the cutter on the tube until the blade is advanced to make the first cut. The blade, slider block, and clamping roller form a unit that is mounted on a ratchet in the main body of the cutter.

To use the cutter, the operator snaps it onto the tube, where it is held in place by the spring-loaded roller. Then the screw ratchet is rotated to advance the cutting wheel until it contacts the tube. After each full rotation of the body, the screw ratchet is turned so that the cutting blade penetrates deeper into the tube for the next cut.

A powered version of the tubing cutter would add a motorized drive to the basic unit shown. The motor could be made part of the cutter, or a fitting could be added to take power from a conventional drill motor. An automated advance of the slider block, synchronized with the cutting action, could also be designed.

This work was done by Anthony S. Girala of **Johnson Space Center.** *For further information, Circle 65 on the TSP Request Card.*

This invention is owned by NASA, and a patent application has been filed. Inquiries concerning nonexclusive or exclusive license for its commercial development should be addressed to the Patent Counsel, Johnson Space Center [see page A5]. Refer to MSC-18538.

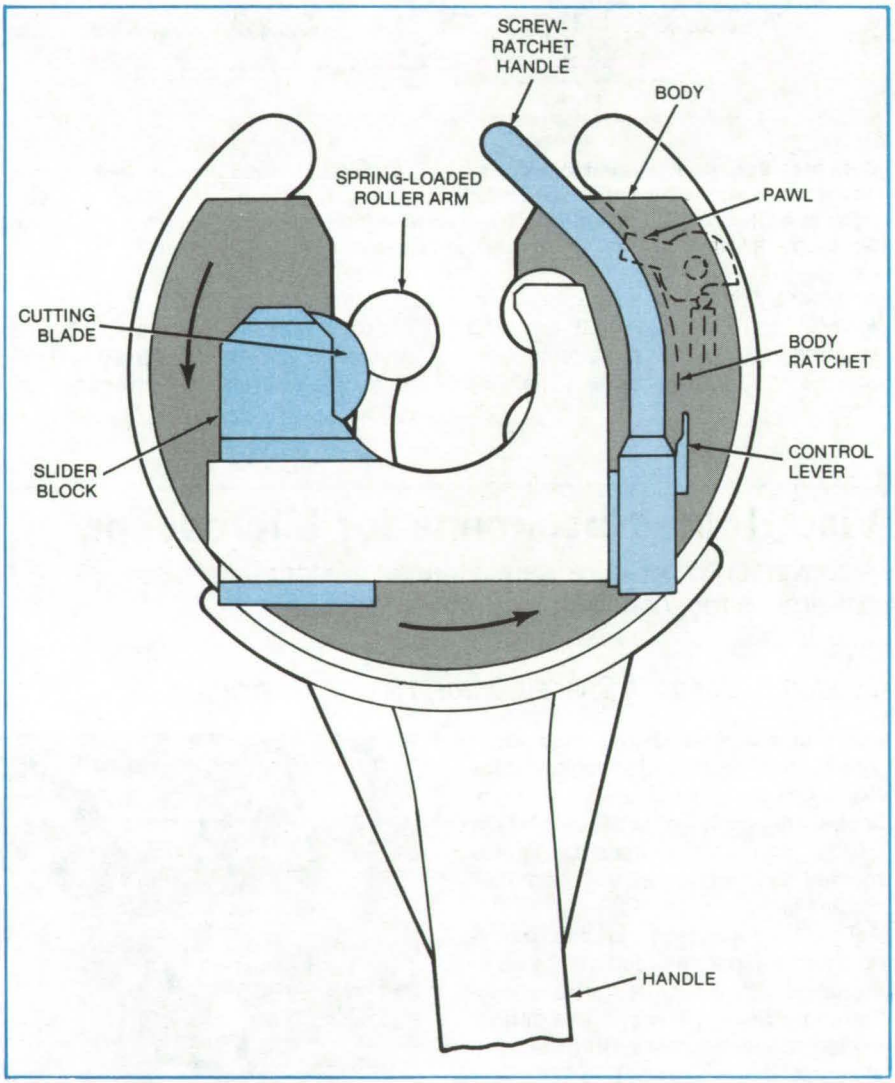

This **Tubing Cutter** is held on a tube by the spring-loaded clamp. The cutting wheel is advanced until it contacts the tube by moving the screw-ratchet handle. An existing model cuts titanium, iron/nickel alloys, or plastic tubing, 1/2 to 1 in. (1.2 to 2.5 cm) in diameter. It can be redesigned for other tubing materials and sizes.

Aluminum-Encased Lead Mallet

A durable, safe hammer for general shop use

Lyndon B. Johnson Space Center, Houston, Texas

A lead mallet for general shop use has an aluminum casing surrounding a lead core to retain its shape and balance. The aluminum casing reduces the amount and rate at which lead expands at the striking surface, greatly increasing the mallet service life. The casing also improves safety by eliminating major changes in balance and reducing the flaking of lead particles.

The mallet head, as shown, can be fabricated from aluminum tube. The handle can be made from heavy-wall pipe and either welded or flared to the head at the top end. The handle is also welded to the inside of the head shell at the handle end. If the handle is flared, a steel pin is installed perpendicular to the handle, inside the head shell; and the lead is cast around it. The pin prevents rotation of the handle. By melting out and recasting the head, shops can easily refurbish the mallets when the head is worn out.

Nonferrous soft hammers (plastic, lead, and aluminum) are widely used throughout industry to strike a workpiece without distorting it. Thus, the aluminum-encased lead mallet should find wide use.

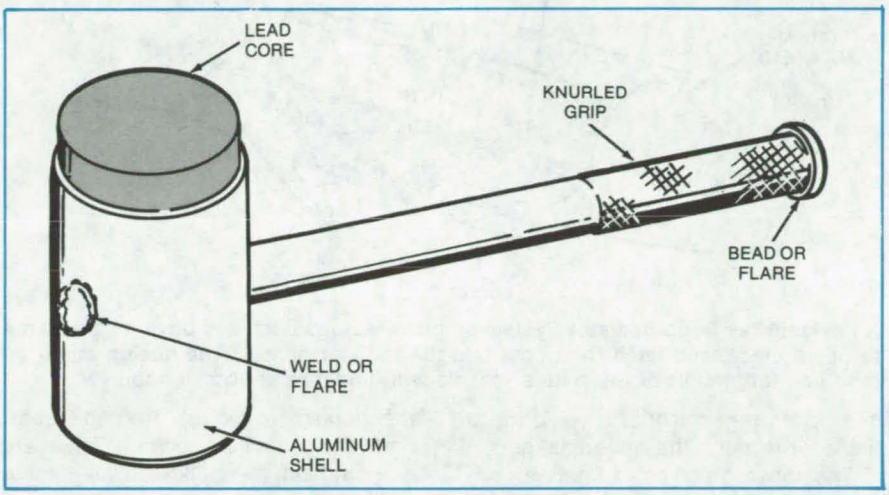

The Lead Core of the mallet is encased in aluminum. The knurled handle can be either welded or flared to the head at the top end. The handle is also welded to the inside of the head shell at the handle end.

This work was done by Floyd Chin and Ira F. Pardue of Rockwell International Corp. for **Johnson Space Center.** *No further documentation is available.*
MSC-18529

Clamshell Door System

Mechanisms that open, close, and latch large clamshell doors

Lyndon B. Johnson Space Center, Houston, Texas

A new system designed for the Space Shuttle orbiter consists of mechanisms that open, close, and latch the payload-bay doors and radiator panels under various gravity and temperature environments. It incorporates a remotely-controlled "zipper latch" operated by a mechanical sequence that accommodates thermal and structural deflections and misalinements in the doors. The entire system could be modified for commercial jetliners and marine vessels with underwater access doors.

The doors as shown in the illustration are opened, closed, and latched sequentially by electromechanical actuators controlled either manually from the onboard control panel or automatically from the onboard computer. There are four basic subelements: the door drive actuator, the forward bulkhead latches, the aft bulkhead latches, and the centerline latches.

Enclosed by the doors are radiator panels that are deployed to a predetermined position once the doors are opened. Basically these are two-sided radiative surfaces that dissipate accumulated heat from the orbiter systems. They are opened, closed, and latched by electromechanical actuators operated manually from the onboard control panel. The radiator mechanisms comprise two basic subelements: the radiator drive actuator and the radiator latches.

Two actuator systems, one on each side of the orbiter, open the doors. Each operates a "half door" at six points along the hinge line. Six

(continued on next page)

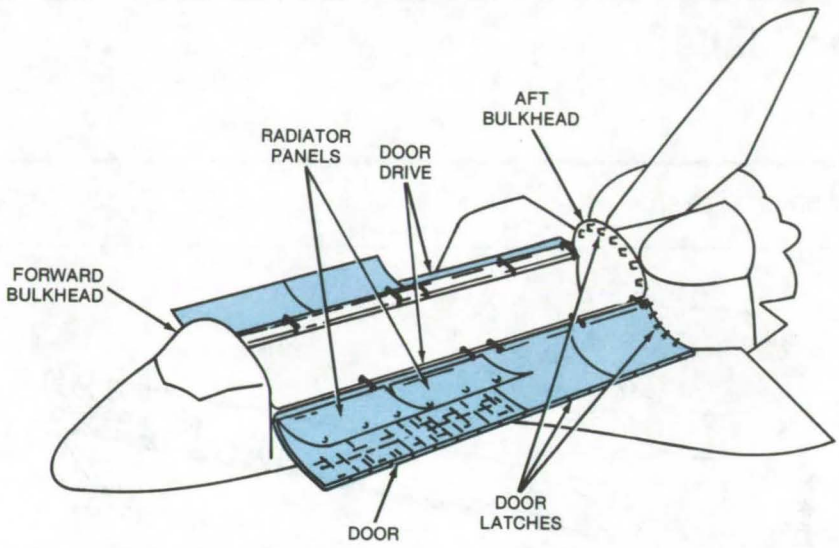

A **Payload-Bay Door/Radiator System** employs various latch and drive mechanisms to open, close, and latch the doors and the radiator panels. The design could be modified for aircraft or for marine vessels with underwater access doors.

gearboxes transmit the drive force to the door through the drive linkage.

The forward bulkhead latches consist of right-hand (four latches) and left-hand (four latches) gangs. The mechanism is mounted on the door, and the mating hook rollers are mounted on the bulkhead. A similar arrangement is used on the aft bulkhead latches.

The upper centerline latches connect the right- and left-hand doors along the upper centerline. There are four gangs of these (four latches each). The active latches are on the right-hand door, and the mating rollers are on the left-hand door.

The actuator system for the radiator mechanism drives the radiator panels to a position 35.5° away from the bay door. The drive system is similar to that of the bay door. Each radiator incorporates 12 latches in two groups of 6. Each group is driven by a single electromechanical unit.

The opening, closing, and latching follow specific sequences, and the status of each is monitored on a CRT in the cockpit. The ganged latches are mechanically sequenced in a "zippering effect," which helps to overcome thermal and mechanical distortion.

This work was done by Dean R. Helble of Rockwell International Corp. for **Johnson Space Center.** *For further information, Circle 66 on the TSP Request Card.*
MSC-18468

Measuring Ball-Bearing Loads

A tool that measures the contour of the wear path aids in bearing design.

Marshall Space Flight Center, Alabama

The dynamic load on a ball bearing is difficult to predict accurately. It can sometimes be measured while the bearing is in service; however, for low- or high-temperature bearings and bearings in confined spaces, such measurements are difficult at best.

A simple diagnostic for characterizing the bearing load has been to remove the bearing race and measure the width of the wear path. Very often the width can be related to the load magnitude and direction, and load imbalances can be identified.

Recent experience with ball bearings on turbopumps for NASA's Space Shuttle shows that the contour of the wear-path boundary contains even more precise information about the load than does the width. A simple tool that measures the boundary has been used successfully for bearing-load estimates and bearing design. Shown in the figure, the tool measures the height

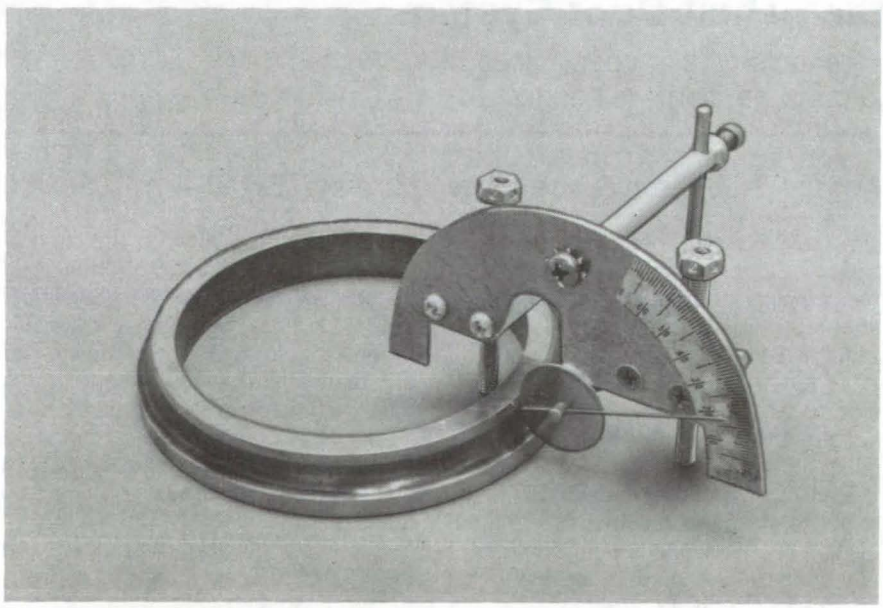

The **Ball-Bearing Load Path Boundary** is measured as an angular deflection of the pointer as the bearing race is rotated.

of the path perimeter as the horizontal bearing race is rotated manually. The height is read as an angle measurement. A set of interchangeable disks allows the pivot of the pointer to be located at the center of the raceway curvature. Leveling screws are adjusted to position the disk perimeter in the raceway. The tool can be used on the inner or outer race to measure both the upper and lower edges of the wear path.

Among bearing-load parameters that can be determined by interpreting the angle measurements are: whether the load is purely radial, purely axial, or a combination; whether it is stationary radial or rotating radial; and whether a rotating radial load is synchronous or asynchronous with the fundamental rotation frequency of the bearing.

This work was done by M. F. Butner of Rockwell International Corp. for **Marshall Space Flight Center.** *For further information, Circle 67 on the TSP Request Card.*
MFS-19505

Retaining a Sleeve on a Shaft

A fastener secures the sleeve to the shaft.

Marshall Space Flight Center, Alabama

The method used for holding the heat-shield retainer in place on the main injector of the Space Shuttle main engine may easily be adapted to many sleeve-on-shaft applications. A fastener was designed to keep a metal sleeve from slipping axially on a moving shaft.

The design (see figure) includes a slotted snapring fastener, a machined groove on the shaft, and a closely fitting sleeve. Before the sleeve is installed, the fastener is expanded and slipped over the shaft until it engages a groove. After the sleeve is slid into position, the fastener tabs are bent to lock it into position. To remove the sleeve, the procedure is reversed.

This work was done by Richard Pessin of Rockwell International Corp. for **Marshall Space Flight Center.** *No further documentation is available.*

Inquiries concerning rights for the commercial use of this invention should be addressed to the Patent Counsel, Marshall Space Flight Center [see page A5]. Refer to MFS-19518.

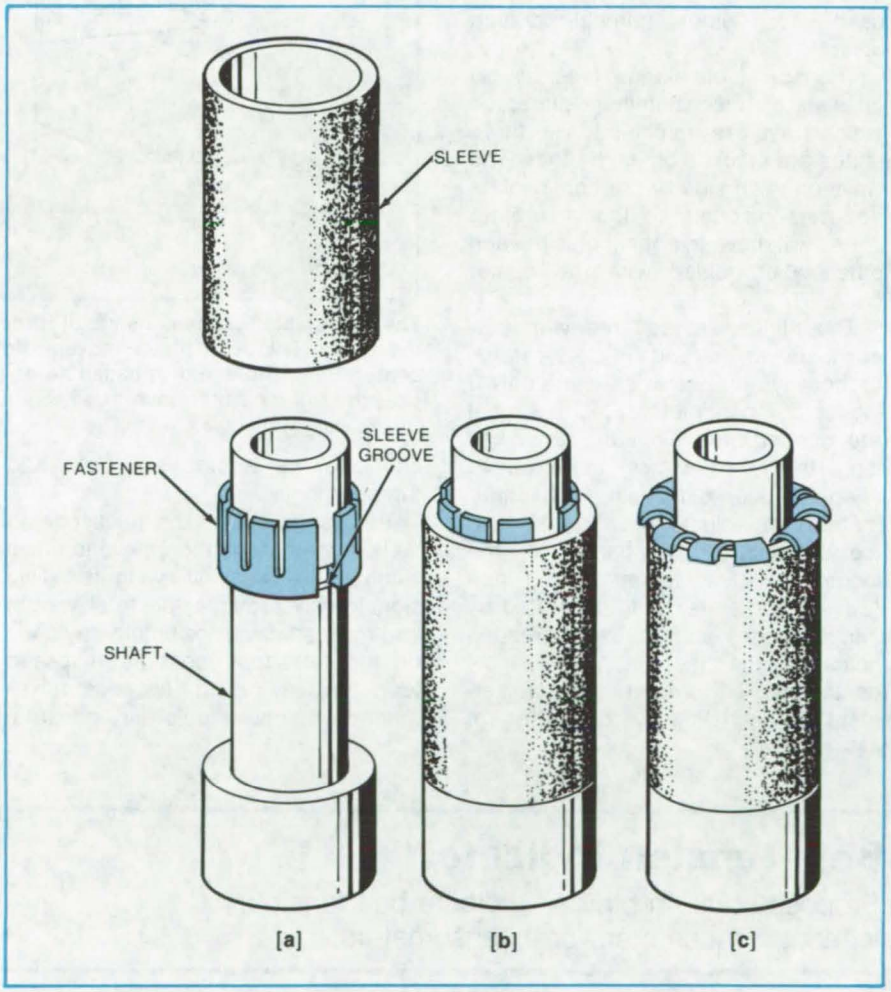

Slotted Snapring Fastener is held in place by the shaft groove (a). When the sleeve is positioned on the shaft (b), the fastener tabs are bent (c), locking the sleeve in place and preventing it from slipping along the shaft axis.

Compact Positioning Flange

A flange originally developed for a balloon-borne telescope allows easy repositioning of the center of gravity of gimbal-mounted objects.

Lyndon B. Johnson Space Center, Houston, Texas

A compact adjustable flange simplifies repositioning of the center of gravity of a balloon-borne telescope. Prior to development of the flange, counterbalancing was required because the center of gravity of the telescope was not along the elevation axis. Furthermore, since the elevation gimbal is inside the azimuth gimbal on this telescope, any mass added in elevation required additional weights in azimuth. The flange can also be used for other gimbal-mounted objects.

The adjustable flange (see figure) consists of three aluminum plates on which ways are machined. The three plates are stacked on each other. The ways on each side of the center plate are perpendicular so that the outer plates will move at right angles to each other when joined with the center plate.

The plates are secured with machine screws that slide in slots parallel to the ways. In one axis, where only 3 inches (7.6 centimeters) of adjustment are needed, the slots are 3 inches long. In the other axis, there was a need for over 6 inches (15.2 centimeters) of adjustment. To maintain the stiffness of the flange for the longer axis, a series of 1-inch (2.54-centimeters) slots separated by 1-inch bridges is used. Extra threaded holes in the mating plates allow continuous adjustment. The adjustment is then simply a matter of choosing the appropriate slots and threaded holes.

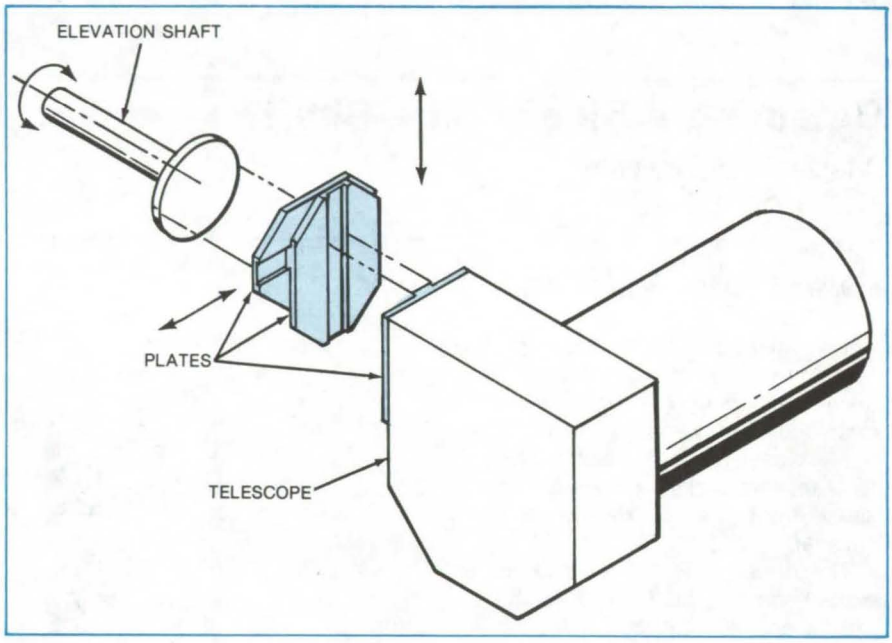

The **Adjustable Flange** consists of three aluminum plates on which ways have been machined. The outer plates move at right angles to each other when joined to the center plate. Slots and threaded holes (not shown) in the plates allow adjustment over the full length of each axis.

The flange allows the telescope to be balanced around the elevation axis without the use of weights. This significantly reduces the total weight and makes heavier scientific payloads on the telescope possible. Crossed ways typically provide two-axis movement on machine tools and industrial equipment. In this application, the overall thickness of the ways has been reduced significantly to minimize shifting of the centerline of the telescope along the elevation axis.

This work was done by Sonne L. Hooper of Kentron Hawaii, Ltd., for **Johnson Space Center.** *No further documentation is available.*
MSC-14876

Bolt-Tension Indicator

Proposed built-in pin can indicate bolt tension without torquemeters or extensometers.

Marshall Space Flight Center, Alabama

A proposed bolt has a built-in pin that indicates bolt tension. As the bolt is tightened, the pin is pulled into the bolt by the stretching bolt shaft. The amount of the pin remaining above the top of the bolt would correspond to the tension on the bolt. This pin-indicator bolt would be a more-accurate tension indicator than a torquemeter and would be less expensive than using an electronic extensometer.

The pin (see illustration) would be retained in the bolt by interference fit at the bottom of a hole step-drilled inside the bolt shaft. The length of the pin would be chosen according to the bolt design limits. The pinhead would be marked by two steps, correspond-

ing to minimum and maximum acceptable tensions. As the bolt is tightened and the pin pulled in, the first step on the pinhead would become flush with the bolthead to indicate a minimum tension limit. Further tightening to the maximum allowable design limit will pull the top of the pin flush with the bolthead.

The counterbore inside the bolthead would be filled by elastic material to dampen pin vibration and prevent contamination. Initially, finished bolts could be "coarse" tightened with a torque wrench. A fine adjustment would follow by further tightening and observing the position of the pin ends relative to the bolt faces. These can be checked using a flat gage block to feel the steps extending above the bolt surface. When, as is often the case, the tension is set somewhere between the minimum and maximum limits, any part of the pin extending above the bolt can be filed off.

The proposed method would be particularly convenient for assembly in field locations without electronic and other specialized instruments. The installed bolts can be rapidly rechecked for any loss in tension by simply going over them with the flat gage block. [Also see "Eddy-Current Sensor Measures Bolt Loading" (MFS-19486) on page 68.]

This work was done by Kenneth L. Wilson of Rockwell International Corp. for **Marshall Space Flight Center.** *No further documentation is available. MFS-19324*

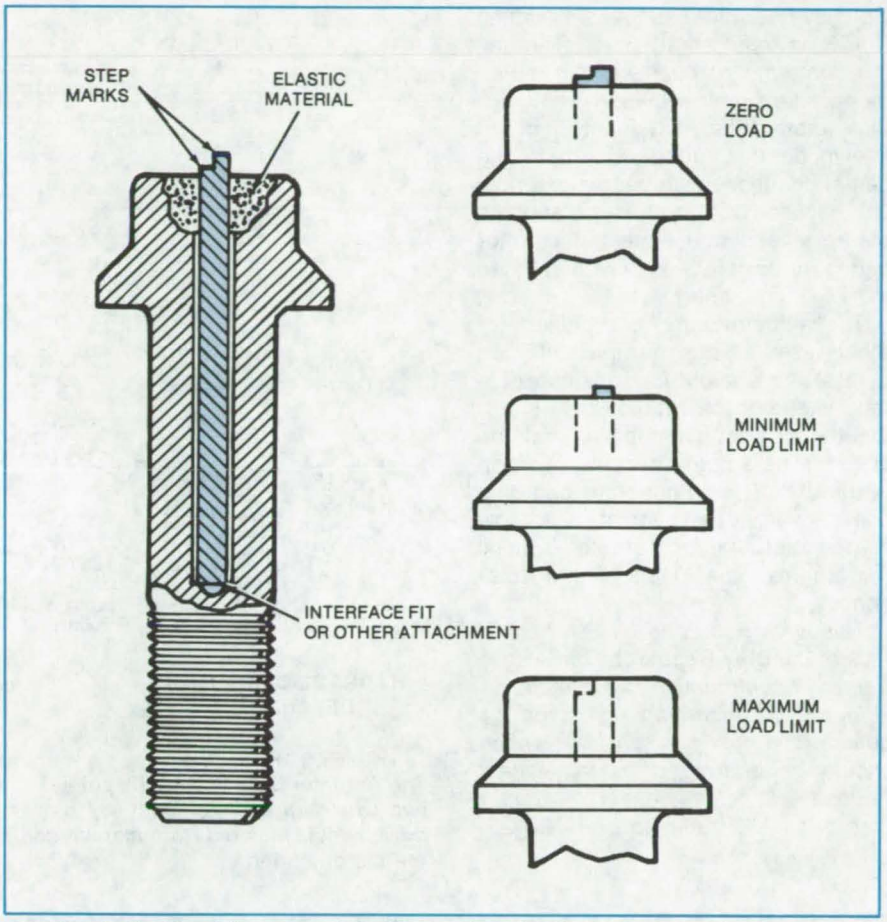

Tension-Indicating Pin secured to the center of a bolt shaft can be an accurate indicator of bolt tension. When the bolt is tightened, the stretching bolt shaft pulls the pin into the center hole. Minimum tension is indicated when the first step mark on the pinhead is flush with the bolthead surface. Maximum allowable tension is reached when the top edge of the pinhead is flush with the bolthead surface.

Dual-Mode Actuator

Compact mechanism functions under automatic control, manual control, or both.

Langley Research Center, Hampton, Virginia

The compact actuator shown in the figure accepts inputs from a person, a computer, or both in combination. It was developed as a retrofit to be attached to the spoiler position control unit (PCU) of existing aircraft where it is controlled by the pilot or by a computerized flight-control system. In the dual mode, the pilot can place the spoiler at an initial setting while the computer makes adjustments around the pilot-selected position.

In the computer-controlled mode, fluid enters the actuator hydraulic cylinders from a closed-loop servosystem. The computer controls the direction and amount of actuator movement and monitors its position. The hydraulic cylinder moves the control lever, thus rotating the PCU input lever and causing a corresponding movement of the aircraft spoilers. The control lever is resisted by a spring system in the centering mechanism, that deflects during operation and returns the mechanism to the zero position when hydraulic power is removed.

In the manual mode, movement of a control system by the pilot causes the

(continued on next page)

input lever to rotate about its mounting (the PCU input shaft) point. Through the centering mechanism this movement in turn moves the control lever, thus rotating the PCU input shaft. In this mode the spring system in the centering mechanism becomes a rigid link between the input lever and the control lever because the springs offer a greater resistance to movement than the PCU input shaft.

The actuator can be modified for other uses. For example, it can control the straight-line position of a rod instead of the rotation of a shaft. Electric or pneumatic power can be used for the automatic-control portion of the unit. The output shaft can also operate valves that regulate fluid flow in the actuator to create special movements other than simple rotations.

This work was done by Stephen C. Irick of **Langley Research Center.** *No further documentation is available.*

Inquiries concerning rights for the commercial use of this invention should be addressed to the Patent Counsel, Langley Research Center [see page A5]. Refer to LAR-12412.

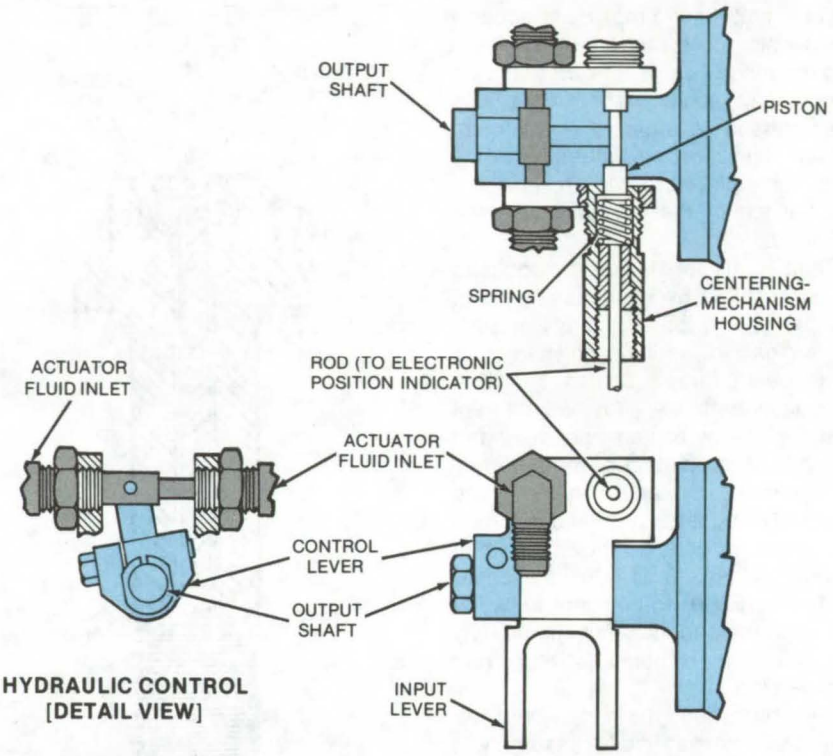

The **Actuator Output Shaft** (in color) is controlled automatically by hydraulic fluid in two cylinders and manually by movement of the input lever. Automatic-control movement is isolated from manual-control movement by adjustment of the force on the piston spring.

Zero-Torque Spanner Wrench

With this proposed tool, a coupling is rotated by simply tightening a grip.

Lyndon B. Johnson Space Center, Houston, Texas

A proposed spanner wrench converts the gripping action of a hand to rotary motion. It does so without imparting reactive moments or forces on the part being turned or on the operator.

The tool was originally proposed for use by astronauts in the weightless environment of outer space. Conventional spanner wrenches are difficult to manipulate in zero gravity because they generate moments and forces that rotate and push the astronaut's body. Because it eliminates this problem, the new wrench should also be useful in undersea operations and in other delicate work where reactive forces and torques have to be controlled.

In a design for valve tightening (see figure), the tool resembles a cross between a conventional spanner

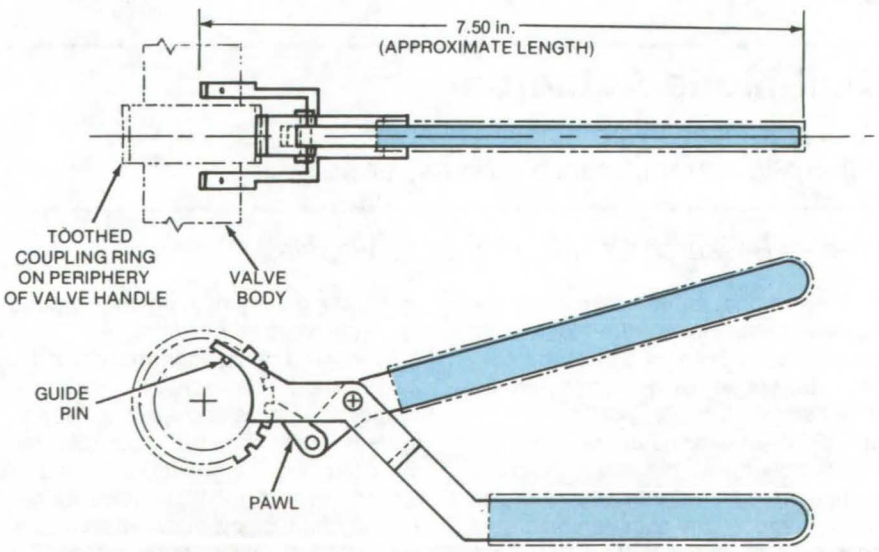

No Unbalanced Moments or Forces are created when rotating the valve handle with this proposed spanner wrench. It thus prevents damage to lightweight shafts, which can be bent or broken when turned with a conventional spanner wrench.

wrench and a pliers. Through locating and holding pins, one handle of the tool engages the valve body. The second handle has a ratchet pawl that engages a toothed coupling ring on the periphery of the valve handle.

Two springs would be used in the tool. One would open the handle grips when they are released, and the other would be installed at the pawl to hold it against the toothed coupling ring.

By incorporating a torque wrench in the handle, the operator could monitor the torque as he manipulates the tool. This would prevent overtightening and damage to valve seats and seals. Since it imparts rotary motion more gently than conventional spanner wrenches, the tool would also allow the use of larger rotary handles and shafts than are presently practical for lightweight assemblies.

This work was done by Morley V. Friedell of Martin Marietta Corp. for **Johnson Space Center.** *No further documentation is available.*
MSC-14843

Drill-Motor Holding Fixture

Fixture prevents bit breakage and helps improve drilling accuracy.

Lyndon B. Johnson Space Center, Houston, Texas

A simple fixture prevents bit breakage and improves accuracy when drilling items that are too large or too awkward to be clamped in a drill press. As shown in the figure, a drill motor is mounted on a furniture clamp fitted with a 3/4-in. (1.9-cm) pipe. The pipe length and diameter are chosen to suit the size of the item being drilled.

The motor mount includes a short length of pipe that slides along the pipe on the furniture clamp. Hose clamps are used to attach the motor to the fixture.

As the hole is being drilled, the operator turns the handle on the furniture clamp. This slides the short length of pipe on the drillholder along the pipe on the furniture clamp, advancing the bit. At the same time, the fixture alines the bit so that it is perpendicular to the surface being drilled. Previously, the drill motor was hand-held, which often resulted in skewed holes and broken drill bits.

This work was done by Eldon N. Chartier and Lee N. Culp of Rockwell International Corp. for **Johnson Space Center.** *No further documentation is available.*
MSC-18582

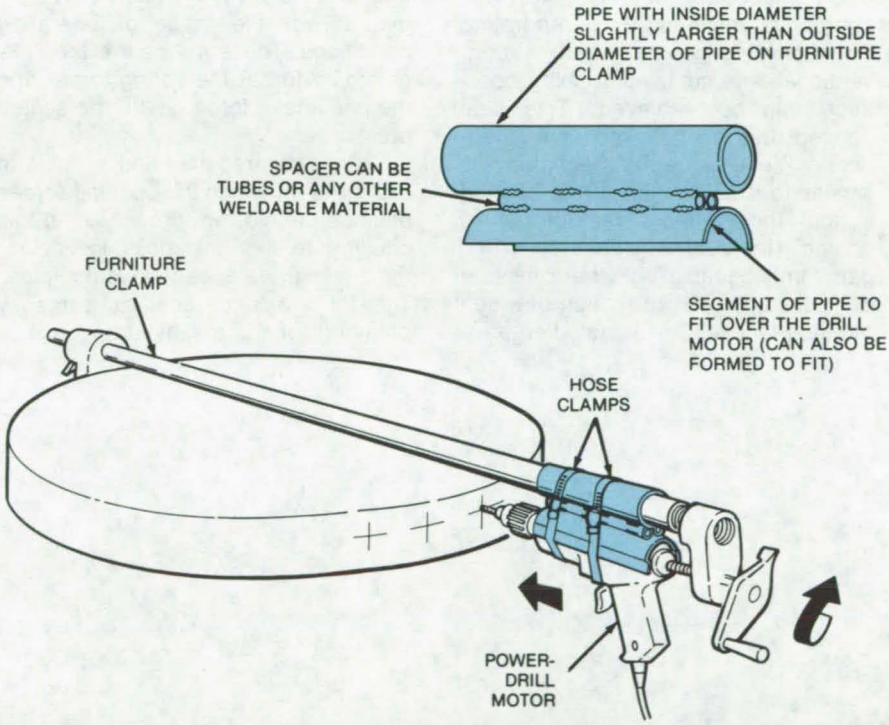

The **Drillholder** advances the drill motor as the bit pierces the edge of the disk. It is being used to drill 3/8-inch (0.93-cm) holes in iron/nickel alloy disks.

Books and Reports

These reports, studies, and handbooks are available from NASA as Technical Support Packages (TSP's) when a Request Card number is cited; otherwise they are available from the National Technical Information Service.

Self-Acting Shaft Seals

Operating principles and design

A paper has been published that reviews the operating principle and design of the self-acting shaft seal and also points out the effects of adverse operating conditions. By incorporating thrust-bearing geometry into a conventional face seal, nonrubbing operation can be achieved. This seal concept has been termed the "self-acting" seal, since the mechanism is similar to a self-acting thrust bearing in that the mating faces lift out of contact (the seal ring rides on a thin gas film) because of the pressure developed by relative motion between the seal faces. Previous studies have demonstrated that the self-acting seals can operate at advanced aircraft engine conditions and have lower leakage rates than labyrinth seals; thus they are attractive from the standpoint of efficiency.

The design of a self-acting seal requires that nonrubbing operation be achieved at all operating conditions (e.g., takeoff and cruise). Therefore, a crucial design consideration is the thickness of the gas film that separates the sealing faces.

To determine film thicknesses and associated leakage in a self-acting seal, the axial forces acting on the seal head (assembly of the primary ring and its carrier) must be determined over the range of operating conditions. These forces are the self-acting lift force, the spring force, and the pneumatic force due to the sealed pressure.

An analysis requires finding the film thickness for which the opening forces balance the closing forces. When this equilibrium film thickness is known, the leakage rate can be calculated. This force balance analysis is readily obtained for the steady-state case in which the seat face has zero runout with respect to the shaft centerline.

Elements of the analysis used to obtain seal performance predictions are described and evaluated. These elements are:

- Primary seal-pressure gradient
- Self-acting geometry and lift force
- Closing forces
- Equilibrium film thickness
- Performance maps
- Inlet effects

Elements of adverse operating conditions for seals are also described and evaluated. These elements are:

- Effect of nonparallel sealing faces
- Effect of seat face runout

The mathematical models for obtaining a seal force balance and the equilibrium operating film thickness are outlined in the paper.

This work was done by Lawrence P. Ludwig of **Lewis Research Center.** *Further information may be found in NASA TM-73856 [N78-19513/NSP], "Self-Acting Shaft Seals" [**$6**]. A copy may be purchased [prepayment required] from the National Technical Information Service, Springfield, Virginia 22161.*

LEW-13229

Fabrication Technology

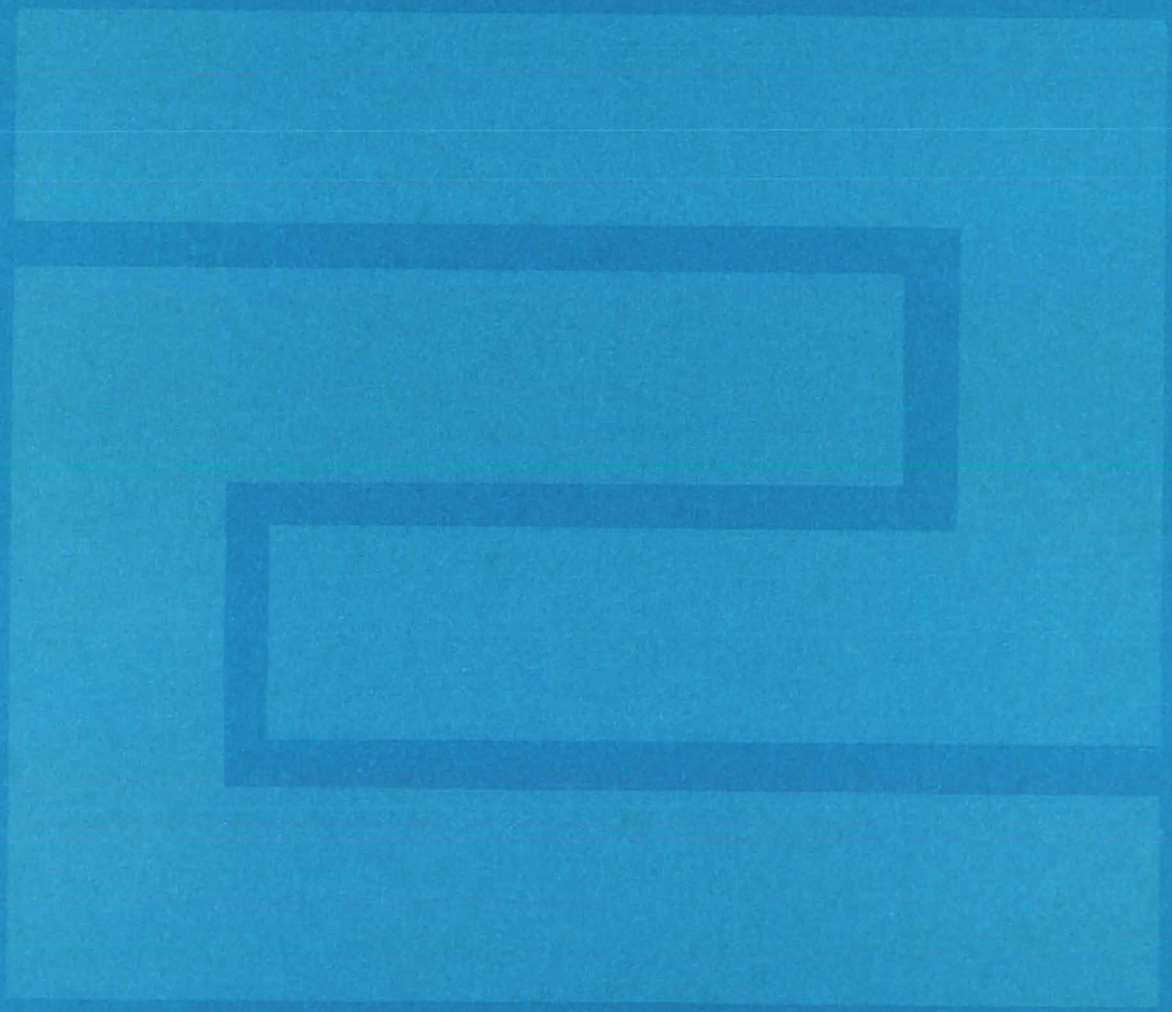

Hardware, Techniques, and Processes

Books and Reports

Verifying Root Fusion in Electron-Beam Welds

Ultrasonic equipment and recorder verify that the back side of the joint is welded.

Marshall Space Flight Center, Alabama

A new technique assures adequate penetration of an electron-beam weld to the back side (root) of the joint. A magnetostrictive wire waveguide inserted in the joint root is monitored by ultrasonic equipment using an x-y recorder. As the joint is welded, signals on the recorder indicate where the penetration is incomplete. The method is particularly valuable when the back side of the joint is inaccessible to conventional inspection after the welding. It is more accurate than most standard ultrasonic and X-ray inspection methods.

An electrical pulse applied to the transducer shown in the figure generates an ultrasonic signal in the magnetostrictive wire waveguide. This ultrasonic wave propagates in the thin rod (extensional mode of propagation). The portion of the wire in the weld joint is about 0.020 in. (0.51 mm) in diameter and may be of the same material as the sample. The wire is placed in a groove (slightly larger than the wire) at the root of the joint. As the welding head moves along the part, the end of the wire is melted and fused if the joint is adequately penetrated. Because of the difference in acoustic impedance between the liquid and solid phases, the ultrasonic signal is reflected, detected by the transducer, and amplified by the receiver. The time of arrival of this signal is measured. An analog position signal, representing the welding-head position and the propagation time (time of flight) of the signal, is differentiated and recorded on an x-y recorder.

For an acceptable weld, the x-y output is very nearly constant. In an area where the joint is not fully penetrated and the wire is not melted, a large reflected signal is received from the area where the wire was last fused. This signal remains constant with time until the beam melts the wire. The length of time that the signal is constant is directly related to the length of the unfused zone, and its position can be located from the x position of the recording.

The method permits a determination of penetration depth in preweld samples without the time-consuming opening of the vacuum chamber of the electron-beam welder and sectioning of the sample.

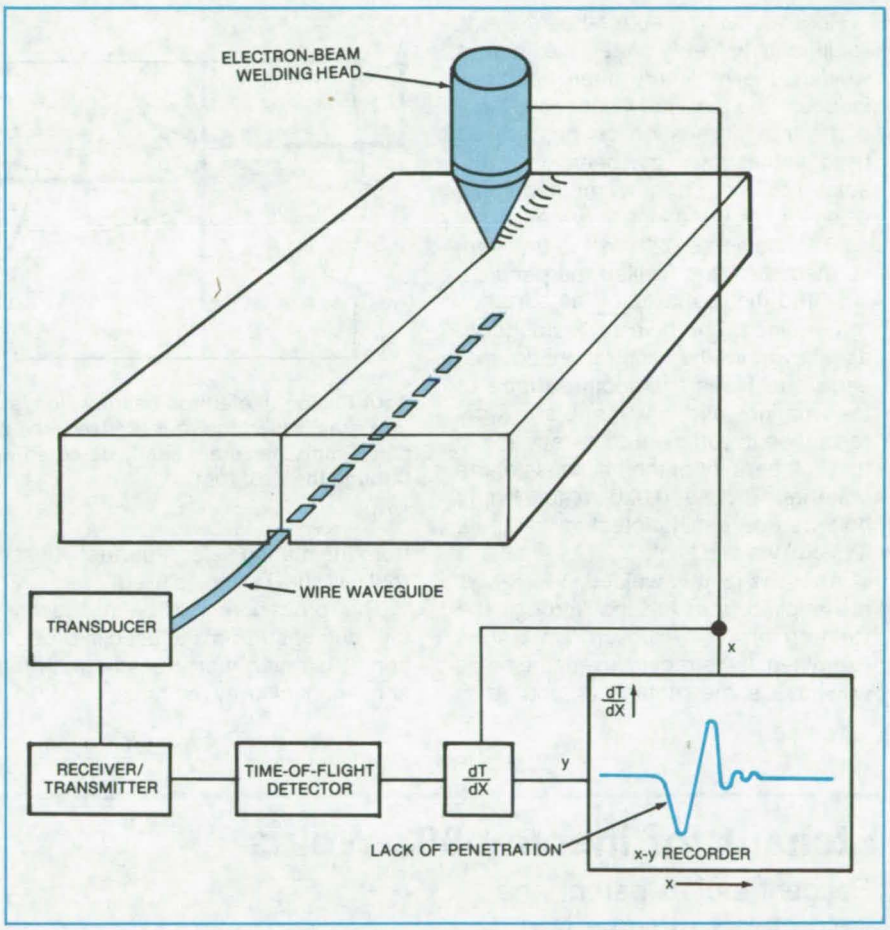

Monitoring Apparatus verifies root fusion in electron-beam welds. A magnetostrictive wire waveguide inserted in the back side of the joint transmits ultrasonic signals to the point where the weld is fully penetrated. The reflected signal is time-detected (similar to radar) and is fed to the x-y recorder. When the joint below the welding head is completely penetrated, the recorder indicates a steady signal. The point where the penetration is incomplete is indicated by a large signal on the recorder.

This work was done by F. L. Becker, Steve Doctor, and R. E. Kleint of Rockwell International Corp. for **Marshall Space Flight Center.** *No further documentation is available.*
MFS-19499

X-Ray Technique Verifies Weld-Root Fusion

X-ray inspection of small holes shows whether the root is welded.

Marshall Space Flight Center, Alabama

Root fusion in electron-beam welds is difficult to verify. After the joint is welded, the root very often becomes inaccessible to visual inspection. X-ray and ultrasonic inspection procedures used earlier have not been very reliable; however, a new method, also using X-rays, is working very well.

Tiny holes [0.020 in. (0.51 mm) in diameter] are drilled perpendicularly into the root area of the surfaces to be joined. The holes are staggered as shown in the illustration so that each one faces a smooth surface of the mating part. In general, X-ray resolution is sufficient to detect a void that is 2 percent of the thickness of the material. Thus a 0.020-in. (0.51-mm) hole can be easily detected in a 1-in. (2.5-cm) welded joint.

After the joint is welded, the X-rays are applied from the top, through the weld crown. The exposed film is then examined. If the root is fused, the holes will have some metal that poured in from the mating side. A perfectly fused root will show all holes filled.

This procedure has been successfully demonstrated and used in production. It is much more reliable than the conventional X-ray methods.

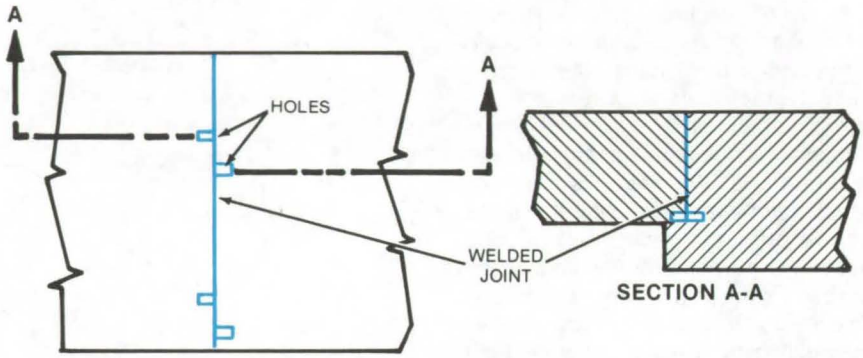

Root Fusion in electron-beam welds is inspected using predrilled small holes in the root area. When the root is fused, the holes are filled with material from the mating part. Empty holes are easily detected with X-rays applied from the weld crown down through the weld root.

This work was done by R. E. Kleint of Rockwell International Corp. for **Marshall Space Flight Center**. *No further documentation is available.*
MFS-19468

Etchant for Incoloy-903 Welds

Reagent etches parent and weld metals at same rate.

Marshall Space Flight Center, Alabama

When etching the surface of a weld area to reveal the underlying grain structure, it is important that the reagent not "overetch" and disguise the microstructure being examined. The etchant should also remove both the welded metal and the parent metal at the same rates. Often, a different etchant is used for each phase to prevent preferential etching.

When the welded material is Incoloy-903 (an iron/nickel alloy), a lactic/nitric/hydrochloric acid formulation can be used successfully. The reagent etches welded specimens uniformly without overetching. It exposes the grain structure of both the welded metal and the parent metal in fused Incoloy-903 joints.

1 part	lactic acid ($CH_3CHOHCOOH$)	90-percent concentration
1 part	nitric acid (HNO_3)	70-percent concentration
4 parts	hydrochloric acid (HCl)	37-percent concentration

The **Etchant Formulation** for Incoloy-903 welds satisfactorily etches both weld and parent metal. It must be freshly mixed for each application.

The reagent composition is shown in the table. The proportions may be altered slightly to improve the ability to reveal particular, finely dispersed constituents. The reagent was developed for autogenous Incoloy-903 welds, in which pieces of the same metal are fused without the addition of a filler metal.

This work was done by Joseph A. Gerstmeyer of Rockwell International Corp. for **Marshall Space Flight Center.** *No further documentation is available.*
MFS-19378

Chemical-Milling Solution for Invar Alloy

Excellent surface finishes and tolerances are possible with two nitric/hydrofluoric formulations.

Marshall Space Flight Center, Alabama

Two chemical-milling solutions for Invar (and equivalent alloys) give excellent surface finishes with none of the problems that plagued previous formulations. A finish of 125 μin. (3.17 μm) is possible with solution A (see table) if milling is done at 135° to 145° F (57° to 63° C). For finishes of 85μin. (2.16 μm), solution B is used. The latter has essentially the same composition as solution A, except for an additional 7 percent of phosphoric acid.

An effective chemical-milling solution is needed for Invar, because this 36-percent-Ni/Fe alloy is very often chosen for dimension-critical components because of its low thermal-expansion coefficient at temperatures up to 400° F (204° C). With the discovery of the two formulations, chemical milling can now complement conventional machining and electric-discharge machining when fabricating precise parts with high surface finishes and tolerances.

Solution A		Solution B	
HF (70 percent)	5.8 oz/gal	HF (70 percent)	5.8 oz/gal
HNO_3 (40 to 42 °Bé)	40 oz/gal	HNO_3 (42 °Bé)	40 oz/gal
H_2O	balance	H_2PO_4 (75 percent)	10 to 13 oz/gal
		H_2O	balance

Chemical-Milling Solutions for Invar and equivalent alloys are applied at temperatures between 135° and 145° C. Control ranges, etch rates, and other process details are available in the Technical Support Package for this article.

The new formulations eliminate problems of channeling at root fillets, dishing, island formation, and overhangs, all of which can occur during chemical processing. Previous attempts to use dilute hydrochloric acid (recommended for Invar) gave unsatisfactory results.

This work was done by Walter Batiuk of The Perkin-Elmer Corp. for **Marshall Space Flight Center.** *For further information, Circle 68 on the TSP Request Card.*

Inquiries concerning rights for the commercial use of this invention should be addressed to the Patent Counsel, Marshall Space Flight Center [see page A5]. *Refer to MFS-25365.*

Eliminating Underbead Fissuring in Superalloys

Reduced weld velocity eliminates underbead fissuring in superalloys.

Marshall Space Flight Center, Alabama

Severe underbead cracking had occurred in weld overlays of Incoloy-903, Incoloy-88, and Inconel-718. This problem was eliminated by carefully controlling the welding-speed parameter.

The weld parameters that produce high-integrity superalloy welds under overlay conditions (piling metal upon itself) were found to differ from those used for conventional welds (metal put in a recessed groove). The thermal and metallurgical properties of these overlays are critically tied to stress/strain and time/temperature threshold characteristics determined by the inherited strength and microstructure of the prior weld bead. The weld microstructure (grain size and segregation) is principally determined by the rate and direction of solidification. Each successive weld bead will tend to nucleate and solidify in a similar fashion as the previous underbead. Results show that weld velocity is critically associated with solidification rates and thermal gradients.

The upper limits of the weld velocity (travel speed) were established to eliminate the underbead fissuring. A maximum weld velocity of 4 in./min (10.2 cm/min) was applied to Incoloy-88 and Inconel-718 overlays, and a maximum travel speed of 3 in./min (7.8 cm/min) was used for Incoloy-903 overlay work. These limits are below the commonly used rates and keep the thermally induced forces to below crack-inducing levels on the grain boundaries of the heat-affected zone of the previous weld bead.

This work was done by R. D. Betts of Rockwell International Corp. for **Marshall Space Flight Center.** *No further documentation is available.*
MFS-19460

Ion-Beam Cleaning for Cold Welds

Ion-beam cleaning results in strong bonds with minimal deformation.

Lewis Research Center, Cleveland, Ohio

A variation of cold welding has been developed that utilizes an ion beam to clean mating metal surfaces prior to joining in a vacuum environment. High-quality solid-state welds are produced with minimal deformation (<1 percent).

In theory, if you bring two perfectly-clean metal surfaces into intimate contact so that the atoms of one surface are sufficiently close to the atoms of the other surface, the interatomic force-of-attraction becomes effective across the interface, and a solid-state weld is obtained. Theoretically, such a weld can be as strong as the parent metals involved.

In reality, metal surfaces are not "clean" but are contaminated with oxides, nitrites, water vapor, organics, and the like, so that sufficiently-intimate metal-to-metal contact cannot be readily established. The effectiveness of an oxide layer to interrupt or prevent metal-to-metal bonds has been shown to exist down to one or two monolayers of coverage. Oxide monolayers are extremely tenacious and especially difficult to remove from most metal surfaces. They are stable even at vacuum levels below their bulk vapor pressure. Thus, an effective cleaning method is necessary to remove completely the oxide or contamination layer in order to obtain a high-quality cold weld with minimal deformation.

In conventional practice it is possible to achieve reliable cold welding in aluminum, as well as some other materials, for many applications by applying sufficient pressure to cause plastic flow of the material at the interface of the pieces to be welded. By using welding dies or indenters to cause plastic flow, the oxide layers at the interface are broken up and dispersed, allowing clean underlying metal to squeeze through to the interface for clean metal-to-metal bonding. Additionally, under plastic flow the atomic contact and registry between the two metals are greatly increased. Thus a good solid-state weld is formed.

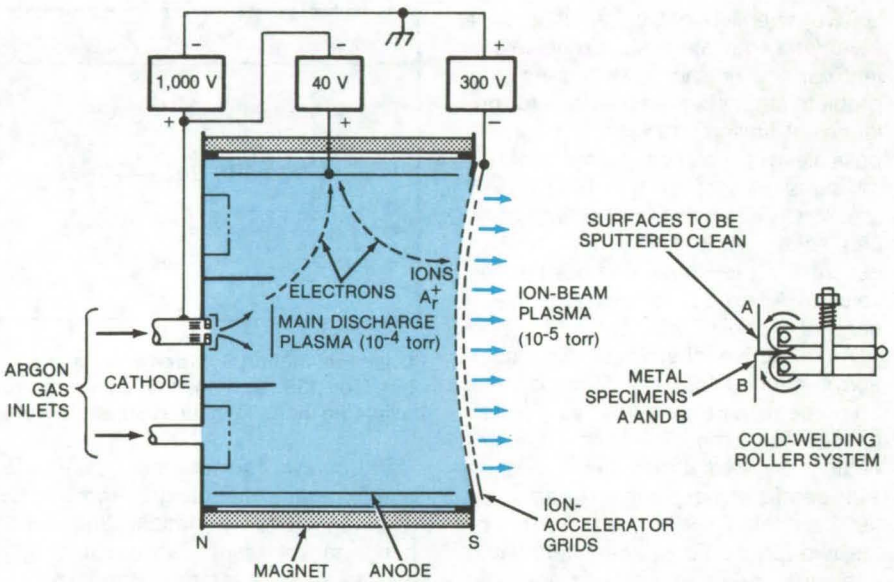

Electron Bombardment Ion Source and Roller System are used to clean metal surfaces and cold-weld them together with minimal deformation.

Past studies have shown that for conventional cold welding of aluminum, no welding was detected with less than 40 percent deformation. At about 70 percent deformation, however, the weld strength approached the strength of the parent metal, which had been thinned by the same amount.

Such plastic flow and deformation, however, have several drawbacks. First, the temper of the metal is increased by cold-working in the bond area so that it is less ductile than the parent metal, and second, the strength of the bond will eventually equal the strength of the thinned metal that resulted from the deformation.

The ion-beam cold-welding method overcomes these drawbacks by removing the oxide layer to expose clean metal that can be cold-welded with greatly reduced pressures so as not to cause gross deformation and thinning of the material at the weld. A minimal amount of deformation is necessary since most metal surfaces are not atomically flat. When two metal surfaces are brought together, the actual contact surface may be only a small portion of the apparent contact area of high points or spots, called asperities. The deformation process requires a loading force to cause sufficient elastic deformation and plastic flow of the surface asperities to increase the actual contact area at the interface to achieve a high-quality cold weld. With ion-beam cleaning, high-quality cold welds were observed in aluminum with deformation of less than 1 percent.

The ion-beam source used for cleaning is based on the technology developed by NASA for ion-propulsion space applications. A schematic diagram of the ion source modified for inert-gas ion-beam cleaning with the metal specimens and roller system is shown in the figure. The ion-beam source and roller system are mounted in a vacuum tank with a pressure range from 10^{-6} to 10^{-4} torr.

The ion-beam source operates as follows: Argon, an inert gas that is easily ionized, is introduced into the cylindrical main discharge chamber.

There the argon atoms are bombarded by electrons and ionized as they flow through the discharge chamber. The electrons are emitted from the cathode and accelerated to anode potential with an energy of the order of 40 eV. At the discharge operating pressure the electrons must travel an average distance of 1 meter before encountering an ionizing collision with an argon atom. Thus a magnetic field is applied in order to increase the electron mean path and enhance the ionization process within the limited dimension of the discharge chamber. Argon ions from the discharge plasma as they approach the acceleration grids are extracted and accelerated through the large number of small holes in the grids by the electrostatic field associated with the high voltages applied to the grid elements. These ions are directed onto the surface of the material to be sputter-cleaned, typically with an energy of 1,000 eV and with a current density of 1 mA/cm^2.

When a 1,000-eV ion beam bombards a metal surface, it imparts sufficient energy to break any chemical bond between the surface and near-surface atoms. All metals can be sputtered by this process, and in general the sputter removal rate is in the range of quite a few atomic layers per second for an ion-beam current density of 1 mA/cm^2.

The roller system used to cold-weld the ion-beam-cleaned surfaces is also shown in the figure. Metal specimens are inserted between the two steel rollers at one end and are separated and bent outward as indicated schematically. This configuration exposes both mating surfaces to a normal incident ion beam for sputter cleaning. The surfaces were mounted approximately 10 cm from the ion-beam source. After ion-beam-cleaning the exposed mating surfaces, the rollers were rotated to pull the specimens through. Rotational torque was applied manually from outside the vacuum chamber through a vacuum shaft feedthrough.

The force between the rollers was controlled by the spring compression, which was approximately 670 N (150 lb) maximum for 0.25 mm separation. Typically, metal specimens were cut from 0.127 mm foil into 25-mm-wide strips with a length of 12 to 15 cm for test purposes. Welding occurred down the center of the strips where the upper roller forced the specimens together. Work was limited in scope to low-yield-strength material due to the limitation of the experimental fixture used to apply pressure at the ion-beam-cleaned interface.

The following low-yield-strength materials were successfully cold-welded using the ion-beam cleaning technique and the experimental fixture: aluminum to aluminum, copper to copper, copper to aluminum, copper to nickel, and silver to iron. These materials could not be pulled apart in peel tests; instead, the base metal failed adjacent to the weld. Photomicrographs of as-welded and heat-treated-weld specimens demonstrated that metal-to-metal bonding had been achieved.

This work was done by Bernard L. Slater of **Lewis Research Center.** *Further information may be found in NASA TM-78933 [N78-27257/NSP], "Use of Ion Beam Cleaning to Obtain High Quality Cold Welds with Minimal Deformation" price [$5]. A copy may be purchased [prepayment required] from the National Technical Information Service, Springfield, Virginia 22161.*

This invention is owned by NASA, and a patent application has been filed. Inquiries concerning nonexclusive or exclusive license for its commercial development should be addressed to the Patent Counsel, Lewis Research Center [see page A5]. *Refer to LEW-12982.*

Coatings for Hybrid Microcircuits

Tests show the efficacy of protective coatings, but indicate problems with PIND tests.

Marshall Space Flight Center, Alabama

Leak Test	MIL-STD-883A (Fine and Gross)
PIND Test	
Electrical Test	
Stabilization Bake	24 hours at 150° C
Thermal Cycling	MIL-STD-883A (-65° to +150° C, 100 cycles)
Thermal Shock	MIL-STD-883A (0° to 100° C)
Mechanical Shock	MIL-STD-883A — Condition B
Acceleration	MIL-STD-883A — Condition A
High-Temperature Storage	168 hours at 125° C
Final Electrical	
External Visual	

Coated and Uncoated Microcircuits were subjected to the tests listed here. The leak test and the electrical test were performed after each of the environmental tests.

Uncoated hybrid microcircuits are vulnerable to electrical failures due to loose solder and other metal particles that cause shorts. In tests of two coating materials to prevent such failures — parylene and silicone, the only electrical failures were in uncoated control samples.

Although the coatings protect microcircuits from contamination by particles, there is the danger that the coating may entrap contamination that will degrade circuit performance over the long term. The tests showed, however, that particle entrapment need not be a concern.

(continued on next page)

A group of 30 microcircuits was subjected to the tests listed in the table. One-third of the units were coated with silicone and one-third with parylene; one-third were left uncoated.

The particle-impact noise detection (PIND) test produced contradictory results that raise doubts about its reliability as a failure predictor. In a PIND test, a packaged microcircuit is shaken while sensitive microphones listen for sounds from loose particles within the package. Although such sounds were detected in PIND tests of parylene-coated microcircuits, none of these circuits failed the electrical tests.

The high incidence of misleading PIND failures is probably a result of the parylene-coating process. Part of the microcircuit surface is masked during coating; when the masking material is removed, a small amount of the nonconducting coating material is dislodged. In small quantities, however, the loose coating particles are harmless.

Failures of uncoated microcircuits were also not predicted reliably by PIND testing. Only one-fourth of the electrical failures in uncoated specimens were anticipated in PIND test results.

This work was done by D. L. Kinser of Vanderbilt University for **Marshall Space Flight Center.** *For further information, Circle 69 on the TSP Request Card.*
MFS-25292

Placement Technique for Semicustom Digital LSI Circuits

An automated cell-placement technique modified to speed up new LSI circuit fabrication

Marshall Space Flight Center, Alabama

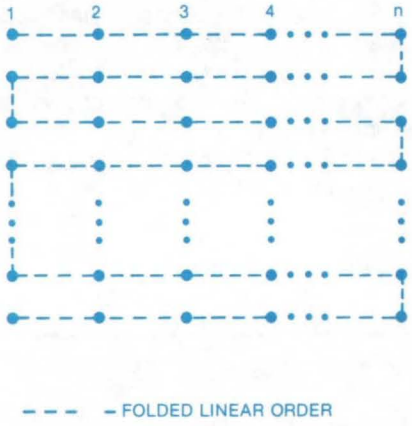

Block-Oriented Folding (block depth = 1) is one of the strategies used in the STAR cell-placement problem. The technique combines the aspects of both horizontal and vertical alinements. Vertically alined segments of the linear order are replicated horizontally across the STAR to form a block. The blocks are then stacked vertically. In this simplest layout the blocks are the horizontal rows of n cells each.

An automated placement technique that has been used with several LSI (large-scale integration) circuits was modified for new LSI technology developed at the Marshall Space Flight Center. The technique called STAR, for standard transistor array, uses a prefabricated transistor understructure and a comprehensive library of digital logic cells to fabricate semicustom LSI circuits efficiently. This technology is intended for small lots of special-purpose IC's and is generally less expensive than customized fabrication.

The STAR system was developed for bulk-metal CMOS technology, although its organization is adaptable to other technologies. The LSI cell placement is based on a linear ordering/folding technique.

Linear ordering produces a one-dimensional chain in which the total interconnection length is nearly minimum (considering the cell width). The folding methods (see example in figure) rely on the assumption that the linear order represents a near-optimum one-dimensional cell placement with respect to the total interconnection distance. The strategy is to decrease the distance between the connected cells or to place a higher percentage of cells in juxtaposition than specified in the linear order.

The entire placement technique is carried out via computer program (CAPSTAR) developed as an integral part of a system of programs for the STAR technology.

This work was done by B. D. Carroll and G. W. Cox of Auburn University for **Marshall Space Flight Center.** *For further information, Circle 70 on the TSP Request Card.*
MFS-25324

A General Logic Structure for Custom LSI's

A proposed concept to reduce the cost and complexity of producing custom LSI's

NASA's Jet Propulsion Laboratory, Pasadena, California

A proposed approach to fabricating custom LSI (large-scale integration) circuits would use a general logic structure (GLS) composed of standardized circuit arrays. Custom LSI's would be made by defining cut and contact points in the basic GLS mask set.

An approximation of the logical equivalent of a programed NMOS GLS is shown in the figure. Each of the m column lines may be formed into two or more NOR gates from physically disjoint partitions of the n implicant rows. A gate is created by connecting pulldown transistors at desired implicant rows to a column and connecting the column to a pullup resistor. The output of the NOR gate may be taken anywhere on the column segment on which the gate is built. Pullup resistors are located periodically along each column. This permits a column to be cut and formed into several independent NOR gates.

A NOR gate output may be connected to any unused implicant row that it crosses. The connection is made by forming a contact point at the desired row-and-column intersection. The formation of multiple contact points allows the NOR output to be transmitted to different locations within the structure.

Implicant rows may be cut into several segments. Each segment can be used to transmit a different implicant. In this way, for example, an implicant row carrying an input term may be cut after the last pulldown transistor that uses it. The segment after the cut can then be reused to transmit a NOR output.

In general the GLS structure consists of two types of rows: One row type transmits implicant terms; the other row is connected to ground. Transistors are created at the intersection of a column and implicant row where the implicant is needed in the NOR function. Transistor channels form a switchable path from columns to the ground row. Pulldown transistors are enchancement-mode devices.

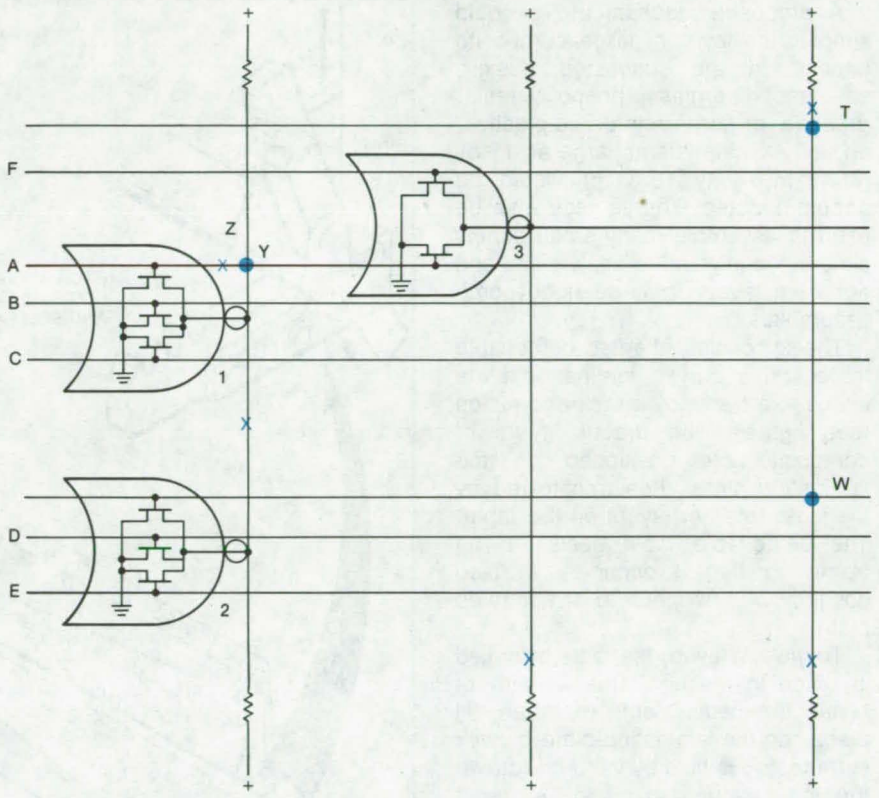

The **General Logic Structure** for custom LSI shows contact points indicated by a dot and cuts by an X. NOR gate 1 forms the result A+B+C. The implicant row carrying input A is cut at Z, and a contact point is created at Y. This connects gate 1 output to the implicant row freed by cut Z. Gate 1 output is then available as an input to NOR gate 3. Gate 3 is connected to an unused implicant row, which in turn is connected at T to a column. Contact W places the output of gate 3 on an implicant row, which makes it available to the input of gate 2.

The channels of these transistors conduct when a positive gate-to-source voltage is present. Pullup resistors are implemented by depletion-mode transistors that are shorted from gate to source.

The GLS can also be used to form shift registers by using a multiplexer in front of a flip-flop. In this configuration the register may be continually clocked. The multiplexer determines whether a left or right shift, load, or no operation is to occur on the next clock transition.

The GLS may be designed using an interactive color graphics system. A user could specify the function to be mapped, design guidelines, and analysis to be performed. By viewing the GLS created by the computer, or the results of an analysis, the user could suggest other mapping approaches or request changes be made.

This work was done by Michael W. Sievers of Caltech for **NASA's Jet Propulsion Laboratory.** *For further information, Circle 71 on the TSP Request Card.*

This invention is owned by NASA, and a patent application has been filed. Inquiries concerning nonexclusive or exclusive license for its commercial development should be addressed to the Patent Counsel, NASA Resident Legal Office-JPL [see page A5]. Refer to NPO-14410.

Jig for Assembling Large Composite Panels

Composite layers are accurately positioned by a mechanical jig.

Langley Research Center, Hampton, Virginia

A proposed mechanical jig could simplify the layup of large composite panels. In the suggested design, sheets of fiberglass, phenolic resin, graphite- or boron-reinforced plastics, and other materials as large as 15 by 60 ft (4.57 by 18.3 m) would be accommodated. The jig may also be used to assemble many small panels simultaneously and to apply skins and adhesive layers to large honeycomb assemblies.

The jig consists of a flat, detachable table and a curved laminating plate joined to a frame by a rack and pinion (see figure). The precut layers of composite are positioned on the laminating plate, then transferred by the plate to other layers on the table. The detachable table nests in the frame so that it occupies a fixed position with respect to the curved plate.

To make a layup, the table is locked in place in the jig frame. A film of Mylar (or equivalent material) is placed on the laminating-plate convex surface and is held by vacuum (drawn through a vacuum manifold). A precut sheet of the preimpregnated material of the first composite layer is applied to the film, within an outline scribed on the plate. The prepreg resin temporarily bonds the composite sheet to the film.

The laminating plate is raised to vertical, then lowered face down on the table. Registration between the curved plate and the flat table is ensured by engagement of the rack and pinion. With the plate positioned on the table, the vacuum is cut off, releasing the layer and the film. The film can then be peeled off the layup, leaving the new layer in place.

The transfer procedure is repeated until the composite panel is complete. Then, the table is released and wheeled away from the fixture so that the composite can be cured.

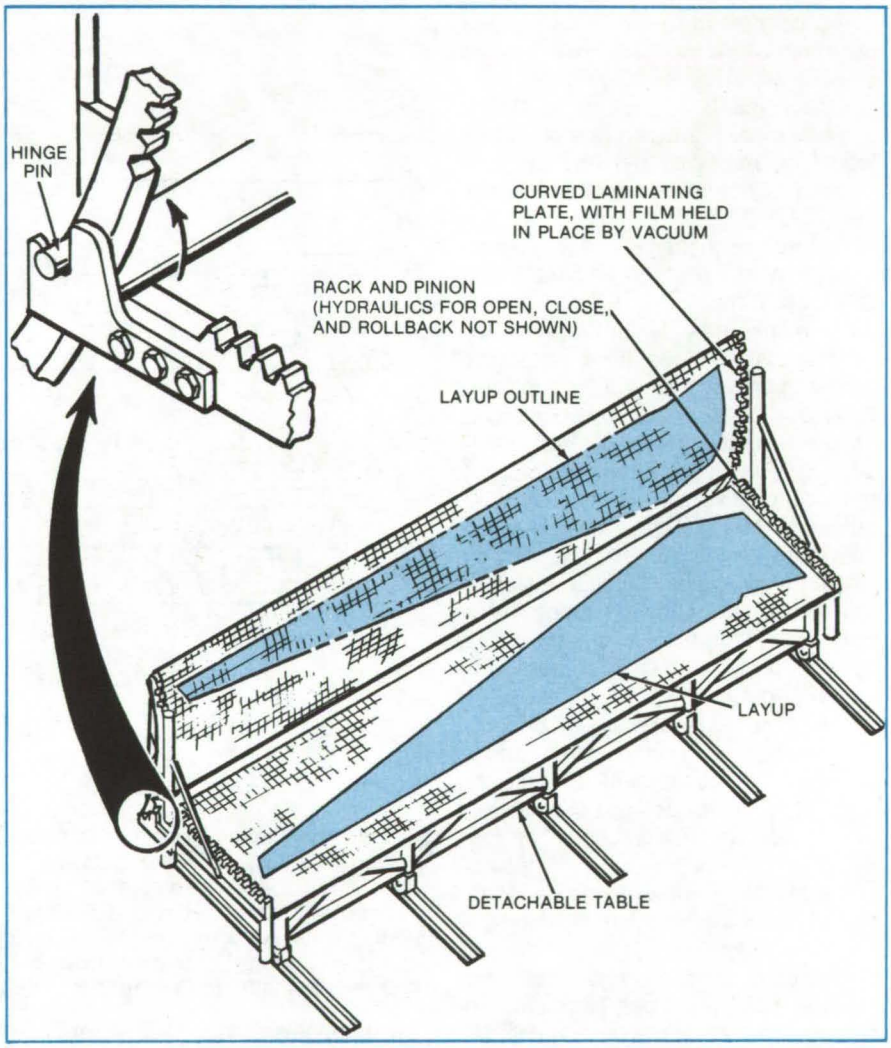

The **Curved Plate of the Bonding Jig** deposits a resin-impregnated layer on the table in a precise location, without disturbing other layers. After the layer is deposited, the vacuum chuck releases the film backing, and the film is peeled off the layup.

This work was done by John T. Watts of McDonnell Douglas Corp. for **Langley Research Center.** *For further information, Circle 72 on the TSP Request Card.*
LAR-12394

Shaping Graphite/Epoxy Stiffeners

A simple procedure produces long curved laminates without wrinkles or voids.

Lyndon B. Johnson Space Center, Houston, Texas

A method of shaping graphite-fiber-reinforced/epoxy parts eliminates wrinkles and voids and reduces fabrication time. Originally developed to make ribs (Figure 1) for the Space Shuttle payload-bay doors, the method may also find use in the fabrication of strong lightweight structural members in cars, trucks, and other vehicles.

A fixture shaped like the upper cap and lower flange of the rib is utilized (Figure 2). Twenty-five to thirty-eight layers of graphite/epoxy tape, 1 inch (2.5 centimeters) wide, are laid on each cap and flange of the fixture. Bleeder cloth covers the strips, and the fixture is placed in a vacuum bag and inserted in an oven at 175° F (79° C) for 15 to 20 minutes. The heat and external pressure on the vacuum bag shape the tape stacks smoothly around the contours of the fixture. (The stacks also retain their shape when they are removed from the fixture.) The caps and flanges are then interleaved with plies of graphite/epoxy fabric, 13 mils (0.33 millimeter) in thickness, to complete the rib.

Previously, layers of tape were shaped and applied by hand with the aid of a laminating adhesive. However, this method produced unacceptable ribs because of wrinkles and voids in the tape stacks.

This work was done by Jim L. Cupp of Rockwell International Corp. for **Johnson Space Center.** *For further information, Circle 73 on the TSP Request Card.*
MSC-18494

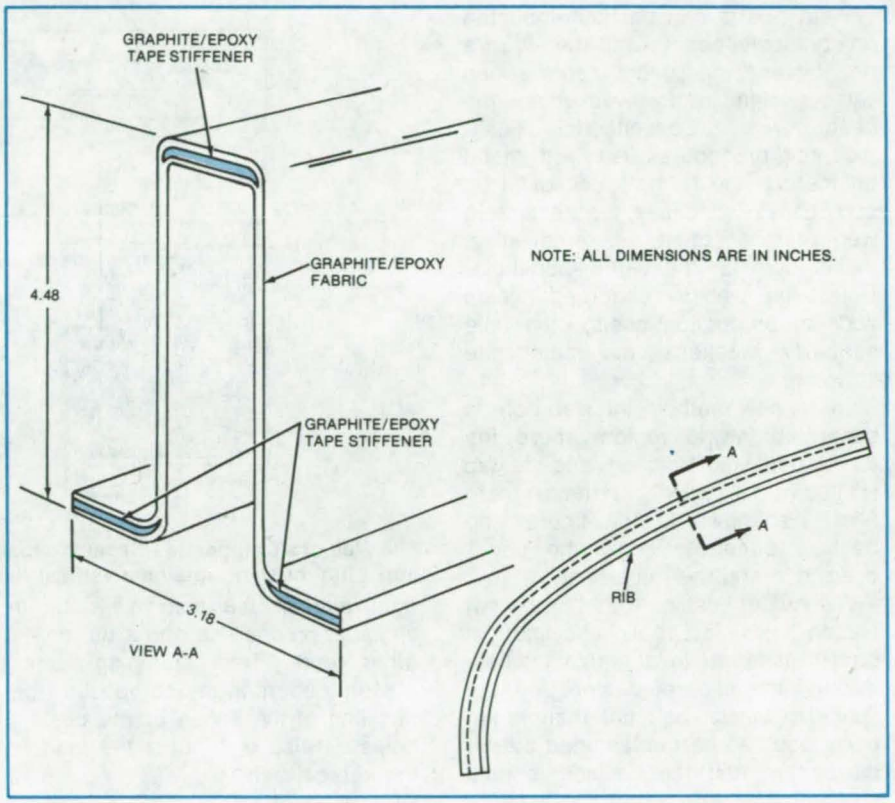

Figure 1. **Graphite/Epoxy Stiffeners** (in color) are embedded in the cap and flanges of a long, curved channelike rib.

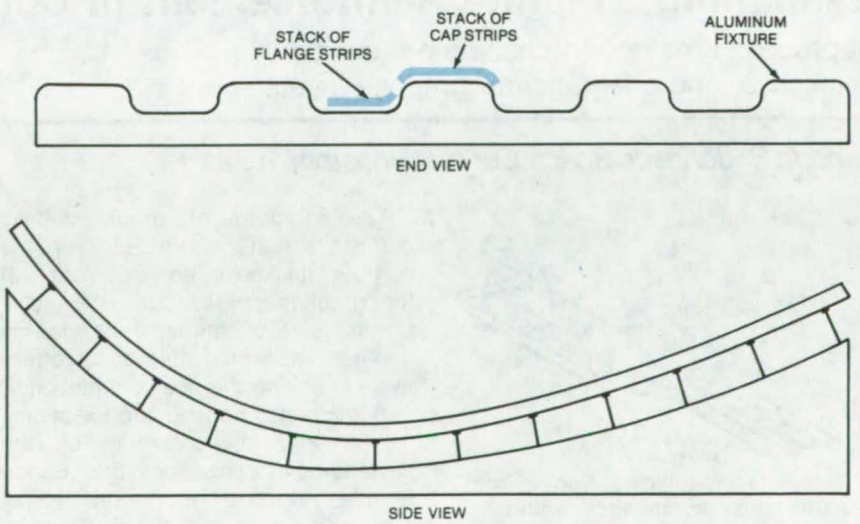

Figure 2. The **Shaping Fixture** contains ridges and grooves shaped like the cap and flanges of the rib and following the same longitudinal curve. Layers of graphite/epoxy tape are stacked on the ridges and in the grooves. The layup is vacuum-bagged in an oven to form caps and flanges free of wrinkles and voids.

Flush-Mounting Technique for Composite Beams

Tension bolts are retained by a transverse bushing.

Langley Research Center, Hampton, Virginia

Heavy parts can be flush-mounted on composite beams with the aid of a new fastener that distributes the load without significantly weakening the beam web. Conventional flush-mounting procedures used with metal beams are usually not successful on composites because considerable web material must be removed to make room for the vertical bolthole. Unless the web is reinforced (which adds to production costs), the hole seriously weakens the composite structure.

In the new method, the web core is separated in the region where the attachment is to be made, and the gap is filled with a lightweight precast foam filler. As shown in the figure, the bolthole penetrates only the upper beam cap and the foam filler.

A shoulder bushing with a barrel nut placed inside its hollow cylindrical core is inserted in a horizontal hole through the separated web and the filler. The tension bolt that anchors the flush-mounted part is fastened by the barrel nut, and the bushing is held tight against the web walls by its shoulder on one end and a nut on the other end. This clamping action prevents fibers in the composite from buckling at the edges of the bushing holes. It also distributes the load on the vertical bolt.

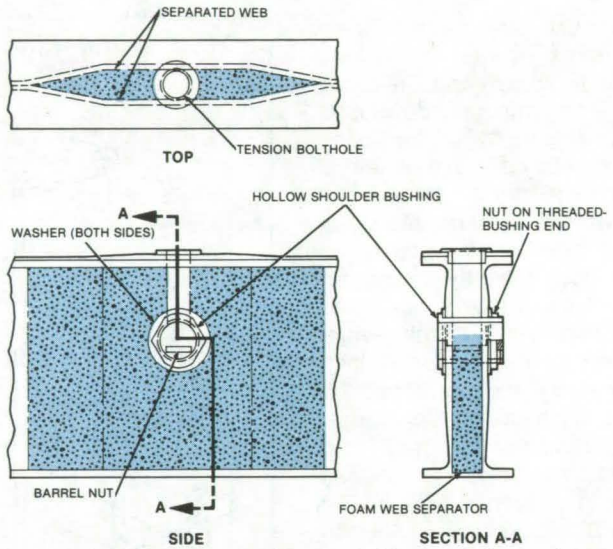

The Web of a Composite I-Beam is separated and filled with foam. A barrel nut in the horizontal bushing retains a vertical flush-mounting bolt.

This work was done by Thomas C. Harman and Bruce F. Kay of United Technologies Corp. for **Langley Research Center.** *For further information, Circle 74 on the TSP Request Card.*
LAR-12389

Examining Graphite Reinforcement in Composites

A proposed method to check the number, thickness, and orientation of graphite layers

Lyndon B. Johnson Space Center, Houston, Texas

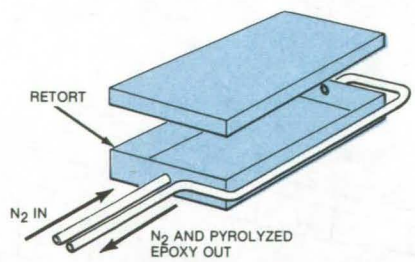

A **Retort for Pyrolyzing Epoxy** from graphite/epoxy composites would retain only the graphite fibers in their original orientation. The retort is placed in a furnace; the nitrogen inlet and outlet tubes extend through an opening in the furnace.

The strength of graphite/epoxy composite materials depends on the number, thickness, and orientation of the graphite fibers. Once the composite is fabricated, there is no generally accepted method of effectively checking the fiber orientation.

A method proposed for examining the graphite reinforcement on the payload-bay doors on the Space Shuttle utilizes a retort (see figure) filled with a nonreactive gas. Samples of graphite/epoxy compound would be placed in the retort, which would be tightly closed, purged with nitrogen gas, and heated in a furnace at 1,000° F (540° C) for 2 to 3 hours.

After several hours, the epoxy is pyrolyzed and carried away through the retort exhaust by a continuous flow of nitrogen gas. The retort is then cooled and opened. The graphite fibers remain and are easily separated to check the number, thickness, and orientation of the layers.

This work was done by Robert E. Sanders and Clyde I. Yates of Rockwell International Corp. for **Johnson Space Center.** *No further documentation is available.*
MSC-19594

Cryogenic Machining of Polyurethane Foam

Complex configurations can be machined in low-density foam.

Lyndon B. Johnson Space Center, Houston, Texas

A method for precisely machining low-density polyurethane foam in thin cross sections begins by cooling foam to cryogenic temperatures. Once "frozen," the foam is machined as if it were any other solid material. Developed to make foam lens seals on the Space Shuttle closed-circuit television cameras, the technique could also be used to make vibration dampers, mounting cushions, and other parts.

The Shuttle lens seal calls for a low-density[1.0 to 2.0 lb/ft^3 (16 to 32 kg/m^3)] closed-cell polyurethane foam disk with a cross section of 0.25 in. (0.64 cm). A narrow slot must be machined in the edge of the disk.

The outer diameter and inner diameter of the disk are first cut with a tool similar to a cookie cutter; the outer diameter is 4.25 in. (10.80 cm), and the inner diameter is 3.15 in. (7.99 cm). After the foam is cut, it is placed on a massive aluminum machining fixture; a cover plate keeps it in place. A handle is attached to the fixture, and the entire assembly is lowered into a tank of liquid nitrogen for 60 seconds. Upon removal, the fixture is placed in the chuck of a lathe, and a slot 0.05±0.005 in. (0.127±0.013 cm) in width by 0.485 in. (1.232 cm) deep is machined into the edge of the disk.

The massive fixture acts as a thermal "sink" that keeps the foam frozen during the entire machining operation. When machining is complete, the disk is removed from the fixture and allowed to reach room temperature.

This work was done by Edward A. Moshey and Peter Prychka of RCA Corp. for **Johnson Space Center.** *No further documentation is available.*
MSC-18572

"Grinding" Cavities in Polyurethane Foam

Foam blocks are cut by a grinding tool on a conventional milling machine.

Lyndon B. Johnson Space Center, Houston, Texas

A **Grinding Tool Removes Material** from a foam block as the milling-machine table moves in the pattern established by a template.

Cavities of precisely controlled size and shape can be cut into blocks of polyurethane foam by a grinding tool installed in a conventional milling machine. The cutting method was developed to produce foam cushions for holding loose tools and small equipment aboard the Space Shuttle. It can also be used to shape foam containers for the storage or shipment of delicate items.

As shown in the figure, the polyurethane foam block is mounted on the milling-machine table, and an air-powered high-speed grinder is attached to the milling-machine head. As the table movement follows a template cut with the required pattern, the grinder is pressed into the foam so that the cavities are formed. The grinding tool can be extended further into the foam to cut smaller cavities within the initial cut.

The method is well suited for prototype or midsize production runs and can easily be adapted to computer control for mass production. Previously, shaped-cavity foam blocks were formed from many small blocks bonded together around a wooden mandrel. Alternatively, a hot wire was used to scoop pieces of foam from a block. The new method saves time and material and allows last-minute changes to be made in the cavity shape.

This work was done by James R. Brower, Raymond E. Davey, William F. Dixon, Paula H. Robb, and Paul P. Zebus of Rockwell International Corp. for **Johnson Space Center.** *No further documentation is available.*
MSC-18564

Alumina Barrier for Vacuum Brazing

Aluminum oxide "paper" protects tooling and improves brazed-joint quality.

Lyndon B. Johnson Space Center, Houston, Texas

Thin sheets of alumina-enriched paper prevent the workpiece from attaching to the tooling in brazing operations. Used in fluxless vacuum brazing of stainless-steel parts (Figure 1), the paper acts as a barrier that prevents the brazing alloy from bonding to the tooling. Because of the high chemical stability of alumina (aluminum oxide), the paper does not react with the parts or the tooling, even at the high temperatures and pressures required for brazing.

The alumina barrier is especially useful in brazing parts with perforated or otherwise irregular surfaces, since it prevents the brazing alloy from extruding through the perforations and contacting the platens of the brazing press. Unlike other common barrier materials (various powders and solids), the alumina paper does not disintegrate in the press. Because the paper does not outgas, there is no contamination of the braze alloy, ensuring a uniform reliable joint without voids. As seen in the section of stainless-steel heat exchanger shown in Figure 2, the paper helps to form a smoothly-contoured regular fillet at the edges of the brazed pieces. On the heat exchanger, used on the vertical stabilizer of the Space Shuttle, the brazing was so successful it eliminated the need for a 130-inch (3.3-meter) peripheral closeout weld.

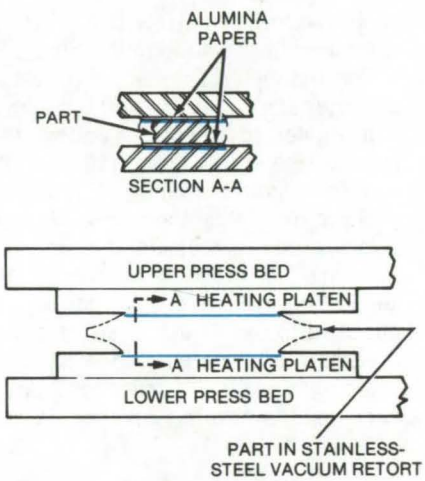

Figure 1. A **Sheet of Alumina Paper** is placed between the parts to be brazed and the heating platens of the press.

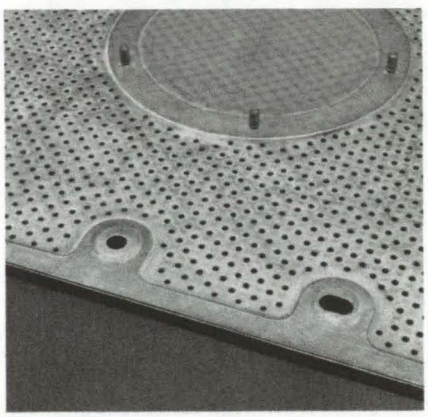

Figure 2. This **Perforated Heat Exchanger** was assembled, using alumina paper as a barrier between the braze alloy and the heating platens of the vacuum-brazing press. Note the smooth fillets.

This work was done by Charles S. Beuyukian of Rockwell International Corp. for **Johnson Space Center.** *No further documentation is available.*
MSC-18528

Connector Heat Shield

Polytetrafluoroethylene protects coated electrical connectors during soldering.

Lyndon B. Johnson Space Center, Houston, Texas

The use of heat sinks and shields to protect electronic components during soldering is widely known. Often overlooked, however, is the susceptibility of plated electrical connectors to heat blistering. A blistered connector secured in place with epoxy potting will eventually corrode, requiring replacement. The cost of this relatively simple problem can be substantial, once the circuit is in operation.

The connectors can be protected against heat damage by wrapping them with polytetrafluoroethylene tape (e.g., Mystik Tape No. 7503 or equivalent) before soldering. The tape can be removed easily after the contacts are joined.

This method was used in soldering connectors to stainless-steel solenoid housings. Earlier, a polytetrafluoroethylene coating was used as the protection. However, this coating is difficult to remove after soldering.

This work was done by Shirley Clarke of Wright Components, Inc., for **Johnson Space Center.** *No further documentation is available.*
MSC-16282

Foam-Filled Cushions for Sliding Trays

Tubular dampers
absorb vibrations.

Lyndon B. Johnson Space Center, Houston, Texas

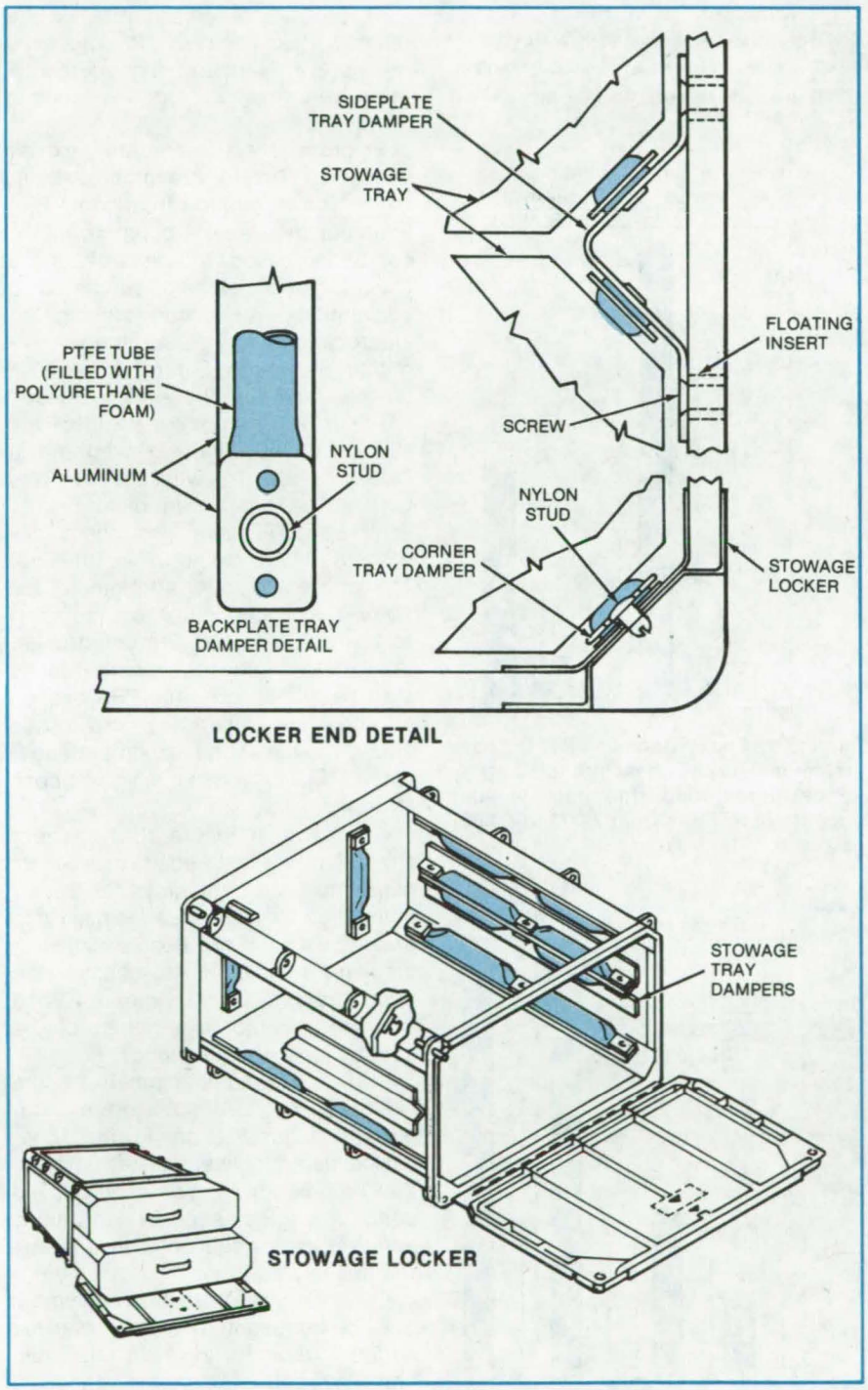

Foam-Filled PTFE Tubes are fastened to the inside of stowage lockers by snap-in nylon studs. The configuration shown accommodates two stowage trays. With the sideplate dampers removed, the locker can accommodate one double-sized stowage tray. The PTFE tubes used for stowage trays on the Space Shuttle are 0.375 in. (0.95 cm) in diameter.

The cushioning of polyurethane foam and the durability of PTFE are combined in vibration dampers for sliding trays aboard the Space Shuttle. Consisting of polyurethane foam inside a PTFE tube, the dampers are fastened to the inside of modular "lockers" that hold the plastic trays. Each foam-filled tube offers a low-friction sliding surface that cushions vibrations, absorbs misalinements and manufacturing tolerances, and prevents accidental movement of the tray during normal crew operations. Possible uses for the dampers are in the packaging of components for shipping and in doors for lockers, refrigerators, automobiles, and other vehicles.

As shown in the figure, the PTFE tubes containing polyurethane foam are fastened to an aluminum strip prior to their installation in the lockers. The dampers are held in place by snap-in nylon studs, which permit easy installation.

This work was done by Samuel B. Nahin and Paula H. Robb of Rockwell International Corp. for **Johnson Space Center.** *No further documentation is available.*
MSC-18565

Ion-Beam Etching Enhances Adhesive Bonding

Ion-beam etching is superior to chemical etching for both metals and plastics.

Lewis Research Center, Cleveland, Ohio

Electron bombardment by an argon ion-beam source was used to etch various metals and fluoropolymers, which were then adhesively joined to themselves. Bond-strength tests on the fluoropolymers showed that there was a substantial improvement in bond strength over current state-of-the-art chemical-etching techniques. Two of the metals also showed substantial bond-strength improvement over untextured metals.

The materials tested were: fluorinated ethylene propylene (FEP), polytetrafluoroethylene (PTFE), perfluoroalkoxy (PFA), and polychlorotrifluoroethylene (CTFE), graphite, nickel, titanium, and type 304 stainless steel.

The metals and fluoropolymers were exposed to Ar ions of 0.5 to 1.0 keV at ion current densities of 0.2 to 1.5 mA/cm^2 for various exposure times. The resulting surface texture is in the form of needles or spires with vertical dimensions that may range from tenths to hundreds of micrometers, depending on the selection of beam energy, ion current density, and etch time. The bonding of textured surfaces was accomplished by ion-beam texturing mating pieces of either metals or fluoropolymers and applying a bonding agent, which flows around the microscopic conelike structures.

The 30-cm ion source used was developed from electric propulsion technology; it operates at beam energies between 300 and 1,500 eV. For the fluoropolymer samples, the source ion energy was 750 eV; for metal specimens, in the range 950 to 1,200 eV. The fluoropolymers and graphite samples were placed in a holder, and the surface to be textured was oriented normal to the ion beam 23 cm from the source-grid plane. The nickel, stainless-steel, and titanium samples were placed in the same position as the fluoropolymers with an additional tantalum target located above them at a 45° angle relative to the metals to provide seeding and sustain surface texturing.

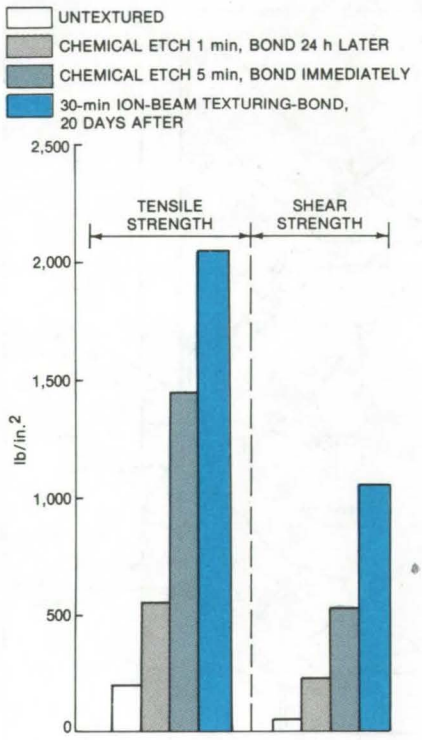

Figure 1. **Epoxy-Bonded PTFE** has greater tensile and shear strengths after ion-beam texturing (the bulk tensile strength of PTFE is from 2,000 to 5,000 psi).

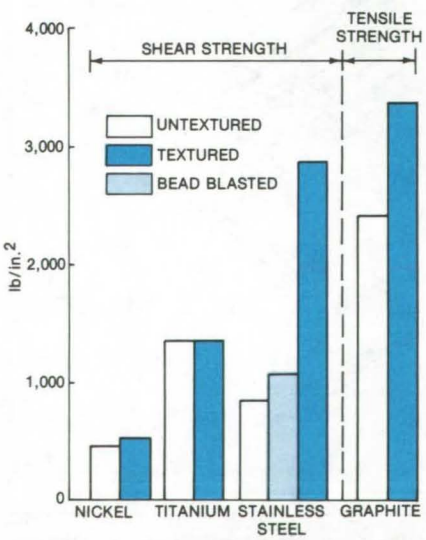

Figure 2. **Epoxy-Bonded Metals and Graphite** show, in some cases, greater tensile and shear strengths when textured by an ion beam.

To obtain textured structure on the metals, it was necessary to expose the metals 3 to 4 hours; the fluoropolymers were textured from 5 seconds to 30 minutes.

Fluoropolymers generally exhibit negligible bond strengths without some type of surface treatment. FEP fluoropolymer epoxy bond strengths can be increased by factors of 5 to 10 using ion-beam etching, compared to conventional chemical etching or electrical-discharge surface treatment. Shown in Figure 1 are the tensile and shear strengths of bonded PTFE using an epoxy resin after the surface for bonding was prepared in different ways. The weakest bond was that of the untextured or untreated samples. PTFE was also chemically etched using sodium/naphthalene. The tensile and shear strengths of the epoxy-resin ion-beam-textured surface are 46 and 100 percent stronger than those of the chemically etched surface. PTFE, FEP, and PFA exhibited about the same shear and tensile strengths when bonded with the epoxy resin. CTFE exhibited the highest bond strengths.

As shown in Figure 2, the shear strength of the textured stainless-steel bond improved by a factor of 3 over untextured stainless steel. Exposure to an ion beam did not texture nickel or titanium sufficiently to change the bond strength of these metals. Bond strength of carbon was helped only a little by ion-beam texturing.

Surface features similar to the polymers are also obtained by ion-beam texturing Kapton. Furthermore, all the fluoropolymers tested showed that ion-beam texturing produced bond strengths superior to those achieved with conventional surface treatments.

Chemically etched fluoropolymers must be bonded immediately after the surface treatment to attain maximum bond strength. Also, the chemical etchant residue must be thoroughly cleaned from the substrate to avoid a

continuous deterioration of the bond, and environmental safeguards must be observed because of the deleterious effects of the chemicals used. The bond strength of ion-beam-etched fluoropolymers is not a function of shelf life; bonding may be done hours, days, or months after surface treatment.

This work was done by B. A. Banks, M. J. Mirtich, and J. S. Sovey of **Lewis Research Center.** *Further information may be found in:*

NASA TM-79004 [N79-12909/NSP], "Adhesive Bonding of Ion Beam Textured Metals and Fluoropolymers" [$4]; and

NASA TM-78888 [N78-24358/NSP], "Ion Beam Sputter Etching and Deposition of Fluoropolymers" [$4].

Copies may be purchased [prepayment required] from the National Technical Information Service, Springfield, Virginia 22161.

This invention is owned by NASA, and a patent application has been filed. Inquiries concerning nonexclusive or exclusive license for its commercial development should be addressed to the Patent Counsel, Lewis Research Center [see page A5]. Refer to LEW-13028.

Room-Temperature Adhesive for High-Temperature Use

Room-temperature-curing adhesive retains strong bond in extreme temperature environments.

Lyndon B. Johnson Space Center, Houston, Texas

Adhesives used in bonding reusable surface-insulation tiles to metallic substrates must withstand extreme temperature environments that may be encountered by the tile surface. Typical adhesives used in this application are the thermosetting type, which are cured at temperatures at least as high as those expected in service, and adhesives cured by chemical reaction in controlled humidity. One chemically curing adhesive requires careful weighing and thorough mixing of catalyst for proper cure. Its service temperature range is between -170° F (-113° C) to 500° F (262° C).

A significant improvement is obtained with polyphenylquinoxaline (PPQ). PPQ cures at room temperatures and withstands temperature extremes between -300° F (-186° C) and 750° F (402° C). Laboratory studies have shown that PPQ used with chloroform as solvent produces the best bond capable of withstanding both mechanical and thermal stresses (see figure).

Basically the PPQ-chloroform solution is sprayed or brushed onto a precleaned metal substrate. The other adherent, typically a porous material to permit quick solvent evaporation, is brought into contact with the PPQ film. The solvent is then allowed to evaporate at room temperature, leaving a strong bond. Evaporation of the solvent may be speeded up by the application of vacuum and/or elevated temperature.

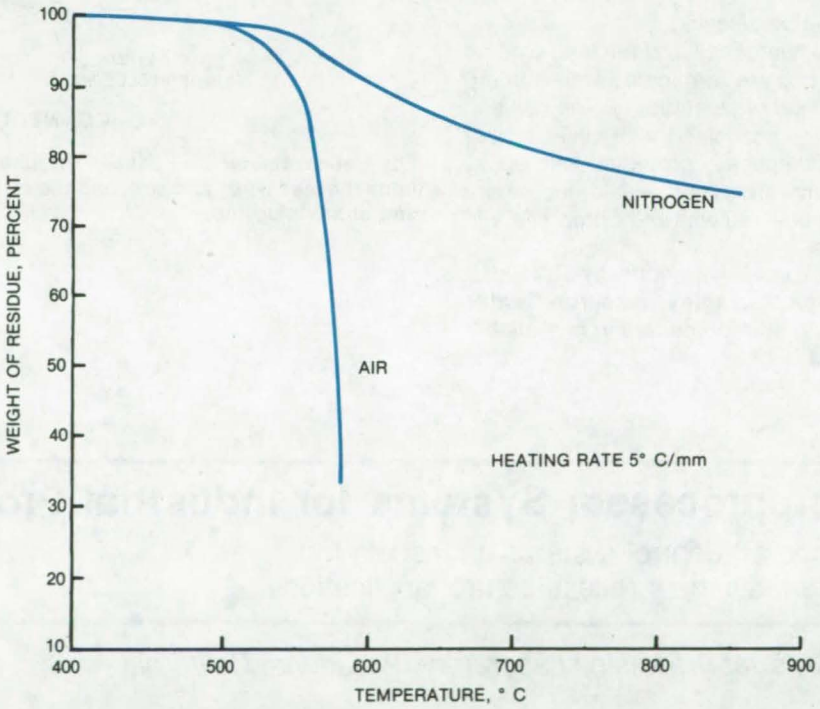

Excellent Thermal Stability of PPQ is demonstrated by thermogravimetric analysis as the polymer is heated. Decomposition in air or nitrogen does not begin until the temperature exceeds about 440° C.

This work was done by Jon L. Brooks, William L. Hill, and Charles R. Rousseau of Rockwell International Corp. for **Johnson Space Center.** *For further information, Circle 75 on the TSP Request Card.*

MSC-16930

Easily-Assembled Helical Heater

A rugged, compact coil heater

Langley Research Center, Hampton, Virginia

A rugged, low-current heater is assembled from readily available materials. The helical heater element is Inconel (or equivalent alloy) 0.004 in. (0.1 mm) in diameter with a resistance of 38 ohms per foot (125 ohms per meter). In a design for heating biological samples on the Viking lander, the total coil resistance is 195 ± 10 ohms, and the inner diameter of the coil is only 0.015 in. (0.38 mm).

Each end of the helical coil passes through a ceramic spool (see figure). The coil and spools are covered with 0.045-in. (1.14-mm) clear PTFE heat-shrinkable sleeving.

The heater coil and the lead wire on each end are terminated with a crimp clip made of steel tubing. The coil and the wire are joined with silver braze, and the splice is protected with epoxy adhesive or silicon elastomer before being covered with the crimp clip and sleeve.

This work was done by Donald E. Pizzeck of **Langley Research Center.** *No further documentation is available. LAR-11712*

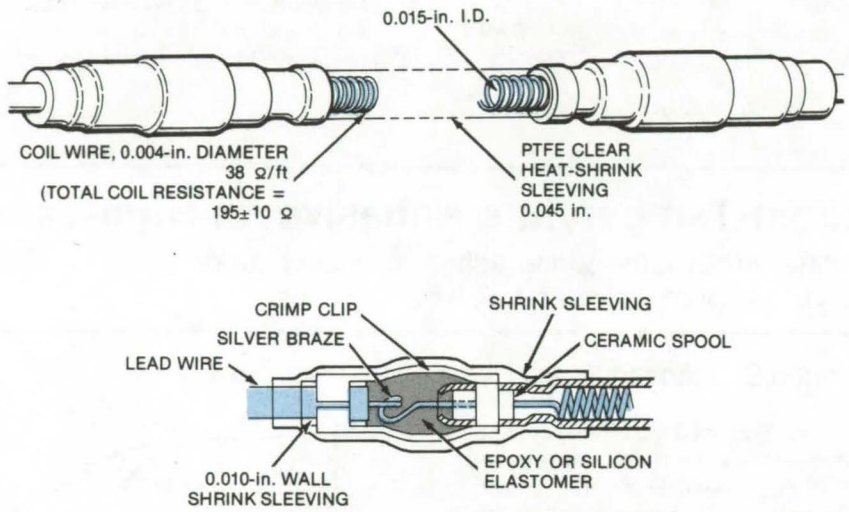

CONNECTOR DETAIL

The **Helical Heater Coil** passes through a ceramic spool at each end. Silver braze joins the lead wires and coil, and the splices are covered with epoxy, a crimp sleeve, and shrink sleeving.

Microprocessor Systems for Industrial-Process Control

Spacecraft control systems as models for future industrial-process control applications.

NASA's Jet Propulsion Laboratory, Pasadena, California

Several promising spacecraft control systems are possible models for future industrial-process controls. Two versions have been examined: One uses minicomputers, and the other uses microprocessors. Both systems utilize distributed microprocessor architecture characterized by a number of microprocessors that are each dedicated to one subsystem. Each microprocessor (or minicomputer) is structured to control sensors and actuators of the subsystem, to collect data, and to maintain synchronization. This approach might be adapted for controlling complex packaging machinery, a steel-rolling plant, an automobile assembly line, and similar processes.

The first example, The Unified Data System (UDS), is an experimental breadboard system equipped with six minicomputers. Each minicomputer has 8,192 16-bit words and an average execution time of about 2.5 μs. It includes a ground computer with a CRT (cathode-ray-tube) display and, on the spacecraft, a processor that exerts overall spacecraft mission control. A format processor collects telemetry data in fixed-length blocks from other processors and moves the data to a modulation/demodulation subsystem computer. Another processor controls a television camera, and a data-storage subsystem computer controls a tape recorder.

The computers operate synchronously and are all interconnected with a set of three independent data buses. Each bus can transfer data at 1 megabit per second. The ground, command, and format processors are each equipped with a bus control and constitute the so-called "high-level

modules." The others without the bus controllers constitute "terminal modules."

The UDS is synchronized using a single interrupt that occurs simultaneously on all processors every 2.5 ms. During the interrupt, each processor examines a list of things to be done during that interval. Any function is performed in a small fraction of the interval.

The system timing is obtained from its TV camera operation as reference. A special UDS design language is used in conjunction with the camera signals to control the timing.

A second example currently under development will be based on commercially available microprocessors with an 8-bit capacity using a different bus arrangement also capable of transferring data at 1-MHz rates in packets of up to 32 words (32-bit words) in length. This version will use a modified software arrangement permitting several programs to be operated concurrently in a single microprocessor.

This work was done by Fred H. Lesh of Caltech for **NASA's Jet Propulsion Laboratory.** *For further information, Circle 76 on the TSP Request Card.*
NPO-14661

Wire Harness Twisting Aid

Handtool and spacers separate and control the wires as they are twisted into a harness.

Lyndon B. Johnson Space Center, Houston, Texas

Long wire bundles are twisted into uniform spiral harnesses by the apparatus shown in the figure. The twisting aid uses a hand-held sliding tool, spacers, control tubes, a wire plate, and a slow-turning bench motor to twist a group of wires into a tight spiral harness. The handtool and spacers separate the wires as they are twisted by the bench motor.

To make a harness, individual wires are fed through the tubes and spacers, which are secured with tape to a table. They are then fed through the hand-held sliding tool and secured at the wire plate to the motor.

The sliding tool is held firmly and pulled along the wires away from the motor. This generates smooth twists in the wires between the motor and the sliding tool. As the spiral length increases, the operator continues to move the sliding tool away from the motor. One at a time the individual spacers are encountered and pushed toward the end of the wires. The sliding tool will be the last member off the wire bundle when the entire length of wires is smoothly twisted.

Besides reducing cost and improving the appearance of the harness, the technique produces wire harnesses that generate less radio-frequency interference when conducting current than do irregularly twisted cables. The tooling aid is ideal for prototype work and low-production runs.

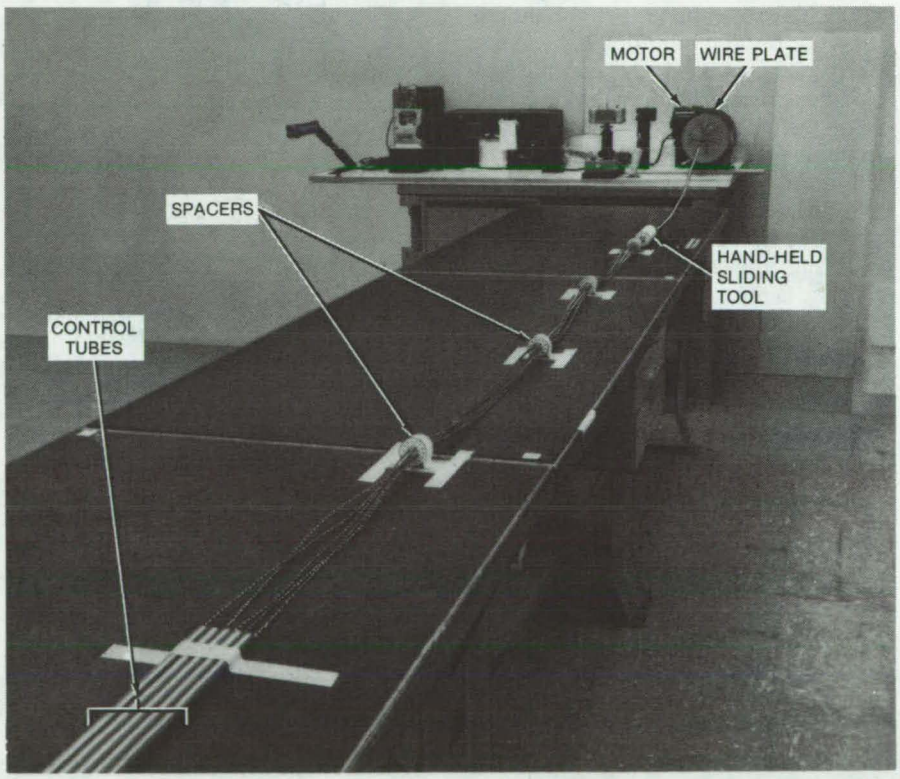

The Hand-Held Sliding Tool, spacers, and control tubes separate the wires while they are twisted by a bench motor into a harness. Smooth twists are generated between the motor and sliding tool by pulling the tool along the wires and away from the motor.

This work was done by Emil J. Casey, Curtis C. Commadore, and Mel E. Ingles of Rockwell International Corp. for **Johnson Space Center.** *No further documentation is available.*
MSC-18581

Adjustable Base for Centering Staked Bearings

A new base compensates for dimensional differences between the parts.

Lyndon B. Johnson Space Center, Houston, Texas

Bearings are normally staked into their housings with a conventional roller staking tool. As the tool is rotated around a flange on the race to stake the bearing, the bearing race and the housing are supported by a flat fixed locator base (see figure, left). For best results, the race must be centered with respect to the housing. If it is not, the misalined bearings are likely to fail under load.

Because slight dimensional differences in widths often occur between the housing and the bearing race during their manufacture, the bearings may not be centered if a flat base is used. One staking flange may be slightly smaller than the other; and when the roller swaging tool is applied to the longer flange, the race may be shifted off center, as in the figure, left.

A new adjustable base prevents that shift (see figure, right). The difference in widths between the race and the housing is measured and divided by 2. Part 1 of the base is then adjusted to support the race at the proper height so that it is staked on center with respect to the housing. The base is adjusted separately for each flange.

This work was done by Leo A. Berson of Rockwell International Corp. for **Johnson Space Center.** *No further documentation is available.*
MSC-19660

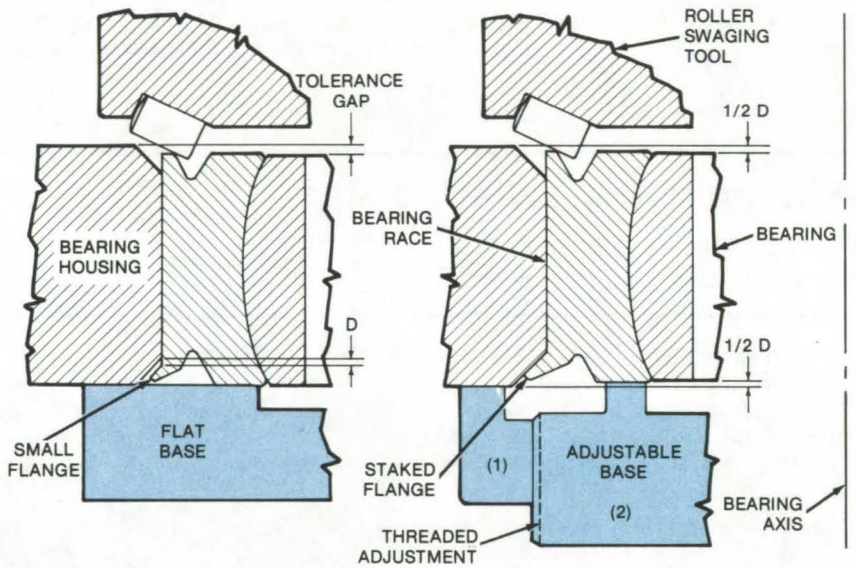

(a) STANDARD ONE-PIECE BASE (NO EQUALIZATION FOR D, SMALL FLANGE SLIDES DOWN ON TURNOVER)

(b) NEW ADJUSTABLE BASE (ADJUSTED TO EQUALIZE FOR 1/2 D, FULL FLANGE HELD TIGHT ON TURNOVER)

If the **Bearing Race Is Centered** and staked with the assistance of a flat base (left), the bearing may be set off center if there is a dimensional difference between the housing and the bearing race. The offset occurs when the roller swaging tool is applied to the top flange. The new adjustable base (right) prevents the shift by supporting the race and housing separately.

Safely Splicing Glass Optical Fibers

A fusion field-repair technique for use in flammable environment.

John F. Kennedy Space Center, Florida

A safer fusion splicing method for optical glass fibers can be used in explosive gas atmospheres. Splicing equipment is inside a box pressurized with inert-gas atmosphere. The method designed for fieldwork replaces earlier methods that use an unprotected electric arc not suitable for a flammable environment.

The new splicing apparatus includes:

a. V-groove vacuum chucks mounted on xyz micromanipulators for accurately positioning the fiber ends to be fused;
b. A high-voltage dc power supply to produce an arc between two tungsten electrodes for fusion of the butt-joint region of fibers;
c. A microscope to observe the joint alinement and fusion;
d. A means of monitoring optical transmission through the joint for

accurate fiber alinement before fusion; and

e. A gastight box containing inert gas under pressure and enclosing the electrodes, fiber holders, and micropositioners with feedthroughs for the electrical wiring and fibers.

A successfully-tested prototype unit uses a 0-to-10-kV dc power supply with current output from 0 to 20 mA. A 10X to 100X magnification microscope and high-resolution micropositioners are included. The fibers are fused in a 12- by 6- by 6-in. (30- by 15- by 15-cm) inert-gas box. Micromanipulator and other control knobs inside the box are projected into rubber sheaths, forming sealed, easily operated controls.

Other equipment necessary to produce a good splice joint includes: a fiber cutting tool, coating material, coating stripper (e.g., acetone), protective sleeve, vacuum pump, about 50 ft (15 m) of high-voltage power cable, an optical generator and receiver, a digital voltmeter, and lock-in amplifier.

About 2 ft (60 cm) of fiber ends are necessary for splicing. Typically, a single fiber is spliced. Typically, a single fiber is spliced at a time from a fiber-bundle tape. After the fibers are spliced, they are taken outside the box and laid on the splice housing one at a time until the entire bundle is finished. The spliced joints are tested with the optical transmitter and receiver for minimum optical energy loss across the joints.

This work was done by K. Korbelak of General Cable Corp. for **Kennedy Space Center.** *No further documentation is available.*
KSC-11107

Knife-Edge Seal for Vacuum Bagging

No adhesive, tape, or sealing groove is needed.

Marshall Space Flight Center, Alabama

In an improved clamping method for high-temperature vacuum bagging, a cam-actuated knife edge holds the perimeter of the film bag against a rubber cushion (see figure). This allows the bag to be quickly installed and removed, without using tape, adhesives, or tedious stripping procedures. Moreover, no permanent modifications to the aluminum baseplate are necessary, in contrast to a previous approach in which a sealing groove was machined in the aluminum surface.

To implement the method, which has been used for vacuum-bagging and cure cycles above 400° F (204° C), the rubber cushion is bonded to the baseplate with a high-temperature cement. The cushion is also a high-temperature-resistant material. The cam-actuated clamps are bolted to aluminum angle stock at approximately 22-in. (55-cm) intervals.

The sealing surface is a 0.005-in. (0.013-cm) knife edge that is machined on the vertical side of the angle stock. After the vacuum-bagging sheet is spread over the work with its edges draped over the rubber cushion, the clamps are used to force the knife edge against the bag and the cushion. This creates a tight seal that is effective at high temperatures.

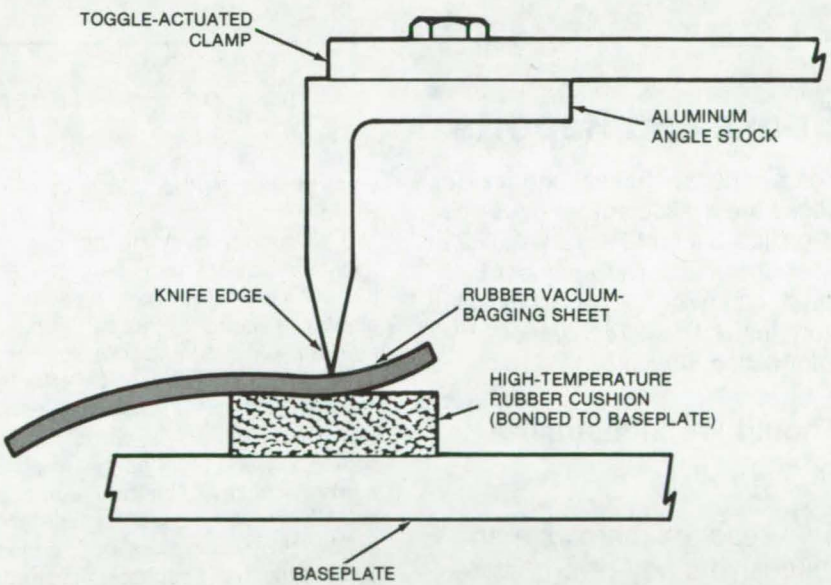

A Tight Seal is formed by clamping a vacuum-bagging sheet between a knife edge and a rubber cushion. Several cam-actuated clamps are spaced along the periphery of the sheet.

This work was done by Joseph A. Rauschl of Rockwell International Corp. for **Marshall Space Flight Center.** *No further documentation is available.*
MFS-24049

A Precoat Prevents Ceramic Stopoffs From Spalling

Nickel-alloy precoat secures ceramic stopoff to the metal surface.

Marshall Space Flight Center, Alabama

Ceramic stopoff materials, such as zirconium oxide, aluminum oxide, and boron nitride, are used to protect areas from unintentional brazing. However, if applied directly to the metal surface, these materials tend to spall during the brazing process. The problem is easily corrected using a nickel-alloy precoat (e.g., Nichrome or Inconel X, or equivalent) before the ceramic is applied. The precoat improves the ceramic adhesion and makes the ceramic more tolerant to any deformation.

The precoat is applied with a plasma gun. The prepared metal surface is sprayed with the alloy to a film thickness of 0.002 to 0.003 in. (0.05 to 0.08 mm). The covered surface is then coated with the ceramic, using the same procedure. The thickness (same as the precoat) of the ceramic coat and its texture can be varied to accommodate heavy tooling by changing the mesh size of the precoat.

Before the precoat, the metal surface is usually grit-blasted, which is the best and the cheapest method for most heavy-duty applications (e.g., in brazing machinery components). Fine aluminum oxide or silicon carbide can be used for light grit blasting. Furnace cleaning and abrasive cleaning can also be used to prepare the surface prior to plasma application. The coating easily adheres to an extremely-thin precoat sheet, as long as the sheet surface is oxide-free.

The stopoff coating does not interfere with the brazing process. When used in a vacuum, the coating does not contaminate the pumping system.

The process has been successfully used in brazing tubes inside the Space Shuttle main-engine nozzle. It is 100 percent reliable and totally controllable. The ceramics are more durable stopoffs than the conventional cloth-type materials.

This work was done by Alex Brennan of Rockwell International Corp. for **Marshall Space Flight Center.** *No further documentation is available.*
MFS-19495

Books and Reports

These reports, studies, and handbooks are available from NASA as Technical Support Packages (TSP's) when a Request Card number is cited; otherwise they are available from the National Technical Information Service.

Should We Industrialize Space?

Two reports summarize an extensive study of a complex question.

Whether or not to make a commitment to space industrialization is a question enmeshed with complex social, economic, and political issues. Space offers the possibility for benefits in the areas of energy, resources, services, and human activity; but the costs are large, and the risks, as with any venture into the unknown, are substantial. Since much of the reward would not be realized for several years, even if a program is immediately initiated, the issue is further complicated by uncertainties in the future course of world events.

A 20-month study of this question, sponsored by NASA, is summarized in two companion reports that can help to clarify the issues for those interested in the implications and possibilities of space industrialization. The effects of diminishing world resources and of expected changes in world markets, population, and technology are considered in assessing the industrial potential of space. Possible benefits of industrialization are outlined, and specific hardware concepts are treated along with cost estimates. A section of one report deals with possible legal implications.

In general, the reports try to project world needs over the next 30 to 50 years (with admitted uncertainty) and to correlate them with space opportunities. The opportunities are broken down into the broad categories of *services*, *products*, *energy*, and *human activities*. Each category is subdivided into numerous specific examples. Among over 100 *service* opportunities are:

- electronic mail,
- personal "wrist radio,"
- disaster warning relay,
- nuclear fuel locator, and
- forest-fire detection.

Products opportunities include:

- isoenzyme production in zero gravity,
- radioisotope separation,
- materials processing, and
- integrated-circuit manufacturing.

Opportunities in the *energy* area include:

- solar/electrical conversion,
- fusion,
- nuclear waste disposal, and
- night illumination for special applications.

In the area of *human activities*, space industrialization offers a diversity of new careers and new challenges, and space colonization is a possibility intimately linked with space industrialization.

This work was done by G. W. Driggers of Science Applications, Inc., and C. L. Gould of Rockwell International Corp. for **Marshall Space Flight Center.** *To obtain copies of the reports, "Space Industrialization," Circle 77 on the TSP Request Card.*
MFS-23963

Cost Models and Economical Packaging of LSI's

New developments in cost modeling and packaging hybrid microcircuits

A report, an extension of an earlier study [see "Cost Savings in LSI Fabrication" (MFS-25079) on page 580 of *NASA Tech Briefs,* Vol. 4, No. 4], presents recent developments in cost modeling and economical packaging of LSI hybrid microcircuits. The mathematical cost models that were developed for hybrid microelectronic subsystems have been refined and expanded. Improvements have also been made in the tape chip carrier (TCC) technology — a promising low-cost technique for packaging the LSI chips.

The report discusses the mathematical cost models that will be used in estimating the costs of developing and fabricating the microcircuits. Earlier models have been expanded to include rework terms related to substrate fabrication, nonrecurring developmental and manufacturing operations, and prototype production. Sample computer programs have been written to demonstrate how these cost models are applied. The programs will analyze the total development and manufacturing costs, calculate the cost variations when nonconventional technologies, such as TCC, become more widely used, and examine the behavior of the cost functions relative to the production volume.

These modeling techniques were also expanded to evaluate the total manufacturing costs of fully-assembled printed-wiring boards (PWB's). This is an important step leading to models that will handle a large variety of electronic technologies and yield comparative costs of the various development and manufacturing approaches. The models will not only indicate cost reductions but will clearly identify areas requiring technological improvements to reduce the costs.

The second part of the report discusses the development of LSI packaging utilizing the TCC technology, particularly in the areas of tape processing, wafer bumping, and inner/outer lead bonding. One section is devoted to studies and laboratory efforts to show the feasibility of interconnecting the LSI chips using the TCC and semiautomatic wire-bonding technology.

The report includes a number of cost plots and hardware illustrations. The appendix sections include references and sample program runs.

This work was done by R. P. Himmel, R. G. Ravetti, C. W. Rothrock, S. M. Stuhlbarg, and P. J. Zulueta of Hughes Aircraft Co. for **Marshall Space Flight Center.** *To obtain a copy of the report, "Design, Processing and Testing of LSI Arrays Hybrid Microelectronics Task," Circle 78 on the TSP Request Card.*
MFS-25359

Automated Ion Implantation for IC's

A semiconductor fabrication facility reduces operator costs and increases product yield.

A 24-page report discusses an automated ion-implantation facility being developed at the Marshall Space Flight Center. [Also see following article "An Automated Photolithography Facility for IC's" (MFS-25073).] This facility will be a part of a larger system that will process IC's from start to finish with minimal human intervention. The chips will be transported automatically from one processing station to another, eliminating the damage that occurs from manual handling. The facility will produce ultrareliable IC's that will function for 25 years or longer in spaceflights and other critical applications.

The facility will use four types of carriers according to the processing function: (a) an aluminum carrier designed for all regular IC operations, (b) a polypropylene carrier for processing in chemical solutions and caustic agents, (c) quartz boats for processing IC's in high-temperature environments, and (d) an interface for the other three to flip-transfer the wafer loads from one carrier type to another.

The facility will incorporate a commercially-available ion implanter modified for loading and unloading with an air-track input and output, respectively. Its continuously-variable energy output of 20 to 200 keV can generate ion-beam currents in excess of 40 μA using boron, phosphorus, or arsenic.

A 200-keV accelerator will be used. Its power supply will operate the cold-cathode ion source and also will include provision for operating optional hot-cathode and RF ion sources.

Three complete gas-handling systems will be used to supply dry nitrogen for backfilling the implantation chamber and system, dry air for operating electropneumatic valves, and liquid nitrogen as a cold trap for a high-speed oil-diffusion pump. The implanter will be furnished with two identical oil-diffusion pumping systems. These will control the electropneumatic valves and maintain the necessary vacuum and venting during the process cycles.

The entire operation will be controlled from a console, and the system will be more fully automated with an implant programer. The programer will receive command signals to interrupt the beam and initiate a wafer-indexing function until all the wafers receive the ion dose preset in the integrator. The integrator will have 15 current ranges.

This work was done by Bobby W. Kennedy of **Marshall Space Flight Center.** *To obtain a copy of the report, "Ion Implantation for Automatic Processing of Integrated Circuits," Circle 79 on the TSP Request Card.*
MFS-25193

An Automated Photolithography Facility for IC's

A facility for fully automated production of IC's

A 35-page report discusses various subsystems that will constitute a new fully-automated photolithography facility for the processing of IC's. [Also see preceding article "Automated Ion Implantation for IC's" (MFS-25193).] This facility being developed at the

(continued on next page)

Marshall Space Flight Center will be a part of a larger system that will process the IC's from start to finish with minimal human intervention. A number of carriers will be used to transport the chips from one station to another, eliminating the damage that occurs from manual handling. The facility will produce ultrareliable IC's that will last 25 years or longer in spaceflights and other critical applications.

The reported facility consists of an automatic scrubber, photoresist coater and developer, mask aliner, IR (infrared) bake, and inspection stations. The heart of the facility is the wafer carrier system. Four distinct carriers are utilized, depending on the nature of wafer processing. There is a standard aluminum carrier for all regular operations, a polypropylene carrier for areas with chemical solutions and caustic agents, quartz boats for high-temperature environments, and an inverting carrier for flip-transferring the wafers from one carrier system to another. Each carrier can handle 25 wafers at a time, the wafer diameter being 3 in. (7.5 cm).

An automatic in-line scrubber cleans the wafers with high-speed brush and solvent prior to other processing. This program-controlled station scrubs the wafers without creating mechanical stresses.

A single-head photoresist-coater and developer station is program-controlled and may include nitrogen purge, a spray wash, spin drying, precoating, and photoresist coating in its photoresist-coating cycle. A develop cycle may include various solvent washes and developer rinses with spin drying.

The automatic mask-aliner station alines the mask with the wafers using an optical-scanning computer control. The alined wafers are exposed to ultraviolet light for printing the pattern on the wafers and are then fed to the developer station.

The hard-bake IR station processes the coated wafers in 1 to 4 min and in 4 to 7 min after developing. The station includes a nitrogen purge available from two built-in nozzles.

The inspection station equipped with a micromanipulator includes a microscope to examine the wafers under low and high magnifications. A pantograph with template is also available for quick inspection. Acceptable wafers are returned to the wafer carrier by foot-switch command, while the rejects are sent to a holding position.

The report includes a number of illustrations showing various optical schemes for detecting and alining the chips. Photographs of the facility are also included.

This work was done by Bobby W. Kennedy of **Marshall Space Flight Center.** *To obtain a copy of the report, "Photolithography for Automatic Processing of Integrated Circuits," Circle 80 on the TSP Request Card.*
MFS-25073

Models of MOS and SOS Devices

A report on progress in the processing of metal-oxide-semiconductor and silicon-on-sapphire IC's

A quarterly report on trends and techniques for space-base electronics describes progress in three programs:

1. The development of a dc sputtering machine for aluminum and aluminum alloys,
2. The development of two-dimensional computer models of metal-oxide-semiconductor (MOS) transistors, and
3. The development of a computer program for calculating the redistribution diffusion of dopants in silicon-on-sapphire (SOS) films.

The sputtering machine can accommodate eight wafers for aluminum deposition. It rotates the wafers through three sputter-gun positions and two mask positions. The sputtering chamber opens into a clean bench located in a clean room.

The finite-element method of analysis was investigated as a means of modeling MOS transistors. Although the finite-element method is reportedly convenient in treating nonrectangular geometries and irregular boundaries, it produced disappointing results in the study; its accuracy was no better than that of the finite-difference method.

An MOS algorithm has been developed on the assumption that mobile carriers are included in an infinitesimally thin layer of charge at the silicon/silicon dioxide interface. The algorithm proceeds in an iterative fashion to solve simultaneously a one-dimensional current equation and Poisson's equation. The solution yields the potential distribution from which current is calculated as a function of the gate, drain, and body voltages.

The MOS model as it stands neglects generation/recombination mechanisms and therefore cannot treat impact-avalanche and bulk-generated leakage currents. However, it is likely that such effects can be treated by adding another iterative loop to the algorithm.

The SOS redistribution diffusion computer program is intended to produce curves showing the effects of diffusion time and temperature on junction depth, sheet resistance, and integrated ion-implanted impurity dose. These data have been generated for boron and phosphorus redistribution in nitrogen, dry oxygen, and steam ambients for SOS films in ⟨111⟩ crystal orientation. (The report furnishes the data in an appendix.)

The program contains three basic mathematical models: (1) an implantation profile, (2) an oxidation model, and (3) a diffusivity model. It was developed to account for both thin and thick oxides, but at present is limited to thin oxides because the simulation of both thick and thin oxides requires that a warped grid system be incorporated in the program — a modification that would demand considerable additional effort.

This work was done by J. D. Gassaway, Q. Mahmood, and J. D. Trotter of Mississippi State University for **Marshall Space Flight Center.** *To obtain a copy of the report, "Trends and Techniques for Space Base Electronics," Circle 81 on the TSP Request Card.*
MFS-25153

Mathematics and Information Sciences

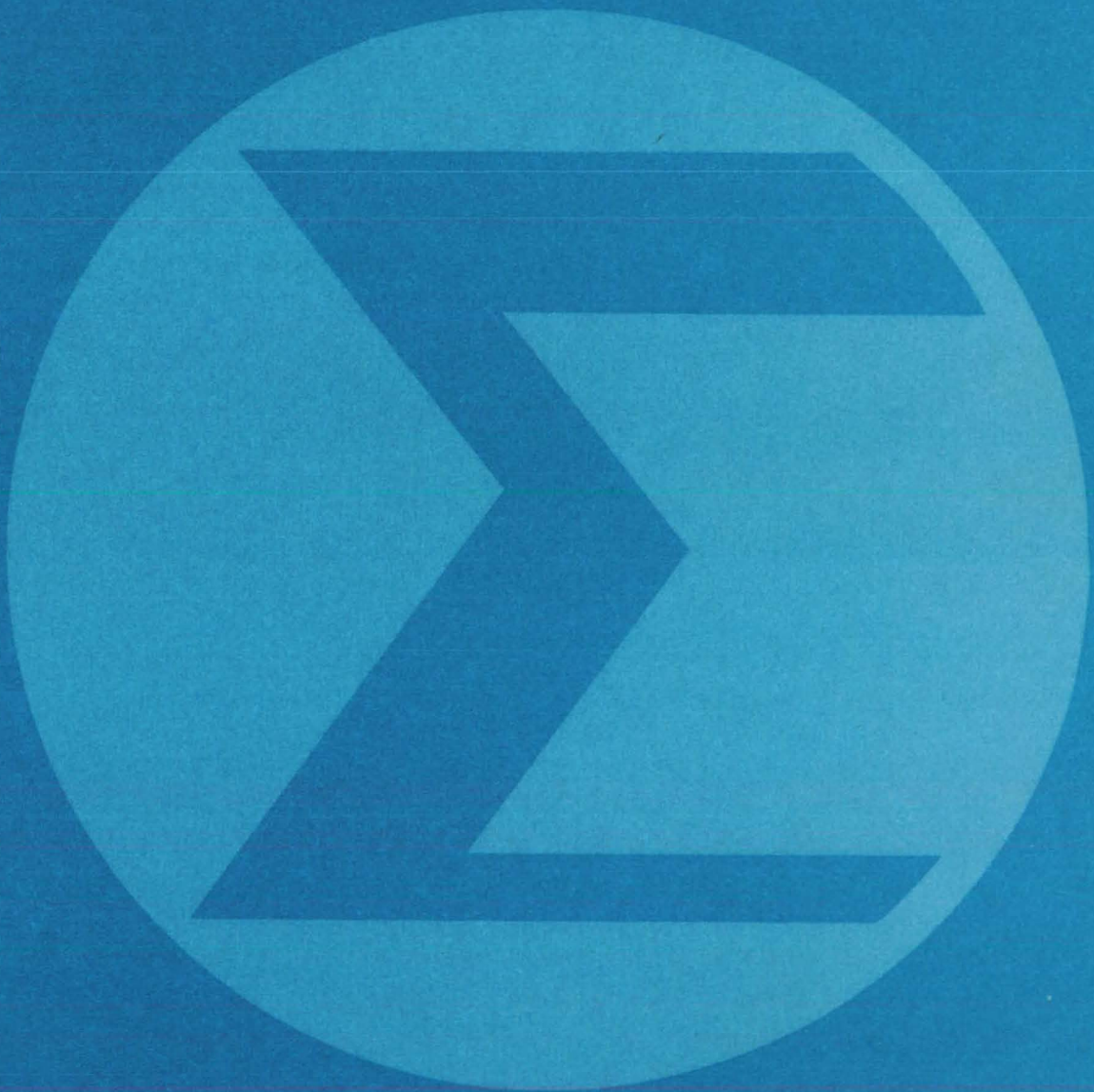

Efficient Telemetry Format

A proposed format promises to simplify ground processing of spacecraft data.

NASA's Jet Propulsion Laboratory, Pasadena, California

A recently-proposed telemetry format can organize spacecraft data from various sources into autonomous blocks. Each block would begin with a standard synchronization code, and contain a block-type identification, measurement-time information, and a data set from a particular source. Because all the blocks would be autonomous and would contain all the information needed for processing and routing, the processing at the receiving end (ground station) would be less complicated than in a time-multiplexed system. Thus, the complexity and cost of ground processing equipment could be reduced.

In the new format, complete data sets from each source are assembled into autonomous blocks via onboard buffering. The telemetry formats are assembled by sequentially transmitting the blocks from each source, and data mode changes are accommodated by changing the order or frequency of transmission of the block stream. Because of the standard-length blocks, much of the data can be edited, and format changes become readily apparent. Any errors in the transmission block would affect only one source. In effect the data are preprocessed, simplifying the function of the central processing computer to determine the received-block type and process the data set as a batch.

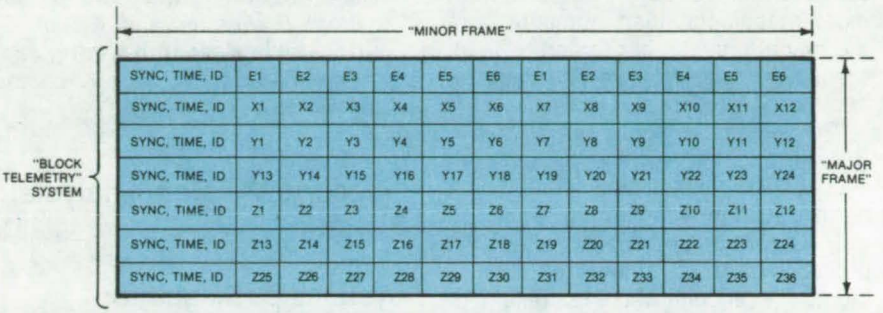

A **Proposed Telemetry Data Format** organizes data from various sources into autonomous blocks. Four spacecraft data sources are represented here by E, x, y, and z. In the "blocked" system, only one or several minor frames must be received, depending on the set, to reconstruct the data set. This approach is less error-prone and is more compatible with the packet-organized ground systems than the currently-used time-multiplexed transmission format.

The proposed format is illustrated using simple data sources E, x, y, and z representing, for example, spacecraft engineering data, scatterometer data, microwave radiometer data, and altimeter data, respectively. For each source, the data samples (E1 through E6, x1 through x12, etc.) are assumed to define completely the output of that source for one cycle of its operation.

In a "blocked" system, as shown, each minor frame is devoted to data from one specific source; some onboard source buffering is thus implied. The minor frame contains all or part of the data set. In order to reconstruct the set, it is only necessary to receive one E, x, two y, or three z minor frames. A missing minor frame creates an error in one set of source data only, whereas in a conventional system, all sets would be disrupted.

This work was done by Edward Greenberg and Adrian J. Hooke of Caltech for **NASA's Jet Propulsion Laboratory.** *For further information, Circle 82 on the TSP Request Card.*
NPO-13679

Computer Programs

These programs may be obtained at very reasonable cost from COSMIC, a facility sponsored by NASA to make new programs available to the public. For information on program price, size, and availability, circle the reference letter on the COSMIC Request Card in this issue.

User's Guide to SFTRAN

Programing language has been expanded and improved.

SFTRAN, a structured-programing language, has been given additional language features, has had some operating limitations removed, and has been designed to run more efficiently. In addition, the concepts of modularity and top-down development have been extended to the area of task management, and a set of command-level procedures has been provided for this purpose. Thus, the programer is able to select one of several jobs, and one of several parts of that job, and to invoke one of several operations to be performed on that part. This is done by simple brief statements, freeing the programer of bothersome details of an operational nature in order to concentrate his attention on those areas where his skill and effort are of a maximum benefit.

SFTRAN (Structured FORTRAN) is a programing language combining the two principles of "GO-TO-less" programing and stepwise refinement. A more appropriate description of "GO-TO-less" programing might be "avoidance of numbered statements." When

(continued on next page)

this concept is employed, program flow is controlled by constructs, or structures, that imply a certain flowchart function; the name given each construct is selected to be suggestive of its function. A principal benefit of "GO-TO-less" programing is that the resulting code is easier to read because the structure names are more meaningful than numbers and the reader's eye is not forced to leap around the page or from one page to another.

The second principle of stepwise refinement involves the process of successively refining one's description of the solution method in terms of evermore primitive components or processes. At each level of refinement, only enough detail is presented to make the method clear. Anything of a complicated nature is merely referred to, with its precise definition postponed until later. Sometimes called top-down programing, this technique is another that results in an easier-to-read code. Only a few ideas need be kept in mind at each level of description; and the important ones can be put first, at the top, where they belong.

The combined techniques have more to offer than merely good readability. They also provide a natural sequence of steps to be taken in the programing process and replace much of the *art* of programing with a methodology that is easy for the novice to learn and very efficient in the hands of the experienced. In addition, a high degree of program modularity is obtained, which means the code produced can be easily changed, extended, or adapted for other uses.

SFTRAN was created by John T. Flynn (NASA's Jet Propulsion Laboratory, Pasadena, California) for the specific purpose of providing a language suitable for structured programing. Flynn's implementation of an SFTRAN language was a precompiler that translated from SFTRAN to FORTRAN. This permitted a great degree of simplification in the precompiler program, as it only had to recognize the few special structures that control program flow. Also, by translating to FORTRAN, the benefits of program portability were automatically obtained. The new SFTRAN precompiler retains all of Flynn's original structures in addition to the improvements described above.

This program is written in SFTRAN for use on the UNIVAC 1100 computer and is also written in SFTRAN for use on the IBM 360 computer (reference LEW-13165).

This program was written by Theodore E. Fessler and William F. Ford of **Lewis Research Center.** *For further information, Circle P on the COSMIC Request Card.*
LEW-13172

Goddard Mission Analysis System

Systems packages for controlling many dynamic modules

In conventional mission analysis systems, requirements to meet varying user demands have been met by developing large, cumbersome systems encompassing many options or by developing many small, individually tailored systems that require significant setup and deck-handling time between runs. The Goddard Mission Analysis System (GMAS) is a collection of software modules that can be readily configured by the user to solve a wide variety of specific mission analysis problems.

The setup time and machine resources required to analyze a particular problem are greatly decreased through the dynamic-execution-time loading of modules in a user-specified sequence. The GMAS design is based on the philosophy that multiple options and variably-sized data areas can be most effectively provided through dynamic allocation, rather than through a planned overlay structure. The user can command the full potential of the GMAS with a simple control language, similar to a programing language, that defines data and controls the order in which load modules are executed.

The GMAS includes modules for performing a large selection of standard mission analysis procedures. One may modify existing modules or add new modules to enhance the abilities of GMAS without modifying the GMAS control structure because the load modules are identified through the input control language. The GMAS could also be used to control the processing of user-supplied modules that are not necessarily mission analysis oriented.

The major components of GMAS are the executive and the dynamic load modules and the dynamic arrays. The GMAS executive is primarily responsible for interpretation of user-control directives and data management. The executive passes control to user-designated utility load modules after having prepared user-specified and default data for the utilities. The executive also controls the dynamic assignment and release of core space for user-specified modules and data areas.

The dynamic load modules represent the applications software to be used in specific problem solutions. They may consist of the GMAS library of standard routines along with user-developed libraries of routines. Each dynamic load module is a separate group of subroutines that, when loading during GMAS execution, can be executed to solve part of the assigned problem and then be deleted from core. Dynamic-load-module input and output can be transferred through out-of-core files or through user-specified dynamic arrays located in a core area separate from the executive and any dynamic load modules. GMAS also contains a graphics executive system for providing interactive graphics in the form of tables, plots, and displayed messages for the IBM 2250, IBM 2260, and Anagraph 6600.

The GMAS is written in FORTRAN IV and Assembler for batch or interactive execution on an IBM 360-series computer system. The executive component, which is always resident in core, has a central memory requirement of approximately 220K of 8-bit bytes. The GMAS was developed in 1977.

This program was written by Francis E. McGarry of **Goddard Space Flight Center.** *For further information, Circle R on the COSMIC Request Card.*
GSC-12392

Software Design and Documentation Language

Processor and methodology for using structured programing

The Software Design and Documentation Language (SDDL) supports the design and documentation of complex software. It comprises (1) a design and documentation language for expressing design concepts, with forms and syntax that are simple, unrestrictive, and communicative; (2) a processor that can take design specifications written in this language and produce an intelligible, informative, and machine-reproducible documentation; and (3) a methodology for effectively using the language and processor to create well-structured, top-down programs and documentation.

The SDDL syntax is based on concepts of structured programing that have been expanded in scope to accommodate the communication requirements of software design. The SDDL syntax supports the top-down development of the design as a hierarchy of modules that specify the important concepts of the program. Each module represents a design abstraction and contains only as much detailed information as is needed to communicate its own intent and purpose. Lower level detail is represented by other modules; i.e., abstractions; and the interrelationships between the modules are expressed by module-invocation statements. The details of each module are expressed in terms of iterations, conditional branches, and sequences.

In addition to the syntax for specifying design concepts, SDDL also provides extensive controls over actions of the processor. These include the capability to add or delete any keywords used to express the concepts described above, to supply title pages, to control formatting (e.g., page width and length, indentation, page eject, page headings, line, and page numbering), and to specify the means by which identifiers and names in the document will be caught and cross-referenced.

The SDDL processor reformats and prints the design specifications with indentation, flow lines, and page reference numbers that provide a two-dimensional representation superior to flow charts. In addition the processor checks for logic errors and summarizes important design information as a Table of Contents, a Module Hierarchy report (i.e., "calls to" and "calls from"), or Cross-Reference Listings of identifiers and names used in the design.

The combination of a language that supports the expression of design concepts and a processor that supplies machine-reproducible documentation with enhanced information content makes iterative, incremental, software design a practical reality.

Documentation provided with SDDL contains an introduction to the concepts, a description of the syntax, and a methodology for effective use of language and processor. The SDDL processor is written in the SIMSCRIPT II.5 Programing Language and is currently implemented on UNIVAC, IBM, and CDC machines.

This program was written by Henry Kleine of Caltech for **NASA's Jet Propulsion Laboratory.** *For further information, Circle S on the COSMIC Request Card.*
NPO-14610

Estimation of Incomplete Multinomial Data

For classification of multinomial data when observations are incomplete

At times during the collection of multinomial data, an observation may be only partially classified. Each such partially classified observation is observed to fall in one of two or more selected categories but cannot be further classified into a single category. A computer program was developed to estimate the multinomial cell probabilities from such incomplete data.

The data are assumed to be randomly incomplete; the estimation criterion is the minimization of risk for quadratic loss. The estimators are the classical maximum-likelihood estimate, the Bayesian posterior mode, and an approximate Bayesian posterior mean. For both Bayesian estimators, the conjugate prior for the multinomial distribution (the Dirichlet) is assumed. The program performs Monte Carlo simulation studies on small- and medium-size samples to assess which estimate — the maximum-likelihood, posterior mode, or approximate posterior mean — best minimizes risk for specified values of the probability vector. For trinomial samples the program can also assess how well each of these functions approximates the exact posterior mean and how well a Taylor-series function approximates elements of the posterior covariance matrix. Various properties of the estimators can be evaluated. This program should prove useful in any project involving the collection of multinomial data where observations are sometimes incomplete.

This program is written in FORTRAN IV and Assembler for batch execution and has been implemented on the CDC CYBER 173 with a central memory requirement of approximately 112K (octal) of 60-bit words. This estimator program was documented in 1978.

This program was written by Karen R. Credeur of **Langley Research Center.** *For further information, Circle T on the COSMIC Request Card.*
LAR-12593

Automated Flow-Chart System

Accurate flow chart produced for FORTRAN programs

The TAMU Flow-Chart System will produce a flow chart of any program written in the FORTRAN language. With your program as input, TAMU generates, as line-printer output, a detailed representation of the action taken as each program statement is executed.

Each statement in a flow-charted program is displayed within a symbol that represents the program action during processing of the enclosed statement. Symbols available include: subroutine, function, and entry statements; arithmetic statements; input

(continued on next page)

and output statements; arithmetical and logical IF statements; subroutine calls with or without argument list returns; computed and assigned GO TO statements; DO statements; STOP and RETURN statements; and CONTINUE and ASSIGN statements. Comment cards within the source program may be suppressed or may be displayed and associated with a succeeding source statement. Each symbol is annotated with a label (if present in the source code), a block number, and the statement-sequence number. Program flow and options within the program are represented by line segments and direction indicators connecting symbols.

This program is written in COBOL for batch execution and has been implemented on an IBM 370-series computer with a central memory requirement of approximately 380K of 8-bit bytes. It was developed in 1977.

This program was written by William Woodford of **Goddard Space Flight Center.** *For further information, Circle U on the COSMIC Request Card.*
GSC-12514

Systems Improved Numerical Differencing Analyzer

SINDA program for CDC computers

The program SINDA (Systems Improved Numerical Differencing Analyzer) solves physical problems governed by diffusion-type equations that can be modeled by lumped-parameter representation. Previously available only to UNIVAC users [see *NASA Tech Briefs*, Vol. 1, No. 4, page 658 (MSC-13805)], the SINDA program has now been adapted for use on CDC machines.

The system is most widely used as a general thermal analyzer with resistor/capacitor network representations, but it may be adapted to a wide range of problems represented by differential equations, such as Fourier, Poisson, or Laplace equations. SINDA can solve numerically most any set of ordinary differential equations which may be used to represent the transient behavior of a lumped-parameter system, or any set of nonlinear algebraic equations, which might represent the steady-state conditions of a physical system.

For flexibility, SINDA offers numerical solution techniques including finite-difference formulations of the explicit method, such as the forward-difference explicit approximation, the Dufort-Frankel approximation, the exponential approximation, and the alternating-direction approximation. Also available are formulations of the implicit method, such as the backward-difference implicit approximation and the Crank-Nicholson approximation. Many physical problems, particularly those in thermal analysis, can be readily analyzed with the SINDA system.

The SINDA system consists mainly of a preprocessor and a subroutine library. The preprocessor accepts programs written in the SINDA language and converts them into standard FORTRAN programs. The SINDA language is designed for working with lumped-parameter representations and finite-difference solution techniques. The SINDA library consists of a large number of prewritten FORTRAN subroutines that perform a variety of commonly needed actions. The user may call these subroutines from the user's SINDA language program, thus greatly reducing the programing efforts required to solve many problems.

Most of the subroutines in the SINDA library were developed for use in solving thermal analysis problems. As a thermal analyzer, SINDA can handle such interrelated complex phenomena as sublimation, diffuse radiation within enclosures, transport delay effects, sensitivity analysis, and thermal network error correction. Special subroutines are included in the SINDA library to facilitate the thermal analysis of systems incorporating fluid flow networks. SINDA can easily account for pumps, valves, and heat exchangers during a thermal analysis. The user-written SINDA language program determines the input data required and the information that is produced as output by the program.

This program is written in FORTRAN IV and Assembler and has been implemented on a UNIVAC 1100-series computer operating under EXEC 8 with a central memory that varies depending on input but never exceeds 65K of 36-bit words. For plotted output, a Stromberg-Carlson SC 4020 plotter is required. The SINDA program was developed in 1971 with the fluid capability added in 1975. SINDA was adapted to the CDC computer in 1978. The CDC version has been implemented on a CDC CYBER 175 operating under NOS with a central memory requirement of approximately 175K (octal) of 60-bit words.

This program was written for **Johnson Space Center.** *For further information, Circle V on the COSMIC Request Card.*
MSC-18597

SUBJECT INDEX

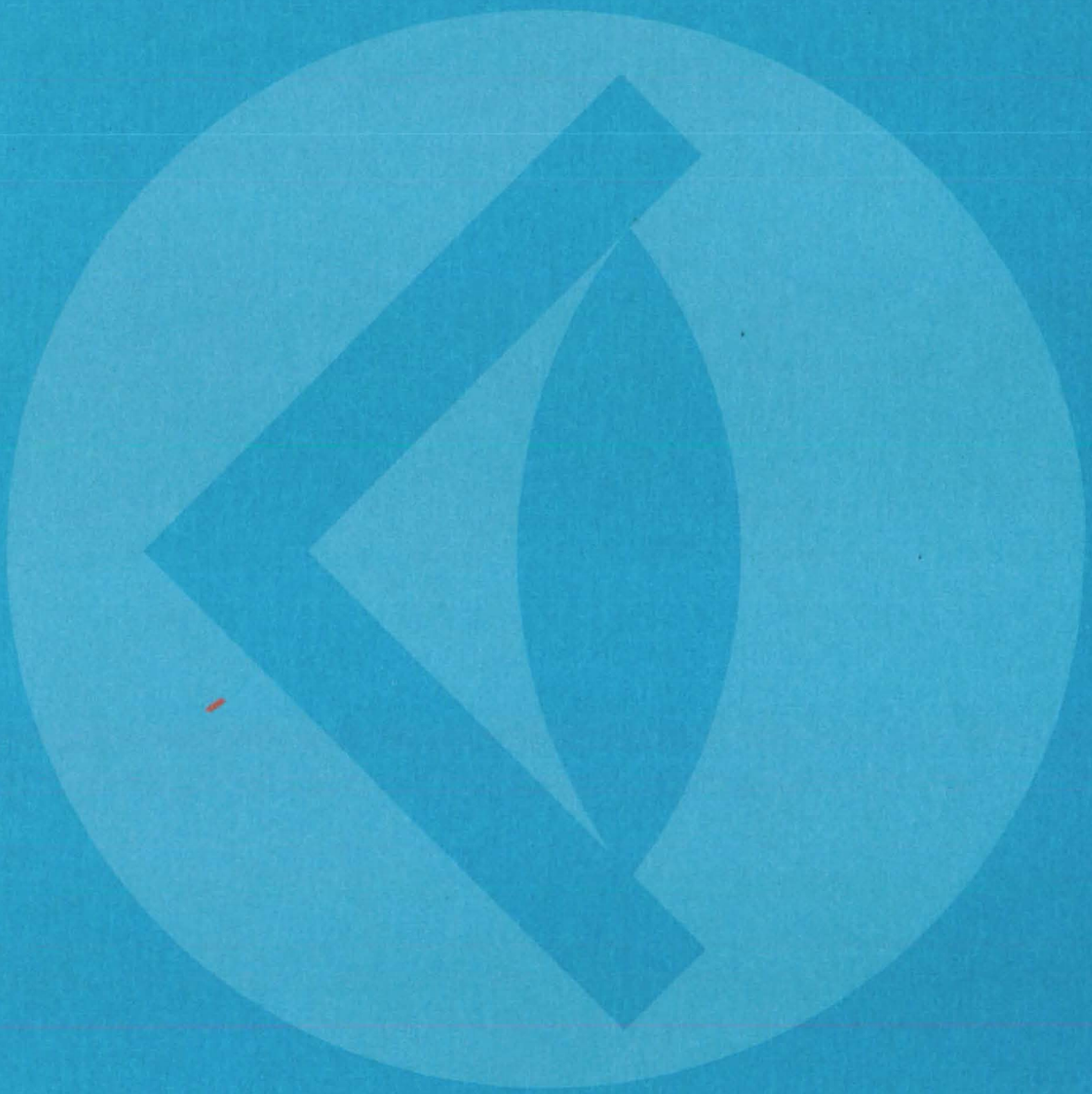

National Aeronautics and
Space Administration

Washington, D.C.
20546

THIRD-CLASS BULK

NASA

A commercial seismic testing facility, shown here ready for testing of a 25-ton diesel generator, evolved from related work by a NASA contractor on the Saturn V launch vehicle. The Saturn V had to be tested for its ability to withstand launch vibration. Similarly, massive equipment, such as that used in nuclear power generating stations, is tested [at lower frequencies] for Earthquake resistance. [See page A1.]